DOC.20071018.0019

QA: QA

MDL-EBS-PA-000004 REV 03

October 2007

Waste Form and In-Drift Colloids-Associated Radionuclide Concentrations: Abstraction and Summary

THIS DOCUMENT IS IMPACTED BY THE FOLLOWING "ERROR RESOLUTION DOCUMENTS", WHICH SHOULD BE REVIEWED PRIOR TO USING THIS DOCUMENT:

----

1) MDL-EBS-PA-000004 ERD 01 - ACCESSION NO. LLR.20080325.0281

Prepared for:
U.S. Department of Energy
Office of Civilian Radioactive Waste Management
Office of Repository Development
1551 Hillshire Drive
Las Vegas, Nevada 89134-6321

Prepared by:
Sandia National Laboratories
OCRWM Lead Laboratory for Repository Systems
1180 Town Center Drive
Las Vegas, Nevada 89144

Under Contract Number
DE-AC04-94AL85000

DISCLAIMER

This report was prepared as an account of work sponsored by an agency of the United States Government. Neither the United States Government nor any agency thereof, nor any of their employees, nor any of their contractors, subcontractors or their employees, makes any warranty, express or implied, or assumes any legal liability or responsibility for the accuracy, completeness, or any third party's use or the results of such use of any information, apparatus, product, or process disclosed, or represents that its use would not infringe privately owned rights. Reference herein to any specific commercial product, process, or service by trade name, trademark, manufacturer, or otherwise, does not necessarily constitute or imply its endorsement, recommendation, or favoring by the United States Government or any agency thereof or its contractors or subcontractors. The views and opinions of authors expressed herein do not necessarily state or reflect those of the United States Government or any agency thereof.

QA: QA

Waste Form and In-Drift Colloids-Associated Radionuclide Concentrations: Abstraction and Summary

MDL-EBS-PA-000004 REV 03

October 2007

Model Signature Page/Change History

Complete only applicable items.

1. Total Pages: 278

2. Type of Mathematical Model

☐ Process Model ☒ Abstraction Model ☐ System Model

Describe Intended Use of Model

Colloids process models for the waste form and engineered barrier system components of the Total System Performance Assessment for the License Application.

3. Title

Waste Form and In-Drift Colloids-Associated Radionuclide Concentrations: Abstraction and Summary

4. DI (including Rev. No.):

MDL-EBS-PA-000004 REV 03

	Printed Name	Signature	Date
5. Originator	Edgar Buck ← GAF 10/16/07 for David Sassani		10/08/2007 10/08/2007
6. Independent Technical Reviewer	Patrick Brady		10/09/2007
7. Checker	Stephen Alcorn		10/09/2007
8. QCS	Robert Spencer		10/09/07
9. Responsible Manager/Lead	Patrick Brady		10/09/2007
10. Responsible Manager	Geoff Freeze		10/16/07

11. Remarks

Change History

12 Revision No.	13. Description of Change
00	Initial Issue.
00/ICN01	Modified model report to include a discussion on the development of the Forward Rate Constant (k) for irreversible sorption of Pu and Am on iron hydroxide colloids and corrosion products. Other modifications included changing the model output DTN references to reflect the latest versions of these data records and also changing the reference to the NRC's Yucca Mountain Review Plan to reflect the current version of this guidance document.
01	Complete revision to incorporate comments for regulatory integration. Changes were too extensive for change bars to be practical.

02	Two new alternate conceptual models have been included to cover possible reversible and irreversible spent nuclear fuel-derived waste form colloids. The special case of oxidized high burn-up spent nuclear fuel has been considered. A new sorption kinetic model has been developed. Validation section has been altered. Changes were too extensive for change bars to be practical. **CR-5286** High Sorption, see Appendix IV. **CR-4724** Incorrect statement in validation section of colloid report. This statement has been removed and most of the section has been rewritten. **CR-5278** Insufficient documentation to reproduce data independently. Additional plots have been added and new text to link data to Table 6-6 **CR-5185** DTN does not agree with source report. Errors were made in writing some values in Table 6-6. These have been corrected. **CR-5254** Rev 01 deleted Table 16 and note on Table 10. Reader is pointed to Table 6-6, note added back. **CR-5598** DTN MO0311ANLGCOLL.564 incorrectly labeled Qualified, Product Output. References to DTN replaced with references to original sources. **CR-6234** Assumptions on gravitational settling and filtration removed from Rev 01. Statement that gravitational settling and filtration are excluded was added to Section 7.2. **CR5600** The- following citations and DIRS entries were changed accordingly: CRWMS M&O 2001 [DIRS 154071] was changed from “Direct” to “Indirect Input” Liang and Morgan 1990 [DIRS 109524] was moved “Entire” to indirect input row Mertz et al. 2003 [DIRS 162032] was changed from “Direct” to “Indirect Input.”
03	New direct data sources. Extensive revision of Section 6. Changes were too extensive for change bars to be practical. Introduction of new colloidal particles and radionuclides, additional assumptions added. Validation section modified to deal with new model and new validation questions. **CR-7291** Figure 6.7 is no longer used and the issue no longer exists in the report. See discussion in Section 1.0. **CR-8555** All output is included within the DTN, no input-output files were generated with EQ3/6 for this revision of the report. See discussion in Section 1.0.

ACKNOWLEDGEMENTS

Contributions to this report were made by:

- Richard Aguilar, REV 00 and REV 00, ICN 01
- Stephen Alcorn, REV 00; REV 00, ICN 01; and REV 01
- Jim Cunnane, REV 02, Section 6.3.1.2.

INTENTIONALLY LEFT BLANK

EXECUTIVE SUMMARY

This report describes the types and concentrations of colloids that could be: (1) generated in the waste package from degradation of the waste forms and the corrosion of the waste package materials, (2) produced from the steel components of the repository and their potential role in radionuclide transport, and (3) present in natural waters in the vicinity of Yucca Mountain. In addition, sorption and desorption characteristics and mechanisms of colloids anticipated in the repository are addressed. The model considers radionuclide–colloid behavior and radionuclide-sorption by representing colloids in the waste package as smectite clay, a mixed actinide-bearing rare earth-zirconium oxide, iron oxyhydroxide, and uranophane $\{Ca(UO_2)_2(SiO_3OH)_2(H_2O)_5\}$. For the purposes of predictive stability modeling of these colloidal suspensions, these colloids that comprise the types expected to have any potential contribution to radionuclide transport are conceptually represented as montmorillonite, ZrO_2, hematite, and meta-autunite, respectively. The model uses theoretical calculations and laboratory data to determine the stability of modeled colloids with ionic strength and pH. The true nature of colloid composition and heterogeneity, generation, and flocculation in the waste package will be extremely complex, involving the formation of numerous types of phases, often depending on the composition of the various waste forms and waste package materials. This model strives to capture the uncertainty of the real system using theoretical models of four representative colloids to capture the behavior of the colloid types most likely to influence dose.

Data used to develop model parameters and model process elements are based on colloidal particle theory, field data, Yucca Mountain Project-developed laboratory data, and open-literature data. Theoretical calculations and experimental data have been used to establish parameters associated with colloid stability and to develop ranges for anticipated concentrations of colloids in groundwaters, generated during waste form and waste package corrosion, and sorption–desorption characteristics of radionuclides associated with colloids.

Colloids can be produced from the degradation of defense high-level waste glass (DHLWG), commercial spent nuclear fuel (CSNF), defense spent nuclear fuel (DSNF), and metallic waste package components. The abundance of these colloids within the breached waste package will depend on the extent and rate of degradation and the degradation products formed. Colloid abundance and stability also depend on environmental factors including the ionic strength, pH, colloid–colloid interactions, and colloid concentrations of waters entering the waste package from the surrounding drift. The model considers the potential effects of these factors and processes on colloid formation and subsequent suspension stability.

Waste form corrosion tests have been used to provide data on the colloid crystal structure and composition, concentration, and transuranic content. Radionuclide-bearing colloids can be produced by several mechanisms: by precipitation of released species (sometimes termed condensation), by sorption of transuranics onto natural seepage colloids and onto iron oxide corrosion products from the waste package (pseudocolloid formation), and by spallation of the weathered corrosion rind (termed primary colloid formation). The migration of radionuclides generated from waste degradation are included in an analysis of potential radionuclide transport within the engineered barrier system, as documented in *EBS Radionuclide Transport Abstraction* (SNL 2007 [DIRS 177407]).

Studies by van Middlesworth and Wood (1998 [DIRS 170927]) represent possibly one of the best validations for the colloid model. Alteration of the granite resulted in the precipitation of monazite and rhabdophane analogous to the laboratory tests on waste glasses. The analysis of filtered and unfiltered samples indicated that the majority of the mobilized rare earths and thorium were associated with colloids (albeit in minute quantities (10^{-10} to 10^{-11} mol/L Th), while the mobilized uranium fraction was mostly soluble. An interesting aspect of these studies was the application of ferric-hydroxide coprecipitation for the analysis of trace-level actinides and rare earths in solution, which supports the contention that attenuation of actinides in the waste package will occur by reaction with iron corrosion products. Studies by Kersting et al. (1999 [DIRS 103282]) and Novikov et al. (2006 DIRS 179554]) have demonstrated the impact of colloidal-assisted transport of plutonium by attachment to silicate (clay) particles and iron oxide particles, respectively. The model developed here predicts the formation of these types of particles and provides information on their properties but does not implement long-range transport.

Specific parameters developed in this model analysis for use elsewhere in the TSPA-LA model include waste form colloid mass concentrations (derived from DHLWG, CSNF, and DSNF), corrosion product colloid mass concentrations, the distribution of sorption partition coefficients (K_d values) for selected radionuclides onto smectite clay and uranophane phases, rate of plutonium and americium irreversible attachment onto ferrihydrite, and range of specific surface areas and surface site densities for smectite and uranophane.

CONTENTS

Page

ACKNOWLEDGEMENTS v

EXECUTIVE SUMMARY vii

ACRONYMS AND ABBREVIATIONS xix

1. PURPOSE 1-1
   - 1.1 OVERVIEW 1-2
   - 1.2 BACKGROUND 1-2
   - 1.3 DOCUMENT DEVELOPMENT 1-3
   - 1.4 MODEL REPORT OVERVIEW 1-4

2. QUALITY ASSURANCE 2-1

3. USE OF SOFTWARE 3-1

4. INPUTS 4-1
   - 4.1 DIRECT INPUT 4-1
     - 4.1.1 Developed Parameters 4-9
     - 4.1.2 Other Parameters Critical to the Implementation of This Abstraction in the TSPA-LA Model 4-9
   - 4.2 CRITERIA 4-9
   - 4.3 CODES AND STANDARDS 4-10

5. ASSUMPTIONS 5-1
   - 5.1 DISTRIBUTION COEFFICIENTS OF THORIUM AND PROTACTINIUM ARE THE SAME AS THAT OF AMERICIUM 5-1
   - 5.2 EFFECT OF TEMPERATURE ON WASTE FORM COLLOIDS 5-1
   - 5.3 DIAMETER OF COLLOIDS IN THE WASTE PACKAGE IS FIXED 5-2
   - 5.4 ATTACHMENT OF PLUTONIUM AND AMERICIUM TO DHLWG COLLOIDS IS EITHER REVERSIBLE OR EMBEDDED (IRREVERSIBLE) 5-2
   - 5.5 "EMBEDDED" COLLOIDS FROM SNF MAY BE DESCRIBED AS ZRO_2 PARTICLES 5-2
   - 5.6 COLLOIDAL META-AUTUNITE IS A REASONABLE ANALOGUE FOR A URANOPHANE COLLOID 5-3
   - 5.7 COLLOIDS DERIVED FROM THE CORROSION OF WASTE PACKAGE MATERIALS CAN BE REPRESENTED AS HEMATITE FOR STABILITY CALCULATIONS 5-3
   - 5.8 COLLOID SORPTION AT THE AIR–WATER INTERFACE 5-4

6. MODEL DISCUSSION 6-1
   - 6.1 MODEL OBJECTIVES 6-1
   - 6.2 FEATURES, EVENTS, AND PROCESSES CONSIDERED IN MODEL 6-2

CONTENTS (Continued)

Page

6.3 BASE-CASE MODEL 6-2
6.3.1 Colloid Formation and Occurrence 6-3
6.3.2 Colloid Suspension Stability and Concentration 6-8
6.3.3 Experimental Evidence for the Concentration and Nature of Colloids from Borosilicate Waste Glass Corrosion Tests 6-34
6.3.4 Experimental Evidence for Irreversible CSNF Colloids 6-36
6.3.5 Experimental Evidence for U(VI) Colloidal Phases 6-37
6.3.6 Evidence of Colloids from DSNF 6-38
6.3.7 Field Evidence of Colloids from Natural Analogues 6-43
6.3.8 Colloids from the Corrosion of Waste Package and Metallic Invert Materials 6-44
6.3.9 Type, Abundance, and Stabilities of Natural Colloids within UZ Seepage Water and/or Groundwater 6-47
6.3.10 Re-Stabilization of Colloids at Very High Ionic Strength 6-49
6.3.11 Literature and Site-Specific Data on Stability and Concentration of Seepage Water Colloid Suspensions 6-49
6.3.12 Radionuclide Sorption to Colloids 6-53
6.3.13 Potential Effects of Microbes and Organic Compounds 6-72
6.4 CONSIDERATION OF ALTERNATIVE MODELS 6-73
6.4.1 Kinetic Sorption Model: An Alternative to Irreversible Attachment 6-74
6.4.2 Rate of Colloid Generation Model 6-77
6.4.3 Mechanisms of Colloid Generation 6-80
6.5 MODEL FORMULATION FOR BASE-CASE ASSESSMENT 6-81
6.5.1 Waste Form Abstraction Implementation in TSPA–LA 6-82
6.5.2 In-Drift Abstraction Implementation in TSPA–LA 6-90
6.5.3 Implementation of Colloid-Facilitated Transport in the Natural Barrier System 6-92
6.6 BASE-CASE MODEL RESULTS 6-94
6.6.1 Uncertainty Associated with the Model Analysis 6-94
6.6.2 Uncertainty Associated with DHLWG Colloid Formation 6-97
6.6.3 Uncertainty Associated with Irreversible CSNF Colloid Formation 6-99
6.6.4 Uncertainty Associated with Reversible Colloid Formation from DSNF and CSNF 6-102
6.6.5 Uncertainty Associated with Corrosion Product Colloid Formation 6-105
6.6.6 Uncertainty Associated with the Measurement of Seepage Water/Groundwater Colloids 6-108
6.6.7 Uncertainty Associated with the Determination of Colloid Stability 6-108
6.6.8 Uncertainty Associated with Radionuclide Sorption onto Colloids 6-108
6.7 DESCRIPTION AND ANALYSES OF THE BARRIER CAPABILITY 6-121
6.8 EVALUATION OF ALTERNATIVE MODELS 6-121

CONTENTS (Continued)

Page

7. VALIDATION 7-1
7.1 VALIDATION OF MODEL 7-9
7.1.1 Validation of Mathematical Form of Model 7-9
7.1.2 Validation of Model Results for Colloid and Plutonium Concentrations 7-13
7.1.3 Validation of CSNF and DSNF Model Results 7-15
7.1.4 Validation of Corrosion Product and Groundwater Colloid Concentration Model Results 7-20
7.1.5 Optional Additional Confidence Building for Distribution Coefficient Values 7-23
7.1.6 Post-Model Development Validation Conclusion 7-30
7.2 PROCESSES NOT INCORPORATED INTO THE ABSTRACTION 7-30
7.3 VALIDATION ACTIVITIES EXTENDING BEYOND THE CURRENT DOCUMENTATION OF THE MODEL 7-31

8. CONCLUSIONS 8-1
8.1 MODEL SUMMARY AND IMPLEMENTATION 8-1
8.2 MODEL OUTPUTS 8-2

9. INPUTS AND REFERENCES 9-1
9.1 DOCUMENTS CITED 9-1
9.2 CODES, STANDARDS, REGULATIONS, AND PROCEDURES 9-17
9.3 SOURCE DATA, LISTED BY DATA TRACKING NUMBER 9-17
9.4 OUTPUT DATA, LISTED BY DATA TRACKING NUMBER 9-19
9.5 SOFTWARE CODES 9-20

APPENDIX I: CALCULATION OF GROUNDWATER COLLOID PARAMETERS I-1

APPENDIX II: QUALIFICATION OF UNQUALIFIED DATA FROM OUTSIDE SOURCES USED AS DIRECT INPUTS II-1

APPENDIX III: DATA QUALIFICATION PLANS III-1

APPENDIX IV: CRITICAL REVIEW IV-1

INTENTIONALLY LEFT BLANK

FIGURES

Page

6-1. Radionuclide-Bearing Colloid Types 6-4
6-2. Schematic of Colloid Formation from Waste-Form Corrosion 6-7
6-3. Stability Ratio (W) for ZrO_2 Colloids, Showing Experimental Data from Bitea et al. (2003 [DIRS 174504]) with Calculation Fit Using Parameters in Table 6-2 6-11
6-4. Experimental Zeta Potential with pH at Different Ionic Strengths with Fits Used in Model Development 6-12
6-5. Calculated Stability Plot for Hematite with Fits to the DLVO Model at the Low and High pH Regions (Equations 6-8a and 6-8b) and Experimental Values from Liang and Morgan (1990 [DIRS 109524], Figure 1, p. 40) 6-13
6-6. Relationship between Plutonium Colloid Concentration and Colloid Mass Concentration 6-15
6-7. Cumulative Distribution of Plutonium Colloid Concentration from DHLWG Corrosion Tests with Monolith Results in Large Symbols (i.e., red squares and blue triangles) 6-17
6-8. Experimental Zeta Potential with pH at Different Ionic Strengths for Montmorillonite 6-20
6-9. Plot Showing the DLVO-Calculated Stability of Montmorillonite Colloids at $W = 10$ with a Quadratic Fit (Equation 6-9) to the DLVO Model and Experimental Values from Tombácz et al. (1990 [DIRS 112690]) 6-21
6-10. Cumulative Distribution of Concentrations of Plutonium Colloids from SNF Corrosion Tests 6-24
6-11. Measured Variation in Zeta Potential with pH at an Ionic Strength of 0.001 mol/kg for ZrO_2 6-25
6-12a. Calculated DLVO Stability Plots with Polynomial Fit (Equation 6-10a) to the DLVO Model for ZrO_2 Colloids Suspension at Low pH 6-26
6-12b. Calculated DLVO Stability Plots with Polynomial Fit (Equation 6-10b) to the DLVO Model for ZrO_2 Colloids Suspensions at High pH 6-26
6-13. Experimental Zeta Potential with pH at Different Ionic Strengths for Meta-Autunite 6-28
6-14. Calculated Stability Plots with a Polynomial Fit (Equation 6-11) to the DLVO Model for Uranophane Colloids Suspensions 6-29
6-15. Distribution of Colloidal Mass from 8- to 10-year Testing of UO_2 under Unsaturated Conditions Assuming 2% to 5% of Released Uranium Is from Uranophane Colloids 6-30
6-16. Summaries of Radionuclide Sorption Data on Uranyl Phases 6-32
6-17. Calculated Surface Area of Two Types of Uranyl Secondary Phase (Čejakite and Uranophane) 6-34
6-18. Concentrations of Plutonium and Colloids as a Function of Ionic Strength in Corrosion Tests 6-35
6-19. Transmission Electron Microscope Images of DHLWG and CSNF Corrosion Rinds and Colloids 6-36
6-20. Log_e Normal Fit to Iron Oxide Colloid Mass 6-45
6-21. Modeled Distribution Iron Oxide Colloid Mass from Stainless Steel Corrosion 6-46

FIGURES (Continued)

Page

6-22. Colloid Concentrations versus Alkali and Alkaline-Earth Concentration for Groundwaters from around the World 6-50
6-23. Groundwater Colloid Concentration Data Collected in the Vicinity of Yucca Mountain Compared with Data Collected from Groundwaters around the World 6-51
6-24. Cumulative Distribution Function Showing the Probability of Occurrence of Colloid Concentration Levels in Groundwater Samples in the Yucca Mountain Area and Idaho National Laboratory 6-52
6-24a. Summaries of Np and U Sorption Data on Montmorillonite between pH 5 and 9 6-60
6-24b. Summaries of Cs, Sn, and Ra Sorption Data on Montmorillonite 6-61
6-24c. Summaries of Pu, Am, Th, and Pa Sorption Data on Montmorillonite 6-61
6-25a. Kinetic Sorption Model Predictions for Plutonium Sorption onto Colloids 6-75
6-25b. Three-Site Sorption Model 6-75
6-26. Processes within the Waste Package 6-83
6-27. Processes within the Drift (invert) 6-84
6-28. Flow Chart and Logic Statements: Transfer of Colloid-Associated Radionuclide Source Term to Invert 6-89
6-29. Inputs to Drift from Waste Package 6-90
6-30. Recalculation of Colloid-Associated Radionuclides in Drift 6-91
6-31. Source Term Summation for Colloid-Associated Radionuclide Concentrations in Drift 6-92
6-32. Stability Ratio (W) of Colloids Calculated from Particle Concentrations Reported by Mertz et al. (2003 [DIRS 162032], Table A3-1) 6-96
6-33. Predicted Change in Glass Colloid Concentration Based on DHLWG Tests 6-98
6-34. Stability of Montmorillonite Colloids with pH and a Series of W Values 6-99
6-35. Predicted Stability of Plutonium Colloids from CSNF based on Data from Wilson (1990 [DIRS 100793]) with $W = 1 \times 10^6$ 6-100
6-36. Stability of CSNF Irreversible Colloid (ZrO_2) with pH and Ionic Strength 6-101
6-37. Stability of U(VI) Phase with pH and Ionic Strength 6-103
6-38. Distribution of Radionuclide-Associated Colloid Partitioning between the Fluid and the Colloid 6-104
6-39. Variation in Stability Ratio with pH and Ionic Strength 6-106
6-40. Plots Showing pH Dependent Sorption of (a) U(VI) and (b) Np(V) on Montmorillonite 6-111
6-41. (a) Cumulative Distribution Functions for the K_c of Smectite Colloids Using Transport Parameters Defined for the Conditions within the EBS; (b) Cumulative Distribution Functions for Uranium K_c for Smectite Colloids in the Yucca Mountain Volcanic Regions 6-112
7-1. Total Plutonium and Americium Concentration from Static Tests on Actinide-Doped R7T7 Borosilicate Glass Conducted at 90°C with an SA/V of 50/m 7-14
7-2. Released Fraction per Day of ^{239}Pu and ^{241}Am as a Function of Test Duration for the CSNF High Drip-Rate Tests 7-16

FIGURES (Continued)

Page

7-3. Microscopic Images of Colloidal U(VI) Phases and Analogues of Possible CSNF Irreversible Colloids 7-19
7-4. Comparison of Plutonium Concentration with pH Reported on Iron Oxide Colloids at the Mayak Facility in Russia and DLVO Predicted Stability of Iron Oxides from Current Model with $W = 100$ 7-21
7-5. Transmission Electron Micrograph of Corroded Stainless Steel Showing Iron Oxide Surface 7-22
7-6. Cumulative Distribution Plot of Values Calculated from Results Reported by Dietz (2005 [DIRS 179542]; see Output DTN: MO0705COLCONCS.000) Compared to the Stainless Steel Corrosion Product Colloid Distribution Used in the Model 7-23
7-7. Cumulative Distribution Function Showing the Distribution of Cesium Sorption Coefficients Obtained on Clay, Zeolite, and Glass 7-24
7-8. Schematic Plot Adapted from Data Reported for Cesium Sorption on Montmorillonite with pH and NaCl Concentration 7-25
7-9. Plot Showing Sorption Rate for Plutonium on Iron Oxides 7-29

INTENTIONALLY LEFT BLANK

TABLES

Page

4-1. Direct Inputs for Colloid Models 4-3
4-2. Summary of Corroborating/Supporting Information 4-6
4-3. Applicable Project Requirements 4-10
6-1. FEPs Included (screened in) in the TSPA Model and Addressed in This Report 6-2
6-2. Definition of Colloid Potential Energy for Stability Calculations 6-10
6-3. Range of Colloid Concentrations for Scaling 6-16
6-4. Distribution of Plutonium Colloid Concentration Values (mL/g) Used for DHLWG Colloids in TSPA-LA Calculations 6-16
6-5. Plutonium Colloid Concentrations Obtained from Immersion Tests on DHLWG 6-18
6-6a. Plutonium Colloid Concentrations Obtained from Immersion Tests on SNF 6-22
6-6b. Distribution of Plutonium Colloid Concentration Values (mL/g) and Cumulative Probabilities Used for SNF Colloids in TSPA-LA Calculations 6-23
6-7. Concentration of Released Uranium from Unsaturated Drip Tests 6-31
6-8. Uncertainty Distribution for Stable Uranophane Colloids from Corroded CSNF and DSNF 6-31
6-9. Developed Sorption Coefficient Distributions for Radionuclide Sorption onto U(VI) Colloidal Phases 6-33
6-10. Radionuclide Concentrations Associated with Colloids from Immersion Tests at 25°C on SNF 6-38
6-11. Uncertainty Distribution for Stable Colloids from Corroded Stainless Steel Waste Package Colloid 6-47
6-12a. Critical Coagulation Concentration Values 6-48
6-12b. Concentrations of Counter-ions in Input Water Compositions 6-48
6-13. Uncertainty Distribution for Groundwater Colloid Concentrations for the TSPA-LA Analyses Based on Ionic Strength (I) of the Water Sample 6-53
6-14. Experimentally Determined K_d Values for Plutonium and Americium Sorption onto Hematite and Montmorillonite 6-57
6-15. K_d Values (mL/g) and Cumulative Probabilities Used for Reversible Sorption of U, Np, Sn, and Ra on Iron Oxide and Smectite Type Colloids in TSPA-LA Calculations 6-63
6-16. Cesium Sorption Coefficients on Yucca Mountain Tuffs 6-64
6-17. Selected Published Values for Specific Surface Area (S_A) for Iron Phases 6-66
6-18. Time-Dependent FeO_x Colloid Sorption Fraction for Plutonium and Rate Constant Calculation 6-68
6-19. Alternative Conceptual Models Considered 6-74
6-20. Plutonium Sorption Coefficients Developed from Kinetic Sorption Model 6-76
6-21. Ranges and Bounds for Constants, *a* and *b*, in Equation 6-24 6-78
6-22. Parameters Used in Description of Alternative Model 6-79
6-23. Conditions from Experiments by Zarrabi et al. (2003 [DIRS 171238]) and Predicted Outcome Based on DLVO Model 6-107
6-24. Parameters Used in Model 6-115
7-1. Supporting (Corroborating) Information Used to Validate the Colloid Model and/or Provide Additional Confidence in Parameter Values and Analyses Results 7-7

TABLES (Continued)

Page

7-2. pH_{pzc} of Iron Oxides 7-11
7-3. Actinide Levels in Borosilicate Glasses Used for Testing 7-14
7-4. Colloid Data on Rare Earths and Actinides from Locations in the Cretaceous Idaho Batholith 7-18
7-5. Cesium Sorption with 95% Lower- and Upper-Confidence Bounds (mL/g) 7-24
7-6. Summary of Sorption Data Developed by National Cooperative for the Disposal of Radioactive Waste for Bentonite, Crystalline Rock, and Marl 7-26
7-7. Summary of Sorption Data Developed by U.S. Environmental Protection Agency 7-27
7-8. Modeled K_d Values for Plutonium, Americium, Thorium, Neptunium, and Uranium Sorption onto Yucca Mountain-Vicinity Colloids 7-28
7-9. Rate of Plutonium Uptake on Iron Oxide Phases 7-28
8-1. Summary of Model Output Parameters 8-2
I-1. Groundwater Samples Used to Develop Cumulative Distribution Function Developed to Establish Colloid Concentration Sampling Frequency in GoldSim Calculations for TSPA-LA for Solutions with Stable Colloids I-2
I-2. Example Calculation for Total Colloid Mass in Well NC-EWDP-01s, Depth 170 ..... I-4
II-1a. Data Qualified for Direct Input Using SCI-PRO-006, Section 6.2.1(K) II-1
II-1b. Data Qualified for Direct Input Using SCI-PRO-001 ..... II-3

ACRONYMS AND ABBREVIATIONS

ACM	alternative conceptual model
A_H	Hamaker constant
ANL	Argonne National Laboratory
ATM	Approved Testing Material
BET	Brunauer-Emmett-Teller (method for surface area determination)
CCC	critical coagulation concentration
CDF	cumulative distribution function
CR	condition report
CSNF	commercial spent nuclear fuel
DHLWG	defense high-level waste glass (sometimes referred to as DOE-owned high-level waste glass)
DIW	de-ionized water
DLVO	Derjaguin, Landau, Verwey, and Overbeek (colloidal interaction theory)
DOE	U.S. Department of Energy
DSNF	defense spent nuclear fuel (sometimes referred to as DOE-owned spent nuclear fuel)
DTN	data tracking number
ε_0	free-space permittivity
EBS	Engineered Barrier System
ε_r	dielectric constant of water
FeO_x	iron oxide hydroxide corrosion products
FEPs	features, events, and processes
HLW	high-level (radioactive) waste
$I_{Threshold}$	ionic strength above which colloid are considered unstable
JNC	Japan Nuclear Cycle Development Institute
k_B	Boltzmann constant (1.38066×10^{-23} J K^{-1})
K_c	ratio of colloidal radionuclide concentration to dissolved radionuclide concentration
K_d	distribution coefficient (mL/g) (sometimes also referred to as sorption coefficient)
k_f	diffusion constant
k_{smol}	Smoluchowski theoretical value for fast coagulation (6.16×10^{-18} $m^3 s^{-1}$)
LANL	Los Alamos National Laboratory
MOX	mixed oxide (fuel)

ACRONYMS AND ABBREVIATIONS (Continued)

NAGRA	National Cooperative for the Disposal of Radioactive Waste
NFE	Near-Field Environment
NTS	Nevada Test Site
PNNL	Pacific Northwest National Laboratory
pzc	point of zero charge
QA	quality assurance
r_D	Debye length
S_A	surface area (m^2)
SEM	scanning electron microscopy
SNF	spent nuclear fuel
SRL	Savannah River Laboratories (as in experimental testing glass formulations SRL-131, -202)
SZ	saturated zone
T	temperature
TEM	transmission electron microscopy
TSPA	total system performance assessment
TSPA-LA	total system performance assessment for the license application
TWP	technical work plan
$U_E(h)$	electrostatic repulsion energy term
$U_T(h)$	total interaction energy term (where h = is the particle–particle separation distance)
$U_v(h)$	van der Waals attractive energy term
UZ	unsaturated zone
VA	validation activity
W	stability ratio
WHC	Westinghouse Hanford Company
W_T	stability ratio (total energy)
W_V	stability ratio (van der Waals)
YMP	Yucca Mountain Project
YMRP	*Yucca Mountain Review Plan, Final Report*
ζ_{eff}	effective surface potential (see also "zeta potential" in the Definitions)

MINERAL NAMES AND FORMULAE

Akaganéite	β-FeOOH
Boltwoodite	$K(H_3O)[(UO_2)(SiO_4)]•0.5H_2O$
Cejkaite	$Na_4(UO_2)(CO_3)_3$
Ferrihydrite	$Fe_5O_3(OH)_9$ (more commonly written as FeOOH)
Goethite	α-FeOOH
Hematite	Fe_2O_3
Lepidocrocite	γ-FeOOH
Meta-autunite	$Ca(UO_2)_2(PO_4)_2•6\text{-}8H_2O$
Meta-schoepite	$[(UO_2)_4O(OH)_6](H_2O)_5$
Meta-studtite	$UO_4•2H_2O$
Meta-torbernite	$\{Cu[(UO_2)(PO_4)]_2(H_2O)_8\}$
Monazite	$(Ce,La, Nd, Th, Y)PO_4$
Montmorillonite	$(Na,Ca)_{0.3}(Al,Mg)_2Si_4O_{10}(OH)_2•n(H_2O)$
Rhabdophane	$(Ce,La)PO_2•(H_2O)$
Saléeite	$\{Mg[(UO_2)(PO_4)]_2(H_2O)_{10}\}$
Smectite	Represents a group of minerals including montmorillonite, nontronite, and saponite, as well as other minerals (see Definitions below).
Schoepite	$[(UO_2)_8O_2(OH)_{12}](H_2O)_{12}$
Uraninite	UO_2
Uranophane	$Ca(UO_2)_2(SiO_3OH)_2(H_2O)_5$

UNITS

a	years
°C	degrees centigrade
g	gram
J	Joules
L	liter
µg	microgram
µm	micrometer
M	molarity, mole/liter
m	meter

Ma	Million years
mg	milligram
mL	milliliter
nm	nanometer

DEFINITIONS

Aggregation	In this report, colloid aggregation occurs when the stability ratio (W) is 10. The colloid double layer collapses, rapid flocculation occurs, and colloids are removed from solution.
Colloid	A finely divided dispersion of one material in a second continuous phase. With respect to this model report, the second continuous phase is water. Colloidal particles are generally between individual molecules and macroscopic objects. A useful limit is that a colloid is <1 μm in at least one dimension.
Debye length (nm)	The Debye length (r_D) is defined in Equation 6-2 in this report and represents the distance over which charge separation (where repulsive forces will operate) can occur and is proportional to the ionic strength.
Distribution coefficient (mL/g)	The distribution coefficient, K_d, is the ratio of sorbed constituent concentration (mol/mL) to dissolved constituent concentration (mol/g). The K_d approach tends to include multiple thermodynamic and kinetic processes and is best thought of as a "snap-shot" of partitioning between the aqueous and surface-bound state. In a system where equilibrium has been clearly attained, K_d is sometimes referred to as a sorption coefficient. Where the system may not have attained equilibrium, the distribution coefficient is sometimes represented by the retention value, R_d (see Bradbury and Baeyens 2005 [DIRS 179538]).
DLVO theory	DLVO theory accounts for the interaction between charged colloidal particles. It is based on the sum of a van der Waals attractive potential and a screened electrostatic potential arising from the "double layer" potential screened by ions in solution. The name DLVO comes from the two groups who separately developed this model: Derjaguin and Landau, and Verwey and Overbeek. The application of the theory is discussed in Section 6.3.2.
Double layer interactions	Ionized particles in aqueous solution interact with each other by electrostatic forces. The simple charged interactions are moderated by two effects: first, counter-ions will tend to associate at least loosely with opposite charges; second, the bulk concentration of ions in solution screens those electrostatic forces. These forces can be calculated by solving the Poisson-Boltzmann equation to determine the distribution of charged species given a thermal distribution of energies.

Flocculation	The process of particle–particle aggregation leading to the formation of larger colloid flocs that may still be stable in solution (see studies on montmorillonite by Tombacz et al. 2004 [DIRS 174073]).
Hamaker constant (Joules)	The constant in the van der Waals (vdW) force equation is termed the Hamaker constant. It is a material property (units in Joules) and its magnitude reflects the strength of the vdW attractive force arising from that material. The Hamaker constant is difficult to determine experimentally, although it can be approximated from the decrease in particle concentrations under conditions when $W = 1$, as particle aggregation will be driven only by VdW forces.
Hydrophobic	In this model report, a hydrophobic colloid is one that repels contact with water or an aqueous phase.
Langmuir isotherm	In this model the Langmuir isotherm relates the adsorption of radionuclides on a colloid surface to the concentration of the radionuclide in solution at a fixed temperature as follows: $\theta = \frac{\alpha P}{1 + \alpha P}$, where θ is the percentage coverage on the colloid surface, P is the solution radionuclide concentration, and α is the Langmuir absorption constant.
Pendular ring discontinuity	When the water content in a rock is low, as in unsaturated environments, the water is trapped in rings around the contact points of the rock or mineral grains, called pendular rings. Colloid immobilization will depend on the probability of pendular discontinuity and also on the ratio of the colloid size to the film thickness. Pendular discontinuity increases as the moisture content decreases. The particles are trapped at the air–water interface film unless the film thickness increases because of increasing moisture content.
Primary colloid	Term first adopted by Bates et al. (1992 [DIRS 100704]) to describe the generation of colloids directly from surface waste form alteration. For instance, release of colloids from waste forms that were initially altered under vapor conditions before being in contact with liquid water. This process of primary colloid generation may lead to the "embedding" of Pu, Am, and Th in waste form colloids.
Smectite clay	This mineral group includes montmorillonite $(Na,Ca)_{0.3}(Al,Mg)_2Si_4O_{10}(OH)_2 \bullet n(H_2O)$, nontronite $Na_{0.3},Fe_2(Si,Al)_4O_{10}(OH)_2 \bullet n(H_2O)$, and beidellite $(Na,Ca_{0.5})_{0.3}Al_2(Si,Al)_4O_{10}(OH)_2 \bullet n(H_2O)$. Poorly crystalline iron-rich smectite clays have been identified as the initial corrosion products from the majority of DHLWG laboratory PCT-B and unsaturated drip tests conducted (Feng et al. 1994 [DIRS 101611]; Buck and Bates 1999 [DIRS 109494]; Fortner et al. 1997 [DIRS 114452]).

Stability	In this report, stability refers to the property of a particle suspension in which the particles have no tendency to aggregate. The key to understanding colloid stability is the pair-potential (total potential energy of interaction). In this report, expressions for describing the distance-dependent potential energy of intereaction of two particles are used to address colloid stability.
Stability ratio (dimensionless)	The colloid stability can be expressed through the stability ratio, W, which is the ratio between the rate constants of rapid (van der Waals dominated attraction) and slow coagulation. Stability ratios can be calculated from DLVO theory or estimated experimentally based on the decrease in particle concentrations with time.
Zeta potential (mV)	The zeta (ζ) potential of a colloidal particle is the interaction potential observed by hydrodynamic measurements such as electrophoresis. Note that the *surface potential* is the actual potential at the particle surface, which is generally derived based on measurements of the *effective surface potential*. The effective surface potential occurs within the double layer that is on the particle surface, and includes the effects of shielding by ions in solution. The zeta potential is an effective surface potential that exists in the double layer at the boundary between the stationary portion and the mobile portion of the double layer. The force on an electric charge in an electric field is balanced by the viscous drag such that the particle moves at a constant velocity. The potential measured in this way can differ from those seen in static measurements or the titration of charge as it will depend on details of viscous drag (the hydrodynamic radius) and the screening of charge by ions in the solution. When the zeta potential is reduced to zero, repulsion among/between particles will be eliminated and flocculation will occur.

1. PURPOSE

The purpose of this report is to present and describe the abstraction of the colloids process model for the waste form and Engineered Barrier System (EBS) components of the total system performance assessment (TSPA). The model describes the types and concentrations of colloids that could be: (1) generated in the waste package from degradation of the waste forms and the corrosion of the waste package materials, (2) produced from the steel components of the repository and their potential role in radionuclide transport, and (3) present in natural waters in the vicinity of Yucca Mountain. In addition, sorption and desorption characteristics and mechanisms of colloids anticipated in the repository are addressed and discussed.

The abstraction of the process model simplifies radionuclide–colloid behavior and radionuclide sorption by assuming that all colloids in the waste package are either smectite clay $\{(Na,Ca)_{0.3}(Al,Fe)_{2-3}(Si,Al)_4O_{10}(OH)_2 \cdot nH_2O\}$, a mixed actinide-bearing rare earth-zirconium oxide, iron oxyhydroxide, or uranophane $\{Ca(UO_2)_2(SiO_3OH)_2(H_2O)_5\}$, where the modeled colloids are montmorillonite $\{(Na,Ca)_{0.3}(Al,Mg)_2Si_4O_{10}(OH)_2•n(H_2O)\}$, ZrO_2, hematite $\{Fe_2O_3\}$, and meta-autunite $\{Ca(UO_2)_2(PO_4)_2•6\text{-}8H_2O\}$, respectively. The rationale for the selection of the modeled colloids is discussed in Assumptions 5.5, 5.6, and 5.7. The model uses theoretical calculations and laboratory data to determine the stability of modeled colloids with ionic strength and pH. The true nature of colloid composition and heterogeneity, generation, and flocculation in the waste package will be complex, involving the formation of numerous types of phases, often depending on the composition of the various waste forms and waste package materials. Traexler et al. (2004 [DIRS 172072]) have listed potential colloidal products from waste glass and spent fuel degradation, but there is insufficient data to model all types of particles. This method for modeling the waste package and in-drift colloid system is anticipated to bound the potential impact of colloid-facilitated radionuclide transport on repository performance.

In addition, this revision (Revision 03) of this report addresses the following condition reports (CRs):

- CR-7291 was written to describe a condition where Figure 6-7 in Revision 02 of this report plotted the colloid stability as a function of pH, for three different ionic strengths. Two of the curves were not plotted correctly for the change of the y-axis from logarithmic (log(W) in the source) to linear (W in the Revision 02 of this report). Hence, they were shifted about 1 pH unit below where they should have been. The text in Revision 02 of this report reflects the values in the source document accurately, and it is only the figure that is incorrect. Therefore, this error does not appear to have propagated into the colloid stability model, and is of low impact.

  Revision 03 of this report no longer uses the figure, so the Condition Adverse to Quality no longer exists, and the CR Action 7291-001 to perform an Administrative Change Notice on the report with a corrected figure has been overcome by events (Revision 03) and can be processed to closure when this revision is approved.

- CR-8555 identified a condition where input-output files had been described in the report but not submitted to the Model Warehouse Data. For Revision 03, all output is included within the various output data tracking numbers (DTNs), and no input/output

files were generated with EQ3/6 (or other geochemical code package) for this revision of the report. This condition has been evaluated for Revision 03 and found to not be applicable. Therefore, Corrective Action 8555-003 is addressed by this revision, so far as to determine that the extent of the condition does not apply.

1.1 OVERVIEW

The colloid model abstraction is used in total system performance assessment for the license application (TSPA-LA) to estimate the stability and concentration of colloid suspensions, as well as concentrations of radionuclides associated with the colloids, based on in-package and in-drift fluid chemistry and in-package dissolved radionuclide concentrations. As such, the colloid parameters are estimated based on fluid chemistry only (i.e., regardless of fluid quantity and spatial distribution). Feeds for in-package ionic strength and pH are received from *In-Package Chemistry Abstraction* (SNL 2007 [DIRS 180506]) and feeds for in-drift ionic strength and pH are received from *Engineered Barrier System: Physical and Chemical Environment* (SNL 2007 [DIRS 177412]). Feeds for dissolved radionuclide concentrations are developed in *Dissolved Concentrations of Radioactive Elements* (SNL 2007 [DIRS 177418]).

Colloid properties have been modeled with the Derjaguin, Landau, Verwey, and Overbeek (DLVO) theory. This model is bounding because it does not account for filtration and/or thin-film straining, two processes that tend to limit colloid concentrations in unsaturated environments.

1.2 BACKGROUND

For the purposes of this report, colloidal systems are defined as those in which the component phases are dispersed in an aqueous medium ranging in size from approximately 1 nm to 1 μm (Kim 1994 [DIRS 109521]). The effective experimental range for particle detection may be narrower depending on the analysis technique and is typically between 6 nm to 450 nm in diameter.

Knowledge on the weathering of alkali borosilicate waste glasses is well established from a broad range of national and international sources. With respect to data on colloids, at least 26 individual intermittent drip tests were conducted over several years on actinide-doped glasses generated at Savannah River Laboratories (SRL) (e.g., SRL-165A, SRL-200R), and at Approved Testing Material (ATM) (e.g., ATM-10; West Valley composition) (Bates et al. 1995 [DIRS 170880]). One hundred immersion tests have been conducted on actinide-doped borosilicate glasses (e.g., SRL-131A, SRL-202A, and SRL-200R) (Bates et al. 1995 [DIRS 170880]; DTN: LL000123351021.117 [DIRS 143308]). Immersion corrosion tests on SRL-131A and SRL-202A glasses (DTNs: MO0705ANLGSV01.258 [DIRS 181399]; LL991109751021.094 [DIRS 142910] (MOL.20000124.0207, pp. 27 and 32); LL000905312241.018 [DIRS 152621] (MOL.20001130.0021, pp. 29, 30, and 70)) have been used as direct input in the model. The nature of these waste glass corrosion tests prevents pH or ionic strength control (i.e., the dissolution of the waste form affects both the pH and ionic strength of the leachate). Waste glass corrosion tests were performed at 90°C. Newer production waste glasses tend to be more corrosion-resistant and will be likely to produce lower concentrations of colloids than the glasses used in the development of this model abstraction

(i.e., SRL-131A, SRL-200R, SRL-202A, and ATM-10). Colloid data on spent nuclear fuel (SNF) has been provided by Wilson (1990 [DIRS 100793]) and McNamara et al. (2005 [DIRS 174068]). Wilson (1990 [DIRS 100793]) ran a number of immersion tests on bare fragments of spent nuclear fuel and spent nuclear fuel fragments with partial cladding at 25°C and 85°C. McNamara et al. (2005 [DIRS 174068]) reported analyses of suspended colloidal particles from spent nuclear fuel corrosion tests run at 25°C. Data from these sources have been used as direct input to this model to obtain radionuclide associated colloid concentrations from defense high-level waste glass (DHLWG), commercial spent nuclear fuel (CSNF), and defense spent nuclear fuel (DSNF).

The model for DHLWG colloids has been validated (see Section 7.1.2) through the use of glass corrosion data from Ménard et al. (1998 [DIRS 171053], Luckscheiter and Nesovic (2002 [DIRS 170884]), and Pirlet (2001 [DIRS 174351]). The model for CSNF colloids has been validated using the four intermittent long-term drip tests conducted on SNF fragments at 90°C (Finn et al. 1994 [DIRS 100746]; Mertz et al. 2003 [DIRS 162032]), spent fuel studies presented by Grambow et al. (1996 [DIRS 113253]), natural analogue studies (van Middlesworth and Wood 1997 [DIRS 170927]; Murakami et al. 1997 [DIRS 113272]), tests on uranium oxide (UO_2) ceramic pellets (Wronkiewicz et al. 1996 [DIRS 102047]), and tests on uranium metal fuels (Mertz et al. 2000 [DIRS 162161]; Kaminski et al. 2005 [DIRS 179550]).

Traexler et al. (2004 [DIRS 172072]) and Zhao and Steward (1997 [DIRS 170892]) extensively reviewed colloid formation from nuclear waste forms and concluded that all waste forms, including DHLWG, CSNF, and DSNF, will generate colloids during weathering. The model described in this report focuses first on the factors that lead to the formation of colloids from waste form degradation and secondly on their subsequent stability within the waste package and the surrounding EBS environment. Other analyses and models developed for TSPA-LA address the processes and mechanisms responsible for the stability and transport or retardation of radionuclides associated with colloids released from the EBS to the underlying unsaturated zone (UZ) and saturated zone (SZ) environments.

The colloid source term is defined here as the total of those radionuclides associated in some manner with colloids that: (1) are mobilized at the surface of the waste form, (2) are transported within the waste package to the waste package wall, (3) leave the waste package at a breach or breaches in the waste package wall, and (4) enter the drift.

The model describing colloid formation through waste form degradation and the subsequent stability of colloidal suspensions within the drift is valid over the range of chemical and hydrological conditions anticipated within the waste package and drift during the postclosure regulatory assessment period. Discussion on the valid range of application for the various process models is included in Section 7.

1.3 DOCUMENT DEVELOPMENT

This report revision was developed in accordance with *Technical Work Plan for Waste Form Testing and Modeling* (BSC 2006 [DIRS 177389]). Section 7 contains a deviation from the post-development validation activities listed in the technical work plan (TWP) (BSC 2006 [DIRS 177389], Table 2-3).

1.4 MODEL REPORT OVERVIEW

Section 2 lists the procedures, technical work plan, and requirements under which this report was prepared. Section 3 discusses the software used to perform the analyses described in this report.

Section 4 describes the development of inputs for the colloid model abstraction and lists the information used in Table 4-1 (direct input, qualified data) and Table 4-2 (other input, including corroborative unqualified data). Acceptance criteria from *Yucca Mountain Review Plan, Final Report* (YMRP) (NRC 2003 [DIRS 163274]) and the codes and standards that apply to this report are outlined in Sections 4.2, 4.3, and Table 4-3.

Section 5 presents the assumptions used in the colloid abstraction with their rationale, confirmation status, and the report sections in which the assumptions are used. In those cases where data are inadequate to support a particular concept or model technique, a bounding assumption is used.

Section 6 presents conceptual models and background information on colloid formation and behavior (including potential stability and their potential role in radionuclide transport).

- Section 6.1 presents a description of the model and its objectives.
- Section 6.2 addresses pertinent features, events, and processes (FEPs) evaluated for their significance to this analysis.
- Section 6.3 presents the base-case colloid model elements in several subsections. The processes occurring within the waste package and within the drift are detailed and summarized in this section (e.g., see Section 6.3.1 for more detail). The background information and rationale are provided for the approaches used, as well as for elements considered but not incorporated into the model. Key subsections include Section 6.3.2, which discusses the DLVO theory for predicting colloid stability and describes the four colloid types modeled, and Section 6.3.12, which covers radionuclide sorption.
- Section 6.4 describes alternative models that were considered during the development of the colloid model and the rationale for not adopting them.
- Section 6.5 presents the abstraction of the colloid model elements and the methodology and logic for implementing the abstraction in the TSPA-LA model calculations. The section begins with a summary description of the abstraction and a schematic overview. Section 6.5.1 presents the in-package abstraction in some detail, with figures; Section 6.5.2 similarly provides the in-drift abstraction. Section 6.5.3 presents an overview of the disposition of colloids and associated radionuclides "downstream" from the EBS in the UZ and the SZ.

- Section 6.6 discusses uncertainty in the model analysis.
- Sections 6.7 and 6.8 present the analyses of the barrier capability and an evaluation of the alternative models.

Section 7 validates the colloids model. It also describes the waste form, corrosion products, and groundwater colloid parameters (used as surrogates for seepage water colloids in this analysis); radionuclide sorption characteristics; model uncertainty; and processes not incorporated into the model abstraction.

Section 8 provides a summary of the analysis, describes the developed output parameters and uncertainties, and presents conclusions drawn from the model results.

Section 9 lists references cited, standards, regulations, and procedures, source data, output data, and software codes.

There are four appendices. The first describes data for determination of natural abundances of colloids, the second describes the qualification of unqualified data for use as direct input in the model, the third lists required qualification plans, and the fourth presents a critical review of the model.

INTENTIONALLY LEFT BLANK

2. QUALITY ASSURANCE

Development of this report and the supporting analyses have been determined in the TWP (BSC 2006 [DIRS 177389], Section 8) to be subject to the Yucca Mountain Project's quality assurance (QA) program. *Quality Assurance Requirements and Description* (DOE 2007 [DIRS 182051]) applies to the development of this report. Approved quality assurance procedures identified in the TWP (BSC 2006 [DIRS 177389], Section 4) have been used to conduct and document the activities described in this report. The TWP (BSC 2006 [DIRS 177389], Section 8) also identifies the methods used to control the electronic management of data , and there were no deviations from these methods.

This report contributes to the analysis and modeling data used to support performance assessment by developing and providing source terms for waste form colloids, corrosion product colloids, and natural groundwater colloids for the TSPA-LA model; the conclusions do not directly impact engineered features or engineered and natural barriers important to waste isolation, as discussed in *Q-List* (BSC 2005 [DIRS 175539]).

INTENTIONALLY LEFT BLANK

3. USE OF SOFTWARE

Reference is made in this report to parameters used in calculations by the TSPA-LA model. The parameters are provided for use by the TSPA-LA model, but no TSPA model calculations were performed for this report. The qualified version of GoldSim (Goldsim V. 9.60.100 [DIRS 181903], STN: 10344-9.60-01) was used to calculate the convolution of two probability distributions as discussed below. The logic presented in this report is intended for implementation in the TSPA-LA model, but no computer runs of the colloid models within GoldSim were executed for this report.

The calculations performed in this analysis used commercial, off-the-shelf software (Microsoft Excel 2003 (11.8117.8107) SP-2) on a personal computer running Windows XP Service Pack 2. This use of Microsoft Excel is exempt in accordance with Section 2 of IM-PRO-003 (last bullet) and its use is considered appropriate because it provides: (a) the ability to derive final calculation results using simple mathematical expressions, and (b) built-in graphical charting capabilities. Workbooks containing colloid stability, radionuclide sorption, and colloid concentration calculations were created and have been submitted to the Technical Data Management System. These workbooks comprise the intermediate Output DTNs: MO0705CSIONSTH.000 (colloid stability), MO0705DSCSCUSS.000 (radionuclide sorption), and MO0705COLCONCS.000 (colloid concentration).

Stability calculations are detailed in Excel workbooks in Output DTN: MO0705CSIONSTH.000 and described in Section 6.3.2. The input value is pH, and the surface charge is calculated by a fit to literature data describing the surface charge with pH. Using the "Solver" function in Excel, and fixing *W* at 10, the corresponding ionic strength threshold value can be determined.

Output DTN: MO0705DSCSCUSS.000 includes Excel workbooks that describe the development of K_d values for smectite and uranophane colloids, as well as GoldSim output files (*.gsm) that contain the convolution results for the distributions of these K_d values with the colloid concentrations to evaluate the corresponding K_c parameter values that are used within the natural system transport models.

Output DTN: MO0705COLCONCS.000 includes an Excel workbook that describes the development of colloid concentrations from corroded carbon steel. The workbook also contains validation information on the generation of colloids from stainless steel.

INTENTIONALLY LEFT BLANK

4. INPUTS

Technical product inputs and sources used as direct inputs to develop the model are listed in Table 4-1. Corroborating and supporting data and information used as indirect inputs in the analysis and used to validate the model are listed in Table 4-2 following the procedures described in SCI-PRO-006, *Models*.

4.1 DIRECT INPUT

Direct technical inputs, listed in Table 4-1, address the types of colloids formed from waste form degradation, steel corrosion degradation products, and natural seepage water colloids that might potentially come in contact with waste forms and the surrounding EBS. Four primary particles were selected to represent the major colloid types in the waste package and in-drift environment: (1) smectite clay, (2) iron oxyhydroxide, (3) Pu-Zr oxide particles, and (4) uranophane. The selection of these phases was based on the evaluation of the likely long-term alteration of the waste forms and waste package materials and the secondary phases most capable of forming viable colloids. However, specific physical data on these particular particles is lacking. For model implementation of the DLVO-based stability model, the required data included the relationship between zeta potential and pH and the Hamaker constants.

A summary of the model representation of the four primary particles follows:

- In the case of the clay minerals formed from the corrosion of DHLWG and/or silicate tuff rock, **montmorillonite** was considered a reasonable choice for modeling. For seepage water (groundwater) colloids, which consist of many types of particles including zeolites, iron oxides, silica, and smectite clays, the model colloid is also montmorillonite. This phase has the highest specific surface area and will be the dominant radionuclide-bearing colloid under groundwater conditions. Montmorillonite is a compositionally well-defined mineral, whereas the smectites that form during glass corrosion are poorly crystallized and may possess variable compositions. This compositional variability might lead to different electrical surface properties and possible decrease in colloid stability. Hence, application of a bounding stability criterion in the model effectively bounds the uncertainty.

- Several phases are known to form during the corrosion of steels, including ferrihydrite, which may in turn undergo alteration to hematite or goethite over time depending on temperature and Eh conditions. For instance, hydrothermal corrosion tests on Stainless Steel Type 316 reported by Dietz (2005 [DIRS 179542]) did not result in ferrihydrite formation as this phase is unstable under high temperature conditions and will transform to hematite. Hence, **hematite** was considered to be a representative phase for waste package-derived colloids resulting from carbon steel and stainless steel weathering. Although ferrihydrite (HFO) and goethite are used in the competitive surface complexation model for radionuclide sorption onto waste package materials, the sorption and colloid stability properties for these various Fe(III)-polymorphs is similar.

- A phase that forms on the surface of corroded CSNF has been demonstrated to consist of Pu, Zr, and rare earths oxides (Buck et al. 2004 [DIRS 172668], pp. 77 to 79). This

phase could be modeled as either plutonium oxide, a rare earth oxide, or zirconium oxide. Many of the metal oxides have similar points of zero charge (pzc) near pH 8 (Parks 1965 [DIRS 174361]); however, the magnitude of the surface charge may be different resulting in different stabilities. The **zirconium oxide** colloid was selected because of the available data that could be developed into an effective model and because the pzc was at a relatively high pH, the modeled colloid would provide a conservative range for stability.

- Meta-autunite is a layered uranyl phosphate, whereas uranophane is a uranyl silicate with a slightly different layered configuration. These structural and compositional differences may result in uncertain changes in the surface electrical characteristics. Data from a mixed schoepite/UO_{2+x} system reported by Mertz et al. (2003 [DIRS 162032]) indicated a pzc near pH 2 and a high negative surface charge at all pH values above 4. This is similar to the data reported on meta-autunite (Zheng et al. 2006 [DIRS 179565]). These results suggest that the layered uranyl phases may share similar surface charge properties despite the compositional differences. Hence, the use of **meta-autunite** as a substitute for uranophane is appropriate for model implementation.

Also included in the input tables are sources of data used for the development of sorption partition coefficients (K_d values), which are used to model radionuclide sorption to colloids:

- "Sorption" as used here is a general term that has been used throughout the literature to include interactions between dissolved ions and mineral surfaces governed by processes such as: (1) electrostatic forces, (2) ion exchange, (3) surface reaction, and (4) coprecipitation. Although the term is used here similarly, it is used primarily to denote processes that involve surface interactions between the ions and minerals that do not dramatically alter the nature of the dissolved species (e.g., do not change its oxidation state). Note that where the reaction mechanism is not being even loosely specified, the term "attachment" is used to be purposely general. Sorption may occur by a number of mechanisms and all of these may be considered (1) reversible (i.e., attachment to the surface and detachment from the surface occur *instantaneously* at an established dynamic equilibrium value represented by the equilibrium sorption coefficient—K_d), (2) irreversible (i.e., the attachment rate or detachment rate is kinetically slow such that the apparent distribution coefficient is not the equilibrium value), or (3) appear to be effectively completely irreversible (i.e., desorption is so slow that the detachment does not even matter relative to the time frame of transport). This last case is only an effective property because even very small rates may effectively detach material if the time frame of interest is large enough (e.g., as is the case for stationary materials). The relative rates of sorption, desorption, and transport determine the approach to reversibility of the sorption. When sorption reactions are fast (i.e., reversible), equilibrium conditions apply and the linear isotherm model is applicable for describing radionuclide uptake and release. Even in cases of slightly irreversible sorption processes, such an equilibrium approach is a reasonable approximation if the transport rates are slow in comparison. When sorption is highly irreversible (i.e., desorption is slow relative to transport times), then local equilibrium models are less accurate, resulting in over- or under-predictions of transport, and kinetic (i.e., rate-based) models

can facilitate evaluation. In this report, K_d values that may not have been obtained under equilibrium conditions are reported as retention values (R_d values) (see "Distribution Coefficients" in the Definitions).

The selection of modeled colloids was based on relevance to the actual system, available data for sorption, and colloid properties. These parameter groups are described in the next section, and the parameters are listed and described in Table 4-1. The parameters listed in Table 4-1 are based technically on findings from applicable analytical, laboratory, and field research, including investigations specific to the Yucca Mountain region and the Yucca Mountain Project (YMP). More detailed discussion on the technical bases for the development of these parameters may be found in Sections 5 and 6. Data used to develop the model were not used to validate the model.

Uncertainty associated with the model analysis, including development of parameter values and their implementation in the TSPA-LA model, is discussed in Sections 6.6.2 through 6.6.8. Many of the parameters are derived from data directly relevant to colloid formation, colloid suspension stability, and capacity to associate with radionuclides. Departure from anticipated repository conditions is addressed by acknowledging uncertainties in the parameters, bounding calculations, and by providing a means to incorporate these uncertainties into the TSPA calculations. These uncertainties are addressed by providing ranges, probability distributions, and bounding assumptions as appropriate for each given parameter or process.

Table 4-1. Direct Inputs for Colloid Models

DTN or Report	Data or Parameter Description
Waste Form Colloids and Associated Radionuclide Concentrations	
LL991109751021.094 [DIRS 142910] (MOL.20000124.0207, p.27)	Ionic strength of solutions associated with DHLWG colloids; silica concentrations associated with DHLWG colloids
LL000905312241.018 [DIRS 152621] (MOL.20001130.0021, pp. 29, 30)	Plutonium concentrations associated with DHLWG colloids; silica concentrations associated with DHLWG colloids
LL000905312241.018 [DIRS 152621] (MOL.20001130.0021, p.70)	Plutonium and americium association with clay particles; plutonium concentrations associated with DHLWG colloids
LL991109751021.094 [DIRS 142910] (MOL.20000124.0207, p.32)	Colloid concentration associated with measured colloidal plutonium concentration
MO0705ANLGSV01.258 [DIRS 181399]	Ionic strength of solutions associated with DHLWG colloids; plutonium concentrations associated with DHLWG colloids
Wilson 1990 [DIRS 100793], Tables A.2 through A.7 for $^{239/240}$Pu (pp. A9/A10 to A19/A20) (data converted from activities to concentrations)	Plutonium and americium concentrations associated with colloids from spent nuclear fuel; description of uranium particles released
Liu et al. 1992 [DIRS 172864], Figure 2-4	Fraction of particles under 1 µm following oxidation of UO_2
Corrosion-Generated (Iron Oxyhydroxide) Colloids	
Zarrabi et al. 2003 [DIRS 171238], Excel spreadsheet and Table 6, p. 32	Concentration of iron oxyhydroxide colloids from the corrosion of waste packages
Lu et al. 2000 [DIRS 166315], Table 1, p. 9	Experimental concentration of iron oxyhydroxide colloids [mass of waste package corrosion product colloid/water volume]
Lu et al. 2000 [DIRS 166315], Table 1, p. 10	Experimental value of specific surface area of iron oxyhydroxide colloid

Table 4-1. Direct Inputs for Colloid Models (Continued)

DTN or Report	Data or Parameter Description
Groundwater Colloids	
Lide et al. 1995 [DIRS 101876], pp. 4-132 through 4-138	Particle density values for silicate (montmorillonite and quartz) (iron oxide minerals were not included in the analysis) – used to estimate general particle density value for groundwater colloids.
Groundwater Colloid Concentrations LA0002SK831352.001 [DIRS 149232]; LA0002SK831352.002 [DIRS 149194]; LA9910SK831341.005 [DIRS 144991]; LA0211SK831352.002 [DIRS 161581]; LA0211SK831352.004 [DIRS 161458]; LA0211SK831352.001 [DIRS 161580]; LA0211SK831352.003 [DIRS 161582]	Colloid particle size distributions and concentration values for groundwater samples in the Yucca Mountain vicinity
DLVO Stability Model Development	
Zheng et al. 2006 [DIRS 179565], p. 53, Figure 7b; p. 53, Section 3.2.4, line 4	Variation in zeta potential with pH for meta-autunite; Hamaker constant, A_H, and plate thickness (δ) for meta-autunite
Bitea et al. 2003 [DIRS 174504], p. 59, Figure 3	Variation in surface potential with pH of ZrO_2 (Hamaker constant for ZrO_2 was derived from stability data)
Gunnarsson et al. 2001 [DIRS 179547], Figure 7, p. 456; p. 454, Section 3.3, line 14	Variation of zeta potential with pH and ionic strength for hematite; Hamaker constant for hematite
Tombácz et al. 1990 [DIRS 112690], Figure 3, p. 77 ; Figure 4, p. 78, legend (Hamaker constant (A) reported in Joules; plate thickness (δ) taken from p. 79, half the d_{001} spacing)	Variation in surface potential with pH and ionic strength for montmorillonite; Hamaker constant, A_H, and plate thickness (δ) for montmorillonite
Lide 1991 [DIRS 131202], back cover	Viscosity of water, Boltzmann's constant, Avogadro's number
Sorption Coefficients and Related Parameters	
Ilton et al. 2006 [DIRS 178810, p. 4837, Section 2.1, last line; p. 4839, Figure 1	Specific surface area for uranophane (boltwoodite)
Pabalan and Turner 1997 [DIRS 179555], Table II, p. 213	Specific surface area for montmorillonite
Pabalan and Turner 1997 [DIRS 179555], Table II, p. 213	Sorption site densities for montmorillonite
LA0003NL831352.002 [DIRS 148526]; LA0005NL831352.001 [DIRS 149623], LA0003NL831352.001 [DIRS 149172]	K_d values for plutonium and americium on hematite, goethite, and montmorillonite in J-13 groundwater; uptake with time, ionic strength, and temperature
LA0003AM831341.001 [DIRS 148751]; LA0407AM831341.002 [DIRS 170621]	K_d values for cesium on (a) clay (as part of the devitrified tuff mineral assemblage), and (b) other tuff rock types (vitric and zeolitic) and (c) iron oxide
Bradbury and Baeyens 2005 [DIRS 179538], Figure A4(c and d), p. 889; Figure A4b, p. 889; Figure A4a, p. 889	R_d values used for K_d values for Np and Sn on clay minerals; (data for Th and Pa included but used in model development)
Pabalan and Turner 1997 [DIRS 179555], Figure 4, p. 211	K_d values for U on clay minerals
Tachi et al. 2001 [DIRS 179561], Table 2 and 3, pp. 176 and 177	K_d values for Ra on clay minerals
Kim et al. 2006 [DIRS 179551]; p. 153, Table 2; p. 154, Table 3; p. 156, Table 4	Development of K_d values for Pu, Am, and Th on U(VI) minerals. Values were based on analog chemical behavior of rare earth elements for Pu, Am, and Th.

Table 4-1. Direct Inputs for Colloid Models (Continued)

DTN or Report	Data or Parameter Description
Sorption Coefficients and Related Parameters (continued)	
Burns 1999 [DIRS 110975]; p. 218, abstract demonstrating exchange of K^+ and Na^+ for Cs^+, Table 4, p. 222	Development of K_d values for Cs on U(VI) minerals (uranyl minerals). No specific K_d values were reported in the reference. Values were based on chemical behavior of Cs with uranyl minerals reported in the input report.
Douglas et al. 2005 [DIRS 173086], calculated from Table 1, p. 268	Development of K_d values for Np on U(VI) minerals
Douglas et al. 2002 [DIRS 179546], report of incorporation of Sr and Cs in uranophane in abstract, p. 504	Development of K_d values for Cs and Ra on U(VI) minerals. No specific K_d values were reported in the reference. Values were based on analogue chemical behavior of Sr for Ra.
McNamara et al. 2005 [DIRS 174068], Calculated based on values presented on p. 171 (Table 1) and p. 172 (Table 2)	Development of K_d values for Pu, Am, Np, Th, Cs, Ra on U(VI) minerals
LA0004NL831352.001 [DIRS 150272]	Fraction of Pu(V) and Pu(IV) sorbed to Fe_2O_3 and FeO(OH) colloids in J-13 well water and information for rates

Table 4-2. Summary of Corroborating/Supporting Information

Reference	Data or Parameter Description	Units	Selected Location(s) Used in Report
DHLWG Colloids and Associated Radionuclide Concentrations			
Ménard et al. 1998 [DIRS 171053], p. 105	Clay colloids with plutonium and thorium, description of alkali borosilicate glass weathering	N/A	Section 7.1.2, Table 7-3
Luckscheiter and Kienzler 2001 [DIRS 180831], Figure 2, p. 157	Association of americium and thorium on corroded waste glass	mL/g	Section 7.1.2
Advocat et al. 2001 [DIRS 163198], Tables 1 and 2, p. 56 Pirlet 2001 [DIRS174351], Figure 1, p. 48; Section 4, p. 51 Vernaz and Gordon 1992 [DIRS 174503], Table 3	Estimation of Pu content in R7T7 glass, evidence for strong retention of actinides in alteration layers	wt %	Section 7.1.2, Table 7-3, Figure 7-2
Bates et al. 1992 [DIRS 100704], Figure 1, p. 649; Table 1, p. 650	The nature of “embedded” actinide colloids associated with corroded glass	N/A	Section 7.1.2, Table 7-3
CSNF and DSNF Colloids and Associated Radionuclide Concentrations			
Grambow et al. 1996 [DIRS 113253], Section IV.3.2, p. 119; Figure IV.8, p. 123	Plutonium colloids from spent nuclear fuel, description of uranium particles released from CSNF; characteristics of U(VI) particles and PuO_2 particles	mol/L	Section 7.1.3
Kaminski et al. 2005 [DIRS 179550], Section 3.3, p. 82	Evidence for the formation of U(VI) colloidal phases from corroded N-reactor fuel	mol /L	Section 7.1.3
Mertz et al. 2000 [DIRS 162161], Figures 4 and 5	Images of U(VI) colloids	N/A	Output DTN: MO0705DSCSCUSS.000
Finn et al. 1994 [DIRS 100392], Table 1-4, pp. 191 and 192; Figure 2a, p. 193	Plutonium colloid concentrations from corroded CSNF; image of CSNF colloid	mol/L	Section 7.1.3
Wronkiewicz et al. 1996 [DIRS 102047], Table 1, p. 80; p. 86, 3rd paragraph; Figure 4, p. 86	Concentration of U(VI) colloids in a leachate during corrosion testing	mg/L	Section 7.1.3, Figure 6-15, Output DTN: MO0705DSCSCUSS.000
Wang et al. 2006 [DIRS 179563], Figure 3, p. 168; Buck et al. 2004 [DIRS 171479], Figure 5.4c, p. 5.5	Nature of nano-particles of rare earth oxides and colloid U(VI) phases	N/A	Section 7.1.3, Figure 7-3
Iwasaki et al. 1968 [DIRS 172518]; Spino et al. 1996 [DIRS 174080]	Size fraction of spent nuclear fuel particles in the high burn-up rim and the polygonization of fuel	N/A	Section 6.3.6.2

Table 4-2. Summary of Corroborating/Supporting Information (Continued)

Reference	Data or Parameter Description	Units	Selected Location(s) Used in Report
Corrosion-Generated (Iron Oxyhydroxide) Colloids			
Widerlund et al. 2004 [DIRS 180833]	Concentration of iron oxyhydroxide colloids observed in natural groundwaters	mg/L	Section 7.1.4, Table 7-1
Dietz, 2005 [DIRS 179542], Section 2.3, p. 22 ; Figure 14, p. 23; Ziemniak and Hanson 2001 [DIRS 179566]; Smailos et al. 2003 [DIRS 179559], Section 2.2.1, p. 11	Corrosion rind from stainless steel used to estimate the amount of colloids that might be released into solution	mg/L	Sections 6 and 7.1, Output DTN: MO0705COLCONCS.000
Ruckenstein and Huang 2003 [DIRS 179556], Figure 7, p. 3055	Quantification of re-stabilization effects at high ionic strength (i.e., >1 mol/kg)	mol/kg	Section 6.3.10
Groundwater Colloids			
DTN: LA0002SK831352.003 [DIRS 161771] DTN: LA0002SK831352.004 [DIRS 161579]	Colloid particle size distributions and concentration values for groundwater samples in the Yucca Mountain vicinity	nm (size); pt/mL (conc.)	Section 6.3.11 and Appendix I
Novikov et al. 2006 [DIRS 179554], Table 1, p. 639	Reported plutonium concentrations transported with pH; evidence for plutonium transport at analogue sites	mg/L	Section 7.1.4, Figure 7-4, Output DTN: MO0705CSIONSTH.000
Kersting and Reimus 2003 [DIRS 162421], Figure 1.1, p. 2	Particle types observed in groundwater at the Nevada Test Site	N/A	Section 6.3.1
DLVO Stability Model Development			
Honig et al. 1971 [DIRS 179548], p. 101, Equation 14; p. 98, Equation 6	Derivation of analytical expressions for *W*		Section 6.3.2
Mertz et al. 2003 [DIRS 162032], Figure 11, p. 41 ; Table A3-1, p. 53	Variation in surface potential with pH for UO_{2+x} and schoepite; particle counts with time for UO_{2+x}/schoepite colloids	mV conc/L	Section 7.1.1
Hsu et al. 1985 [DIRS 174350]	Variation in surface potential with pH for CeO_2	mV	Section 7.1.1
Liang and Morgan 1990 [DIRS 109524], Figure 1, p. 40; Madden et al. 2006 [DIRS 180995]	Experimental stability data for hematite. Variation in surface potential with pH for FeO_x		Section 7.1.1
Jara et al. 2005 [DIRS 180834], Figure 6, p. 166; Sondi et al. 1996 [DIRS 170928], Figure 6, p. 518; Figure 12, p. 521; Kraepiel et al. 1999 [DIRS 180997], Figure 6, p. 50	Variation in surface potential with pH for amorphous aluminosilicates and smectite; surface charge with pH for montmorillonite	mV	Section 7.1.1

Table 4-2. Summary of Corroborating/Supporting Information (Continued)

Reference	Data or Parameter Description	Units	Selected Location(s) Used in Report
Sorption Coefficients			
Bradbury and Baeyens 2006 [DIRS 179541], Figure 3, p. 622;	K_d values for Pa and Th on clay minerals	mL/g	Section 6.3.12.1
Beckman et al. 1988 [DIRS 144956]	Cesium sorption to silicates and zeolites	mL/g	Section 7.1.5
EPA 1999 [DIRS 147475], Vol. 2, Appendices D, G, I, and J; Honeyman and Ranville 2003 [DIRS 161657]; Stenhouse 1995 [DIRS 147477]; EPA 2004 [DIRS 172215]	K_d values for plutonium, americium, thorium, protactinium, neptunium, uranium, and cesium on rock, minerals, and colloids; modeling results for partitioning of radionuclides between colloids and stationary phases	mL/g	Section 7.1.5, Tables 7-6 and 7-7
Powell et al. 2004 [DIRS 180836], Table 2, p. 6020; Powell et al. 2005 [DIRS 174726], Table 1, p. 2110, Table 2, p. 2112	Sorption rate of Pu onto iron oxides	Rate/yr	Section 7.1.5, Figure 7-9, Table 7-9
Lu et al. 2000 [DIRS 166315]	Discussion of experimental conditions and observations for measurements of K_d for americium and plutonium on hematite, goethite, montmorillonite	N/A	Sections 6.3.12.1, 6.3.12.2, 6.4.1, and 6.6.8
Surface Areas and Site Densities			
Davis and Kent 1990 [DIRS 143280], Table 1, p. 182	Site density for a U(VI) phase	sites/nm^2	Section 7.1
Kraepiel et al. 1999 [DIRS 180997], Table 2, p. 48	Surface area of montmorillonite	m^2/g	Section 6.3.2.3
McKinley et al. 2006 [DIRS 179552], Figure 4, p. 1879, Figure 6, p. 1881	Nature of U(VI) phases at the Hanford site; estimated surface area of boltwoodite solids from TEM images	m^2/g	Section 7.1.3, Figure 7-3, Output DTN: MO0705COLCONNS.000
Murakami et al. 2005 [DIRS 175700], Figure 3, p. 121, Figure 4, p. 122, Discussion pp. 123 to 124	Characterization of nano-precipitates of U(VI) phases at a natural analogue site	N/A	Table 7-1
Krupka et al. 2006 [DIRS 179654], Figure 3a, p. 3751	Surface area of U(VI) Phases from SEM images	m^2/g	Output DTN: MO0705COLCONNS.000

NOTE: SEM = scanning electron microscopy; TEM = transmission electron microscopy.

4.1.1 Developed Parameters

Modeled Colloid Stability—The parameters in Table 4-1 have been used to determine the range of colloid stability.

Waste Form Colloid Concentrations and Associated Radionuclides—Waste form colloid concentration ranges and distributions were established using the available testing data, utilizing necessary conceptual simplifications, and consideration of measurement error.

Radionuclide Sorption Parameters—Sorption partition coefficients (K_d values) are used in the abstraction to estimate concentrations on colloids of the reversibly sorbed radionuclides considered in the abstraction. The ranges and distributions of these K_d values are given in Table 6-15 for smectite and Table 6-9 for uranophane. Values for iron oxides are included for information purposes and are not intended for model usage.

Waste Package Corrosion-Generated (FeO_x) Colloid Parameters—The colloid parameters listed under "Corrosion-Generated (FeO_x) Colloids" in Table 4-1 are related to estimates of corrosion product colloid mass concentrations in the waste package and the invert and determination of their stability.

Seepage Water Colloid Parameters—The colloid parameters listed under "Groundwater Colloids" in Table 4-1 define seepage water colloid mass concentrations entering the waste package and other components of the EBS. Groundwater parameter ranges and distributions were formulated using data on groundwater colloid concentration in wells evaluated in the vicinity of Yucca Mountain. Data sources are listed in Table 4-1 (direct input).

4.1.2 Other Parameters Critical to the Implementation of This Abstraction in the TSPA-LA Model

Chemical and Environmental Parameters—When this colloids process model is implemented in the TSPA-LA model, it is fed certain chemical and environmental parameters from other submodels implemented in the TSPA-LA. Ionic strength and pH are developed in the in-package chemistry model (SNL 2007 [DIRS 180506]) and the EBS physical and chemical environment model (SNL 2007 [DIRS 177412]) abstractions, and dissolved radionuclide concentrations are developed in *Dissolved Concentrations of Radioactive Elements* (SNL 2007 [DIRS 177418]). In-drift chemical environmental parameters (e.g., seepage water pH and ionic strength) are provided in the EBS physical and chemical environment model (SNL 2007 [DIRS 177412]). The abstraction uses input from pH in the waste package and in-drift to determine the ionic strength below which the colloids would be stable. This value is then compared against the waste package and in-drift ionic strength values.

4.2 CRITERIA

Projects Requirements Document (Canori and Leitner 2003 [DIRS 166275]) identifies the high-level requirements for the YMP. The requirements that pertain to this report, and their link to 10 CFR 63 [DIRS 180319], are shown in Table 4-3. The YMRP (NRC 2003 [DIRS 163274]) lists acceptance criteria pertaining to these requirements. Criteria that are applicable to this report are described below.

Table 4-3. Applicable Project Requirements

Requirement Number	Title	10 CFR 63 Link
PRD-002/T-014	Performance Objectives for the Geologic Repository After Permanent Closure	10 CFR 63.113 [DIRS180319]
PRD-002/T-015	Requirements for Performance Assessment	10 CFR 63.114 [DIRS 180319]
PRD-002/T-016	Requirements for Multiple Barriers	10 CFR 63.115 [DIRS 180319]

The following requirements were taken from Section 2.2.1.3.4.3 of the YMRP (NRC 2003 [DIRS 163274]) and are based on the requirements of 10 CFR 63.114(a)–(c) and (e)–(g) [DIRS 180319], relating to the radionuclide release rates and solubility limits model abstraction:

- Acceptance Criterion 1—System Description and Model Integration Are Adequate
- Acceptance Criterion 2—Data Are Sufficient for Model Justification
- Acceptance Criterion 3—Data Uncertainty Is Characterized and Propagated through the Model Abstraction
- Acceptance Criterion 4—Model Uncertainty Is Characterized and Propagated through the Model Abstraction
- Acceptance Criterion 5—Model Abstraction Output Is Supported by Objective Comparisons.

Section 8.3 quotes the full text of the applicable acceptance criteria with pointers to the information within this report that pertains to the criteria.

4.3 CODES AND STANDARDS

As stated in the TWP (BSC 2006 [DIRS 177389], Section 3), the work presented in this report conforms to the guidance provided in ASTM C 1174-97 [DIRS 105725], *Standard Practice for Prediction of the Long-Term Behavior of Materials, Including Waste Forms, Used in Engineered Barrier Systems (EBS) for Geological Disposal of High-Level Radioactive Waste*.

5. ASSUMPTIONS

The assumptions used in the colloid abstraction are presented here along with their rationale, confirmation status, and the report sections in which the assumptions are implemented. The rationale of an assumption includes the logic and/or the limited available information that enables the assumption to be considered plausible or reasonable (i.e., the justification) and generally states whether the assumption is bounding, conservative, or otherwise suitable for its use. Assumption 5.1 deals with modeling the behavior of thorium and protactinium. Assumption 5.2 deals with the role of temperature on colloids. Assumption 5.3 is required for the development of the DLVO stability model. Assumptions 5.4 and 5.5 deal with the nature of the embedded radionuclide colloidal particles from DHLWG and CSNF. Assumption 5.6 deals with the selection of conceptual modeled particles for U(VI) colloids from CSNF and DSNF. Assumption 5.7 addresses the conceptual colloid stability model for the corroded waste package. Assumption 5.8 provides the rationale for excluding attachment to air–water interfaces.

5.1 DISTRIBUTION COEFFICIENTS OF THORIUM AND PROTACTINIUM ARE THE SAME AS THAT OF AMERICIUM

Assumption: The K_d values for thorium and protactinium are the same as americium for all colloid types because of limited relevant data.

Rationale: In glass corrosion tests conducted by Luckscheiter and Kienzler (2001 [DIRS 180831], Figure 2, p. 157), the pH sorption edge for Th occurred at the lowest pH values with the strongest increase with pH. The Am sorption edge occurred at a slightly higher pH and its sorption coefficients were lower than thorium sorption coefficients by about a factor of 10. The sorption range for protactinium on hematite is less than that of other actinides, as Pa is often present in the 5+ oxidation state. Within the range of pHs under consideration for the model, the assumption is adequate. The sorption edges for Am and Th occur below the lowest pH of interest to the waste package. The modeled sorption range for Am was increased by a factor of 10 to account for the increased sorption capacity of Th. The assumption is bounding within the range of pH of interest in the model.

Use in the Model: Table 6-15 and Section 6.3.12.1.

5.2 EFFECT OF TEMPERATURE ON WASTE FORM COLLOIDS

Assumption: Waste form colloid suspensions produced at 90°C are stable at 25°C.

Rationale: There are no data available on colloid formation at 25°C for DHLWG; however, data are available for SNF colloids between 25°C and 90°C. As flocculation is a particle collision process, temperature will play a role in the rate of coagulation. If colloidal suspensions are stable at 90°C, they should be stable at 25°C. The surface charge is not anticipated to change greatly with temperature. As temperature increases, the total intereaction energy, V_T/k_BT (where k_B is Boltzmann's constant), decreases, making colloids less stable (see Section 7.1.1 and following text). However, without the high temperatures (i.e., 90°C for crushed glass immersion tests) used in the experiments on waste forms, reaction rates would have been slow, resulting in less colloid generation. At lower temperatures, little glass reaction would have occurred and consequently little colloid formation. Advocat et al. (2001 [DIRS 163198], Figure 1, p. 57)

illustrate the decrease in borosilicate waste glass reaction rate with temperature. The assumption that colloid suspensions will remain stable as temperature drops is reasonable.

Use in the Model: Section 6.3.2.

5.3 DIAMETER OF COLLOIDS IN THE WASTE PACKAGE IS FIXED

Assumption: Waste form colloid particles have been assigned a specific diameter for DLVO calculations.

Rationale: For DLVO modeling, a single size particle needed to be selected that best described the particles observed (see Table 6-2). Particle size is not controlled in accelerated corrosion tests, and it is likely that there will be a distribution of particle sizes. *EBS Radionuclide Transport Abstraction* (SNL 2007 [DIRS 177407]) reports particle size ranges from 20 to 300 nm as reasonable for waste form corrosion tests. Particles in the natural state will be irregular in shape; however, for the purposes of modeling, simple geometric shapes (plate–plate interactions) can only be considered for describing the van der Waals attractive energy. Iron oxide and irreversible SNF colloids may be considered spherical with a small diameter, consistent with observations; however, the interaction is still described as a plate–plate form. Smectite and uranophane colloids may be considered plate-like, with larger dimensions consistent with experimental experience. Within the particle size ranges observed experimentally (i.e., 30 and 300 nm in diameter; SNL 2007 [DIRS 177407]) and adopted in the model, there is little change in the van der Waals forces.

Use in the Model: Section 6.3.2.

5.4 ATTACHMENT OF PLUTONIUM AND AMERICIUM TO DHLWG COLLOIDS IS EITHER REVERSIBLE OR EMBEDDED (IRREVERSIBLE)

Assumption: Plutonium and americium are either associated irreversibly (or embedded) with DHLWG colloids or reversibly.

Rationale: Plutonium and americium have been found associated with colloids and suspended particles generated during DHLWG weathering (CRWMS M&O 2001 [DIRS 154071]; DTN: LL000123351021.117 [DIRS 143308]; Bates et al. 1992 [DIRS 100704], Table 1, p. 650). However, it is not clear how representative short-term tests can be for disposal conditions, and these radioisotopes may undergo reversible sorption; hence, the model considers the two cases independently. The assumption that all measured plutonium and americium is associated irreversibly (embedded) with DHLWG colloids is conservative for the TSPA-LA model analysis.

Use in the Model: Sections 6.3.2.2.

5.5 "EMBEDDED" COLLOIDS FROM SNF MAY BE DESCRIBED AS ZrO_2 PARTICLES

Assumption: Irreversible colloids from spent fuel will have particle characteristics similar to that of ZrO_2.

Rationale: A phase that forms on the surface of corroded CSNF consists of Pu, Zr, and rare earth oxides (Buck et al. 2004 [DIRS 172668], pp. 76 to 78). This phase could be modeled as plutonium oxide, a rare earth oxide, or zirconium oxide. All of these metal oxides have similar points of zero charge (pzc) near pH 8 (Parks 1965 [DIRS 174361]); however, the magnitude of the surface charge may be different, resulting in different stabilities. The zirconium oxide colloid was selected because of the available surface charge data that could be developed into an effective model. The assumption that irreversible colloid suspensions can be related to ZrO_2 colloid behavior is reasonable given the experimental observations and analysis of corroded SNF.

Use in the Model: Sections 6.3.1 and 6.3.2.4.

5.6 COLLOIDAL META-AUTUNITE IS A REASONABLE ANALOGUE FOR A URANOPHANE COLLOID

Assumption: The reversible colloids from spent fuel (uranophane) will have particle characteristics similar to that of meta-autunite.

Rationale: Meta-autunite and uranophane are both layered uranyl phases; however, meta-autunite is a uranyl phosphate whereas uranophane is a uranyl silicate with a slightly different layered configuration. Both contain calcium ions as interlayer constituents. In uranophane, the uranyl cation is coordinated to five equatorial anions, while in meta-autunite the uranyl ion is tetra-coordinate. The result is that the valence requirements of the phosphate anions are nearly satisfied in meta-autunite, and the anions do not form strong bonds with the interlayer cations. In uranophane, however, some silicate tetrahedra form bonds with the interlayer calcium ions, which provides additional linkage between sheets. These structural and compositional differences may result in uncertain changes in the surface electrical characteristics. Data from a mixed schoepite/UO_{2+x} system reported by Mertz et al. (2003 [DIRS 162032], Figure 11, p. 41) indicated a pzc near pH 2 and a high negative surface charge at all pHs above 4. This is similar to the data reported on meta-autunite (Zheng et al. 2006 [DIRS 179565]). These results suggest that the layered uranyl phases may share similar surface charge properties despite the compositional differences. The assumption that reversible colloid suspensions can be related to meta-autunite colloid behavior is reasonable given the experimental observations and analysis of various U(VI) phases.

Use in the Model: Sections 6.3.2.5.

5.7 COLLOIDS DERIVED FROM THE CORROSION OF WASTE PACKAGE MATERIALS CAN BE REPRESENTED AS HEMATITE FOR STABILITY CALCULATIONS

Assumption: The colloids from the waste package will have particle characteristics similar to those of hematite for DLVO stability calculations.

Rationale: Several phases are known to form during the corrosion of steels, including ferrihydrite, goethite (α-FeOOH), lepidocrocite (γ-FeOOH), and akaganéite β-FeOOH. Ferrihydrite will in turn undergo alteration to hematite or goethite over time depending on temperature and Eh conditions. For instance, hydrothermal corrosion tests on Stainless Steel

Type 316 reported by Dietz (2005 [DIRS 179542]) did not result in ferrihydrite formation as this phase is unstable under high temperature conditions. Dietz (2005 [DIRS 179542], Section 2.2.2, p. 16) reported the formation of hematite (Fe_2O_3) on vapor-hydrated Stainless Steel Type 304. Hence, hematite was selected as the representative phase for waste package-derived colloids resulting from carbon steel and stainless steel weathering. For the radionuclide uptake, the major waste package corrosion product is considered to be ferrihydrite (HFO) and goethite. The assumption that colloid suspensions from the corroded waste package can be represented as hematite is reasonable given the experimental observations and analyses of corroded steels.

Use in the Model: Sections 6.3.2.1.

5.8 COLLOID SORPTION AT THE AIR–WATER INTERFACE

Assumption: Colloid sorption at the air–water interface will not occur within the waste package.

Rationale: Colloid sorption at the air–water interface may occur within the waste package but is not considered in the abstraction. Colloid attachment to air–water interfaces commonly occurs in unsaturated environments and may limit mobile colloid generation and migration (Wan and Tokunga 1997 [DIRS 108285]). This phenomenon is dependent on the interface surface area, electrostatic charge on the particles, and the salinity of the aqueous phase. At low water saturations, colloid migration is retarded, although colloids may still move through the adsorbed water films. At intermediate water saturations, there is still an interconnected gas phase, although gas flux may be lower. The interface may act as a static sorbing surface, but the estimating geometry and surface area is complicated, more so under changing saturation state. At high water saturations the majority of the gas is present as small gas bubbles that may migrate, transporting sorbed colloids. However, a proportion of the bubbles may become trapped and will effectively immobilize sorbed colloids.

Neglect of colloid sorption onto the air–water interface in the TSPA calculations should be conservative. Wan and Tokunga (1997 [DIRS 108285]) have shown that Na-montmorillonite clay will be excluded from air–water interfaces at any given pH owing to their structure. Colloidal metal oxide particles, including iron oxides and ZrO_2, will exhibit strong pH dependent affinities to the air–water interface; however, the absence of similar behavior for montmorillonite, and possibly uranophane, results from the high permanent negative charge and low edge surface area on these phases. Excluding attachment to air–water interfaces is conservative; however, it is unclear whether many of the waste form colloids would be affected by these processes. Some U(VI) phases (Buck et al. 2004 [DIRS 171479], Figure 5.2, p. 5.2) have a strong attraction to air–water interfaces which is not well understood. Modeling of the air-water attachment process without specific repository relevant data will be speculative. Smectite clay sorption to air–water interfaces should not be significant; hence, the process may be irrelevant for the clay colloidal particles under consideration in this model. If this process occurs with other suspended particles within the waste package, it may result in greater attenuation of colloids than currently predicted.

Use in the Model: This assumption is used throughout this report. This process is not modeled, and therefore a discussion on its application is not included in this report.

6. MODEL DISCUSSION

This section describes the: (1) model objectives, (2) features, events, and processes (FEPs) considered in the analysis, (3) base-case model, (4) consideration of alternative models, (5) model formulation for base-case assessment, (6) base-case model results, (7) description and analysis of the barrier capability, and (8) evaluation of alternative models. The supporting information (indirect/corroborative data) used in the analysis is listed in Table 4-2.

6.1 MODEL OBJECTIVES

The purpose of this colloid model abstraction is to provide colloid source terms to the TSPA system model. Colloids will likely be produced as a result of the alteration of DHLWG, CSNF, and DSNF waste forms, as well as corrosion of waste package and EBS component steel. The abundance of colloids within the breached waste package will depend on the degree of waste form alteration, on the quantity of steel corrosion product colloids formed, and on quantities of natural colloids present in seepage water. Colloid abundance and suspension stability also depend on the ionic strength, pH, and colloid content of waters entering the waste package from the drift.

In this section, the types and concentrations of colloids that could potentially be generated in the waste package from the degradation of the waste (waste form colloids) and corrosion of the waste package internal components (corrosion-generated iron oxyhydroxide colloids) are described. Concrete and cement are excluded from use in the emplacement drifts by project design criteria; colloids from these man-made materials are not addressed. The treatment here on man-made materials is focused only on steel corrosion products. For stability calculations, hematite is the modeled colloid; however, for sorption onto waste package corroded materials including colloids, HFO and goethite are the modeled surfaces. Sorption of radionuclides onto waste package corrosion products is dealt with in *EBS Radionuclide Transport Abstraction* (SNL 2007 [DIRS 177407]). Potential interactions between inorganic colloids and microbes or organics are addressed in Section 6.3.13. Also, the observed types and concentrations of colloids naturally present in groundwater (groundwater colloids) that would potentially seep or flow into the EBS during the postclosure regulatory period are described. In addition, sorption and desorption of dissolved radionuclides to and from colloid surfaces are discussed, as well as the nature of colloids anticipated in the repository environment. The abstraction is intended to capture the most important characteristics of radionuclide–colloid behavior for use in predicting the potential impact of colloid-facilitated radionuclide transport on repository performance. Colloid transport in the waste package and drift is discussed in *EBS Radionuclide Transport Abstraction* (SNL 2007 [DIRS 177407]).

Output quantities from the waste form and EBS colloid abstraction to the UZ include DHLWG colloid concentrations, CSNF and DSNF colloid concentrations, corrosion product (hematite) colloids, and natural groundwater colloids. Five types of radionuclide association with colloids are modeled: (1) irreversibly sorbed (also termed “embedded”) plutonium and americium in the DHLWG waste form colloids; (2) irreversibly sorbed (also termed “embedded”) Pu and Am in the CSNF-derived colloids; (3) reversibly sorbed radionuclides on uranyl silicate colloids from corroded CSNF and DSNF; (4) irreversible attachment of Pu and Am in iron oxyhydroxide

colloids; and (5) reversible sorption of Pu, Am, U, Np, Th, Pa, Ra, Cs, and Sn, onto smectite and uranophane colloids.

Model inputs include ionic strength and pH of the in-package fluid resulting from reaction of water with the waste, ionic strength and pH of the seepage water entering the drift, estimates of colloid masses formed from waste form degradation, the concentrations of radionuclides generated from degradation of the waste, and K_d values for radionuclides on mineral phases and colloids.

Model outputs feed the UZ transport models and include (as described above) DHLWG, CSNF, and DSNF colloids with attached radionuclides, irreversibly and reversibly sorbed radionuclides, and colloid masses.

The uncertainty associated with the development of parameters representing major processes or features modeled in this analysis is described in general terms in Section 6.6.1. Additionally, specific details on the types of uncertainties associated with the various components of the model elements and the cause(s) for these uncertainties are provided within Sections 6.3 and 6.6.

6.2 FEATURES, EVENTS, AND PROCESSES CONSIDERED IN MODEL

As described in *Technical Work Plan for Waste Form Testing and Modeling* (BSC 2006 [DIRS 177389], Table 2-4), this report addresses the key colloid-oriented FEPs for the waste form and EBS components of the repository that are screened in (i.e., Included FEPs) for TSPA-LA. This report summarizes details of FEP implementation in TSPA-LA, and Table 6-1 provides specific references to sections concerning FEPs within this report.

Table 6-1. FEPs Included (screened in) in the TSPA Model and Addressed in This Report

FEP No.	FEP Name	Section in This Report
2.1.09.02.0A	Chemical interaction with corrosion products	6.3.1, 6.3.8, 6.6.5
2.1.09.16.0A	Formation of pseudocolloids (natural) in EBS	6.3.1, 6.3.12.1, 6.6.8
2.1.09.17.0A	Formation of pseudocolloids (corrosion product) in EBS	6.3.1, 6.3.12.1, 6.6.8
2.1.09.23.0A	Stability of colloids in EBS	6.3.2, 6.3.10, 6.3.11, 6.6.7
2.1.09.25.0A	Formation of colloids (waste-form) by coprecipitation in the EBS	6.3.1

6.3 BASE-CASE MODEL

A discussion of the colloid model is presented here, organized by major concepts considered and the specific ideas and values developed and incorporated into the model. Accordingly, the following subjects are discussed: (1) colloid formation from waste forms (DHLWG, CSNF, and DSNF), corrosion products, and naturally occurring groundwater colloids (Section 6.3.1); (2) colloid suspension stability and concentration of all modeled colloid types (Sections 6.3.2 through 6.3.11); and (3) radionuclide sorption to colloids (Section 6.3.12).

As described in Section 6.1, materials introduced during repository construction may include various metals. Concrete and cement are excluded from use in the emplacement drifts, and

therefore colloids derived from these materials are not considered. Colloids formed from corrosion of introduced materials are modeled only as hematite for stability calculations and as ferrihydrite (HFO) and goethite for sorption calculations (as described in SNL 2007 [DIRS 177407]), although other iron oxide phases and mixed Cr-, Ni-, and Mn-oxide phases would be present (see Section 5.7).

Colloid-facilitated transport may facilitate migration of isotopes that sorb highly to both colloids and host rock. Therefore, the radionuclides for direct consideration in the TSPA dose calculations were examined for their relative sorption ability. The radionuclides included for dose calculations are given in Table 7-1 of *Radionuclide Screening* (SNL 2007 [DIRS 177424]), and their sorption class based on adjustment factors for freshwater shoreline deposits (NCRP 1996 [DIRS 101882]) is shown in Table 6-3 of that same report (SNL 2007 [DIRS 177424]). The information from these two tables was evaluated together so that all the highly sorbing radionuclides could be evaluated for colloid-facilitated transport (except ^{227}Ac and ^{210}Pb, which are not explicitly transported in TSPA but assumed to be in secular equilibrium with their parent isotopes). In addition, ^{231}Pa was chosen because its sorption ability was judged to be high like thorium. The medium sorbing elements, neptunium, selenium, strontium, and uranium were also considered for colloid-facilitated transport. Uranium was chosen because it is the dominant element within the waste, and its daughters are important for long-term dose. Neptunium was chosen because it was a major dose contributor in previous TSPAs. Strontium was not chosen because it has a very short half-life, and any retardation will lead to insignificant releases. Selenium was not chosen because, in the absence of organics, selenium is low sorbing. The final list for direct inclusion in EBS colloid-facilitated transport is americium, cesium, neptunium, protactinium, plutonium, radium, tin, thorium, and uranium.

Additional screening of isotopes for representation of colloid-facilitated transport in the UZ and SZ was done based on the additional consideration of transport properties used by those models.

The UZ and SZ transport models use a similar list of isotopes for colloid-facilitated transport, except they do not include representations for radium, uranium and neptunium. Examination of the groundwater K_c (the product of the K_d and the colloid concentration) for these elements shows that colloid-facilitated transport within the UZ and SZ would not be significant (see Section 6.8.8). The final list of radionuclides considered for UZ and SZ colloid-facilitated transport is americium, cesium, protactinium, plutonium, tin, and thorium.

6.3.1 Colloid Formation and Occurrence

Below is a discussion of colloid types, definitions, and pertinence to the repository. A summary of the colloid types modeled in this abstraction is provided at the end of this section, (e.g., Figures 6-26 and 6-27 provide schematic summary of the colloid types and processes evaluated within the waste package and within the drift, respectively). Figure 6-1 is a schematic illustrating colloid types.

Colloids are typically defined as being between 1 nm and 1 μm in size. Often, particularly in reporting of experimental results, the upper end of the colloid size range is 450 nm and the lower limit is >6 nm, due to conventional dimensions of laboratory equipment (primarily filters). Based on light scattering results, waste form corrosion tests have generated particles between 30

and 300 nm in diameter (SNL 2007 [DIRS 177407]); however, these values are based on assumptions regarding particle shape. Omission of <50-nm particle-sized fraction in the mass concentration calculations is reasonable, since the smaller particles have much lower mass. In this model, the particle size was fixed for use in the DLVO calculations.

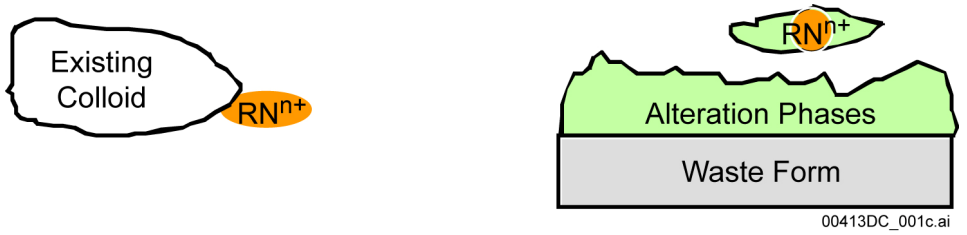

Source: Adapted from CRWMS M&O 2001 [DIRS 154071], Figure 1.

NOTE: The two major types of modeled radionuclide-bearing colloids are depicted: (a) pseudocolloids (clay or iron oxide) and (b) waste form colloids. The radionuclide (RN^{n+}) associated with the waste form colloids and pseudocolloids can be an ionic species, a real colloid, or a discrete radionuclide-bearing phase.

Figure 6-1. Radionuclide-Bearing Colloid Types

True Colloids—True colloids are colloidal-sized assemblages formed from the hydrolysis and polymerization of actinide ions dissolved in solution. They may form in the waste package and EBS during waste form degradation and radionuclide transport. True colloids are also called real colloids, Type I colloids, Eigenkolloide, and intrinsic colloids (Kim 1994 [DIRS 109521]; Ramsay et al. 1988 [DIRS 144603]). The formation of true colloids will depend on the solution chemistry, pH, and temperature.

The speciation and formation of plutonium intrinsic colloids from an initial Pu(V) solution were investigated by Romanovski et al. (1999 [DIRS 170890]) in surrogate Yucca Mountain J-13 well water under an air atmosphere at 25°C. Not all the plutonium was present as colloids in the experiments conducted by Romanovski et al. (1999 [DIRS 170890]); however, the detection of true colloids that may have diameters between 2 and 6 nm is non-trivial and has only been attempted by a few research groups (see results reported by Bitea et al. 2003 [DIRS 173041]). It is possible that similar particles have been produced during waste form testing but were not detected because of instrument and experimental limitations. Only small amounts of colloids are generated from the waste forms (see Section 6.3.4), and only a fraction of these may be intrinsic colloids as the majority are uranyl and/or other silicate colloids. Even the metastable uranyl silicate colloids are expected to dissolve within the groundwater system (see Section 6.3.2.5). As stated in *Colloid-Associated Radionuclide Concentration Limits: ANL* (CRWMS M&O 2001 [DIRS 154071], p. 30), very small amounts of colloids (if any) are detected even using TEM examination of samples, and those that are found tend to be uranyl silicates.

As discussed in Section 6.3.11, transport of radionuclides by groundwater colloids is thought to be generally more prevalent than transport by true colloids (McCarthy and Zachara 1989 [DIRS 100778]). Kersting and Reimus (2003 [DIRS 162421]) reported Pu(V) and Pu(IV) sorption experiments on montmorillonite colloids under conditions relevant to Yucca Mountain. They were able to demonstrate that, in the case of the Pu(V), rapid reduction of Pu(V) to Pu(IV) occurred on the particle surface. This study suggested that true colloids were not present in the

system. Given that the true colloids are unstable phases, it is expected that they will dissolve into the aqueous phase with very little migration and provide radionuclides to be sorbed onto pseudocolloids.

Waste Form Colloids—Waste form colloids, termed primary colloids, may contribute to colloid-facilitated radionuclide transport. These colloids form from the nucleation of colloids from waste form dissolution and from spallation (flaking off) of colloid-sized waste form alteration products. Waste form colloids may contain radionuclides and have the potential for increasing mobile radionuclide concentrations to levels higher than achievable with real colloids or other pseudocolloids. Dissolved radionuclides and other ions may coprecipitate to form colloids. Coprecipitates may consist of radionuclides bound in the crystal lattice of a dominating mineral phase or may consist of radionuclides engulfed by a dominating mineral phase. Traexler et al. (2004 [DIRS 172072]) listed potential waste form-derived colloids from corroded DHLWG and SNF, including schoepite $\{[(UO_2)_8O_2(OH)_{12}](H_2O)_{12}\}$, soddyite $\{(UO_2)_2SiO_4 \cdot 2H_2O\}$, uranophane $\{Ca(UO_2)_2(SiO_3OH)_2 \cdot 5H_2O\}$, boltwoodite $\{KH(UO_2)(SiO_4) \cdot 1.5H_2O\}$, cesium-molybdenum uranyl hydroxide, clay particles with brockite $\{(Ca,Th,Ce)PO_4 \cdot H_2O\}$ inclusions, asbolan $\{(CO,Ni)_{1-y}(MnO_2)_{2-x}(OH)_{2-2y-2x} \cdot nH_2O\}$, birnessite $\{(Na,Ca,K)_x(Mn^{4+},Mn^{3+})_2O_4 \cdot 1.5(H_2O)\}$, weeksite $\{K_2(UO_2)_2Si_6O_{15} \cdot 4(H_2O)\}$, calcite $\{CaCO_3\}$, dolomite$\{CaMg(CO_3)_2\}$, metal oxides, Na-silicates, Al-oxides, analcime $\{NaAlSi_2O_6 \cdot H_2O\}$, hydrated Ca-silicates, and apatite-type phases.

The most abundant waste type is CSNF (uranium oxide) from commercially owned and operated electric power reactors. DSNF is a diverse collection of waste from reactors at U.S. Department of Energy (DOE) nuclear complex sites, although the major contributor is uranium metal. DHLWG is an alkali borosilicate glass-based waste form containing radionuclides. Borosilicate glass corrosion results in the formation of several alteration phases, including iron oxides, alumino-silicates, calcium silicates, weeksite, brockite, and rhabdophane, depending on glass composition and reaction conditions. The major alteration phase is smectite clay.

SNF corrosion can result in the generation of plutonium- and americium-bearing colloids (Wilson 1990 [DIRS 100793]; Wilson 1990 [DIRS 121808]; Finn et al. 1994 [DIRS 100746]; McNamara et al. 2005 [DIRS 174068], p. 171). Other radionuclides have been associated with these phases, including Np and Cs; furthermore, uranium is normally a major component in these colloids. No information on radium and tin association with these phases is available. The potential behavior of these radionuclides must be based on chemical similarities with other elements. Production of plutonium colloids was observed to be highest with bare fuel fragments. In the presence of metal surfaces (e.g., steel vessels or Zircaloy), a reduction in plutonium colloid concentrations was observed (Wilson 1990 [DIRS 100793]; Mertz et al. 2003 [DIRS 162032]). Hence, the inclusion of CSNF colloids in the model is likely to be conservative.

All processes that lead to the elimination of colloids from an aqueous phase might be described as “filtration,” which would include various physical-chemical interactions. However, in this model, physical filtration refers to removal of larger particles due to pore clogging, sieving, or straining in the waste package and in-drift environment (Aguilar et al. 1999 [DIRS 161648]). Physical filtration of colloids is not explicitly called out in the model abstraction because it is extremely difficult to quantify and account for the different mechanisms involved in colloid

retardation and/or retention from advective (flow) experiments. In the majority of colloid transport models, colloid retardation is included through adding an empirical expression to the advective-diffusive transport equation. It is likely that varying amounts of physical filtration occurred depending on the experimental design in all waste form and waste package corrosion tests discussed in this report, so any reported colloid concentrations should be considered conservative. Caution must be taken when using more complex experiments (i.e., tests where colloids were required to be transported any distance before analysis) for estimating colloid concentrations for model implementation.

Pseudocolloids—Pseudocolloids consist of non-radioactive particles with radionuclides sorbed to them. Natural pseudocolloids include mineral fragments formed from the host rock, microbes and microbe fragments, and humic and fulvic acids. Pseudocolloids form as a result of dissolved (aqueous) radionuclides or smaller radionuclide colloids, or both sorbing to existing colloids (e.g., clay, iron oxyhydroxides, silica). At the YMP, pseudocolloids may develop as a result of radionuclide association with waste form colloids formed during degradation of DHLWG, radionuclide association with corrosion-product colloids formed during corrosion of waste package materials and other metallic materials, and radionuclide association with naturally occurring groundwater colloids.

Seepage–Groundwater Colloids—Naturally occurring colloids (referred to in this report as "groundwater colloids") may be inorganic (mineral fragments) or organic (microbes and humic substances). At Yucca Mountain, inorganic groundwater colloids, primarily consisting of clay, zeolites, silica, and iron oxyhydroxides, may be transported in seepage water into the repository from the vadose zone above it or may be formed due to changes in chemical conditions near the repository (e.g., evaporation leading secondary mineral precipitation). At YMP, organic colloids are not important. Humic substances are not sufficiently abundant in YMP groundwaters to impact transport (Section 6.3.9). Microbes, as large colloids, are susceptible to filtration during transport (Minai et al. 1992 [DIRS 100801]).

Colloids are modeled in the abstraction as follows:

Waste Form Colloids—Colloids from the corrosion of DHLWG are modeled as montmorillonite particles with irreversibly associated (embedded) Pu and Am and reversible sorption of Pu, Am, U, Np, Pa, Ra, Sn, and Cs. Colloids from the corrosion of CSNF are conceptually identified as a mixed Pu-Zr-Rare Earth oxide and modeled as "ZrO_2" particles with irreversibly attached Pu and Am with no additional sorption of other radionuclides. Additionally, both CSNF and DSNF are modeled to form uranium colloids that are conceptually identified as uranophane and modeled as meta-autunite with reversibly sorbed Pu, Th, Pa, Am, Np, Cs, Ra, and Sn.

Corrosion Product Colloids—Colloids from the corrosion of steel components in the EBS are modeled as hematite colloids, as they will likely be a mixture or combination of hematite, goethite, lepidocrocite, magnetite, and hydrous ferric oxide (HFO) ferrihydrite (Section 6.3.8). For stability calculations, waste package corrosion colloids are conceptually identified as ferrihydrite and modeled as hematite. For reversible sorption (which is not dealt with in this model), the modeled surfaces are HFO and goethite. Irreversible attachment of Pu and Am is modeled in this report.

In-Drift/Groundwater Colloids—Naturally occurring colloids are modeled as montmorillonite colloids (Section 6.3.11). Groundwaters in the Nevada Test Site (NTS) environment, which is similar to the anticipated repository conditions, contain colloids that are predominantly zeolites and smectite clay (Kersting and Reimus 2003 [DIRS 162421], Figure 1.1, p. 2); however iron oxides and silica colloids may also be present. However, the low sorptive properties of silica are such that they can be ignored, and waste package corrosion products will dwarf the quantity of iron oxides from natural groundwater. Organic colloids in groundwater (humic and fulvic acids, microbes and their detritus and metabolic products) are not modeled.

Above a certain ionic strength (defined in the model as $I_{threshold}$), the concentration of colloids will be negligible and is set to low values for modeling purposes. Under dilute conditions with low particle concentrations, as expected in the repository environment, colloid stability is governed by the Derjaguin-Landau-Verwey-Overbeek (DLVO) theory, and therefore colloids become unstable at higher ionic strengths. The DLVO theory was used to estimate the stability of colloid suspensions. The results were compared to experimental observations for validation.

Figure 6-2 depicts the process of waste form weathering with the subsequent formation of colloids derived from the waste form.

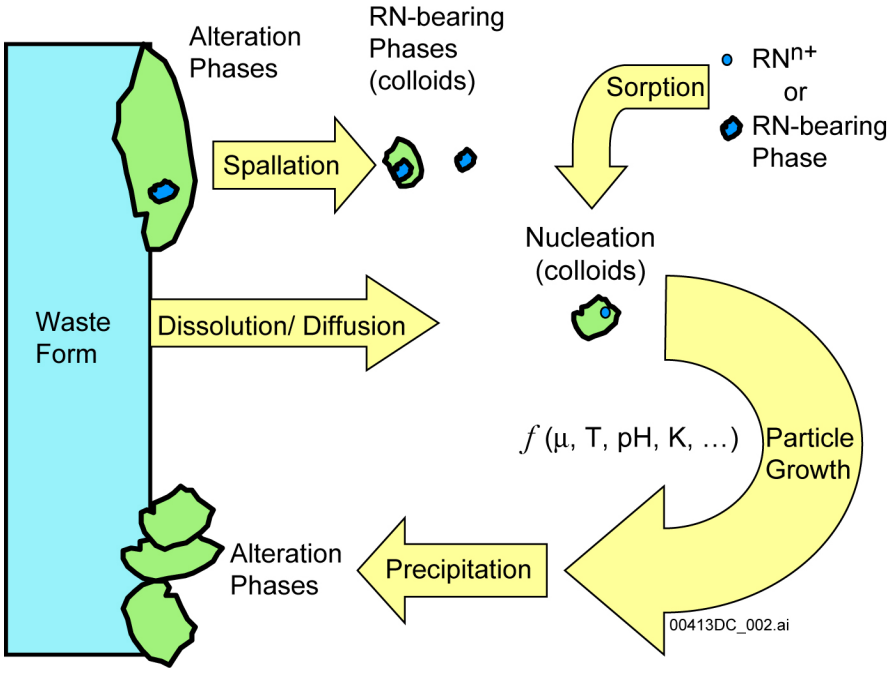

Source: Modified from CRWMS M&O 2001 [DIRS 154071], Figure 2.

NOTE: RN = radionuclide. Schematic of colloid formation from waste-form corrosion whereby several processes are represented: (1) spallation of radionuclide bearing alteration phases from the waste form that are within the colloidal size range, and (2) nucleation of colloids from ions dissolved from the waste form and sorption of ionic radionuclide species or radionuclide-bearing phases. Particle growth occurs by precipitation on nuclei and is controlled by factors such as ionic strength, temperature, pH, and solubility. When particle diameters exceed 1 μm or solution chemistry destabilizes the colloids, deposition or coagulation and gravitational settling of radionuclide-bearing alteration phases occurs.

Figure 6-2. Schematic of Colloid Formation from Waste-Form Corrosion

As the waste form corrodes, an alteration layer forms, grows, and evolves as a layer on its surface. In the case of DHLWG, a smectite-like phase forms initially on the glass surface (CRWMS M&O 2001 [DIRS 154071], Section 6.2.1). Precipitates of actinide phosphates and titanates have been observed embedded within the smectite corrosion rind (DTNs: MO0407ANLGNN02.608 [DIRS 171277] and LL000123351021.117 [DIRS 143308]; CRWMS M&O 2001 [DIRS 154071]; Bates et al. 1992 [DIRS 100704]). In the case of UO_2 SNF, the weathered corrosion rind consists of U(VI) phases and oxide precipitates containing Zr, Pu, and rare earth elements (Buck et al. 2004 [DIRS 172668]).

6.3.2 Colloid Suspension Stability and Concentration

The DLVO theory is the principal method for examining the stability of a colloidal suspension in terms of the repulsive and attractive forces. The theory may have limitations as it does not account for hydrophobic interactions, which may be very important for the types of particles and systems under consideration in this model. Hydration forces and geometric effects are accounted for through an approximation. In this model, the DLVO theory has been used to look at the fundamental constraints on particle stability. In DLVO theory, the total potential energy $U_T(h)$ between two colloid particles of radius a, with their surfaces separated by distance h, includes the sum of both the electrostatic $U_E(h)$ and van der Waals $U_V(h)$ contributions. The colloid stability can be expressed through the stability ratio, W, which is related to the difference in the rate constants of rapid (van der Waals dominated attraction) and slow coagulations (Honig et al. 1971 [DIRS 179548]).

The prediction is based on calculating the average effect of electrostatic repulsion between charged colloid particle surfaces to inhibit the frequency of particle collisions required for coagulation. This report documents the parameters, form of inter-particle potentials, and the surface charge assumptions that were used to develop the stability boundaries for the four colloid types. For each colloid a reference basis was used to establish the required inputs:

1a) Form of electrostatic potential;
1b) Surface potential dependence on pH and ionic strength.
2a) Form of van der Waals potential;
2b) Value for Hamaker constant, A_H, and, in some cases,
2c) Specification of an interaction depth;
3) Particle size consistent with colloid form and reference source.

In all four cases (Table 6-2), the form of the electrostatic potential was expressed according to:

$$U_E(h) = 2\pi a\ \varepsilon_r\ \varepsilon_0\ \zeta_{eff}^2 \ln(1 + e^{-h/r_D}) \qquad \text{(Eq. 6-1)}$$

where ζ_{eff} is the effective surface potential, h is the particle separation distance, and r_D the Debye length. Also, ε_0 and ε_r are the free-space permittivity and dielectric constant of water, respectively. The Debye length squared can be expressed as:

$$r_D^2 = \frac{\varepsilon_r\ \varepsilon_0\ k_B T}{2\ e^2\ N_A I} \qquad \text{(Eq. 6-2)}$$

where k_B is the Boltzmann constant, T is absolute temperature, e is the charge of the electron, N_A is Avogadro's number, and I is the ionic strength in moles per volume units consistent with length scale units of the expression. The fundamental physical constants were obtained from Lide (1991 [DIRS 131202]). In the appropriate units, Equation 6-2 can be inferred from Equation 5 in Appendix A9 of the study by Atkins (1994 [DIRS 134303]).[1]

In each of the cases, the van der Waals potential is expressed according to:

$$U_V(h) = \frac{-A_H}{12h} \frac{a}{(1+\frac{h}{\delta})(1+\frac{h}{2\delta})} \quad \text{(Eq. 6-3)}$$

where δ is the plate thickness. The electrostatic (Equation 6-1) and van der Waals (Equation 6-3) potentials are derived by applying the Derjaguin approximation to the interaction energies per unit area given in Equation 3 of Zheng et al. (2006 [DIRS 179565]). For the van der Waals potential, this expression retains the dependence on both separation distance and surface thickness. Both dependences are needed for montmorillonite and meta-autunite in Table 6-2. The stability factor relating the inhibited collision rate to the uninhibited rate can then be expressed as a ratio $W = W_T/W_V$, where the numerator:

$$W_T = 2\int_0^\infty du \frac{\beta(u)}{(2+u)^2} \exp(U_T(h)/kT) \quad \text{(Eq. 6-4)}$$

and denominator:

$$W_V = 2\int_0^\infty du \frac{\beta(u)}{(2+u)^2} \exp(U_V(h)/kT) \quad \text{(Eq. 6-5)}$$

represent the respective collision probabilities, where k is the Boltzmann constant and T is the absolute temperature. Given the potentials from Equations 6-1 and 6-3, the stability ratio (W) is obtained from the ratio of Equations 6-4 and 6-5 (also as given by Equation 14 of Honig et al. 1971 [DIRS 179548]). The Equation 6-4 and Equation 6-5 integrals evaluate the reduced separation distance $u = h/a$ and the hydrodynamic factor (Equation 6 of Honig et al. 1971 [DIRS 179548]), given by:

$$\beta(u) = \frac{6u^2 + 13u + 2}{6u^2 + 4u} \quad \text{(Eq. 6-6)}$$

Equation 6-6 approximates the deviation from Stokes-law viscous effects on the particle motion, which become large as particle surfaces approach one another (see Output DTN: MO0705CSIONSTH.000).

[1] In Equations listed by Atkins (1994 [DIRS 134303]), $R = k_B \times N_A$ and $\varepsilon = \varepsilon_o \varepsilon_r$. ρL (where $L \equiv N_A$) and ρ is solvent density. The L^2 cancel out, and for water ρ is ~ 1.

Table 6-2. Definition of Colloid Potential Energy for Stability Calculations

Model	Colloid Type			
Parameter	**Montmorillonite**	**Hematite**	**ZrO_2**	**Meta-Autunite**
a (nm) Radius	300	60	30	250
$^{\dagger}\zeta_{eff}$	ζ	ζ	ζ	$\frac{4kT}{e}\tanh\frac{e\zeta}{4kT}$
A_H (J)	5×10^{-20}	5×10^{-20}	1×10^{-20}	2.06×10^{-20}
δ (nm)	0.66[‡]	∞	∞	3.0
Reference	Tombácz et al. 1990 [DIRS 112690], Figure 3, p. 77; Figure 4, p. 78, legend (Hamaker constant (A_H) reported in Joules)	Gunnarsson et al. 2001 [DIRS 179547], Figure 7, p. 456; p. 454, Section 3.3, line 14	[*]Bitea et al. 2003 [DIRS 174504], p. 59, Figure 3	Zheng et al. 2006 [DIRS 179565], p. 53, Figure 7b; p. 53, Section 3.2.4, line 4

† Fits of the surface potentials ζ, contained in each reference are provided in Output DTN: MO0705CSIONSTH.000.
* Parameters determined from fits to data given in reference (see Figure 6-3).
‡ Reported interaction depth (or layer thickness) value of Tombácz et al. (1990 [DIRS 112690], p. 79) was 1.3 nm but may also be between 1.55 and 1.85 nm depending on the ionic strength. Because of the nature of the charge distribution, the plate thickness used in the van der Waals term is half this value at ~0.66 nm. For meta-autunite, a value of 3 nm was reported by Zheng et al. (2006 [DIRS 179565]).

NOTE: Two different values for the Hamaker constant for hematite were documented by Gunnarsson et al. (2001 [DIRS 179547], Section 3.3, p. 454). The selection of the lower energy value is conservative for model application as it results in greater stability for the colloids. Values for the fundamental physical constants reported in spreadsheets were obtained from Lide (1991 [DIRS 131202], back cover).

Table 6-2 presents the specific information to define the inter-particle potential used in the stability calculations for each colloid type. The values for the potential parameters can be found in each of the references in Table 6-2 with the exception of the ZrO_2 colloid. For the ZrO_2 case, the values are selected based on the stability ratio data (Figure 6-3) given by Bitea et al. (2003 [DIRS 174504]). The expressions (and plots) for the fits to surface potential as a function of pH and ionic strength are in Output DTN: MO0705CSIONSTH.000. The files contain sample calculations of the potentials for each colloid along with Equation 6-4 and Equation 6-5 integrals. The integrals are handled numerically with Gauss-Legendre points and weights (Abramowitz and Stegun 1972 [DIRS 156927]) mapped to the interval $(0,\infty)$. The calculations have solved for W by using the "Solver" function in Excel to determine curves of fixed W in the pH–ionic strength plane.

In the case of meta-autunite, the surface potential is related to a surface charge using Equation 4 from Zheng et al. (2006 [DIRS 179565]) for an isolated particle. The expression is valid for a sphere and makes little difference to the precise value used for the small surface potential. The ratios of exponentials:

$$\frac{\exp(x^{-1})}{\exp(x)} = \tanh\left(\frac{x}{2}\right) \qquad \text{(Eq. 6-7)}$$

where x represents any function, was applied in the calculations given in Output DTN: MO0705CSIONSTH.000. In all other cases, the zeta potential was made to equal to the surface potential.

The required inputs to the stability model are the ionic strength and pH of the in-package fluid resulting from reaction of water with the waste and ionic strength and pH of the seepage water entering the drift. The value set as the threshold position was at $W = 10$. The selection of $W = 10$ is discussed in Sections 6.6 and 7.1. Experimental data are used to estimate colloid mass concentration formed from waste form degradation, the concentrations of radionuclides generated from degradation of the waste, and K_d values for radionuclides on mineral phases and colloids.

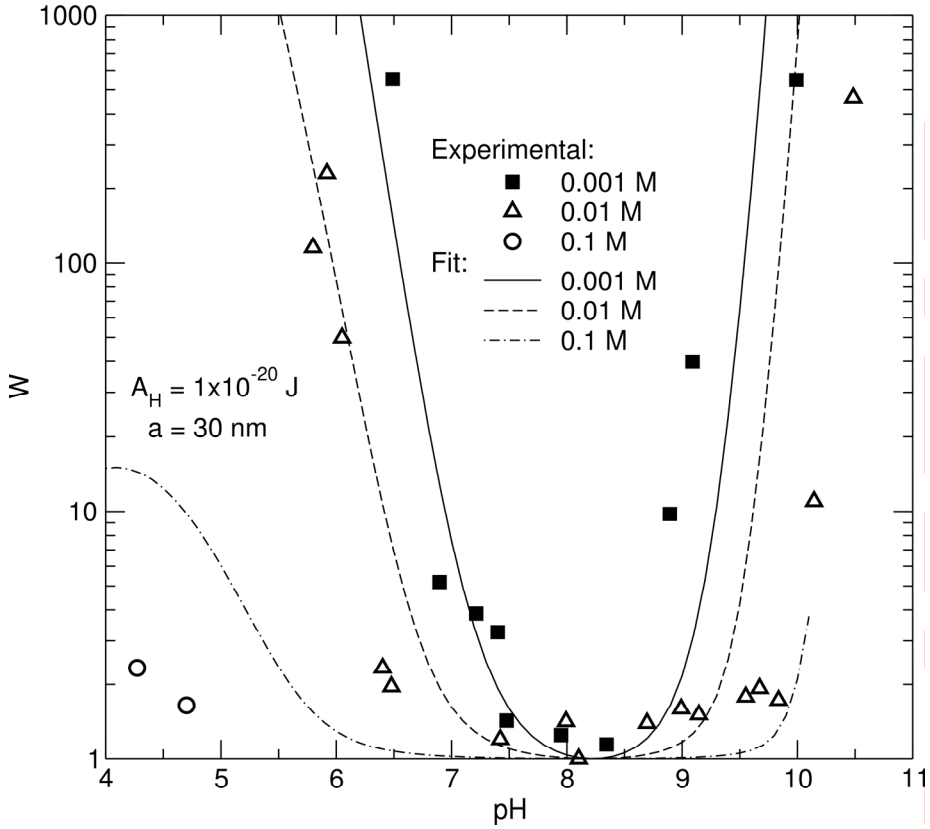

Source: Output DTN: MO0705CSIONSTH.000 and Bitea et al. 2003 [DIRS 174504], Figure 6, p. 61.

Figure 6-3. Stability Ratio (W) for ZrO_2 Colloids, Showing Experimental Data from Bitea et al. (2003 [DIRS 174504]) with Calculation Fit Using Parameters in Table 6-2

TSPA calculates the concentrations of all colloid types as a function of solution chemistry inside and outside the breached waste package. TSPA also calculates the continual interaction of these colloids with radionuclide-bearing fluids and calculates the partitioning of radionuclides onto colloid surfaces.

6.3.2.1 Stability of Hematite Colloid Suspensions as a Function of pH and Ionic Strength

The pzc of iron oxyhydroxide colloids ranges between pH values of approximately 5 and 8.5 (Langmuir 1997 [DIRS 100051], p. 351, Table 10.3), depending on colloid and water composition, and in this range they will tend to be unstable and tend to agglomerate. At higher

or lower pH, however, iron oxyhydroxide colloids are stable, depending upon ionic strength. Liang and Morgan (1990 [DIRS 109524], Figure 1) demonstrated that for a given ionic strength, hematite colloidal suspension stability increases as pH both increases and decreases away from the point of zero charge. The variation in zeta potential with pH at different ionic strengths is displayed in Figure 6-4 based on data from Gunnarsson et al. (2001 [DIRS 179547]). At much higher ionic strengths, particles may be re-stabilized through hydration effects (Ruckenstein and Huang 2003 [DIRS 179556]) and W will be >>1 (see Section 6.3.10).

The waste package will corrode and form iron, chromium, nickel, and manganese oxides and oxyhydroxides. For modeling purposes, two parameters have been established, the expected maximum and minimum mass concentrations of iron oxide colloids, $M_{coll,FeOx,sampled}$ and $M_{coll,FeOx,min}$, respectively.

Although Figure 6-4 demonstrates that there are changes in the surface charge with ionic strength, these variations were incorporated into the $W = 10$ calculation for colloid stability (see Output DTN: MO0705CSIONSTH.000). The solution to when $W = 10$ is unique for a particular pH. In other words, there cannot be two ionic strengths, where $W = 10$ at a fixed pH.

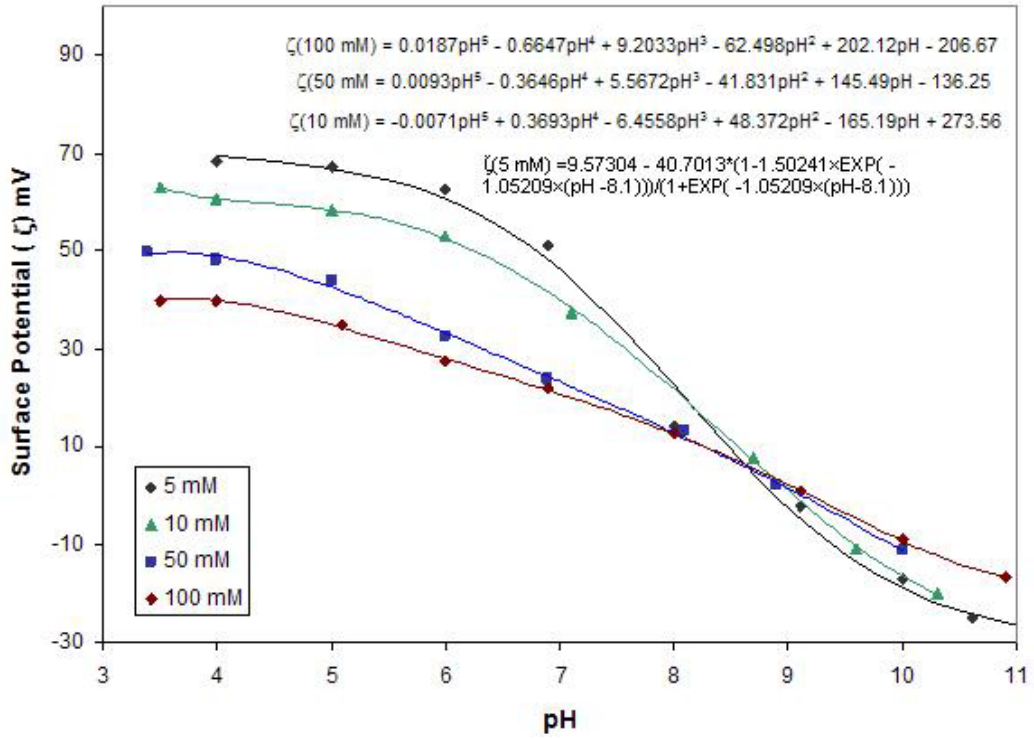

Source: Output DTN: MO0705CSIONSTH.000 and Gunnarsson et al. 2001 [DIRS 179547], Figure 7, p. 456.

NOTE: The fits to the data were obtained with Excel. The fit for the 5mM data set was calculated and then re-plotted in Excel. The results are described in Output DTN: MO0705CSIONSTH.000.

Figure 6-4. Experimental Zeta Potential with pH at Different Ionic Strengths with Fits Used in Model Development

The plot in Figure 6-5 shows the fits to the calculation that are described in Equations 6-8a and 6-8b (see Output DTN: MO0705CSIONSTH.000). The stability of the iron oxide colloids is determined on the basis of the fluid ionic strength and pH. The $I_{threshold}$ is defined as the ionic strength above which the colloids will be unstable. When the pH is between 4.5 and 8.4, the following relationship is used:

$$I_{threshold} = -0.013 \times pH + 0.11 \quad \text{(Eq. 6-8a)}$$

In contrast, when the pH is between 9.4 and 10.4, the following equation is used:

$$I_{threshold} = (0.0017 \times pH^2) - (0.0327 \times pH) + 0.158 \quad \text{(Eq. 6-8b)}$$

If the pH is < 4.5, the $I_{threshold}$ value calculated at pH 4.5 is used, and if the pH > 10.4, the $I_{threshold}$ value calculated at pH 10.4 is used.

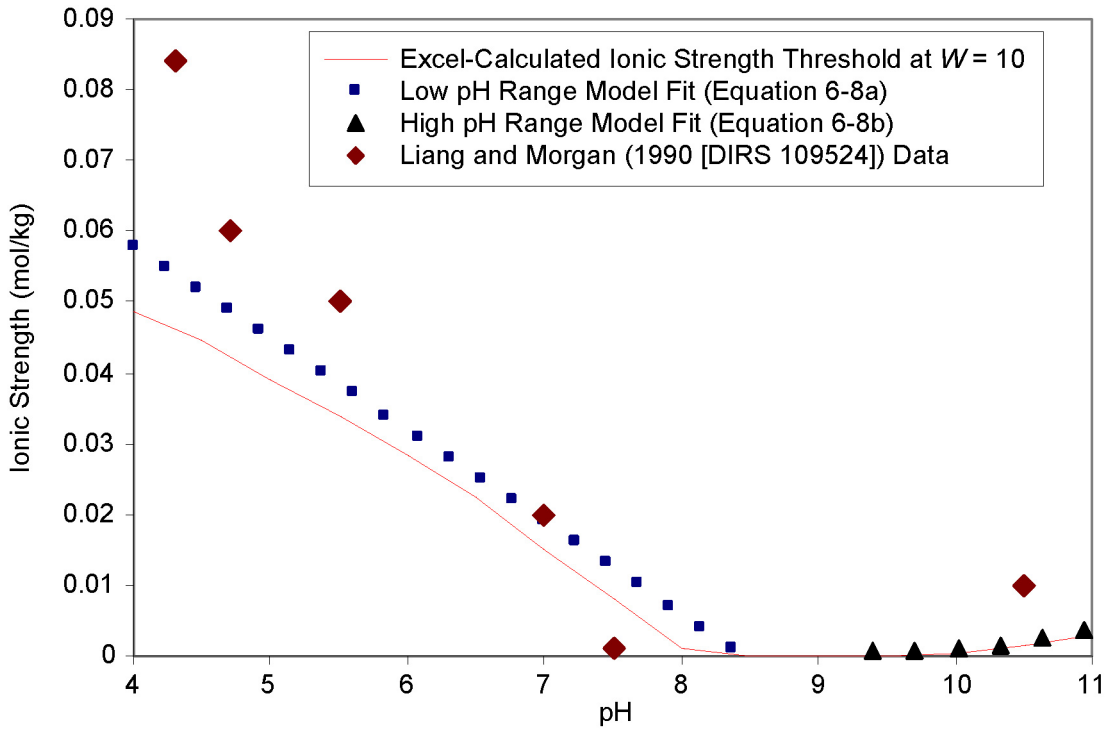

Source: Output DTN: MO0705CSIONSTH.000.

NOTE: Hamaker constant = 5×10^{-20} J (Gunnarsson et al. 2001 [DIRS 179547], Section 3.3, p. 454).

Figure 6-5. Calculated Stability Plot for Hematite with Fits to the DLVO Model at the Low and High pH Regions (Equations 6-8a and 6-8b) and Experimental Values from Liang and Morgan (1990 [DIRS 109524], Figure 1, p. 40)

Experimental data from Liang and Morgan (1990 [DIRS 109524]) are also plotted on the diagram validating the DLVO calculation and approach adopted in this model. A linear fit was used for the low pH region based on visual inspection of the most reasonable approach. All fits were performed using Excel fitting methods. The values from Liang and Morgan (1990

[DIRS 109524]) are outside the bounds of the model, particularly under low pH conditions, and the exact reason for this is uncertain but may reflect different electrical surface characteristics in the particles used in the experiments and the methods used to estimate *W*. In their experiments, stability was determined from the initial slope of particle light scatter extinction data. Assumed differences in particle size and actual shape, as well as initial particle concentration might account for the slight discrepancy between the model and the data from Liang and Morgan (1990 [DIRS 109524]). However, the largest factor effecting these calculations is the Hamaker constant. Very slight variations in the Hamaker constant will alter the stability significantly. In the case of hematite, the Hamaker constant used in the model was the lowest of two values published by Gunnarsson et al. (2001 [DIRS 179547]). The higher value would have resulted in even greater disparity from the data from Liang and Morgan (1990 [DIRS 109524]).

6.3.2.2 Irreversible Colloids from Corroded Borosilicate Waste Glass

Colloids produced from the degradation of alkali borosilicate glasses have been observed to be poorly crystalline clay-like particles occasionally containing discrete radionuclide-bearing phases (DTNs: MO0407ANLGNN02.608 [DIRS 171277] and LL000123351021.117 [DIRS 143308]; CRWMS M&O 2001 [DIRS 154071]; Feng et al. 1994 [DIRS 101611]; Bates et al. (1992 [DIRS 100704]). Depending on the glass composition, different minor phases have been observed; such as brockite (Bates et al. 1992 [DIRS 100704]) or rhabdophane (Buck and Bates 1999 [DIRS 109494]) in thorium- and phosphorus-containing glasses. These phases were not observed in SRL202A and SRL131A glass tests used to establish plutonium concentration with colloids for TSPA-LA. The colloidal properties of any radionuclide-bearing phase associated with smectite clay colloids will be governed by the properties of that smectite clay. Therefore, the stability of smectite (montmorillonite) colloid suspensions will control the mobility of the associated radionuclide-bearing phases.

Determination of the DHLWG colloid concentration is linked to the concentration of Pu that is considered irreversibly attached to the colloids. To obtain the plutonium concentration associated with DHLWG colloids, a range of 1×10^{-11} to 1×10^{-8} mol/L is sampled uniformly. In Figure 6-6, an empirical cumulative distribution function (CDF) is plotted for the plutonium colloid data from the degradation of glass (from DTN: LL991109751021.094 [DIRS 142910] (MOL.20000124.0207, pp. 27 and 32); DTN: LL000905312241.018 [DIRS 152621] (MOL.20001130.0021 pp. 29, 30, and 70); and DTN: MO0705ANLGSV01.258 [DIRS 181399]). These data have been tabulated in Table 6-5 and plotted below in Figures 6-6 and 6-18. These data included powdered samples labeled "_2K" and "_20K," as well as monolith samples labeled "_10." Note that the measured data for the monolith samples reported in DTN: MO0705ANLGSV01.258 [DIRS 181399] have been converted to the values shown in Table 6-5 (within Output DTN: MO0705COLCONCS.000) using the same equations as for the powdered samples (DTN: LL000905312241.018 [DIRS 152621] (MOL.20001130.0021, p. 70)) for the Pu colloid concentrations and for the ionic strength calculation (DTN: LL991109751021.094 [DIRS 142910] (MOL.20000124.0207, p. 27)). The generation of colloids with irreversibly attached plutonium from DHLWG is expected to be more similar to the data measured on the monolith samples because the glass logs are in that state at the beginning of their alteration. Note that for the "non-detectable" values in Table 6-5, the values were assigned, and plotted at, 1×10^{-13} mol/L.

Concentration of DHLWG colloids is obtained by scaling to a triangular distribution (see Table 6-3). This distribution was developed from a high surface area-to-volume glass corrosion test where both the plutonium colloid concentration and the particle concentration were measured. A distribution was developed because of the large degree of the scatter in the available experimental light scattering data and uncertainty in the overall results. Figure 6-6 shows the relationship between colloidal plutonium concentrations and mass of colloids per unit volume. However, as the calculation of the mass of colloids depends on making assumptions on the size and shape of the colloids, it was considered more reasonable to provide a distribution of scaling values for implementation in TSPA.

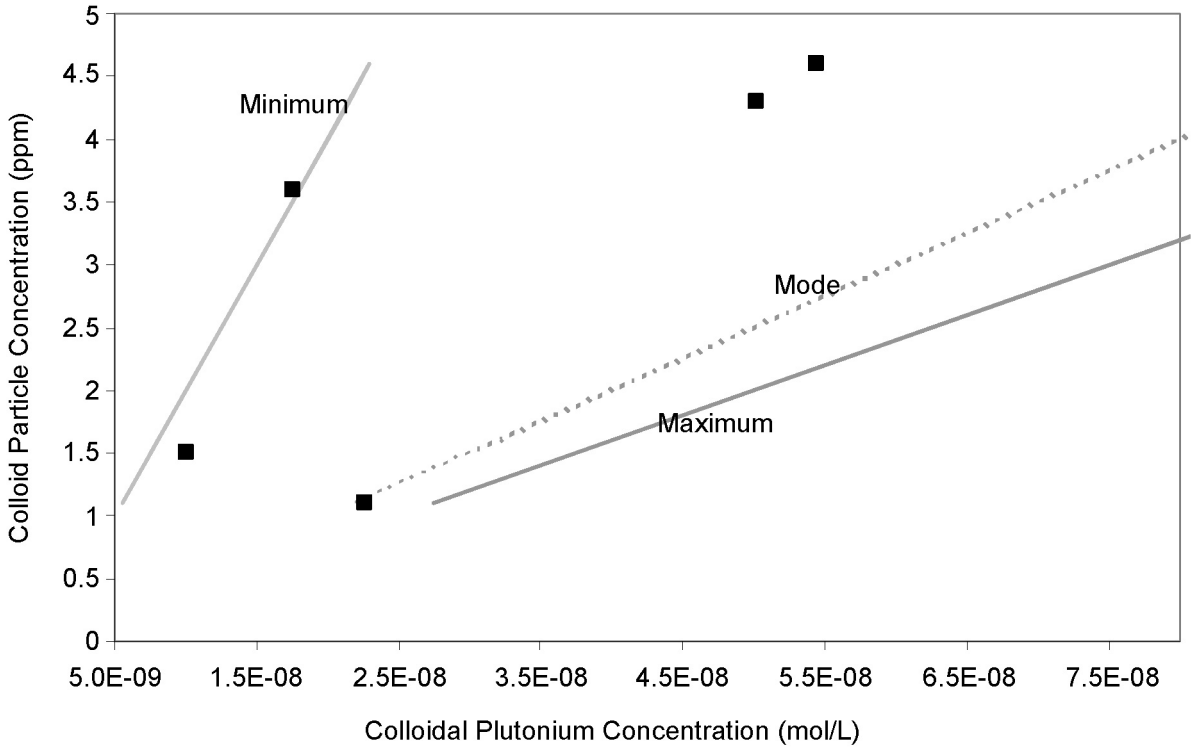

Source: CRWMS M&O 2001 [DIRS 154071] (data re-plotted from Figure 24, p. 40); DTN: LL991109751021.094 [DIRS 142910] (MOL.20000124.0207, p.32).

NOTE: Plutonium concentration associated with colloids. The total colloid concentration was obtained by dynamic light scattering measurements assuming a particle diameter of 73 nm.

Figure 6-6. Relationship between Plutonium Colloid Concentration and Colloid Mass Concentration

Using the relationship described in Figure 6-6, the concentration of colloid plutonium associated with a mass of colloids can be obtained. The relationship suggests that ~1 ppm colloids will have 2×10^{-8} mol/L plutonium; however, there is a good deal of uncertainty in the value. Because the light scattering technique that was used to estimate the concentration of colloids in ppm depends on various assumptions for particle size and shape, it is recommended that the TSPA-LA model use the $DHLWG_{coll,\ med}$ relationship presented in Table 6-3.

Table 6-3. Range of Colloid Concentrations for Scaling

$DHWG_{coll, min}$	5×10^{-9} mol/L
$DHLWG_{coll,mode}$	2×10^{-8} mol/L
$DHLWG_{coll, max}$	2.5×10^{-8} mol/L

Both irreversibly and reversibly sorbed radionuclides are modeled. The concentration of radionuclides irreversibly sorbed is based on DHLWG corrosion data while the concentration of radionuclides reversibly sorbed is calculated using derived sorption K_d values. The concentration of irreversibly sorbed Am is estimated at each TSPA calculation time step by determining the fraction of this element present compared to plutonium in the inventory. Although some borosilicate tests have shown that there can be slightly greater retention of americium in secondary alteration phases than plutonium (Pirlet 2001 [DIRS 174351]) (note that over 80% of the plutonium and 99% of the americium were found as particulates rather than solution species), the direct correlation of americium concentrations from the plutonium values will be adequate for modeling purposes under the conditions anticipated in the repository environment.

Although the data fitted a log-uniform distribution extremely well (see Figure 6-7), a uniform distribution was selected as this implied greater uncertainty in the system. By selecting only the monolith "_10" experiments, the total range of colloidal plutonium concentrations was narrowed (see Figure 6-7). The monolith experiments are a better representation of the actual glass log surface to be disposed (see Table 6-4 and 6-5 for the monolith and all other DHLWG test data).

Table 6-4. Distribution of Plutonium Colloid Concentration Values (mL/g) Used for DHLWG Colloids in TSPA-LA Calculations

Radionuclide	Value Range (mol/L)	Probabilities
Pu	10^{-11} to 10^{-8}	Uniform

Evidence from other DHLWG tests demonstrates that plutonium, thorium, and americium behave similarly (DTNs: MO0407ANLGNN02.608 [DIRS 171277], LL000123351021.117 [DIRS 143308]; Bates et al. 1992 [DIRS 100704]). As the plutonium concentration used in the DHLWG tests is similar to the highest anticipated concentrations in high-level waste production glasses, these results are directly relevant to establishing colloid-associated plutonium concentrations. The effect of the plutonium content from the weapons plutonium disposition lanthanum borosilicate (LaBS) glass on the total plutonium colloid concentration is unclear. The blended composition is likely to have a concentration similar to that used in ^{239}Pu-doped tests on R7T7 reported by Pirlet (2001 [DIRS 174351]) and Ménard et al. (1998 [DIRS 171053]).

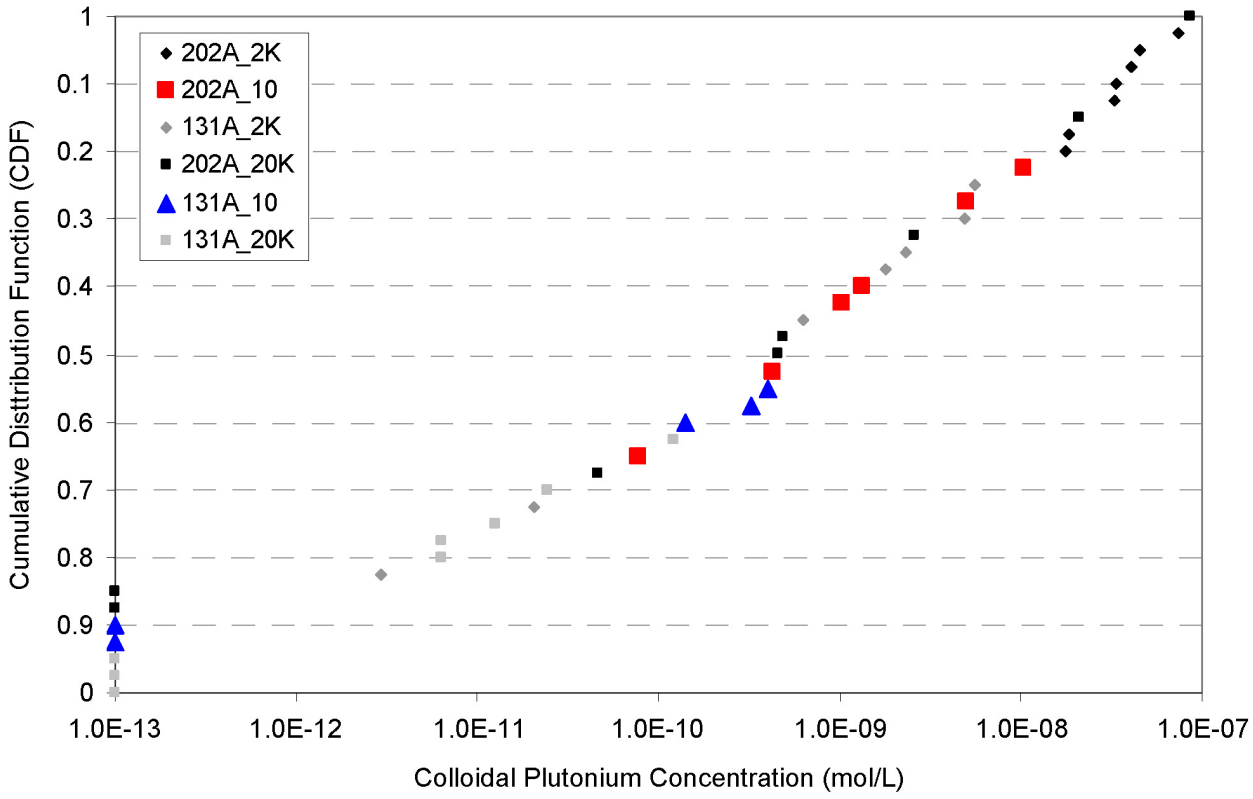

Source: Table 6-5 for the colloidal plutonium concentration data (i.e., abscissa values). Probabilities plotted along the ordinate are based on each abscissa value having the same probability (i.e., 1/n where n is the number of samples given in Table 6-5).

NOTE: Plutonium-bearing colloid concentration (units = mol/L) as a cumulative distribution function for corrosion tests on glass samples SRL 202A and SRL 131A of S_A/V of 10 m^{-1}, 2,000 m^{-1}, and 20,000 m^{-1} (at 90°C). Because monolith tests may represent waste form conditions more accurately, the model distribution was developed based on the 10 m^{-1} tests (202A_10 and 131A_10).

Figure 6-7. Cumulative Distribution of Plutonium Colloid Concentration from DHLWG Corrosion Tests with Monolith Results in Large Symbols (i.e., red squares and blue triangles)

Table 6-5. Plutonium Colloid Concentrations Obtained from Immersion Tests on DHLWG

Test Duration (days)	Test Description	Silicon Concentration, (mol/L) [(a)]	Cation Concentration (mol/L) [(b)]	Colloidal Plutonium Concentration (mol/L) [(c)]
14	131A_20K	4.44E-02	ND	1.21E-10
28	131A_20K	4.44E-02	ND	1.25E-11
56	131A_20K	5.01E-02	ND	6.28E-12
98	131A_20K	5.45E-02	ND	2.43E-11
182	131A_20K	5.92E-02	7.20E-01	1.00E-13
364	131A_20K	ND	ND	6.28E-12
552	131A_20K	ND	ND	1.00E-13
728	131A_20K	ND	ND	1.00E-13
14	131A_2K	6.72E-03	1.20E-02	1.80E-09
30	131A_2K	7.11E-03	ND	2.34E-09
70	131A_2K	9.36E-03	ND	5.61E-09
140	131A_2K	9.01E-03	2.00E-02	4.85E-09
280	131A_2K	1.50E-02	4.10E-02	6.28E-10
560	131A_2K	2.06E-02	7.00E-02	2.05E-11
980	131A_2K	2.00E-02	9.10E-02	2.93E-12
238 [(d)]	131A_10	1.94E-03	2.13E-03	1.00E-13
601 [(d)]	131A_10	2.87E-03	3.06E-03	1.00E-13
601 [(d)]	131A_10	3.47E-03	3.81E-03	1.40E-10
1404 [(d)]	131A_10	2.32E-03	2.17E-03	4.03E-10
1404 [(d)]	131A_10	2.60E-03	2.69E-03	3.26E-10
238 [(d)]	202A_10	2.03E-03	1.92E-03	3.90E-11
1416 [(d)]	202A_10	1.96E-03	1.74E-03	5.22E-09
1416 [(d)]	202A_10	2.29E-03	1.93E-03	2.50E-09
14	202A_2K	3.51E-03	4.40E-03	1.76E-08
30	202A_2K	4.38E-03	5.60E-03	7.49E-08
70	202A_2K	5.27E-03	6.50E-03	4.10E-08
140	202A_2K	5.36E-03	7.50E-03	1.84E-08
280	202A_2K	6.41E-03	8.60E-03	4.56E-08
560	202A_2K	7.88E-03	1.10E-02	3.35E-08
980	202A_2K	8.14E-03	ND	3.26E-08
14	202A_20K	1.17E-02	ND	8.66E-08
28	202A_20K	1.28E-02	2.40E-02	2.09E-08

Table 6-5. Plutonium Colloid Concentrations Obtained from Immersion Tests on DHLWG (Continued)

Test Duration (days)	Test Description	Silicon Concentration, (mol/L) [(a)]	Cation Concentration (mol/L) [(b)]	Colloidal Plutonium Concentration (mol/L) [(c)]
56	202A_20K	1.39E-02	2.80E-02	2.59E-09
98	202A_20K	1.88E-02	3.30E-02	4.85E-10
182	202A_20K	1.81E-02	4.30E-02	4.60E-10
364	202A_20K	4.90E-02	3.30E-01	4.60E-11
504	202A_20K	5.30E-02	6.00E-01	1.00E-13
728	202A_20K	6.17E-02	8.70E-01	1.00E-13

(a) DTN: LL000905312241.018 [DIRS 152621] (MOL.20001130.0021, pp.29 and 30) unless noted otherwise on the "Test Duration" value in the first column.

(b) DTN: LL991109751021.094 [DIRS 142910] (MOL.20000124.0207, p.27) unless noted otherwise on the "Test Duration" value in the first column.

(c) DTN: LL000905312241.018 [DIRS 152621] (MOL.20001130.0021, p. 70) unless noted otherwise on the "Test Duration" value in the first column.

(d) DTN: MO0705ANLGSV01.258 [DIRS 181399] as derived within Output DTN: MO0705COLCONCS.000.

NOTE: ND = not determined or used in the analyses.

6.3.2.3 Stability of Montmorillonite Colloid Suspensions as a Function of pH and Ionic Strength

The stability of DHLWG (smectite) waste form colloids is determined from a quadratic relationship showed in Figure 6-8 . The quadratic relationship was derived as a fit to the DLVO model results using standard Excel fitting routines. The relationship describes the stability of smectite colloids as a function of pH (valid between pH 1.5 and 9). There is assumed to be no change in the ionic strength threshold, $I_{threshold}$, above pH 9. There is no effective zero point of charge for smectite but it is reasonable to suggest a value between 1 and 1.5, below which clay colloids would be unlikely to exist. Experimental data reported by Tombácz et al. (1990 [DIRS 112690], Figure 3, p. 77), Sondi et al. (1996 [DIRS 170928], Figure 6, p. 518), and Kraepiel et al. (1999 [DIRS 180997], Figure 5, p. 50) do not show results for montmorillonite below pH 2.

Tombácz et al. (1990 [DIRS 112690]) investigated the stability of montmorillonite clay colloid suspensions as a function of pH and ionic strength in NaCl solution. It was found that suspensions became unstable and flocculated at pH 2, 4, and 8 in 0.1 M (100 mmol/dm^3), ~0.225 M (200 to 250 mmol/dm^3), and ~0.375 M (350 to 400 mmol/dm^3) NaCl solutions, respectively. In this model, DLVO theory was applied using the applicable van der Waals and repulsive energy terms for plate-like particles. Although Figure 6-8 shows that there are large changes in the surface charge with ionic strength for montmorillonite, these variations were incorporated into the $W = 10$ calculation for colloid stability (see Output DTN: MO0705CSIONSTH.000). The solution to when $W = 10$ is unique for a particular pH as there cannot be two ionic strengths where $W = 10$ at a fixed pH. The potential is a linear interpolation between values of ionic strength shown on Figure 6-8. For instance, at a certain pH and ionic strength of 70 mM, the surface potential is described as: $\zeta_{70mM} = \zeta_{40mM} + (\zeta_{100mM} - \zeta_{40mM}) \times (70 - 40)/(100 - 40)$.

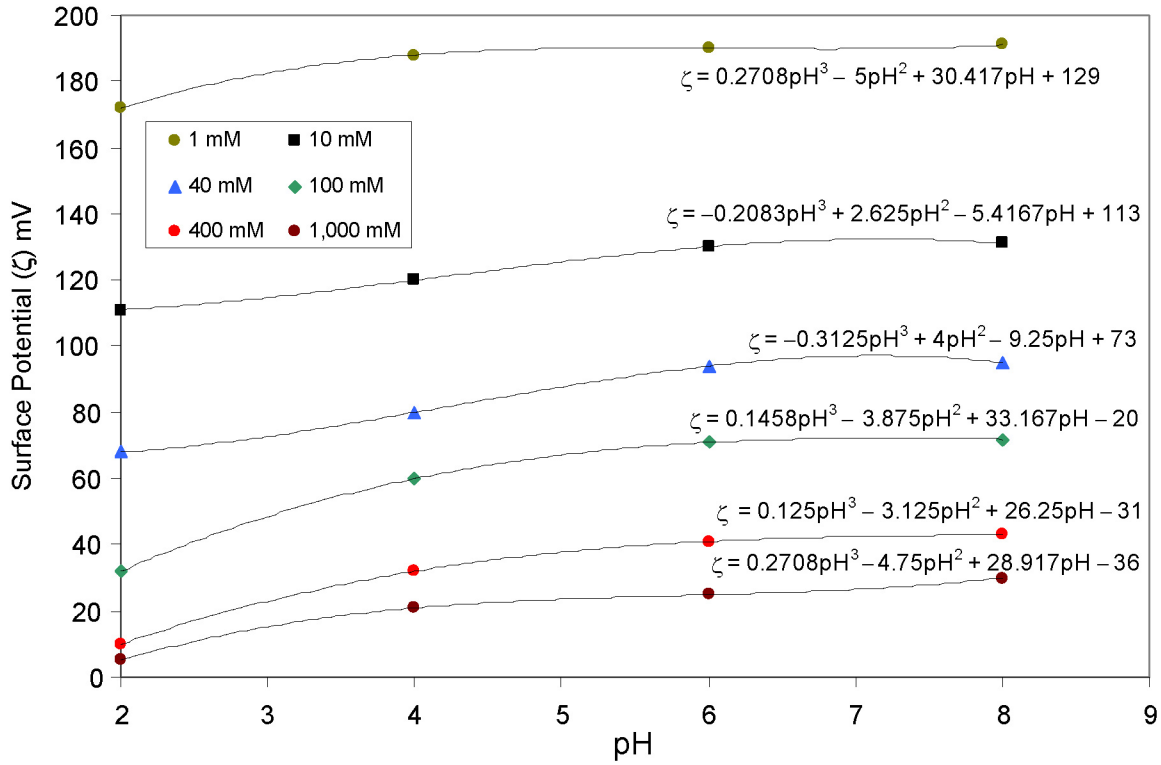

Source: Output DTN: MO0705CSIONSTH.000.

NOTE: Data was extracted by visual inspection of Figure 3 from Tombácz et al. (1990 [DIRS 112690], p. 77). The fits to the variation in zeta potential with ionic strength were made by standard functions in Excel. The polynomial fitting equations are shown on the figure. The interpolation method is described in the text below that allows determination of the surface charge at any pH for the DLVO model.

Figure 6-8. Experimental Zeta Potential with pH at Different Ionic Strengths for Montmorillonite

Figure 6-9 describes the DLVO model prediction using a Hamaker constant taken from Tombácz et al. (1990 [DIRS 112690], Figure 4, p. 78; Hamaker constant, A, reported in Joules), a quadratic fit to the model, and data reported by Tombácz et al. (1990 [DIRS 112690]). The developed model fit (see Equation 6-9) bounds the experimental data and the DLVO prediction (see Figure 6-9 and Output DTN: MO0705CSIONSTH.000).

$$I_{threshold} = (-0.008 \times pH^2) + (0.12 \times pH) - 0.03 \qquad \text{(Eq. 6-9)}$$

If $pH_{wp,inv} > 9$, then the $I_{threshold}$ value calculated at pH 9 is used, and if $pH_{wp,inv} < 1.5$, then colloids are assumed to be unstable. Tombácz et al. (1990 [DIRS 112690]) did not report stability ratios, so the data points represent points where colloids were not observed. This can be inferred as points where $W = 1$. This may account for the values being lower than the model fit. Nevertheless, the experimental data is bounded by the DLVO approach used for the model.

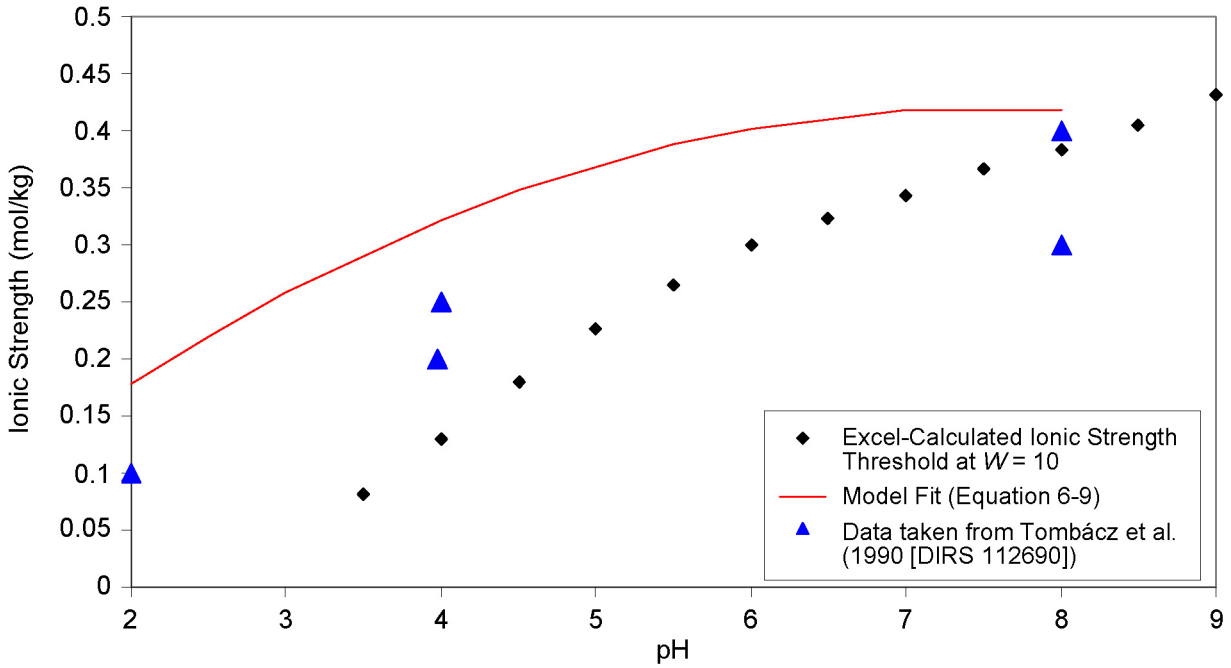

Source: Output DTN: MO0705CSIONSTH.000.

Figure 6-9. Plot Showing the DLVO-Calculated Stability of Montmorillonite Colloids at $W = 10$ with a Quadratic Fit (Equation 6-9) of the DLVO Model and Showing the Experimental Values from Tombácz et al. (1990 [DIRS 112690])

The range of chemical conditions in the laboratory testing represents a subset of the conditions expected in the repository. The pH in product consistency tests depends on the alkali borosilicate glass reaction and is not controlled (Buck and Bates 1999 [DIRS 109494]). The pH range anticipated in the waste-form and drift environments for the majority of the time is expected to be between 4.5 and 8.1. Since the pH never drops below 7 during the reaction of water with alkali borosilicate waste glass (Bates et al. 1995 [DIRS 170880], Figure 2c, p. 25; Figure 4c, p. 28; Figure 6c, p. 30; Figure 7c, p. 32; Figure 8c, p. 33; Figure 9c, p. 34; Figure 10c, p. 35), the range of expected conditions is adequately represented.

6.3.2.3.1 Surface Area of Montmorillonite Colloids

Pabalan and Turner (1996 [DIRS 179555]) used a surface area for montmorillonite of 9.7 m^2/g, which was 10% of the Brunauer-Emmett-Teller (BET) measured surface area. This value accounts for sorption of radionuclides at edge sites and has been used successfully in modeling the sorption of uranium on montmorillonite. However, as cesium and radium are likely to sorb at interlayer sites, the range for smectite clay surface area has been increased. Furthermore, based on images from corroded DHLWG (see Buck and Bates 1999 [DIRS 109494] and Figure 6-19a and c), it is reasonable to increase the expected surface area for clays to 10 to 100 m^2/g.

The site density for smectite clay (2.3 sites/nm^2) is based on recommended values used by Pabalan and Turner (1996 DIRS 179555]) in surface complexation modeling. The surface area and the site density are utilized in the sorption capacity model component as described in Section 6.3.12.3.

6.3.2.4 Irreversible Colloids from Corroded CSNF

The plutonium concentration for CSNF was obtained from data obtained by Wilson (1990 [DIRS 100793]). The data ranged from 1×10^{-12} to 1×10^{-6} mol/L plutonium (see Table 6-6a). Because of the potential unknown interference of metallic components in the tests, the range was biased towards the bare fuel tests which resulted in a range of concentrations from 1×10^{-10} to 5×10^{-6} mol/L. The empirical cumulative distribution function is shown in Figure 6-10.

Table 6-6a. Plutonium Colloid Concentrations Obtained from Immersion Tests on SNF

A.2	HBR/BF-25					
Time (days)	Vol. (mL)	0.4 μm (pCi)	1.8 nm (pCi)	Colloid (pCi)	[Pu] (moles/L)	log [Pu] (mol/L)
1	15	1.23E+04	6.62E+03	5.68E+03	2.51E-07	−6.60017
7	15	8.29E+03	3.90E+03	4.39E+03	1.94E-07	−6.71205
14	20	6.40E+03	2.85E+03	3.55E+03	1.57E-07	−6.80429
33	30	2.94E+03	8.58E+02	2.08E+03	9.20E-08	−7.03603
62	30	1.91E+03	4.48E+02	1.46E+03	6.46E-08	−7.18957
119	30	1.23E+03	2.31E+02	9.99E+02	4.42E-08	−7.35495
174	250	9.14E+02	1.75E+02	7.39E+02	3.27E-08	−7.48587
A.3	TP/BF-85					
1	15	2.59E+03	1.20E+02	2.47E+03	1.06E-07	−6.97516
7	15	5.32E+02	6.08E+01	4.71E+02	2.02E-08	−7.69465
14	20	3.88E+02	9.55E+01	2.93E+02	1.25E-08	−7.90173
33	30	6.76E+01	3.60E+01	3.16E+01	1.35E-09	−8.86817
62	30	1.35E+01	1.44E+01	−9.00E-01	−3.86E-11	NULL
119	30	4.50E+00	4.23E+00	2.70E-01	1.16E-11	−10.9365
174	250	4.05E+00	1.35E+00	2.70E+00	1.16E-10	−9.93649
A.4	HBR/BF-85					
1	15	1.97E+04	7.48E+02	1.90E+04	8.38E-07	−6.07686
7	15	3.68E+03	3.18E+02	3.36E+03	1.49E-07	−6.82792
14	20	1.45E+03	1.91E+02	1.26E+03	5.57E-08	−7.25449
33	30	4.82E+03	1.40E+02	4.68E+03	2.07E-07	−6.68427
62	30	9.28E+02	1.20E+02	8.08E+02	3.57E-08	−7.4471
119	30	9.05E+02	1.31E+00	9.04E+02	3.99E-08	−7.3985
174	250	6.76E+00	9.01E-02	6.67E+00	2.95E-10	−9.5304
A.5	HBR/SD-85					
7	15	2.25E-01	2.25E-01	0.00E+00	0.00E+00	NULL
14	20					
33	30	3.15E-01	2.70E-01	4.50E-02	1.99E-12	−11.7013
119	30	1.26E+00	2.70E-01	9.90E-01	4.38E-11	−10.3589
174	250	1.35E-01	1.35E-01	0.00E+00	0.00E+00	NULL

Table 6-6a. Plutonium Colloid Concentrations Obtained from Immersion Tests on Spent Nuclear Fuel (Continued)

A.6	**HBR/HD-85**					
62	30	1.80E-01	9.01E-02	8.99E-02	3.97E-12	−11.4008
A.7	**HBR/UD-85**					
119	30	5.41E-01	2.70E-01	2.71E-01	1.20E-11	−10.9215

Source: Wilson 1990 [DIRS 100793], Appendices A1 through A7.

NOTE: BF = bare fuel; HBR = H.B. Robinson fuel; HD = hole defect; SD = slit defect; TP = Turkey Point fuel; UD = no defect. Activities reported for plutonium as $^{239+240}$Pu (pCi/mL) from cycle 1. Conversion for HBR is $4.42064 \times 10^{-11} = 0.374*0.0000163/0.577/1000/239$. Conversion for TP is $4.28691 \times 10^{-11} = 0.374*0.0000163/0.595/1000/239$. Example calculation (A.7, 119 days): Pu colloid = 5.41E-01 − 2.70E-01 = 2.71E-01. This is multiplied by 4.42064×10^{-11} to obtain the concentration listed in the last column of Table 6-6a.

An empirical cumulative distribution function was developed to accommodate the variable plutonium colloid concentrations and the uncertainty in testing configurations for CSNF corrosion tests (see Table 6-6b). This allowed for stochastic sampling of the parameter, $C_{RNcoll,SNF,embed,sampled}$, with a median plutonium concentration of $\sim 5 \times 10^{-8}$ mol/L, while probabilistically allowing for the selection of much lower concentrations (i.e., 1×10^{-10} mol/L) which bounded studies to be used in validation to be described in the report.

Table 6-6b. Distribution of Plutonium Colloid Concentration Values (mL/g) and Cumulative Probabilities Used for SNF Colloids in TSPA-LA Calculations

Radionuclide	Value Range (mol/L)	Value Intervals (mol/L)	Cumulative Probabilities
Pu	1×10^{-10} to 5×10^{-6}	1×10^{-10} to 5×10^{-10}	0.05
		5×10^{-10} to 1×10^{-9}	0.10
		1×10^{-9} to 5×10^{-9}	0.15
		5×10^{-9} to 1×10^{-8}	0.20
		1×10^{-8} to 5×10^{-8}	0.30
		5×10^{-8} to 1×10^{-7}	0.50
		1×10^{-7} to 5×10^{-7}	0.70
		5×10^{-7} to 1×10^{-6}	0.90
		1×10^{-6} to 5×10^{-6}	1.00

NOTE: Concentration of Am to be computed from inventory.

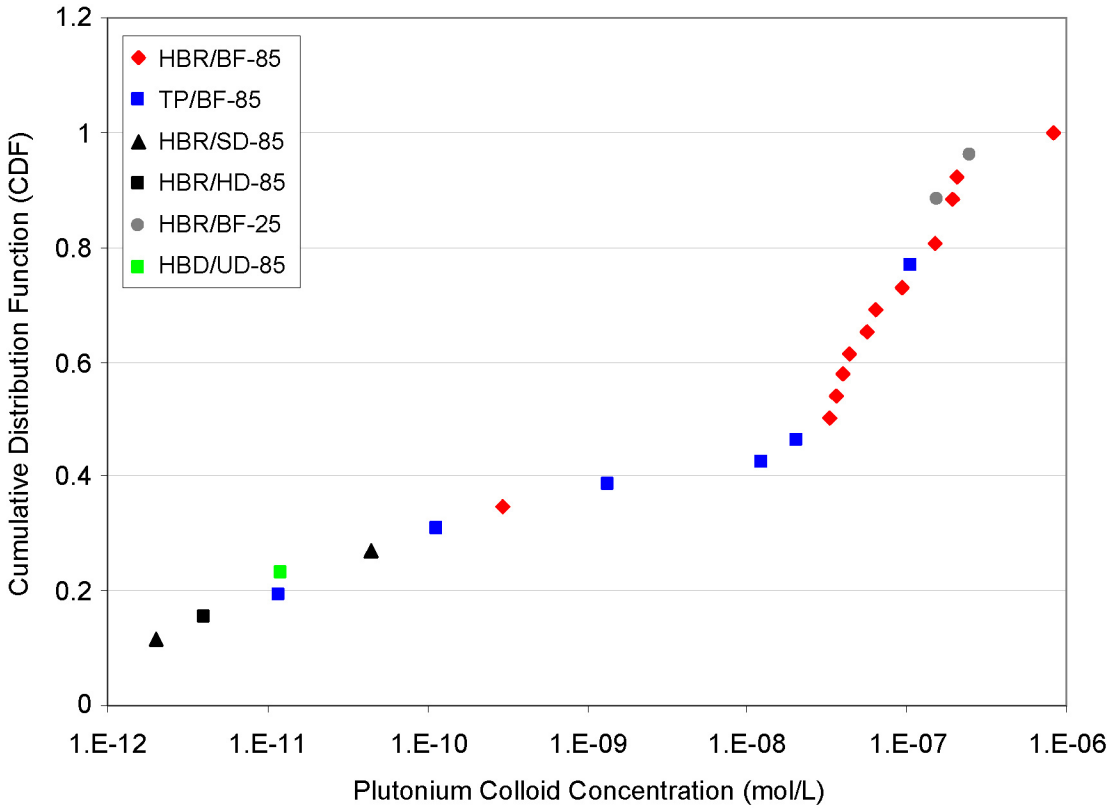

Source: Adapted from Wilson 1990 [DIRS 100793], Appendix A and Table 6-6a.

NOTE: Plutonium colloid concentration (>1.8-nm and <400-nm size fraction from filtration data) for several types of low-burnup spent nuclear fuels. All tests conducted at 85°C except HBR/BF-25, which was conducted at 25°C. HBR = H.B. Robinson fuel (30.2 MWd/KgM); TP = Turkey Point fuel (27.7 MWd/KgM); BF = bare fuel; SD = slit defect; HD = hole defect; UD = no defect.

Figure 6-10. Cumulative Distribution of Concentrations of Plutonium Colloids from SNF Corrosion Tests

Calculation of the mass concentration (mg/L) of waste form colloids from SNF was done by sampling a cumulative distribution based on experimental data and scaling to 1 ppm as follows:

$$C_{RNcoll,SNF,embed,uniform,\ max} = 1 \times 10^{-6}\ \text{mol/L Pu}$$
$$C_{RNcoll,SNF,embed,uniform,\ min} = 5 \times 10^{-7}\ \text{mol/L Pu.}$$

The minimum concentration, $C_{RNcoll,SNF,embed,min}$, is a fixed value of 1×10^{-13} mol/L.

Analysis of plutonium-bearing solids from corrosion tests, including dynamic flow-through and drip tests, suggests that the plutonium is located in nanocrystalline particles that also contain americium, rare earths, zirconium, and some uranium. The surface properties of this material are likely to be similar to ZrO_2 as one of the major oxides in this corrosion rind is zirconium oxide. By extracting colloidal zirconium oxide (ZrO_2) zeta potential data presented in a figure from Bitea et al. (2003 [DIRS 174504], Figure 3, p. 59) (see Output DTN: MO0705CSIONSTH.000 and Figure 6-11 in this report), a stability plot as a function of pH and ionic strength using DLVO theory could be developed (see Figure 6-12). The data from Bitea et al. (2003 [DIRS 174504]) was used to develop a fit that allowed estimation of the surface charge at any pH (see Figure 6-11 and inserted equation for ζ_{ZrO_2}).

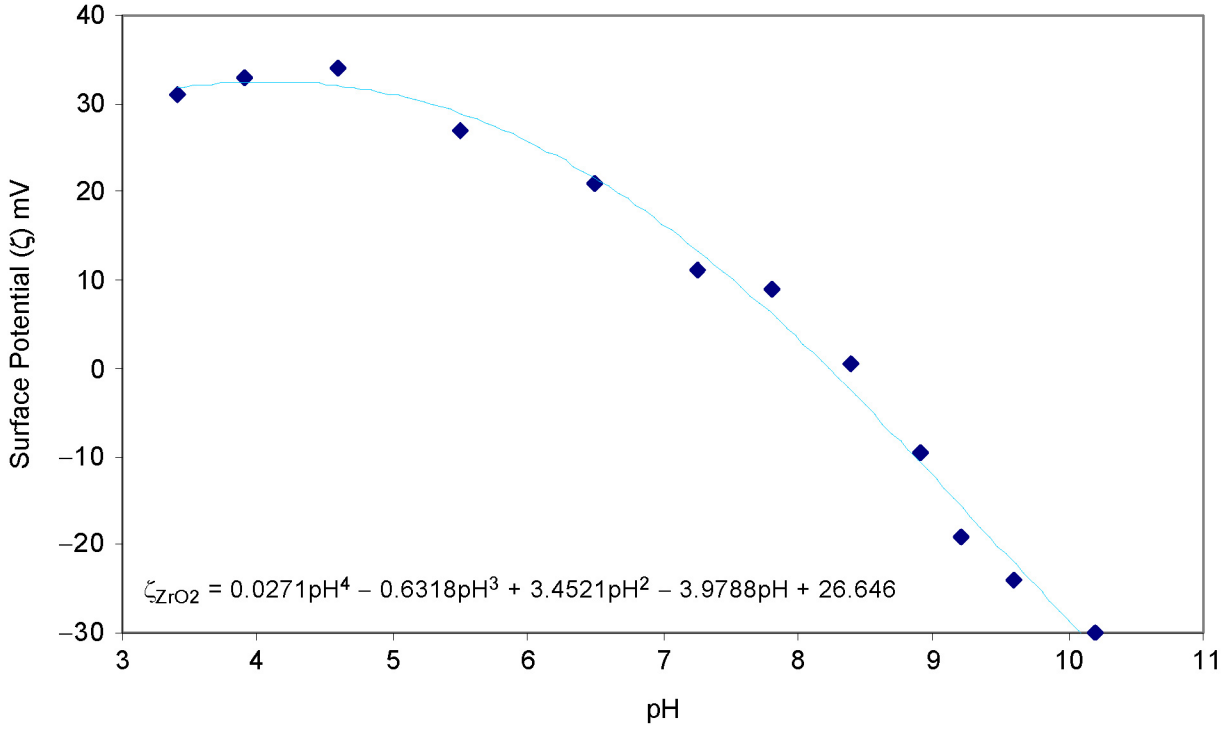

Source: Output DTN: MO0705CSIONSTH.000.

NOTE: Polynomial equation shown on figure was obtained with Excel fitting routines. Experimental points obtained by visual inspection of Figure 3 from Bitea et al. (2003 [DIRS 174504], p. 59).

Figure 6-11. Measured Variation in Zeta Potential with pH at an Ionic Strength of 0.001 mol/kg for ZrO_2

The stability of CSNF ("ZrO_2") colloids is shown in Figures 6-12a and 6-12b. The ionic strength threshold to pH relationship was generated with a polynomial fit to the DLVO theoretical curve. It is important to note that the curve is a purely mathematically fit and has no physical meaning. If the reported ionic strength in the waste package (I_{wp}) is less than the value ($I_{threshold}$) calculated from input pH in the waste package (pH_{wp}) using the polynomial relationships described, the irreversible SNF colloids will be defined as stable.

Between pH 7 and 9.3, the irreversible CSNF colloids are unstable irrespective of the ionic strength.

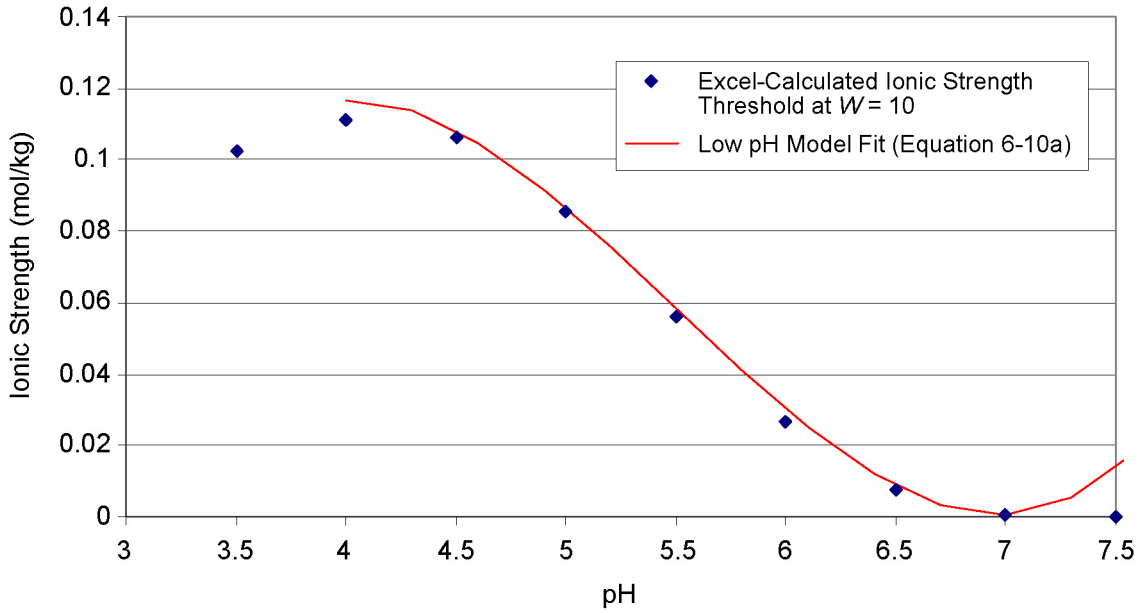

Source: Output DTN: MO0705CSIONSTH.000.

Figure 6-12a. Calculated DLVO Stability Plots with Polynomial Fit (Equation 6-10a) to the DLVO Model for ZrO_2 Colloids Suspension at Low pH

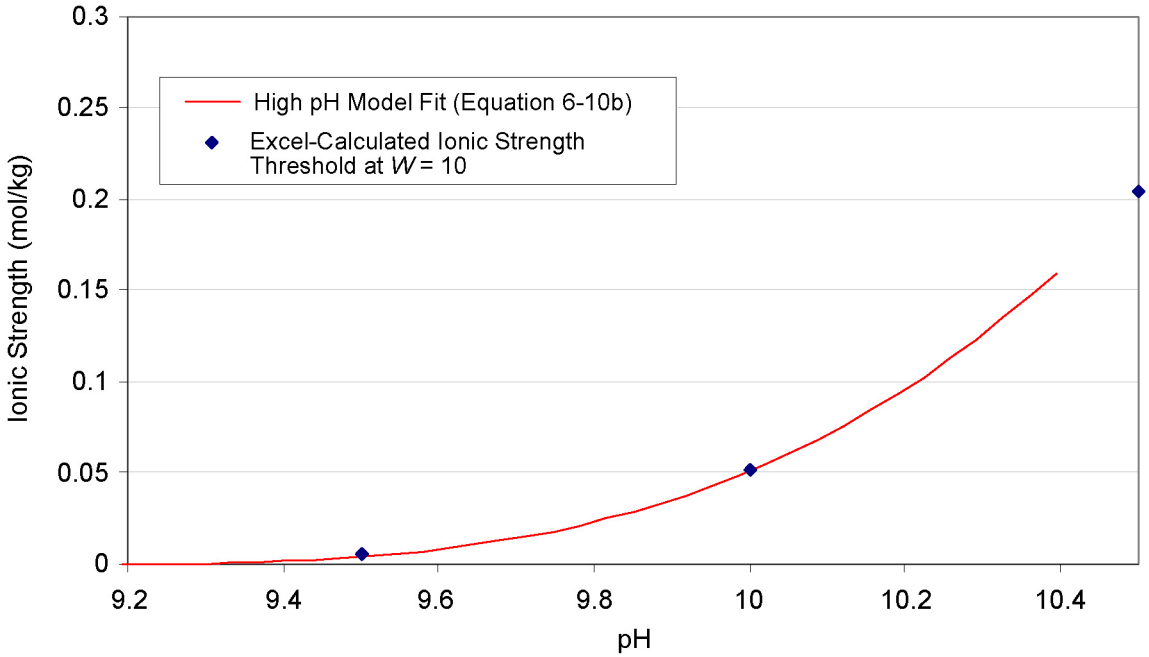

Source: Output DTN: MO0705CSIONSTH.000.

Figure 6-12b. Calculated DLVO Stability Plots with Polynomial Fit (Equation 6-10b) to the DLVO Model for ZrO_2 Colloids Suspensions at High pH

When the pH is between 4 and 7, the following relationship is used based on the fit shown in Equation 6-10a (see Output DTN: MO0705CSIONSTH.000).

$$I_{threshold} = (0.0089 \times pH^3) - (0.1466 \times pH^2) + (0.7462 \times pH) - 1.092 \quad \text{(Eq. 6-10a)}$$

When the pH > 9.3, Equation 6-10b is used:

$$I_{threshold} = (0.087362 \times pH^3) - (2.4078 \times pH^2) + (22.126 \times pH) - 67.791 \quad \text{(Eq. 6-10b)}$$

If the pH is < 4.0, the $I_{threshold}$ value that was calculated at pH 4.0 is used, and if the pH > 10.6, the $I_{threshold}$ value calculated at pH 10.6 is used.

To calculate the total mass of CSNF colloids, the following relationship is applied:

$$M_{coll,SNF} = 1 \text{ (mg/L)} \times C_{RNcoll,SNF,embed,\ sampled} \div C_{RNcoll,SNF,embed,uniform}$$

The concentration of irreversibly sorbed Am is computed by determining the fraction of this element present compared to plutonium in the inventory at each time-step in TSPA.

6.3.2.5 Reversible Colloids from Corroded CSNF and DSNF

Wilson (1990 [DIRS 100793]) observed acicular particles of uranophane $\{Ca(UO_2)_2(SiO_3OH)_2(H_2O)_5\}$ on filters collected from corrosion tests on SNF with J-13 well water. In static tests on CSNF in deionized water, McNamara et al. (2005 [DIRS 174068], p. 171) reported the occurrence of suspended particles of metastudtite ($UO_4 \bullet 2H_2O$). Buck et al. (2004 [DIRS 171479]) reported the presence of meta-schoepite attached to larger UO_2 particles in immersion tests on crushed and sieved UO_2. Any U(VI) oxide hydrate phase that forms initially from the reaction of SNF and water would be anticipated to be thermodynamically unstable with respect to a silica-bearing groundwater. U(VI) silicates will form if the SNF is contacted with a silica-bearing solution and these phases may be the most likely to form colloids as they would be thermodynamically stable in the groundwater. Uranophane could be thermodynamically stable in the Yucca Mountain groundwater environment (Finch and Ewing 1992 [DIRS 113030]), but colloidal uranophane transport remains uncertain. Colloidal uranophane particles may be subject to dissolution in deionized water. Mertz et al. (2003 [DIRS 162032]) examined the stability of meta-schoepite $\{[(UO_2)_4O(OH)_6](H_2O)_5\}$ and UO_{2+x} colloid suspensions after introduction to sodium silicate-bearing (J-13) groundwater and obtained a pH_{pzc} ranging between 2 and 5. Schindler et al. (2004 [DIRS 174507], Equations 11 and 12, p. 1642) calculated the pH_{pzc} values of faces and edges of schoepite and dehydrated schoepite using a rigorous valence bond approach that took account of the structure of these phases. The (001) faces of schoepite and dehydrated schoepite were shown to have pH_{pzc} value of 7.02 and 6.1, respectively, and the edges of these uranyl oxide hydrate minerals were shown to have pH_{pzc}'s between 6.5 and 7.1. Mertz et al. (2003 [DIRS 162032], Figure 10, p. 41) observed a reduction in colloid size and 84% of the uranium was found to be in the dissolved fraction; the absence of precipitated U(VI) silicates and the high proportion of dissolved uranium concentration might suggest that the solution was undersaturated with respect to both schoepite and uranophane. One important consideration in these studies is the morphology of U(VI) phases formed, which depends strongly on pH, presence of other mineral surfaces, and temperature (Schindler et al. 2004

[DIRS 174507]). Morphology may also affect dissolution of the phases and the sorption of radionuclides by changing the nature of the surface of the phase.

In Figure 6-13, the measured variation in zeta potential with pH for meta-autunite colloids reported by Zheng et al. (2006 [DIRS 179565]) is shown. A mathematical fit was made to the available data to allow the determination of a surface charge at any pH for the development of the stability ratio using the DLVO approach. The reasons for selecting meta-autunite to represent uranophane are discussed in Assumption 5.6.

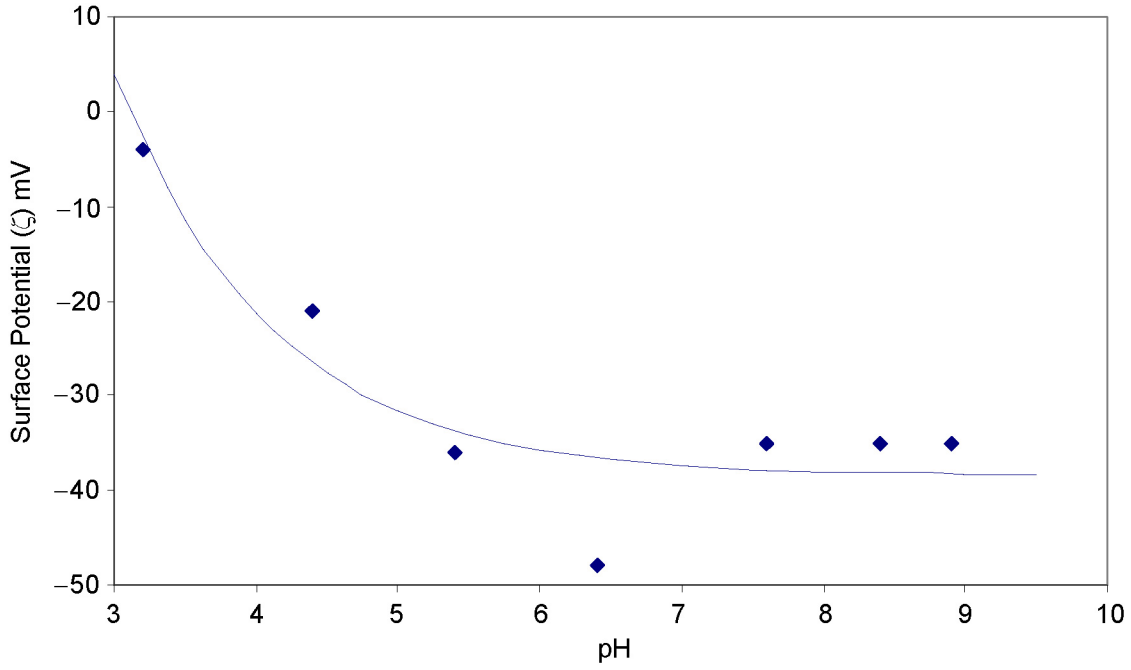

Source: Output DTN: MO0705CSIONSTH.000.

NOTE: The values were obtained by visual inspection of Figure 7b from Zheng et al. (2006 [DIRS 179565], p. 59). The fit to the experimental points was $\zeta_{autunite}(mV) = -38.5012 + 13395 \times \exp[-0.904308 \times (pH + 3.36097)]$, which allows estimation of the surface charge at a pH of interest.

Figure 6-13. Experimental Zeta Potential with pH at Different Ionic Strengths for Meta-Autunite

The stability of U(VI) phase (uranophane) colloids derived from degradation of CSNF and DSNF is determined on the basis of in-package pH and ionic strength (see Figure 6-14). The ionic strength threshold to pH relationship for the uranophane particles was generated with a quadratic fit to the DLVO theoretical curve.

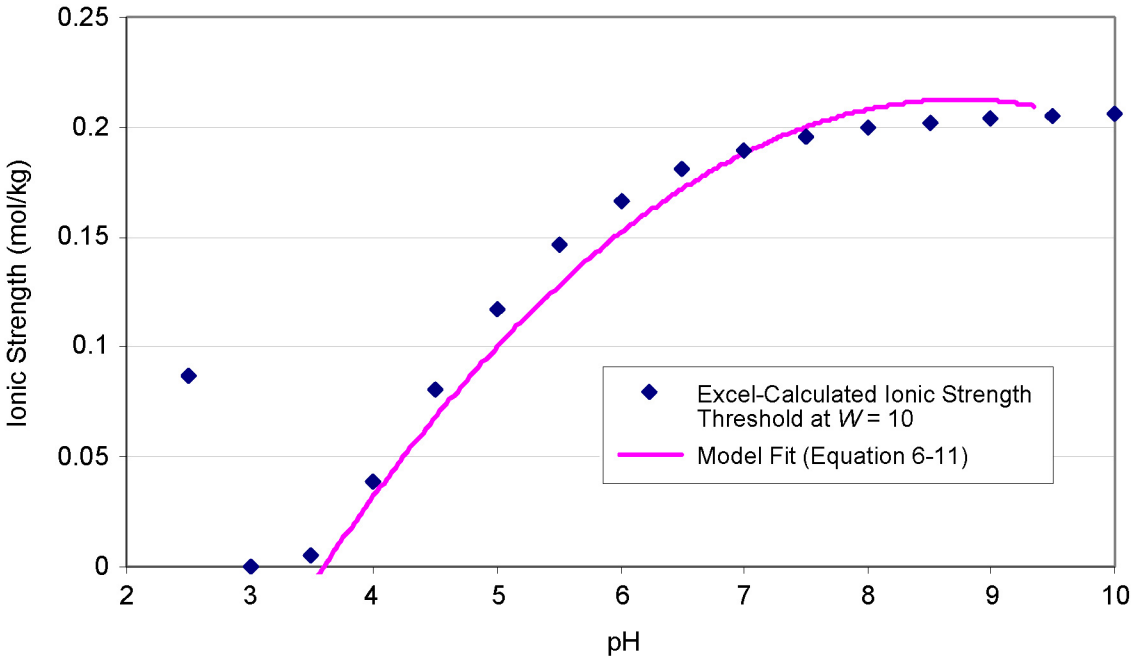

Source: Output DTN: MO0705CSIONSTH.000.

Figure 6-14. Calculated Stability Plots with a Polynomial Fit (Equation 6-11) to the DLVO Model for Uranophane Colloid Suspensions

The model fit (see Equation 6-11) indicates that the U(VI) particles should be stable under most in-package conditions (see Output DTN: MO0705CSIONSTH.000). The ionic strength above which the colloids are deemed unstable is termed $I_{threshold}$, and is defined as:

$$I_{threshold} = -(0.008 \times pH^2) + (0.14 \times pH) - 0.4 \qquad \text{(Eq. 6-11)}$$

Equation 6-11 is a mathematical fit obtained with Excel, which does not convey any physical meaning but allows the determination of the conditions that would favor stable U(VI) particles between a limited pH range of interest to the anticipated repository conditions.

6.3.2.6 Concentration of Reversible DSNF and Reversible CSNF Colloids

The concentration of uranophane colloids from CSNF and DSNF was based on judgment of the analogous behavior of uranophone to natural smectite colloids such that a conservative model distribution was developed. To provide confidence in this model distribution, the information regarding relevant experimental data on uranophane colloids from UO_2 flow testing is discussed below for comparison. The selection of this distribution was based on comparison with commonly observed colloid population distributions of groundwater colloids that are dominated by smectite clay particles. As the uranophane colloids exhibited a stability profile similar to that calculated for smectite colloids, it is reasonable to use a similar population distribution. Unsaturated UO_2 intermittent flow tests reported by Wronkiewicz et al. (1996 [DIRS 102047]) were then used to examine the reasonableness of this distribution. These tests did not provide data directly on colloids at all sampling periods; however, uranophane-type colloids were observed in some of the test leachates. Experiments conducted after eight years underwent

filtration. It was found that <2% of the material passed through a 5-nm filter. Most of the U was associated as plate out (86% to 97%). In these filtered materials, 1% to 12% was 5 nm and may be defined as both colloidal and suspended Uranium particulate. Microscopic analysis proved the occurrence of larger suspended particles (i.e., larger than colloidal) within this set of material; hence a range of 2% to 5% was chosen for this analysis. In Figure 6-15, a cumulative distribution of the mass of uranophane particles based on data from Wronkiewicz et al. (1996 [DIRS 102047]) is shown. The distribution was obtained by assuming that, based on the above discussion, 2% to 5% of the total released uranium was due to colloidal uranophane particles (mwt = 856.331 g) (see Table 6-7). The distribution shown in Figure 6-15 is bounded by the distribution shown in Table 6-8; nevertheless, it is likely that a fraction of the colloidal material may have been greater than 1 μm in length, which would have contributed significantly to the total suspended mass.

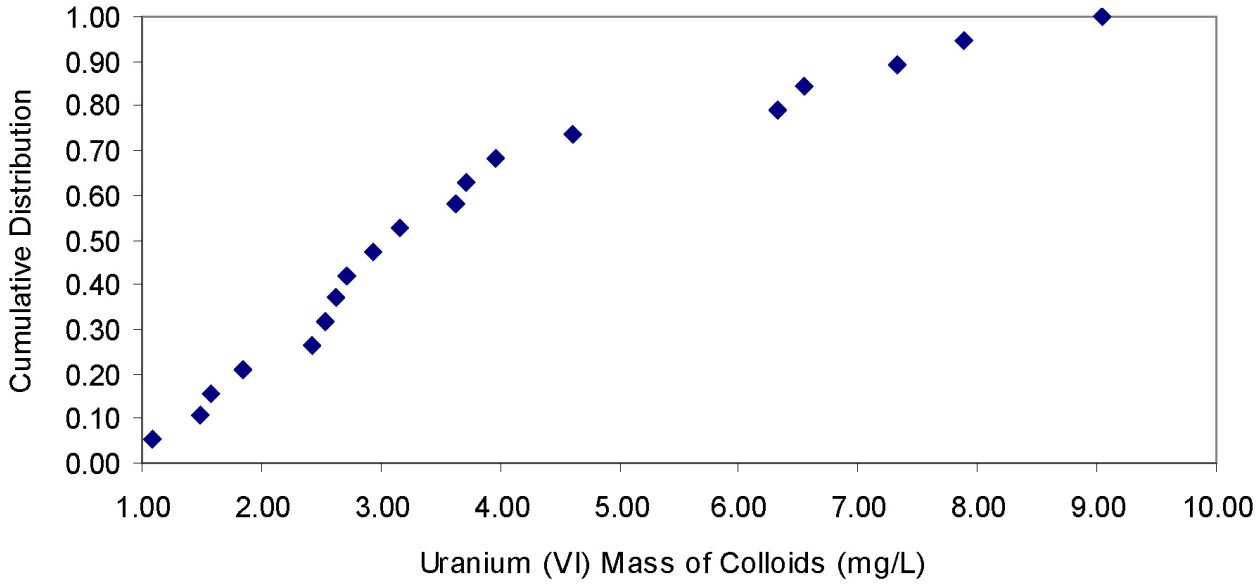

Source: Output DTN: MO0705DSCSCUSS.000.

NOTE: Experiments conducted after eight years underwent filtration. It was found that <2% of the material passed through a 5-nm filter. Most of the U was associated as plate out (86% to 97%). 1% to 12% was 5 nm and may be defined as both colloidal and suspended particulate. Microscopic analysis proved the occurrence of these larger suspended particles; hence a range of 2% to 5% was chosen for this analysis.

Figure 6-15. Distribution of Colloidal Mass from 8- to 10-year Testing of UO_2 under Unsaturated Conditions Assuming That 2% to 5% of Released Uranium Is from Uranophane Colloids

Table 6-7. Concentration of Released Uranium from Unsaturated Drip Tests

Weeks	Experiment 2		Experiment 3		Experiment 6		Experiment 7	
	Sol. Vol (mL)	Total U (μg)	Sol. Vol (mL)	Total U (μg)	Sol. Vol (mL)	Total U (μg)	Sol. Vol (mL)	Total U (μg)
417	4.47	325	5.88	301	5.98	162	1.88	56.8
469	ND	ND	4.24	298	4.80	198	1.58	159.0
521	ND	ND	3.54	288	4.06	356	1.31	57.6

Source: Wronkiewicz et al. 1996 [DIRS 102047], Table 1, p. 80.

NOTE: ND = not determined.

The colloid mass ($M_{coll,uranophane}$) range obtained from the experiments by Wronkiewicz et al. (1996 [DIRS 102047]) is within the bounds set by using the groundwater distribution for the uranophane colloids.

The uranophane colloidal mass was estimated from the distribution shown in Table 6-8. Only reversible sorption onto these colloids is modeled using K_d values that describe the distribution of radionuclides between the fluid and the U(VI) phase (uranophane) colloids. Calculation of the mass concentration of reversible SNF (uranophane) colloids is done by sampling the distribution in cases where uranophane colloids are stable, otherwise the minimum value given in the note to Table 6-8 should be applied in cases where this colloid type is not stable.

Table 6-8. Uncertainty Distribution for Stable Uranophane Colloids from Corroded CSNF and DSNF

Uranophane Colloid Concentration (mg/L), $M_{coll,uranophane}$	Cumulative Probability of Occurrence
0.001 to 0.1	0.50
0.1 to 1.0	0.75
1.0 to 10	0.90
10 to 50	0.98
50 to 200	1.00

NOTE: The minimum concentration ($M_{coll,uranophane,\ min}$) for modeling purposes is set at 1×10^{-6} mg/L.

The selection of this distribution was based on comparison with commonly observed colloid population distributions of groundwater colloids that are dominated by smectite clay particles. As the uranophane colloids exhibited a stability profile similar to that calculated for smectite colloids, it is reasonable to use a similar population distribution.

Sorption of radionuclides onto uranophane particles was based on limited experimental data with actinides and some analogue studies that used rare earth elements (see Figure 6-16 and Table 6-9). The sorption studies were performed on a number of different U(VI) phases, including uranophane.

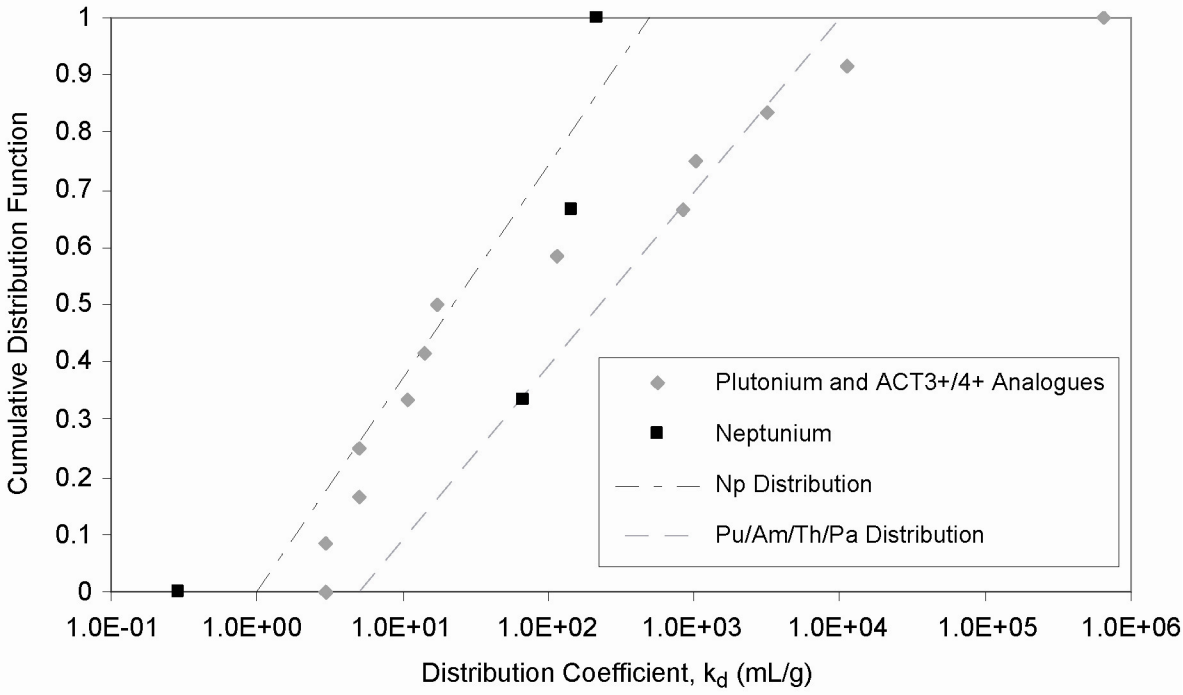

Source: Output DTN: MO0705DSCSCUSS.000.

NOTE: Actinide Analogues (Kim et al. 2005 [DIRS 179551], Table 1, p. 152; Table 2, p. 153; Table 4, p. 156); Plutonium (McNamara et al. 2005 [DIRS 174068], Table 1, p. 171; Table 2, p. 172); Neptunium (Douglas et al. 2005 [DIRS 173086], Table 1, p. 268). Data reported for Np uptake above pH 9 was not included in the distribution. Dotted lines represent log uniform trends described in Table 6-9.

Figure 6-16. Summaries of Radionuclide Sorption Data on Uranyl Phases

Ion exchange of cesium into the interlayer sites of boltwoodite has been demonstrated by Burns (1999 [DIRS 110975], Table 4, p. 222) and both cesium and strontium into uranophane by Douglas et al. (2002 [DIRS 179546]). Douglas et al. (2002 [DIRS 179546]) state that, "While these results suggest that Cs^+ may be incorporated into the uranophane structure at low mole fractions, we cannot exclude the possibility that the Cs^+ is only surface sorbed, or is more effectively partitioned into separate, amorphous solids that are not observable by [x-ray diffraction]." These latter interactions may mean the Cs^+ would be less or more, respectively, strongly bound within the uranophane phase, but the information on the incorporation can be used to assess the apparent sorption coefficients relative to other phases such as smectite. No explicit information on sorption coefficients was provided in either of these reports; however, the studies and the discussion of their results indicate that the uptake of cesium and radium (a reasonable chemical analogue for strontium) will be similar to that observed for cesium sorption on smectite clay (10^1 to 10^3 mL/g).

Table 6-9. Developed Sorption Coefficient Distributions for Radionuclide Sorption onto U(VI) Colloidal Phases

	Min (mL/g)	Max (mL/g)	Form
Plutonium	5×10^0	1×10^4	Log uniform
Americium	5×10^0	1×10^4	Log uniform
Neptunium	1×10^1	5×10^2	Log uniform
Thorium	5×10^0	1×10^4	Log uniform
Protactinium	5×10^0	1×10^4	Log uniform
Radium	1×10^1	1×10^3	Log uniform
Cesium	1×10^1	1×10^3	Log uniform
Tin	1×10^0	1×10^2	Log uniform

Source: Figure 6-16; Output DTN: MO0705DSCSCUSS.000.

6.3.2.7 Surface Area of Uranophane Colloids

The specific surface area data from Ilton et al. (2006 [DIRS 178810]) was available for Na-boltwoodite. In this case, the structures of boltwoodite and uranophane are similar enough for modeling purposes. Based on BET analysis reported by Ilton et al. (2005 [DIRS 178810], Section 2.1, p. 4837) on boltwoodite $\{K(H_3O)[(UO_2)(SiO_4)]\bullet 0.5H_2O\}$, a value of 30 m^2/g was selected as a reasonable value for the surface area of uranophane. Micrographs of a natural uranyl carbonate specimen, čejkaite, and uranophane specimen were examined to determine if the value selected for the model was a reasonable value. In the case of the SEM images, the width and height were considered equal. The total area was then multiplied by a roughing factor of 3. The resolution of the SEM does not allow the surface to be seen in sufficient detail to allow an accurate assessment of the total surface area, therefore this roughing factor is used to compensate so that surface area is not under estimated. In the case of the TEM images, the thickness was assumed to be 30 nm based on visual inspection of the images. The measurements made from the individual images are displayed in Figure 6-17. Note that the surface area values for čejkaite are dramatically smaller than those for uranophane and that there is approximately a 90% probability that the uranophane grains are 30 m^2/g or less. Given that this other naturally occurring uranyl phase has a surface area less than about 1/6 that of uranophane, the uranophane values themselves at least represent a reasonably larger mineral surface area that would tend to enhance surface adsorption processes relative to a phase like čejkaite.

Based on the information in Figure 6-17, a value of 30 m^2/g is a reasonable value for the surface area of uranophane colloids. This value describes the external surface and not any available ion exchange sites. Radionuclides such as radium and cesium may be sorbed at interlayer sites and actinides may only sorb on edges. Therefore, there is uncertainty in the available surface area for sorption. Nevertheless, as little information is available on this parameter, it is recommended to use the single experimental value. The site density for uranophane was set to 2 sites/nm^2, which is similar to the value for kaolinite (1.3 to 3.4 sites/nm^2) (Davis and Kent 1990 [DIRS 143280], Table 1, p. 182). This information is used in the sorption capacity model discussed in Section 6.3.12.3.

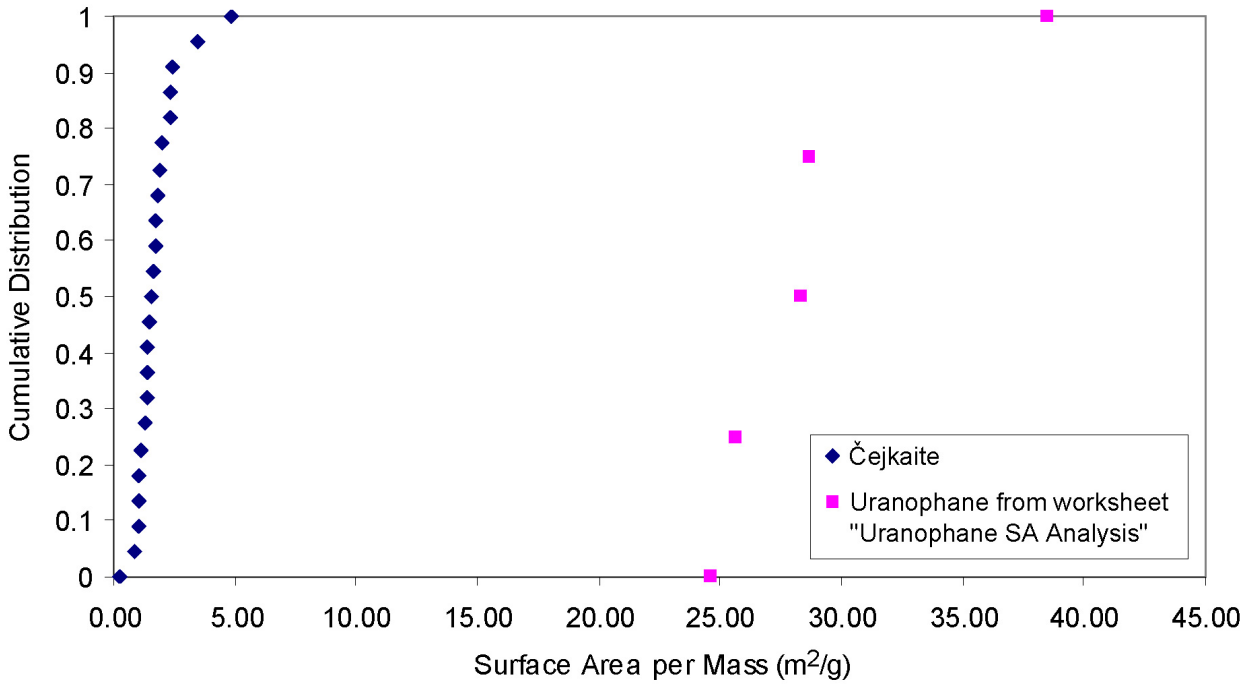

Source: Measurement data and calculations are described in Output DTN: MO0705DSCSCUSS.000.

NOTE: Data obtained by measuring particle sizes from a scanning electron micrograph of natural čejkaite (Krupka et al. 2006 [DIRS 179654], Figure 3a, p. 3751) and a transmission electron micrograph of uranophane from sediments at the Hanford site (McKinley et al. 2006 [DIRS 179552], Figure 6, p. 1881). Surface areas from the SEM analyses were multiplied by a roughing factor of 3 but are still much smaller than those for uranophane and are therefore bounded by them. The images of uranophane were not multiplied by any factor as the resolution of the TEM image was sufficient to indicate any large changes in topology so that the surface areas can be determined more accurately.

Figure 6-17. Calculated Surface Area of Two Types of Uranyl Secondary Phase (Čejakite and Uranophane)

6.3.3 Experimental Evidence for the Concentration and Nature of Colloids from Borosilicate Waste Glass Corrosion Tests

Several investigations into the degradation of DHLWG (DTNs: MO0407ANLGNN02.608 [DIRS 171277] and LL000123351021.117 [DIRS 143308]; CRWMS M&O 2001 [DIRS 154071]; Bates et al. 1992 [DIRS 100704]) concluded that waste form colloids have formed by precipitation of radionuclide-bearing phases within the glass-weathering rind that later became associated with colloid-sized clay phases. Spallation of fragments of clay (primarily) and radionuclide-bearing phases from the alteration layers formed on the waste form surfaces may also result in waste form colloid generation. Colloids were formed in the course of static DHLWG tests on several of the glasses for different S_A/V (glass solid surface area to leachate volume ratio). It was observed that as the ionic strength increased, colloid concentration generally decreased, and ultimately a threshold value was reached above which the colloids were not observed or were observed in low quantities (Figure 6-18).

The stability of smectite colloid suspensions (including smectite colloids formed from DHLWG degradation) can be estimated based on the relationship presented in Equation 6-9.

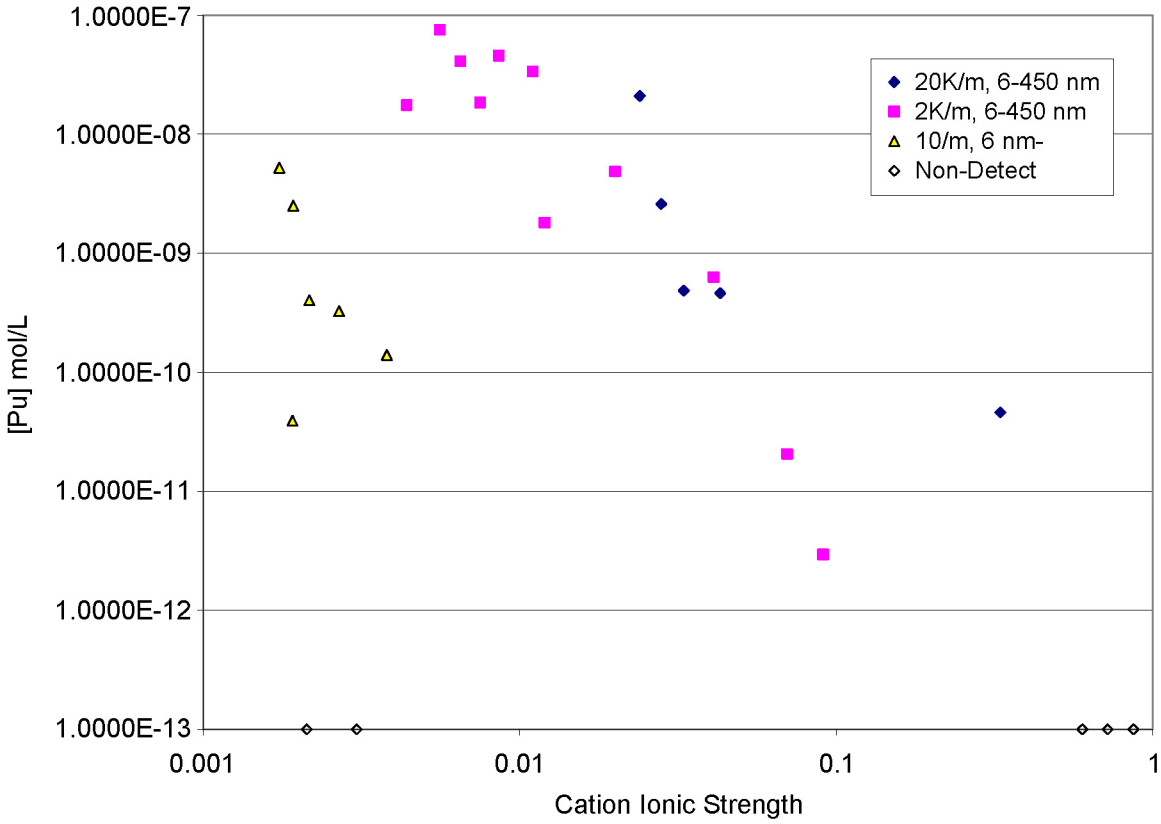

Source: Table 6-5 (5th column versus 4th column).

NOTE: Plutonium-bearing colloids as a function of ionic strength for corrosion tests on glass samples SRL-202A and SRL-131A at SA/V of 10/m, 2,000/m, and 20,000/m (at 90°C). Zero values have been plotted as 1×10^{-13} M. Glass reaction can result in an increase in ionic strength and pH.

Figure 6-18. Concentrations of Plutonium and Colloids as a Function of Ionic Strength in Corrosion Tests

The colloid model abstraction assumes plutonium and americium are associated irreversibly (embedded) within smectite colloids from the DHLWG degradation experiments As such they are treated as a separate colloid subtype, and assuming that the sorbed actinides are an intrinsic part of the colloid, not in equilibrium with the aqueous system. This premise has been based on a limited set of microscopic images obtained from corrosion tests and is not supported by results from waste glass corrosion tests reported by Ménard et al. (1998 [DIRS 171053]) on the plutonium-doped glasses and via product consistency testing DHLWG data from DTN: LL000123351021.117 [DIRS 143308]. However, it not clear that sufficient analyses were performed in these experiments to permit the direct identification of these embedded phases. The actinide particles are assumed to be attached irreversibly (or embedded) to the carrier colloid (see Assumption 5.4).

In Figure 6-19, a series of images from waste form corrosion tests are shown. Each image shows the accumulation of actinides and rare earth elements (i.e., uranium, thorium, plutonium, lanthanides, etc.), in particles found in the leachate or at the surface corrosion rind. Microscopy images represent snap-shots in time and specific location that may not necessarily represent the overall sample conditions. These images demonstrate a similarity in corrosion and colloidal

behavior of glass and SNF. These images may also imply that the actinides are embedded in the carrier colloids; however, it is not known whether these phases persist at longer times. Indeed, thorium not plutonium or americium was identified in the particle in Figure 6-19a, and only uranium and rare earths were observed in the particle agglomerate shown in Figure 6-19b. Furthermore, both particles exceed the nominal dimensions for a colloid and should be referred to as suspended particles, not colloids. However, in the case of DHLWG, modeling americium and plutonium as irreversible colloids is conservative and bounding.

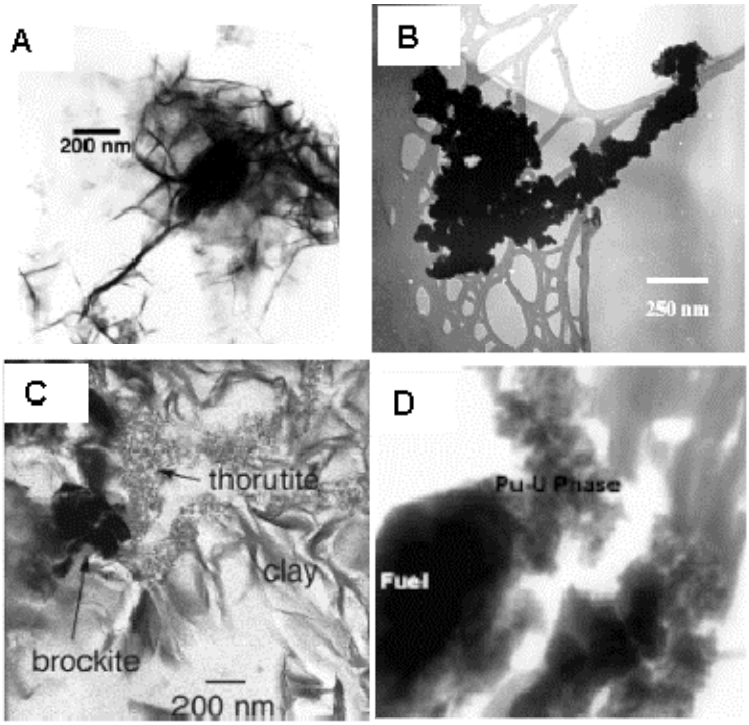

Source: CRWMS M&O 2001 [DIRS 154071], (a) Figure 12, p. 26; (b) Figure 18, p. 31; (c) Figure 15, p. 28; (d) Figure 21a, p. 34.

NOTE: (a) Suspended particle in leachate from thorium-rich glass unsaturated drip test, (b) suspended particle in leachate from SNF drip test, (c) corrosion rind from glass drip test, and (d) corrosion rind from SNF drip test.

Figure 6-19. Transmission Electron Microscope Images of DHLWG and CSNF Corrosion Rinds and Colloids

6.3.4 Experimental Evidence for Irreversible CSNF Colloids

In experiments where cladding was present, plutonium colloid concentrations were reduced by three to four orders of magnitude (Wilson 1990 [DIRS 100793]). These observations may be supported by the intermittent drip SNF corrosion tests on ATM-103 HDR and ATM-106 HDR (Mertz et al. 2003 [DIRS 162032]); however, other uncertainties need to be considered in these tests, such as amount of spent nuclear fuel reaction, the amount and nature of water contact, and the physical barriers that might have limited colloid transport from the altered fuel surface to the collection vessel. Various colloidal phases (e.g., rare earth element-bearing phases) were detected in the leachates at early times (Finn et al. 1994 [DIRS 100746]); but, at later times,

colloids were not observed directly and colloid release may have stopped, possibly due to filtration, attachment to air–water interfaces, or sorption by the metallic holder used in the tests. There was evidence of material buildup consisting of SNF particles and radionuclide-bearing uranium (VI) phases on these Zircaloy holders (Finn et al. 1998 [DIRS 100392]). Unfiltered plutonium concentrations measured from the ATM-103 HDR and ATM-106 HDR following removal of the Zircaloy holder was slightly higher than those reported before the changes. These results indicate that small but measurable levels of plutonium colloids were released between 5.2 and 8.7 years after the physical impediments to colloid release were partially removed (Mertz 2003 [DIRS 162032]). Plutonium concentrations were between 1×10^{-10} and 1×10^{-9} mol/L, only slightly lower than the levels reported by Finn et al. (1994 [DIRS 100746]) for the initial samplings. These values indicate that some plutonium colloids may continue to be released from CSNF. In corrosion tests on spent nuclear fuel under immersion conditions in deionized water, plutonium, americium, and neptunium were found associated with the U(VI) phases (McNamara et al. 2005 [DIRS 174068]).

6.3.5 Experimental Evidence for U(VI) Colloidal Phases

Although the colloid concentrations from the unsaturated drip tests on SNF were extremely low, evidence from examination of the corroded solids and the Zircaloy retainer indicated the presence of fine particulates (Buck et al. 1997 [DIRS 112904]; Finn et al. 1998 [DIRS 100392]). Fully saturated immersion tests by Wilson (1990 [DIRS 121808]) and McNamara et al. (2005 [DIRS 174068]) have shown evidence of plutonium- and americium-bearing particulates, and resulted in effective plutonium concentrations between 10^{-7} M and 10^{-6} M for the duration of these tests.

McNamara et al. (2005 [DIRS 174068]) investigated the formation of suspended solids from samples of a low-burnup CSNF immersed in deionized water. H.B. Robinson CSNF was crushed and sieved into a 100-μm to 500-μm size range and 1-g samples were reacted in 8 mL of deionized water for two years at 25°C. Suspended colloidal-like aggregates were observed to form at the air-water interface for the samples. Results from the analysis of the suspended solutions and leachate from a 1.5-year test demonstrated CSNF-derived waste form particulate formation with uptake of Pu, Np, Am, and Cm, as well as Sr and Cs. The plutonium and americium particulate concentrations were 1.15×10^{-7} M and 1.04×10^{-9} M, respectively. By dividing the solution concentration by the total mass of solid uranium metastudtite ($UO_4 \bullet 2H_2O$) (mwt = 338.06 g), these correspond to effective K_d (mL/g) values for sorption onto metastudtite of 6.4×10^5 and 1.12×10^4 mL/g, respectively (see Table 6-10). These values were used to develop the distributions reported in Table 6-9. Although, the K_d values for plutonium and americium sorption onto metastudtite were high, only a small fraction of the total available for sorption was associated with the particulates, and most remained on the parent-corroding immobile solid. The total uranium filterable fraction amounted to 80 mg/L (80 ppm). There is insufficient information to argue conclusively whether there is irreversible uptake of the radionuclides.

Table 6-10. Radionuclide Concentrations Associated with Colloids from Immersion Tests at 25°C on SNF

Element	Total Uranium	^{237}Np	^{239}Pu	^{241}Am	^{244}Cm
Radionuclide mass (µg)/g uranium	623 µg	330	352	3.23	0.58
Radionuclide inventory (µg)/g uranium	N/A	389	4,689	1,423	9.66
Uptake into U(VI) suspended particles (%)	N/A	85	7.5	0.2	6
Element	**Total Uranium**	**^{237}Np**	**^{239}Pu**	**^{241}Am**	**$^{243+244}$Cm**
Dissolved concentration in leachate (mol/L)	1.44×10^{-6}	1.4×10^{-9}	2.3×10^{-9}	1.2×10^{-9}	2.3×10^{-11}
Sorption coefficient (K_d) (mL/g)	N/A	9.95×10^{5}	6.4×10^{5}	1.12×10^{4}	1.03×10^{5}
Error in sorption measurement	N/A	6.26×10^{6}	1.9×10^{4}	3.27×10^{3}	4.49×10^{3}

Source: McNamara et al. 2005 [DIRS 174068], Table 1, p. 171; Table 2, p. 172.

NOTE: N/A = not applicable. Solutions were at pH 6.3. The solution aliquots were analyzed at 1.5 years and the solids were examined at 2 years. The reported value for ^{237}Np in the leachate has a 629% standard deviation reported, leading to a large uncertainty in the calculated K_d (hence this value was not included in the analysis). The solid analysis by McNamara et al. (2005 [DIRS 174068]) provided a combined value for $^{243+244}$Cm while the leachate analysis listed only ^{244}Cm. This makes the calculated K_d for curium questionable.

6.3.6 Evidence of Colloids from DSNF

Of the approximately 250 different types of fuel in the DSNF inventory, metallic uranium fuel comprises approximately 85% (by metric tons heavy metal) of that inventory. The degradation of metallic uranium fuel under unsaturated drip test conditions has been reported (DOE 2003 [DIRS 166268], Section 3). The reaction of uranium metal with water vapor produces binary oxides (Haschke 1998 [DIRS 174075]). The general reaction is:

$$U + xH_2O \rightarrow UO_x + xH_2 \qquad \text{(Eq. 6-12)}$$

Values of the O:U ratio (x) of the oxide product vary from 2.0 to 2.2, depending on temperature and water pressure. In the case of U + moist air/O_2, x in UO_x is in the range 2.0 to 2.7. The U + air/O_2 is enhanced by moisture, but the U + H_2O reaction is suppressed by oxygen. Haschke (1998 [DIRS 174075]) has shown that the oxide scale formed between 35°C to 100°C has a laminar morphology, consistent with schoepite, with a high surface area (15 m^2/g). Mertz et al. (2000 [DIRS 162161]) lists schoepite, U_4O_9, UO_2, and uranium silicates as alteration products from uranium metal drip tests. The corrosion products observed during the long-term weathering of N-reactor fuel elements in the Hanford K-basins have been identified as meta-schoepite and studtite (McNamara et al. 2005 [DIRS 174068]).

In the unsaturated tests with equilibrated J-13 well water, ~10-nm spheres of uranium oxides were seen after one month, which later became attached to larger clay colloids (DOE 2003 [DIRS 166268], p. 3-37; Kaminski et al. 2005 [DIRS 179550], Section 3). Clays and other

phases may be forming in the leachate of unsaturated drip tests due to evaporation during the course of the test. Sequential filtration showed that the released uranium was 40% colloidal and 45% particulate after seven days, with the colloidal fraction dropping and the particulate fraction increasing with time. After one month, the colloidal fraction had dropped to 10% and then to zero in the 8.5- and 11-month samples. Plutonium showed similar trends with 75% of the released plutonium colloidal at seven days falling to 8% colloidal and 90% particulate in the 8.5- and 11-month samples. It is possible that the colloid population was destabilized by increasing ionic strength as a result of the evaporating equilibrated J-13 well water solution over time, as evidenced by the formation of clay and calcite; however, low colloid concentrations may also be explained by a reduction in the CSNF corrosion rate.

In static batch tests, plutonium was released almost entirely as colloids with colloid concentrations of 2×10^{-8} to 2×10^{-7} M plutonium compared to generally less than 2×10^{-9} M plutonium dissolved. In a static batch test, colloids were not seen above the equilibrated J-13 well water background until the 32-day sample when the colloids were about ten times background. This 32-day sample was reexamined after nine months and no colloids were detectable (DOE 2003 [DIRS 166268], p. 3-43). This is in contrast to the sample from the unirradiated drip test, which showed that the colloid suspensions are stable for one year (DOE 2003 [DIRS 166268], p. 3-39), but it was not clear if these stable colloid suspensions were the original UO_2 spheres or the later clay and uranyl silicate colloids. Flocculation of colloids was observed in the static batch and unsaturated drip tests, leading the authors to conclude that although a large number of colloids are generated (10^{12} particles per liter) they quickly flocculate into a smaller number of large particles (DOE 2003 [DIRS 166268], p. 3-64). Temperature is usually used to accelerate waste form reaction to allow observation of weathering within a reasonable time frame. No tests were performed at lower temperatures, which may have facilitated more stable colloidal sols. Corrosion testing of uranium metal fuel under drip conditions with additional discussion of the uncertainties associated with the DSNF unsaturated testing is reported in DTN: MO0306ANLSF001.459 [DIRS 163910]. The highest observed colloidal uranium concentration was 3.5 mg U/L, and the highest $^{239}Pu/^{238}U$ ratio (0.13) was seen in the colloidal fraction which corresponds to a plutonium concentration of 2×10^{-6} M. Using information from these experiments it is possible to calculate the stability ratio for the colloids in these tests (see Figure 6-32).

6.3.6.1 Colloids from Mixed Oxide Fuel

Initial plutonium release from unsaturated drip corrosion testing of mixed oxide fuel (MOX) and high burn-up fuel (ATM109-A, -B, and -C) has been reported by Cunnane (2001 [DIRS 154818]). These tests resulted in lower release of plutonium than the lower burn-up ATM-106 and ATM-103 HDR tests. Any colloids from MOX are anticipated to behave like CSNF colloids. The test vessels for the ATM109 (-A through -C) HDR experiments were found to be dry in over 50% of the samplings (Thomas 2003 [DIRS 163048]). A dry test may have curtailed colloid transport. Although the potential for rim disintegration should be greater in the high burn-up and MOX fuels, evidence from the initial 0- to 3-year high drip-rate unsaturated drip testing did not indicate increased release.

In conclusion, there is uncertainty in whether mixed oxide or high burn-up fuels will generate stable colloids; however, it is conservative to include them in the analysis.

6.3.6.2 Effects of Dry Oxidation of CSNF on Colloid Formation

This section addresses the potential effects of CSNF oxidation (in the dry and humid air environments to which it might be exposed in nominal, seismic, and igneous intrusion scenarios) on colloid formation.

A consequence of fuel oxidation is the possible disaggregation of the fuel pellets into fuel-grain-sized powders (Dehaudt 2001 [DIRS 164037], Section 7.2.5.3). This can occur as a result of even minor oxidation at the grain boundaries, in low to medium burnup CSNF, to which hot air and water vapor can gain access through connected porosity at the grain boundaries. The as-fabricated fuel grain sizes are close to 10 micrometers (e.g., a mean size of 9 ± 2.4 μm is given in Dehaudt 2001 [DIRS 164019], Section 5.2.2.5.4) and change little with irradiation in low- to medium-burnup CSNF (Dehaudt 2001 [DIRS 164037], Section 7.2.3.3). However, the grain sizes do change in the restructured rim region of high-burnup fuels; in this region the average grain size can be less than a micrometer (Spino et al. 1996 [DIRS 174080], pp. 179 to 190). Oxidation-induced disaggregation of these grains could produce submicrometer particles. Also, grain fragmentation due to the specific volume increase associated with oxidation of SNF with grain sizes greater than a micrometer (i.e., most of the SNF inventory) could also lead to submicrometer powders. If such powders were produced due to fuel oxidation prior to water contacting the fuels, the possible suspension of these particles upon water contact could produce a source of CSNF colloids. This section discusses the available data on the oxidation of CSNF under the conditions in which it is likely to be exposed in the nominal, seismic, and igneous intrusion scenarios and the likelihood that such oxidation will lead to submicrometer particles that could be suspended as colloids upon water contact.

Nominal and Seismic Scenarios—The fuel temperature could be up to about 300°C. Because the pressure (air and water vapor) will not exceed one atmosphere, the air to which the fuel can be exposed will be "dry" (i.e., low relative humidity) until the temperature decreases to approximately 100°C. The relative humidity will slowly approach 100% when the temperature decreases to below 100°C.

Igneous Intrusion Scenario—The fuel could be exposed to temperatures up to about 1,000°C. The gas phase is likely to contain water vapor during and immediately after the intrusion event. During the cool down period (several month periods when the heat associated with the hot magma is dissipated) the gas phase can be considered to be "dry" air until the temperature decreases to approximately 100°C. As in the case of the nominal and seismic scenarios, the relative humidity will approach 100% when the temperature decreases below 100°C.

The following paragraphs summarize available data that are pertinent to assessing if the initial exposure of CSNF to the "dry" air oxidizing conditions followed by exposure to humid air (approaching 100% relative humidity), as would be expected for the above exposure scenarios, is likely to lead to formation of submicrometer particles that would be available for suspension as colloids when water contacts the oxidized fuel. Available data on the size distributions of fuel

powders produced in the oxidation of CSNF are discussed first. The expected behavior of the oxidized fuel, upon contact with humid air and water, is then addressed.

The oxidation of CSNF has been extensively investigated and the available information for temperatures below 400°C has been summarized in a fairly recent comprehensive review (Dehaudt 2001 [DIRS 164037], Section 7.2.). Hanson (1998 [DIRS 101672], p. iii) describes the oxidation of spent nuclear fuel in dry air as a two-step process of the form $UO_2 \rightarrow UO_{2.4} \rightarrow U_3O_8$. At temperatures up to 250°C, UO_2 fuel that is exposed to dry air will oxidize to $UO_{2.4}$ at a rate that is controlled by the rate of diffusion of oxygen into the fuel. The transition from $UO_2 \rightarrow UO_{2.4}$ does not result in appreciable fuel pellet density changes. At higher temperatures, the fuel is oxidized to U_3O_8. Hanson (1998 [DIRS 101672], pp. iii and 5.9) found that the $UO_{2.4} \rightarrow U_3O_8$ reaction rate, which is controlled by nucleation and growth of U_3O_8, is strongly dependent on fuel temperature and burnup. The transition from $UO_{2.4} \rightarrow U_3O_8$ results in a volume expansion of greater than 36%. No oxidation to U_3O_8 has been observed for temperatures below 250°C. The density or specific volume changes associated with fuel oxidation can cause disaggregation of CSNF into grain-sized powders when the connected porosity in the fuel allows oxidation to occur at the grain boundaries and cause intergranular fracturing. The density changes can also result in transgranular fracturing depending on the rate of oxidation involved.

Results from the corrosion of spent UO_2 fuel stored at ambient temperatures in dry air for 10 years, and subsequently stored in a humid-air environment for fifteen years, have shown oxidation processes along the grain boundaries that weaken the intergranular bonding and cause grain-boundary decohesion (Leenaers et al. 2003 [DIRS 168991]). Examination of the fuel showed progression of a grain-boundary corrosion front that extended from the periphery to about the midradius of the pellets. These results were interpreted to be due to the combined effects of two reactions. One reaction consumes oxygen by direct oxidation of the UO_2 fuel to produce U_4O_9. The other produces hydrogen by oxidation of the fuel to U_4O_9 through reaction with H_2O_2 produced by radiolysis; the net reaction involves oxidation of the fuel by water and can be written as one mole of water reacting with four moles of UO_2 to produce one mole of U_4O_9 and one mole of hydrogen. The larger oxygen depletion observed in the humid-air exposure compared to dry-air exposure indicated that the oxidation of the fuel had progressed more rapidly in humid air than in dry air.

Particle size distributions for unirradiated and irradiated UO_2 fuel following high-temperature oxidation (300°C to 900°C) have been reported by Liu et al. (1992 [DIRS 172864]) and Iwasaki et al. (1968 [DIRS 172518]). Liu et al. (1992 [DIRS 172864]) reported the particle size distribution results for unirradiated fuel. Results from both studies indicated that only a small fraction of oxidized material was less than 1 micrometer in diameter. Also, the results showed that the particle size increases as the oxidation temperature increases. This was attributed to an increase in the plasticity of U_3O_8 with increasing temperature, which allows the oxidation-induced stresses to be relaxed and thus minimize intra- and transgranular fracturing. These data suggest that few, if any, colloid-sized particles would be produced when CSNF is oxidized at the higher temperatures to which it would be exposed following an igneous intrusion event.

Data on the particle-size distribution that may result from the oxidation of the restructured fuel in the rim region of high-burnup spent nuclear fuels are not available. The average grain size of the recrystallized fuel is 290 nm, with a standard deviation of 140 nm (Spino et al. 1996

[DIRS 174080], Figure 7). In contrast to the grain boundaries in medium-to-low burnup fuels, the fact that the fully restructured fuel in the rim region contains the exsolved fission gas in pressurized bubbles suggests that there is little if any connected porosity at the grain boundaries in this region (Spino et al. 1996 [DIRS 174080], Figure 9 and associated discussion). The morphological changes associated with oxidation of this material are, therefore, likely to be more similar to those that have been observed in the oxidation of unirradiated sintered UO_2 pellets than to the morphological changes that have been observed in the oxidation of irradiated fuel fragments (Dehaudt 2001 [DIRS 164037], Sections 7.2.5.4). This indicates that the oxidized powder size distributions will likely range upwards from the fuel grain size distribution.

The complex effects of humidity (particularly for relative humidities at and near 100%) on the corrosion of irradiated and unirradiated UO_2 fuels are summarized in a review of the oxidation of UO_2 at temperatures below 400°C (McEachern and Taylor 1998 [DIRS 113270], Section 2.2). Humidity can influence air oxidation in this temperature range by forming hydrated-uranyl phases (e.g., by hydrous disproportionation of U_3O_8), by supporting oxidative dissolution in water films that form on the surface at higher relative humidities, by enhancing grain-boundary oxidation in spent nuclear fuel, and by supporting radiolytic processes at grain boundaries.

When the finer particles that were produced by oxidation at 300°C were exposed to 98% relative humidity, the particle size was observed to increase (from a median size of 7.5 μm to about 100 μm) (Liu et al. 1992 [DIRS 172864]). Although Liu et al. (1992 [DIRS 172864]) attributed this to agglomeration or adhesion of the fine particles to the sieves used for size determination; it is also plausible that the size increase was associated with oxidative dissolution of the fine-grained oxide particles and reprecipitation as uranyl oxide hydrate phases. Results from work by Taylor et al. (1995 [DIRS 125815]) discussed below indicate that upon exposure to humid air with a relative humidity near 100%, any submicrometer particles that are formed as a result of fuel oxidation are likely to grow due to oxidative dissolution and precipitation of coarser uranyl-oxyhydroxide phases in a surface layer of water that condenses onto the particles under these conditions. Hot cell observations on unsaturated SNF drip tests suggest that the fuel underwent considerable disintegration after 3.7 years for ATM-103 (Finn et al. 1998 [DIRS 100392], pp. 25 to 30), and after 4.1 years for ATM-106 (Finn et al. 1998 [DIRS 100392], pp. 40 to 41). Loosely aggregated clumps fell apart on handling. Uncorroded spent nuclear fuel is a hard ceramic material. However, it is unknown whether this would result in particles in the colloidal size range.

Taylor et al. (1995 [DIRS 125815]) investigated the composition and microstructure of corrosion products formed on unirradiated UO_2 fuel exposed at 225°C to humid air with a range of relative humidities. In dry air (relative humidity < approximately 30%), they observed oxidation to U_3O_7 and U_3O_8 via the solid-state mechanisms discussed above. At moderate relative humidities (30% to 70%), they observed surface and grain-boundary corrosion and fine-grained U_3O_8 and dehydrated schoepite crystals sparsely scattered over the surface. These observations were attributed to oxidative dissolution and precipitation of U(VI) phases within a thin (few molecules thick) and perhaps patchy layer of water on the fuel surface. At higher relative humidities (extending to near 100% relative humidity), a continuous and coarse-grained layer of U_3O_8 and dehydrated schoepite were found overlying a U_3O_7 layer. These results were attributed to dissolution and precipitation in a thicker film of water, which closely resembles a bulk liquid-phase film. When the test atmosphere was moisture-saturated (i.e., 100% relative

humidity), large (tens to hundreds of micrometers in length) dehydrated schoepite crystals were observed consistent with precipitation and growth from bulk solution.

Based on the results discussed above the likely effects of CSNF oxidation and subsequent exposure to humid air on colloid formation in the nominal, seismic, and igneous scenarios can be summarized as follows:

- Oxidation and breakup of low- to medium-burnup fuels is expected to produce powders with particle sizes greater than one micrometer. Higher temperature (>500°C) is expected to produce particle sizes greater than the fuel's grain size; lower temperature exposure is likely to produce powders with particle sizes close to the grain size of the unoxidized fuel.

- For the fine-grained restructured fuel in the rim region of high-burnup CSNF, extrapolation of the experimental observations for unirradiated fuel and low- to medium-burnup fuel suggests that the oxidized fuel particle sizes are likely to be larger than the submicrometer grain size of the restructured fuel. However, this extrapolation is uncertain because directly applicable experimental data are not available for high-burnup CSNF.

- If submicrometer particles are generated as a result of fuel oxidation, the subsequent exposure of these particles to humid air approaching 100% relative humidity will result in uranyl oxide phase formation. The particle sizes produced are likely to be similar to those produced in the oxidative dissolution and precipitation of unoxidized CSNF. Secondary phase particles from the spent nuclear fuel unsaturated drip tests have been reported to be <10 μm to 200 μm (Finn et al. 1998 [DIRS 100392], p. 25). This is above the accepted colloidal size range.

- After exposure of the oxidized fuel to humid air, few, if any, submicrometer particles are expected to be available for suspension as colloids.

Based on the above considerations, exposure of CSNF to the "dry" air oxidizing conditions, followed by exposure to humid air, is unlikely to lead to formation of submicrometer particles that would be available for suspension as colloids when water contacts the oxidized fuel.

6.3.7 Field Evidence of Colloids from Natural Analogues

Natural analogues for colloid-facilitated radionuclide behavior have been reviewed by Triay et al. (1995 [DIRS 100789]) and Traexler et al. (2004 [DIRS 172072]). However, few of these reviewed natural analogue sites are relevant to the Yucca Mountain unsaturated oxidizing environment. At the Koongarra deposit in Northern Australia where the groundwater is dominated by Mg and bicarbonate (the pH is between 6 and 7.5), colloids include clay minerals, fine-grained quartz, and iron-oxide particle coatings. Uranium was principally dissolved, whereas thorium was associated with particles. Observations of nanocrystals of U(VI) phosphates by Murakami et al. (1997 [DIRS 113272]) in Koongarra groundwaters that were undersaturated with respect to saléeite $\{Mg[(UO_2)(PO_4)]_2(H_2O)_{10}\}$ and metatorbernite $\{Cu[(UO_2)(PO_4)]_2(H_2O)_8\}$ may support a colloidal transport process. The most appropriate

natural analogue for colloid behavior at Yucca Mountain is the Nopal I uranium deposit at Peña Blanca District, Mexico. Pearcy et al. (1995 [DIRS 110223]) show that uranium has migrated along micro- and meso-fractures in the tuff rock to distances less than 1 mm. The uranium mineralogy at Nopal I consists almost exclusively of the uranyl silicate (uranophane) and uranyl oxyhydroxides produced from uraninite alteration. Stoichiometric uraninite (UO_2) is unknown in nature and is always partially oxidized in addition to containing radiogenic lead and commonly thorium, calcium, and lanthanides. In conclusion, there is little evidence of colloidal transport of uranium or of uranium phases under unsaturated conditions.

6.3.8 Colloids from the Corrosion of Waste Package and Metallic Invert Materials

The occurrence of iron oxyhydroxide colloids from the corrosion of waste package and metallic invert materials is discussed in this report. Conceptually, iron oxyhydroxide colloids are likely to comprise three mineral species under the anticipated repository conditions: goethite, hematite, and ferrihydrite (or hydrous ferric oxide) (Langmuir 1997 [DIRS 100051], pp. 436 to 437). The hydrous ferric oxides are not as stable as hematite and will react irreversibly to form the more stable hematite. Goethite forms from hydrous ferric oxide (HFO) by dissolution-reprecipitation, whereas hematite will form directly by solid–solid transformation ("aging" of hydrous ferric oxide) (Langmuir 1997 [DIRS 100051], p. 437). The various iron oxyhydroxides will occur in three forms: immobile scale, large particles that will settle out, and colloid-sized particles that can be transported. Hematite has been used in the model for constraining stability calculations of the colloids. For the sorption properties of the Fe-oxide surfaces, HFO and goethite have been taken as representative.

The iron oxyhydroxide phases may be expected to provide abundant sorption sites for dissolved (aqueous) radionuclides in amounts determined by the appropriate K_d value. The sorption of radionuclides onto HFO and goethite (as stationary corrosion products) is handled by a competitive sorption model in *EBS Radionuclide Transport Abstraction* (SNL 2007 [DIRS 177407]) that evaluates the competition between actinides (U, Np, Pu, Am, and Th) and Ni for a limited number of surface sites. Even though Ni is not transported within the TSPA, it is a major potential sorbing ion from the steel and its competition for sorption sites is accounted for to more accurately estimate the sorption of the radionuclides. The competitive sorption model contains both equilibrium representations (i.e., reversible sorption) for U, Np, and Th onto HFO and goethite, as well as kinetic sorption-desorption for Pu and Am, where the slow desorption is applied to the stationary corrosion products. Stable iron oxyhydroxide colloid suspensions may serve to increase the mobility of sorbed radionuclides. The stability of such suspensions is evaluated in the stability model, wherein the waste package corrosion product colloids are viewed conceptually as hematite particles.

Corrosion products released from carbon-steel miniature waste packages were characterized (results archived in DTN: MO0302UCC034JC.003 [DIRS 162871]) and the quantity of corrosion products transported out of the waste packages was measured by micro-filtration (DTN: MO0312UCC034JC.008 [DIRS 166367]). Two configurations were used to introduce water into the carbon steel miniature waste packages and induce corrosion: (1) a "bath tub" configuration in which water was introduced from the top of the miniature waste package and exits from an opening on the side of the miniature waste package after it has accumulated along the bottom, and (2) a "flow-through" configuration in which water is introduced from the top of

the miniature waste package and exits directly from the bottom (Zarrabi et al. 2003 [DIRS 171238]). Water chemically similar to J-13 well water (near Yucca Mountain) was used in the experiments and the rate of water introduction was similar to projected rates of water movement within the drifts at Yucca Mountain. To establish the total amount of corrosion material transported out of the carbon steel miniature waste packages, the effluent was passed through a microfiltration system capable of separating particles of 0.1 µm and upward, which is below the range for colloids; hence, this system will under-report colloid concentrations. Identification of the oxidation corrosion products is ongoing, although to date the data suggest a preponderance of cryptocrystalline corrosion products, including magnetite (Fe_3O_4), lepidocrocite {FeO(OH)}, and goethite {FeO(OH)} (DTN: MO0302UCC034JC.003 [DIRS 162871]).

Iron oxyhydroxide colloids would be expected to form as a result of corrosion of the waste package and associated engineered barrier system components. Few peer-reviewed publications present information on iron oxide–oxyhydroxide colloid concentrations as a function of aqueous chemistry. The range of values for maximum iron oxide–oxyhydroxide colloids concentration (0.3 mg/L to 30 mg/L) was chosen so that it was greater than iron oxyhydroxide colloid levels found in groundwater, but high enough to reflect the masses of corroded ferrous metal anticipated in the repository (see Figure 6-20).

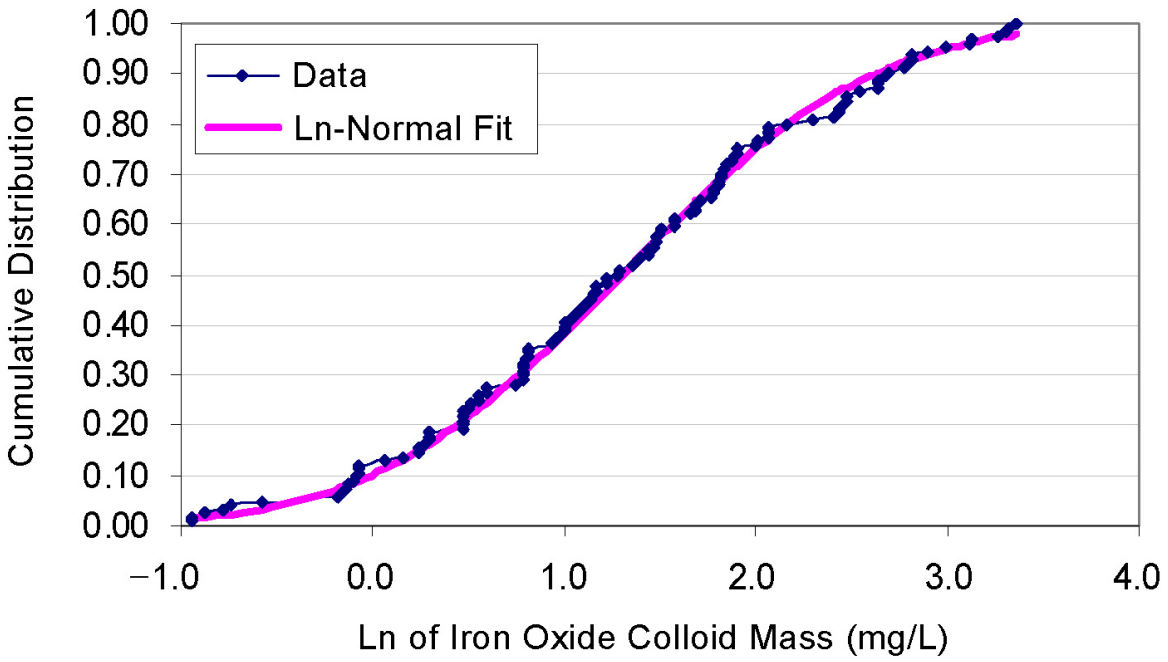

Source: Output DTN: MO0705COLCONCS.000.

NOTE: Data reported in Zarrabi et al. 2003 [DIRS 171238] and DTN: MO0312UCC034JC.008 [DIRS 166367], using the link to the Excel spreadsheet "Data File." The geometric mean = 3.69 mg/L with geometric standard deviation = 2.79.

Figure 6-20. Log_e Normal Fit to Iron Oxide Colloid Mass

The majority of available data from Zarrabi et al. (2003 [DIRS 171238]) was used in the development of the model. However, data obtained under low pH conditions was excluded on the basis that it was well outside the bounds of anticipated conditions in the waste package.

The colloidal size fraction of these materials represents viable analogues for the nature and quantity of corrosion-generated iron oxide colloids that could potentially be produced and transported from the carbon steel-based engineered barrier system during the corrosion of the waste packages after breaching. From the $\log_e$-normal distribution of the miniature waste package corrosion tests results, a geometric average concentrations of 3.69 mg/L was determined for the four-week-long experiments. The carbon steel miniature waste packages became clogged after four weeks, probably due to the formation and accumulation of corrosion products (e.g., iron oxyhydroxide).

For the colloid concentrations associated with stainless steel there is little relevant data. A distribution was selected that was based on an assessment of the amount of corrosion that might be expected (see Figure 6-21 and Table 6-11). This distribution was then compared with corrosion studies reported by Dietz (2005 [DIRS 179542]) on Stainless Steel Type 316, the amount of corrosion is anticipated to be minimal (see Section 7.1.4). Smailos et al. (2003 [DIRS 179559]) have reported small corrosion layers during high temperature oxidation of stainless steels. The assessment of colloid concentrations from stainless steel is subjective as there is insufficient data available to make a reliable analysis. As stainless steel is less corrosive than carbon steel, the overall colloid mass distribution was reduced compared to carbon steel.

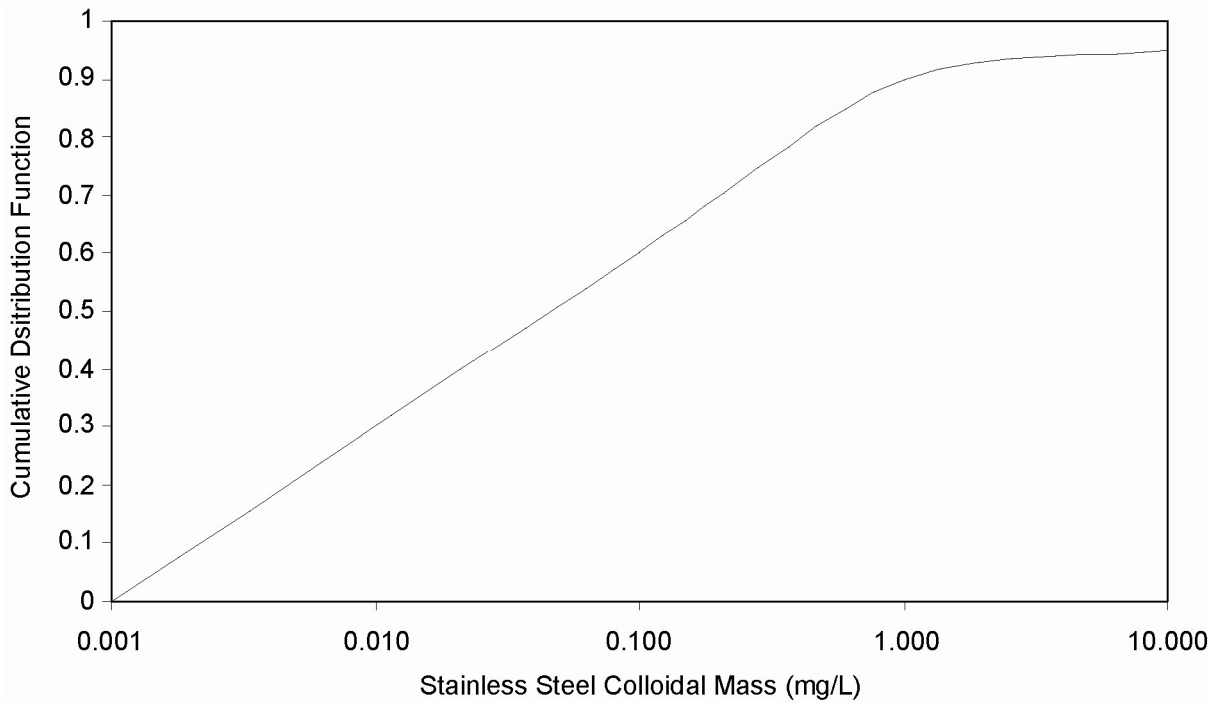

Source: Table 6-11.

Figure 6-21. Modeled Distribution Iron Oxide Colloid Mass from Stainless Steel Corrosion

Table 6-11. Uncertainty Distribution for Stable Colloids from Corroded Stainless Steel Waste Package Colloid

FeOx Colloid Concentration (mg/L)	Cumulative Probability
0.001 to 0.1	0.60
0.1 to 1.0	0.90
1.0 to 10	0.95
10 to 30	1.00

Source: Output DTN: MO0705COLCONCS.000.

NOTE: Minimum value when colloids are unstable: 1×10^{-6} mg/L.

Uncertainty in the data generated by the miniature waste package experiments and the consideration of iron oxyhydroxide colloid concentrations reported in the literature for groundwaters in iron-rich geologic environments is discussed in Section 6.6.5.

6.3.9 Type, Abundance, and Stabilities of Natural Colloids within UZ Seepage Water and/or Groundwater

Natural colloids occurring in seepage water or groundwater in the repository vicinity are modeled as smectite clays. Although silica, zeolites, and iron oxyhydroxides will also be present in seepage water or Yucca Mountain groundwater (Kingston and Whitbeck 1991 [DIRS 113930]), these were not explicitly represented for a number of reasons. First, silica has a much lower sorptive capacity than smectite clay, second, clay colloids have been observed as contributing to radionuclide transport in the natural system within Nevada and are in general the most abundant type (see Section 6.3.1), and third, the abundance of iron oxyhydroxides in the waste package will be more comparable to the abundant natural colloids and exceed the concentrations of iron oxyhydroxides that may occur in the seepage waters. The presence and potential influence of natural seepage water colloids on the formation of radionuclide-bearing colloids in the engineered barrier system are considered by modeling seepage water colloids as smectite, which are referred to as "groundwater colloids" throughout this document. There are a number of aspects that may affect the abundance of groundwater colloids including the two major ones that are temperature and ionic strength (fluid composition) that both can play a role in the concentration of stable colloid suspensions. These are discussed here and the compositional effects are then discussed further in Section 6.3.11 based on data from the site and elsewhere.

Temperature—The stability ratio (*W)* given by the ratio of Equations 6-4 and 6-5 above, indicates that an increase in temperature should result in destabilization of a colloid suspension. For the purposes of this abstraction, the temperature effect has not been represented because it would only serve to decrease colloid abundance. It is assumed here that colloids resulting from waste form corrosion tests conducted at 90°C would also be stable at 25°C (Section 5, Assumption 5.2).

Ionic Strength—The primary effect that solution composition has on the abundance of colloids (i.e., their concentrations in stable suspensions) can be represented by the ionic strength of the solution. The role of ionic strength is captured in the κ term of the Debye equation (van Olphen 1977 [DIRS 114428]). For a given counter-ion concentration, the higher the valence of the counter-ions, the more unstable the colloid suspension and the greater the tendency to flocculate (van Olphen 1977 [DIRS 114428]). So for solutions with highly charged species, the stable

concentration of colloids would be lower than a comparably concentrated solution of monovalent species. The solution concentration point at which the colloids flocculate is represented by the critical coagulation concentration (CCC).

The CCC is one of the most important characteristics of a colloid dispersion. Experimental observations suggest that the variation of CCC with the valence of the counter ions roughly follows an inverse sixth power law, also termed the Schulze-Hardy rule. At the CCC, the stability ratio is one, leading to rapid flocculation. In his treatise on clay colloidal dispersions, van Olphen (1977 [DIRS 114428], p. 24) summarized empirically determined critical coagulation-concentration values (Table 6-12a).

Table 6-12a. Critical Coagulation Concentration Values

Counter-ion Valence	Critical Coagulation Concentration (M)
±1	2.5×10^{-2} to 1.5×10^{-1}
±2	5×10^{-4} to 2×10^{-3}
±3	1×10^{-5} to 1×10^{-4}

Source: van Olphen 1977 [DIRS 114428].

At pH values below the pH_{pzc} (where pzc is the point of zero charge) for a mineral, the negatively charged counter-ions are important; above the pH_{pzc}, positively charged counter-ions are important (van Olphen 1977 [DIRS 114428]). For comparison, concentrations of counter-ions in J-13 well water have been reported and are listed in Table 6-12b.

Table 6-12b. Concentrations of Counter-ions in Input Water Compositions

	Ca Pore Water	Na Pore Water	J-13 Well Water
Ion	Concentration (moles/L)		
Na^+	1.3×10^{-3}	4.1×10^{-3}	2.0×10^{-3}
K^+	2.6×10^{-4}	2.1×10^{-4}	1.3×10^{-4}
Ca^{2+}	3.2×10^{-3}	2.8×10^{-3}	3.2×10^{-4}
Mg^{2+}	6.2×10^{-4}	1.1×10^{-4}	8.3×10^{-5}
Cl^-	7.2×10^{-4}	8.3×10^{-4}	2.0×10^{-4}
SO_4^{2-}	1.2×10^{-3}	1.1×10^{-3}	1.9×10^{-4}
pH	7.6	7.4	7.41

Source: Taken from BSC 2005 [DIRS 180506], Table 4-2, p. 18 (units converted from mg/L to mol/L).

NOTE: Carbonate was not included in table. Although carbonate is important in the chemical behavior of several radionuclides, the table is presented for demonstrating the differences in the ionic strength of the waste package and in-drift groundwaters.

The concentrations of individual ions in J-13 well waters do not exceed empirical CCC values. However, for the Ca and Na pore waters, the CCC value is exceeded. The conclusion is that colloid dispersions will probably be stable in J-13 well water. However, the predicted Ca and Na pore-water compositions as described in *In-Package Chemistry Abstraction* (SNL 2007 [DIRS 180506]) suggest that colloids may be destablized. The ionic strengths of the Ca pore water, Na pore water, and J-13 well water are <0.005 M, <0.02 M, and <0.02 M, respectively.

If the ionic strength were to reach extremely high values (i.e., 1 M), restabilization has been predicted to occur.

6.3.10 Re-Stabilization of Colloids at Very High Ionic Strength

The aggregation of electrostatically stabilized colloids with DLVO theory is well established; however, certain cases exist where the aggregation behavior does not agree with DLVO theory. Several studies have shown that clays, metal oxides, and various organic colloids undergo an increase in stability or a decrease in aggregation rate at high salt concentrations (>1 mol/L). The phenomenon known as colloid re-stabilization can occur above an ionic strength of 1.0 mol/kg. High salt stabilization has been attributed to the ability of acidic and basic sites on the surface to associate with the abundance of counter-ions that exist at high salt concentrations creating ion pairs or surface dipoles. These surface dipoles then polarize the water molecules, ordered as ice-like structures, which propagate generating a repulsive force upon overlap of these hydration shells. It is this repulsive energy term that results in re-stabilization of the colloids. The phenomenon has been observed in laponite (Huang and Berg 2006 [DIRS 179549]) and rutile. It is possible that this behavior explains the increase in colloid concentrations in the two high saline tests performed by Zarrabi et al. (2003 [DIRS 171238]). Ruckenstein and Huang (2003 [DIRS 179556]) have developed a model to describe this behavior, but it has not been implemented in the current abstraction because the model is empirical and difficult to extend to non-idealized systems. A quantitative theory of colloid restabilization has only been developed in the last few years and was not available for consideration during earlier versions of this report.

6.3.11 Literature and Site-Specific Data on Stability and Concentration of Seepage Water Colloid Suspensions

Colloids exist naturally in groundwater in subsurface environments, with the composition and concentration of colloids being site-specific and determined by the geologic nature of the subsurface. Transport of radionuclides by groundwater colloids is a potentially important transport process and is thought to be generally more prevalent than transport by true colloids (McCarthy and Zachara 1989 [DIRS 100778]).

McCarthy and Degueldre (1993 [DIRS 108215]) and Degueldre et al. (2000 [DIRS 153651]) have characterized the colloids from groundwaters sampled at various locations around the world from crystalline and sedimentary rocks in saturated and unsaturated hydrologic regimes. They showed that the colloid concentration and suspension stability are dependent on several factors; however, colloid suspensions tend to be stable if the concentration of alkalis (Na and K) is below approximately 10^{-2} M and if alkali-earth elements (Ca and Mg) are below approximately 10^{-4} M (Figure 6-22). In the case of Ca and Na pore waters, described in *In-Package Chemistry Abstraction* (SNL 2007 [DIRS 180506]), the Ca^{2+} concentration is $>10^{-4}$ M, which would lead to colloid suspension instability in the waste package environment. While the DLVO calculations provide useful inferences on mechanisms of colloid destabilization, these empirical observations may be more useful in developing approaches to performance assessment calculations.

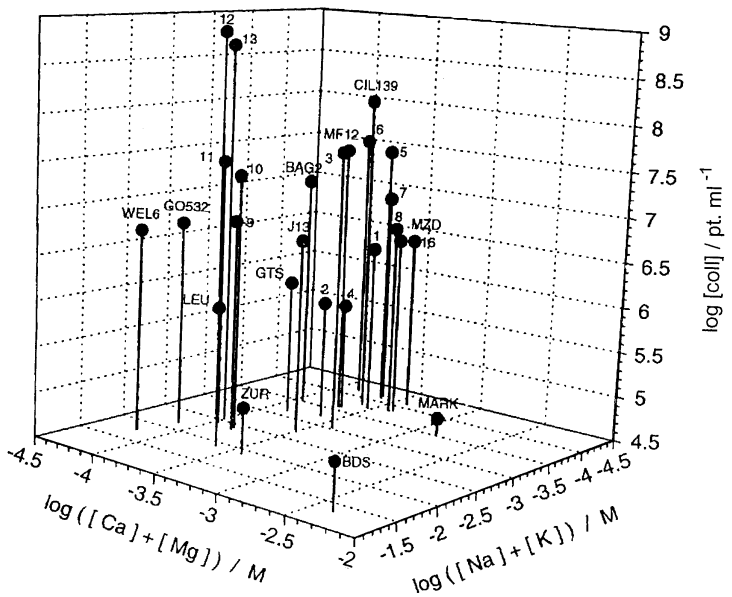

Source: Adapted from Degueldre et al. 2000 [DIRS 153651].

NOTE: pt = particles. Here, concentrations of colloids are compared on the basis of alkali and alkaline-earth element concentration for colloid size greater than 100 nm.

Figure 6-22. Colloid Concentrations versus Alkali and Alkaline-Earth Concentration for Groundwaters from around the World

Data from the Yucca Mountain area and the Nevada Test Site indicated a highly variable colloid concentration over a range of ionic strength (0.001 to 0.02), in agreement with the findings of Kingston and Whitbeck (1991 [DIRS 113930]) and Degueldre et al. (2000 [DIRS 153651]). Figure 6-23 plots the groundwater colloid concentrations in water samples collected in the vicinity of Yucca Mountain. Data sources included in the figure are:

Groundwater Colloid Populations—DTNs: LA0002SK831352.001 [DIRS 149232]; LA0002SK831352.002 [DIRS 149194]; LA0002SK831352.004 [DIRS 161579]; LA9910SK831341.005 [DIRS 144991]; LA0211SK831352.001 [DIRS 161580]; LA0211SK831352.002 [DIRS 161581]; LA0211SK831352.003 [DIRS 161582]; LA0211SK831352.004 [DIRS 161458]; LA0002SK831352.003 [DIRS 161771]) and colloid concentrations in groundwaters sampled around the world by Degueldre et al. (2000 [DIRS 153651]) and from DTN: SNT05080598002.001 [DIRS 162744].

Ionic Strength Data—DTNs: SNT05080598002.001 [DIRS 162744], LA0304PR831232.001 [DIRS 163196], and LA0304PR831232.002 [DIRS 163197].

The groundwater colloid samples analyzed represent colloid particle size distributions from 50 nm to 200 nm in diameter while the data from groundwaters around the world (DTN: SNT05080598002.001 [DIRS 162744]) represent colloid particle size distributions from 100 nm to 1,000 nm (1.0 μm diameter). Evaluation of the colloid populations in the various size fraction classes for each groundwater sample did not reveal a systematic increase in the number of particles with decreasing particle-size class (Table I-2). Therefore, inclusion of particle-size classes smaller than 50 nm should not result in a substantially greater mass concentration in the

water sample, especially since the smaller particles would have exponentially lower mass; therefore, omission of the less than 50-nm particle-sized fraction in the mass concentration calculations is reasonable.

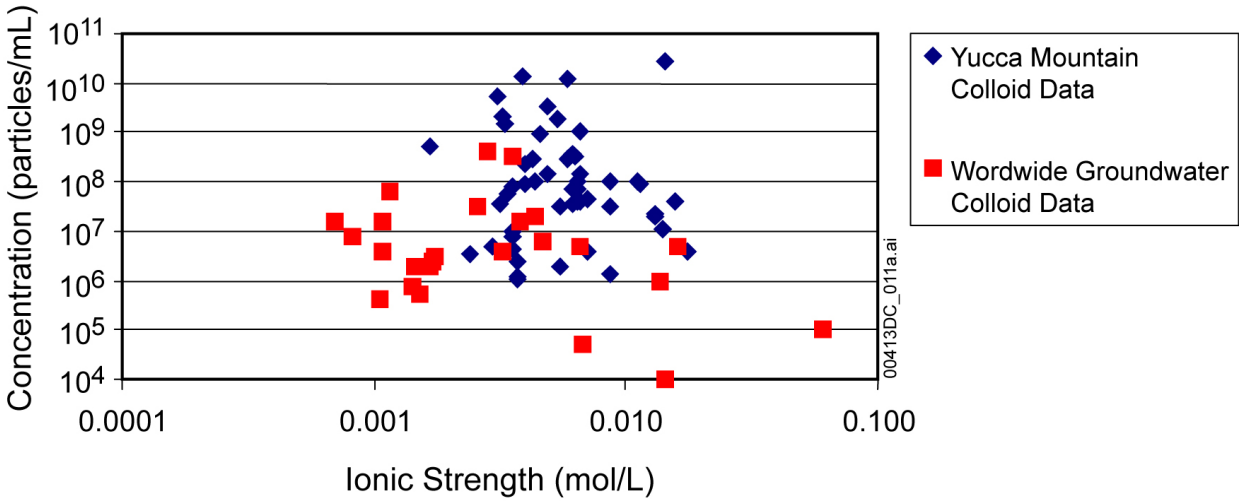

Sources: Yucca Mountain site colloid data: DTNs: LA0002SK831352.001 [DIRS 149232]; LA0002SK831352.002 [DIRS 149194]; LA9910SK831341.005 [DIRS 144991]; LA0211SK831352.001 [DIRS 161580]; LA0211SK831352.002 [DIRS 161581]; LA0211SK831352.003 [DIRS 161582]; LA0211SK831352.004 [DIRS 161458]; LA0002SK831352.003 [DIRS 161771]; LA0002SK831352.004 [DIRS 161579]. Groundwater colloid population data: DTN: SNT05080598002.001 [DIRS 162744].

NOTE: Ordinate values are presented in particles per milliliter.

Figure 6-23. Groundwater Colloid Concentration Data Collected in the Vicinity of Yucca Mountain Compared with Data Collected from Groundwaters around the World

Colloid particle number data (particles (pt)/mL) for groundwater samples from the Yucca Mountain area and the Idaho National Laboratory were converted to mass concentrations (mg/L) (Appendix I). The colloid data from DTN: SNT05080598002.001 [DIRS 162744] were not used to calculate the mass colloid concentrations (mg/L) but were only used to establish a general relationship between ionic strength and colloid populations in groundwaters around the world and, specifically, in the Yucca Mountain area (Figure 6-23).

The groundwater colloid data from the Yucca Mountain site and the Idaho National Laboratory were pooled, and a discrete CDF was established to evaluate the uncertainty in colloid concentration distribution. The colloid concentrations data included the following DTNs:

- LA0002SK831352.001 [DIRS 149232]
- LA0002SK831352.002 [DIRS 149194]
- LA9910SK831341.005 [DIRS 144991]
- LA0211SK831352.001 [DIRS 161580]
- LA0211SK831352.002 [DIRS 161581]
- LA0211SK831352.003 [DIRS 161582]
- LA0211SK831352.004 [DIRS 161458]
- LA0002SK831352.003 [DIRS 161771]
- LA0002SK831352.004 [DIRS 161579].

The Idaho National Laboratory groundwater colloid data (DTN: LA0002SK831352.003 [DIRS 161771]) was deemed appropriate for inclusion in the data analysis as corroborative data even though these groundwater colloid data are not from the vicinity of Yucca Mountain (Appendix I). Water samples that had been filtered were not considered in the development of the uncertainty distribution. Since the colloid particles were measured by dynamic light scattering techniques, any potential error in measurement of colloid populations for the various particle size classes due to filter "ripening" (i.e., clogging of filter pores through time during the filtration process) was avoided by using only non-filtered sample data.

The data shown in Figure 6-23 reflect observed variability in groundwater colloid concentrations. The goal of the uncertainty distribution for groundwater colloid concentrations is to numerically capture our knowledge about uncertainty on a large scale. Based on the groundwater colloid concentration collected at the two sites (Yucca Mountain and the Idaho National Laboratory) and the large uncertainty associated with the collection of groundwater colloids, a reasonable representation of the uncertainty is shown in the discrete cumulative distribution function shown in Figure 6-24 (Table 6-13 shows the probabilities associated with the discrete cumulative distribution function). Major factors that contribute to uncertainty in the collection of groundwater colloids include: (1) collection techniques, (2) differences in pumping rates at each well, and (3) unknown factors including the types of additives introduced in the wells during the drilling process itself.

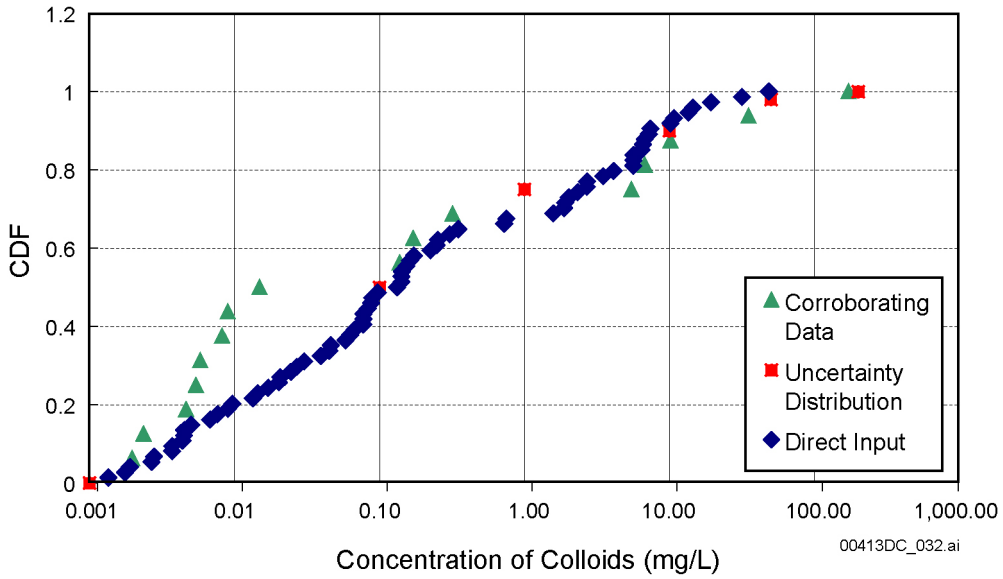

Source: Cumulative distribution was obtained by plotting data (shown as blue diamonds) reported in the last column (colloid concentration per volume (mg/L)) of Table I-1 from Appendix I (in this report) that are derived from the following data sets: DTNs: LA0002SK831352.001 [DIRS 149232]; LA0002SK831352.002 [DIRS 149194]; LA9910SK831341.005 [DIRS 144991]; LA0211SK831352.001 [DIRS 161580]; LA0211SK831352.002 [DIRS 161581]; LA0211SK831352.003 [DIRS 161582]; LA0211SK831352.004 [DIRS 161458]. Note that both DTN: LA0002SK831352.003 [DIRS 161771] and DTN: LA0002SK831352.004 [DIRS 161579] provide data that are evaluated in Appendix I, and the derived values (shown by the green triangles) are used to corroborate the direct input above. Groundwater colloid population data are obtained from DTN: SNT05080598002.001 [DIRS 162744].

Figure 6-24. Cumulative Distribution Function Showing the Probability of Occurrence of Colloid Concentration Levels in Groundwater Samples in the Yucca Mountain Area and Idaho National Laboratory

The waste form and engineered barrier system components of the TSPA-LA analyses implement the uncertainty shown in Figure 6-24 only for ionic strength when colloids are calculated to be stable. Above the ionic strengths at which colloid suspensions become unstable (which depends on the pH and is based on DLVO theory as described above), a single low value (1×10^{-6} mg/L) is used for the concentration of seepage colloids.

Table 6-13. Uncertainty Distribution for Groundwater Colloid Concentrations for the TSPA-LA Analyses Based on Ionic Strength (I) of the Water Sample

Ionic Strength (I)	Groundwater Colloid Concentration (mg/L)	Interval Probability of Occurrence	Cumulative Probability of Occurrence
I < threshold	0.001 to 0.1	50	50
	0.1 to 1.0	25	75
	1.0 to 10	15	90
	10 to 50	8	98
	50 to 200	2	100
I ≥ threshold	1×10^{-6}	100	100

Source: Developed from the data presented in Figure 6-24.

NOTE: Threshold = $-0.008 \times pH^2 + 0.12 \times pH - 0.03$.

Review of the colloid data in Appendix I reveals that the largest proportion of groundwater colloid samples had colloid concentration populations between 0.001 and 0.1 mg/L, and thus the values between these concentrations are modeled as having a sampling probability of 50% if the ionic strength satisfies the stability criteria. Colloid concentration values of 0.1 mg/L to 10 mg/L indicate a reasonable probability of occurrence of 40%. To account for colloid concentrations between 10 mg/L and 50 mg/L, a probability of 8% was included. Some of the corroborative (unqualified) data included values as high as 171 mg/L to 200 mg/L (Table I-1, Appendix I), but the uncertainty distribution based on the direct data indicates that these values have a low probability of occurring.

6.3.12 Radionuclide Sorption to Colloids

A description of radionuclide sorption to colloids is presented in this section. Nonradioactive colloids are only important to repository performance insofar as radionuclides sorb to them. "Sorption" as used here is a general term that has been used throughout the literature to include interactions between dissolved ions and mineral surfaces governed by processes such as : (1) electrostatic forces, (2) ion exchange, (3) surface reaction, and (4) coprecipitation. Although the term is used here similarly, it is used primarily to denote processes that involve surface interactions between the ions and minerals that do not dramatically alter the nature of the dissolved species (e.g., do not change its oxidation state). Note that where the reaction mechanism is not being even loosely specified, the term "attachment" is used to be purposely general. Sorption may occur by a number of mechanisms and all of these may be considered (1) reversible (i.e., attachment to the surface and detachment from the surface occur *instantaneously* at an established dynamic equilibrium value represented by the equilibrium sorption coefficient—K_d), (2) irreversible (i.e., the attachment rate or detachment rate is kinetically slow such that the apparent distribution coefficient is not the equilibrium value), or (3) appear to be effectively completely irreversible (i.e., desorption is so slow that the detachment does not even matter relative to the time frame of transport). This last case is only an effective property because

even very small rates may effectively detach material if the time frame of interest is large enough (e.g., as is the case for stationary materials). The relative rates of sorption, desorption, and transport determine the approach to reversibility of the sorption. When sorption reactions are fast (i.e., reversible), equilibrium conditions apply and the linear isotherm model is applicable for describing radionuclide uptake and release. Even in cases of slightly irreversible sorption processes, such an equilibrium approach is a reasonable approximation if the transport rates are slow in comparison. When sorption is highly irreversible (i.e., desorption is slow relative to transport times), then local equilibrium models are less accurate, resulting in over- or under-predictions of transport, and kinetic (i.e., rate-based) models can facilitate evaluation. Kinetic and competitive sorption models (where each sorbing radioelement competes amongst them all for the fixed number of sites on the mineral surface) have been developed to assess these processes with the linear K_d (SNL 2007 [DIRS 177407]).

6.3.12.1 Reversible Sorption

Perhaps the most common approach used in assessment of contaminant–rock interactions in the subsurface is the linear isotherm, or K_d value (distribution coefficient) approach, based on results of batch sorption experiments. The linear isotherm model relationship may be defined as follows:

$$S = K_d C \quad \text{(Eq. 6-13)}$$

where

S = mass of a solute adsorbed on a unit mass of solid (μg/g)
K_d = distribution coefficient (mL/g)
C = concentration of the adsorbing solute in solution (μg/mL).

The amount of solute adsorbed on a solid can also be defined on the basis of area as follows:

$$S = K_a \times S_A \times C \quad \text{(Eq. 6-14)}$$

where

S = mass of a solute adsorbed on a unit area of solid
K_a = distribution coefficient (area based)
C = concentration of the adsorbing solute in solution
S_A = surface area of solid.

Depending on the size distribution of colloids in the aqueous phase, the impact of choosing a mass-based K_d value, or a surface-area-based K_a value, may be significant. The greatest deviation exists in situations in which a large number of small colloids exist, which have a high surface-area-to-mass ratio. Available sorption information for validation of the model is mass based, and conversion to surface-area-based information is not straightforward.

Three critical conditions must be met for this relationship to be applicable. First, the water-contaminant-rock system must be in thermodynamic equilibrium (i.e., sorption must be completely reversible). Second, contaminant uptake must scale linearly with contaminant

concentration. Third, the presence of other solutes in the system cannot affect the sorption. Because of the nature of the formation of waste form colloids and the interactions of some radionuclides, particularly some actinides, with mineral surfaces, certain conditions of the linear isotherm model are not met; therefore, other approaches must be taken, as described below.

A large quantity of data exists in published literature for sorption, and, in the past several decades, increasing attention has been given to understanding the mechanisms of sorption. In this section, the development of K_d values for uptake of Pu, Am, Th, Pa, U, Np, Ra, Sn, and Cs on colloids is described, along with caveats for their use. Values for americium were assumed to be valid for thorium and protactinium. These radionuclide elements were chosen for analysis because, based on a screening exercise, they are considered by TSPA to be important to dose in the 10,000-year to one-million-year timeframe; high uncertainty surrounds their potential behavior as pseudocolloids; and daughter products of uranium may remain associated with uranium-bearing colloids.

The radionuclides considered for reversible sorption, and the rationale for their selection, are listed below. Characteristics of the radionuclides considered were half-life, sorption characteristics, inventory in the repository, and observed field and laboratory behavior.

- **Plutonium**. Important isotopes with respect to dose calculations include ^{239}Pu, ^{242}Pu, and ^{238}Pu. Plutonium is sparingly soluble but sorbs strongly to oxide mineral surfaces (generally less strongly to silicates) (Lu et al. 2003 [DIRS 170883]; EPA 1999 [DIRS 147475], Volume 2, Appendices D, G, I, and J; Kersting and Reimus 2003 [DIRS 162421]). The formation of pseudocolloids through the sorption of plutonium particularly to iron oxyhydroxide colloids from corrosion of steel in the repository may increase the effective mobility of plutonium.

- **Americium**. Americium is sparingly soluble but sorbs strongly to mineral surfaces, including colloids (Degueldre et al. 1994 [DIRS 174069]). Americium exhibits large K_d values often in the range of 1,000 mL/g to >100,000 mL/g, depending on the Eh. However, the concentrations of dissolved americium may be controlled by precipitation in many environments (EPA 2004 [DIRS 172215]). Therefore, high reported sorption measurements may reflect precipitation reactions. The developed distributions accounted for possible precipitation and also for the possibility that the smectite clays formed from DHLWG have variable compositions and can contain iron oxides (Lu et al. 1998 [DIRS 100946]; Lu et al. 2000 [DIRS 166315]).

- **Thorium**. Thorium adsorption occurs at concentrations $<10^{-9}$ M and will precipitate at concentrations $>10^{-9}$ M based on the solubility of $Th(OH)_4$ at pH 5.5 (Bitea et al. 2003 [DIRS 173041]). Reversible sorption of thorium is not reported in waste glass corrosion tests; indeed, thorium has been observed as a colloidal phosphate (Fortner et al. 1997 [DIRS 114452]). Phosphates will be present in DHLWG formulations (Fowler 2003 [DIRS 164361]). Similar observations have been made in natural systems on thorium phosphates (Tauton et al. 2000 [DIRS 170891]). Whether an equilibrium K_d value is applicable to describing the sorption behavior of thorium is debatable.

- **Neptunium**. The NpO_2^+ ion may be soluble under anticipated repository conditions and will be less likely to participate in colloid formation than the other actinides. The sorption properties of Np(V) have a strong dependence on pH (EPA 2004 [DIRS 172215]; Bradbury and Baeyens 2005 [DIRS 179538], Figure A4 (c and d), p. 889). Retention or sorption of neptunium in alteration products has been observed under high pH conditions (Ménard et al. 1998 [DIRS 171053]; Lu et al. 2000 [DIRS 166315]; McNamara et al. 2005 [DIRS 174068]); however, because these high pH regimes (i.e., >pH 9) are not anticipated to occur in the waste package environment, this high pH data has not been used in the model.

- **Cesium**. Few stable cesium complexes will exist in groundwater. Cs^+ ion exchange will occur with Na^+ or Ca^{2+} in montmorillonite (Atun et al. 1996 [DIRS 164865]) and in uranyl silicates, such as boltwoodite (Burns 1999 [DIRS 110975]) and uranophane (Douglas et al. 2002 [DIRS 179546]). The degree of sorption/desorption will depend on the availability of clays and the concentration of other ions that will compete for adsorption sites; however, within the low ionic strengths anticipated in the repository environment, this is not considered to be an important process. Cesium will only sorb weakly onto iron oxides (Torstenfeld et al. 1982 [DIRS 171770]).

- **Protactinium**. The +5 state is the normal oxidation state for protactinium in solution. Protactinium sorbs strongly to smectite clay (Bradbury and Baeyens 2006 [DIRS 179541], Figure 3, p. 622). The potential colloidal behavior of protactinium has been assumed conservatively to be similar to americium for modeling purposes.

- **Uranium**. Uranium (^{235}U, ^{233}U, and ^{238}U) will be the most abundant radioactive element in the repository. For this reason, uranium was considered in the analysis. The sorption edge for uranium (2×10^{-6} M) on hematite (1 g/L) has been reported to be near pH 5.5 (Hardin 1998 [DIRS 100123], p. 6A-23, Figure 6-28).

- **Radium**. One radium isotope of importance, ^{226}Ra ($t_{½}$ =1.6×10^3 a), is produced by α-decay from ^{230}Th ($t_{½}$ = 7.52×10^4 a). Close chemical analogues for radium are barium and strontium. Development of sorption parameters for radium has required comparison with barium and strontium because of the lack of relevant data. However, the behavior of Th at the surface of altered materials may control Ra release. Transfer of radium from a waste form to the groundwater must occur on a time scale that is rapid relative to the half-lives of the Ra isotopes being considered. Hence, the shorter-lived isotopes, ^{223}Ra ($t_{½}$ =11.68 d), ^{224}Ra ($t_{½}$ = 3.64 d), ^{225}Ra ($t_{½}$ =15 days), and ^{228}Ra ($t_{½}$ = 5.75 a), may be less important. Nevertheless, sorption data for radium is included in the model.

- **Tin**. Tin is stable in its tetravalent form, Sn(IV), and $Sn(OH)_5^-$ and $Sn(OH)_6^{2-}$ are the dominant hydrolytic species. ^{126}Sn is the long lived isotope that has been considered in the analysis for 1 Ma dose estimates. Sparse data is available on the sorption properties of this element on repository relevant surfaces; however, Sn(IV) sorbs strongly to smectite clay (Bradbury and Baeyens 2005 [DIRS 179538]).

The pH and ionic strength (particularly concentrations of Na^+, Ca^{2+}, and K^+) primarily control the behavior of the mineral surface. The effects of pH have not been considered in this model. Within the range of pH anticipated in the repository environment, the changes in K_d values have been accounted for in the distributions developed in Table 6-14. The concentrations of ions (Na^+, Ca^{2+}, and K^+) will alter sorption of Cs^+ and Ra^{2+}. In a study by Wood et al. (2006 DIRS 180970]), cyclic sorption behavior of rare earths elements was observed in a natural environment. The reversible cyclic adsorption-desoprtion of rare earths elements onto hydrous ferric or aluminum oxide was temperature dependent as the water warmed and cooled throughout the day. For minerals in which the sorption mechanism is primarily by ion exchange (e.g., clay minerals), ionic strength impacts sorption of alkali metals on clay minerals (especially at their edges), because cations compete with radionuclides for exchange sites (Atun et al. 1996 [DIRS 164865]).

To develop colloid K_d values, information provided by YMP data and published literature was considered. Lu et al. (1998 [DIRS 100946]; 2000 [DIRS 166315]) provide useful discussion of the sorption of Pu(IV) and Pu(V) on colloidal dispersions of hematite, goethite, montmorillonite, and silica. Discussion of Am(III) is provided for all but goethite; however, all sorption values on iron oxide are presented for information purposes and are not used in the model. Sorption was measured as a function of time up to 4 or 10 days. Desorption was measured after 150 days because desorption tends to be much slower in these mineral-sorbate systems (Lu et al. 1998 [DIRS 100946]; 2000 [DIRS 166315]). The experimentally determined K_d values for plutonium and americium are summarized in Table 6-14.

Table 6-14. Experimentally Determined K_d Values for Plutonium and Americium Sorption onto Hematite and Montmorillonite

Phenomena Investigated	K_d Values, mL/g	
	J-13 Well Water	Synthetic J-13 Well Water
Plutonium-Hematite (DTN: LA0003NL831352.002 [DIRS 148526])		
Sorption (forward, up to 10 days; colloid concentration not specified in DTN)	5.00×10^3 to 1.10×10^5	1.20×10^5 to 7.00×10^5
Desorption (backward, 32 days; colloid concentration not specified in DTN)	3.40×10^5	3.20×10^5
Colloid concentration (forward, 10 mg/L to 150 mg/L, 10 days)	7.50×10^3 to 3.70×10^4	7.70×10^3 to 2.60×10^4
Temperature (forward, 20°C to 80°C, 10 days)	1.70×10^5 to 4.90×10^6	(not in DTN)
Plutonium-Montmorillonite (DTN: LA0003NL831352.002 [DIRS 148526])		
Sorption (forward, up to 10 days; colloid concentration not specified in DTN)	2.30×10^2 to 5.80×10^3	2.40×10^2 to 6.50×10^3
Desorption (backward, 32 days; colloid concentration not specified)	6.70×10^3	6.50×10^3
Colloid concentration (forward, 10 mg/L to 150 mg/L, 10 days)	5.20×10^3 to 2.70×10^4	3.20×10^3 to 2.40×10^4
Temperature (forward, 20°C to 80°C, 10 days)	9.50×10^3 to 2.00×10^5	(not in DTN)

Table 6-14. Experimentally Determined K_d Values for Plutonium and Americium Sorption onto Hematite and Montmorillonite (Continued)

Phenomena Investigated	K_d Values, mL/g	
	J-13 Well Water	Synthetic J-13 Well Water
Americium-Hematite (DTN: LA0005NL831352.001 [DIRS 149623])		
Sorption (forward, up to 10 days; colloid concentration not specified in DTN)	7.90×10^4 to 1.00×10^7	1.20×10^5 to 6.20×10^6
Desorption (backward, 200 days; colloid concentration not specified)	1.90×10^5	8.40×10^4
Colloid concentration (forward, 10 mg/L to 150 mg/L, 10 days)	1.90×10^6 to 1.60×10^7	1.80×10^6 to 2.80×10^7
Temperature (forward, 20°C to 80°C, 10 days)	1.80×10^5 to 6.50×10^5	(not in DTN)
Americium-Montmorillonite (DTN: LA0005NL831352.001 [DIRS 149623])		
Sorption (forward, up to 10 days; colloid concentration not specified in DTN)	7.10×10^3 to 1.0×10^5	2.30×10^4 to 1.10×10^5
Desorption (backward, 200 days; colloid concentration not specified)	9.10×10^4	1.80×10^4
Colloid concentration (forward, 10 mg/L to 150 mg/L, 10 days)	1.60×10^5 to 1.50×10^6	1.60×10^5 to 8.40×10^5
Temperature (forward, 20°C to 80°C, 10 days)	6.00×10^4 to 2.70×10^5	(not in DTN)

Source: DTNs: LA0003NL831352.002 [DIRS 148526] and LA0005NL831352.001 [DIRS 149623].

Waste form colloids from DHLWG and uranophane colloids from corroded CSNF and DSNF and seepage water/groundwater colloids may become pseudocolloids through reversible sorption of aqueous radionuclides onto them. K_d values for combined adsorption and desorption of Pu, Am (Th, Pa), Np, Cs, Ra, and Sn on DHLWG-derived colloids, uranophane colloids from CSNF and DSNF, and groundwater colloids are used to determine effective reversibility of the radionuclides on colloids according to the relationship:

$$RN_{adsorbed/desorbed} = RN_{dissolved} \times K_{d,RN} \times M_{colloid} \quad \text{(Eq. 6-15)}$$

where RN = radionuclide, $K_{d,RN}$ is the sorption coefficient (mL/g) for radionuclide RN, and $M_{colloid}$ is the concentration of colloids in mol/L.

The K_d values in Table 6-15 are based on the following:

- Ranges are drawn from the following sources: Bradbury and Baeyens (2005 [DIRS 179538]; 2006 [DIRS 179541]; note, this latter source only provides corroborative information for thorium and protactinium); Tachi et al. (2001 [DIRS 179561]); Pabalan and Turner (1997 [DIRS 179555]); and qualified project DTNs: LA0003NL831352.002 [DIRS 148526], LA0003AM831341.001 [DIRS 148751], LA0005NL831352.001 [DIRS 149623], and LA0407AM831341.002 [DIRS 170621].

- For a given radionuclide the maximum value of each range is the same to allow for the possibility that iron oxide–oxyhydroxide will occur as colloids and as coatings on,

or microcrystalline aggregates in association with, smectite colloids in the iron-rich waste package environment. Sorption is dissimilar for americium with hematite and montmorillonite; however, the model simplification, in this case, is conservative. The similar sorption characteristics of poorly crystalline, iron-bearing smectite and hematite for plutonium (Lu et al. 2003 [DIRS 170883]) and the dissimilar results for montmorillonite, support the idea that iron oxides can be associated with clays and impact their sorption characteristics.

- The K_d intervals and probabilities are intended to cover the entire ranges and emphasize the higher ends of the ranges but deemphasize the highest intervals. These distributions are used because (1) the ranges are based on data for colloids and larger minerals, and it is believed that K_d values for colloids will be higher than for larger minerals if their specific surface area is higher; and (2) because of the mechanisms of surface phenomena that actually prevail, K_d values tend to overpredict desorption over time of actinide metals from iron oxyhydroxide colloids (i.e., they underpredict retention by the colloids). Redox changes can result in the irreversible association of plutonium with some mineral surfaces (Kersting and Reimus 2003 [DIRS 162421]).

- Although thorium and protactinium generally have high K_d values for sorption onto montmorillonite that are comparable to plutonium and americium, the model has assumed that thorium and protactinium sorption is identical to that of americium (Section 5.1). Hence, the distribution range for thorium and protactinium is larger than the published data reported by Bradbury and Baeyens (2005 [DIRS 179538]; 2006 [DIRS 179541]).

- K_d value ranges for the uranophane particles from corroded CSNF and DSNF are reported in Table 6-9.

- K_d value ranges and distributions for uranium and neptunium can be pH-dependent. These data sets were developed from the results of Pabalan and Turner (1997 [DIRS 179555]) and Bradbury and Baeyens (2005 [DIRS 179538]), respectively, over a selected pH range. The method and associated uncertainty are discussed in Section 6.6.8.

Figure 6-24a shows sorption data for U and Np, Figure 6-24b describes the data from Ra, Sn, and Cs, and Figure 6-24c shows the sorption data for plutonium and americium. Published data on Th and Pa are also shown but were not used in the analysis. The straight lines describe the distribution fits as listed in Table 6-15. As iron oxides will sorb onto clays in a repository environment, the clay colloids in the waste package environment would have an effectively larger K_d range than the pure mineral (montmorillonite) sorption studies from Lu et al. (2000 [DIRS 166315]) show. Indeed, sorption studies by Lu et al. (1998 [DIRS 100946]) demonstrate that smectite, a poorly crystallized phase that contains iron, had similar sorption characteristics to hematite rather than the pure mineral phase, montmorillonite (Lu et al. 2000 [DIRS 166315]). Jara et al. (2005 [DIRS 180834]) have shown that amorphous aluminosilicates have physical characteristics similar to natural allophanes and amorphous iron oxides rather than montmorillonite clays. The high K_d for americium sorption onto hematite reported by Lu et al. (2000 [DIRS 166315]) may have been affected by precipitation. This issue has been raised

(EPA 2004 [DIRS 172215]) regarding use of high K_d values for americium. The distributions shown in Figure 2-24a for Np and U were developed from literature data and reported in the spreadsheets contained in Output DTN: MO0705DSCSCUSS.000. A log uniform distribution was chosen to best capture the uncertainty in the data.

Many cesium sorption tests on Yucca Mountain silicate minerals (including zeolites) have been reported and smectite clay is often a common surface alteration product on these materials. Zeolites display much higher sorption values for cesium, and although zeolites have been sometimes observed as suspended particles in leachates from DHLWG corrosion tests, they are not included in the model abstraction as they were very rare. Sorption of cesium onto hematite is negligible. Values published by Torstenfelt et al. (1982 [DIRS 171770]) are 2 mL/g to 8 mL/g.

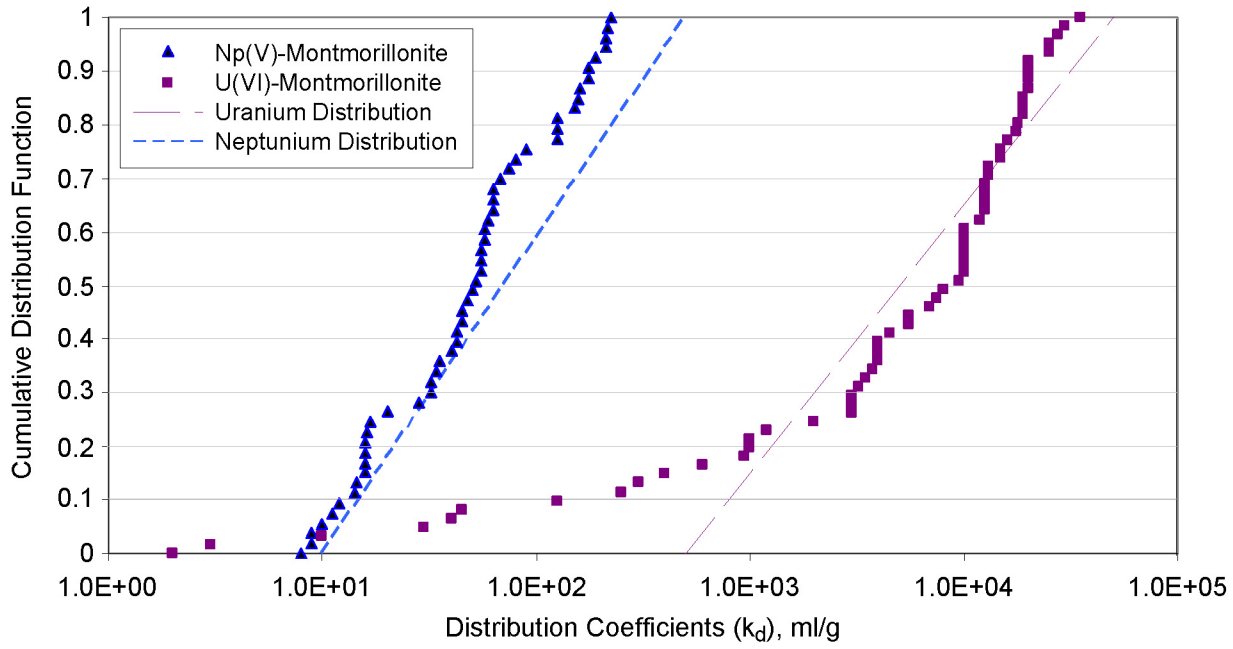

Source: Output DTN: MO0705DSCSCUSS.000.

NOTE: Neptunium (Bradbury and Baeyens 2005 [DIRS 179538], Figures A3 through A4); Uranium (Pabalan and Turner 1997 [DIRS 179555]). The lines are the log uniform distributions as shown in Table 6-15. The distribution fit to the data can be poor, particularly in the case for uranium; however, the distributions are conservative.

Figure 6-24a. Summaries of Np and U Sorption Data on Montmorillonite between pH 5 and 9

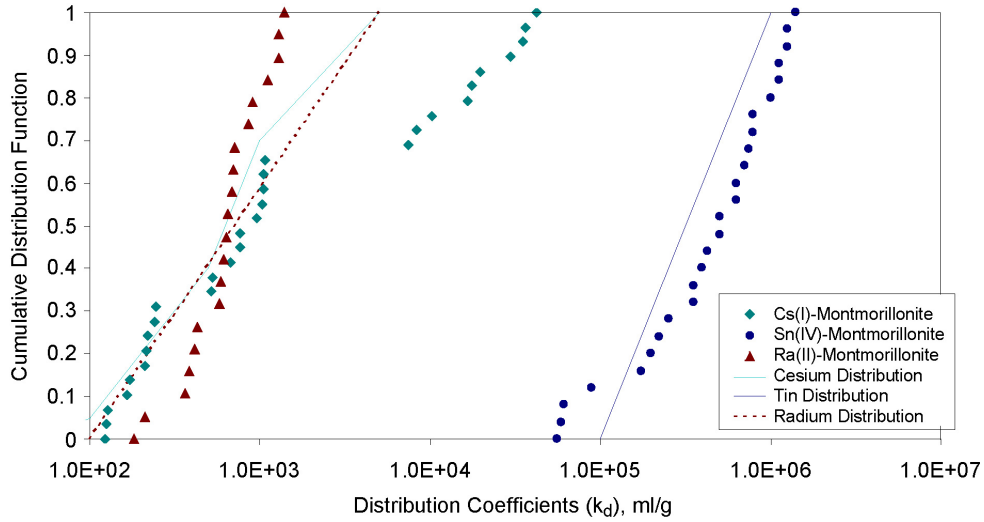

Source: Output DTN: MO0705DSCSCUSS.000.

NOTE: Cesium (DTN: LA0407AM831341.002 [DIRS 170621], Figures A3 through A4). The cesium data exhibits a strong discontinuity in the CDF that is due to the sorption onto tuff dominated by zeolitic phases and clays and an experimental set up that started with very dilute solutions allowing ion exchange reactions to dominate in those cases. The modeled distribution reflects the expected distribution for a smectite clay-dominated system. Tin (Bradbury and Baeyens 2005 [DIRS 179538]); radium (Tachi et al. 2001 [DIRS 179561]). The radium data used does not include tests in de-ionized water (DIW). The lines represent the distributions shown in Table 6-15.

Figure 6-24b. Summaries of Cs, Sn, and Ra Sorption Data on Montmorillonite

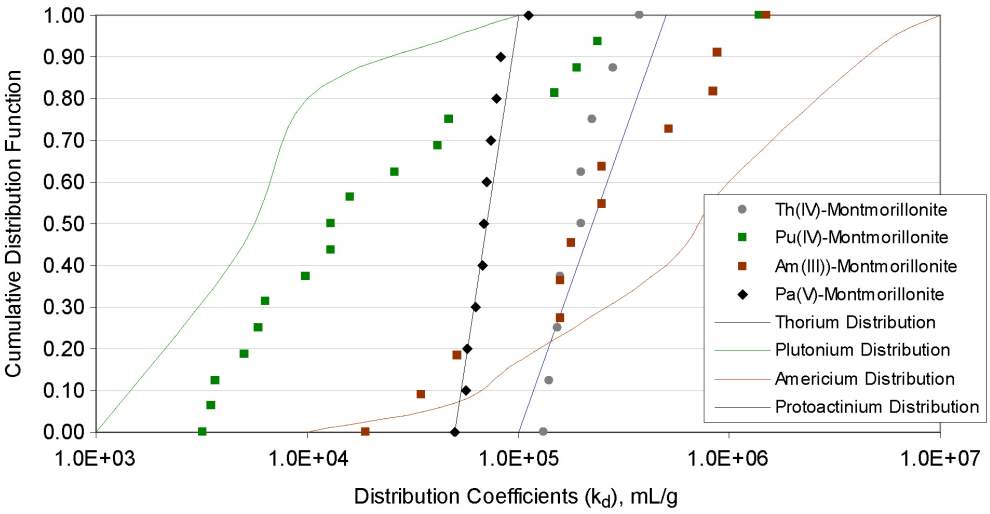

Source: Output DTN: MO0705DSCSCUSS.000.

NOTE: Thorium (Bradbury and Baeyens 2005 [DIRS 179538], Figures A3 through A4) shown for corroborative purposes but not used in the model; plutonium (DTN: LA0003NL831352.001 [DIRS 149172]); americium (Bradbury and Baeyens 2005 [DIRS 179538], Figures A3 through A4); protactinium (Bradbury and Baeyens 2006 [DIRS 179541], Figure 3]) is shown for corroborative purposes but is not used in the model. The lines reflect the distributions provided in Table 6-15. The Am distribution was made highly conservative, relative to the Am data available, to satisfy the model assumption that Th and Pa behave like Am. The plutonium distribution was lowered because of the potential that the highest Kd values reported were due to precipitation.

Figure 6-24c. Summaries of Pu, Am, Th, and Pa Sorption Data on Montmorillonite

The distributions in Figure 6-24 were developed in Output DTN: MO0705DSCSCUSS.000. Cumulative distributions were used to describe the Pu and Am, Th, Pa, Np, U, Ra, and Sn data. The distributions shown as dotted lines in the plots represent the distributions as reported in Table 6-15.

The distributions recommended for neptunium and uranium are shown in Figure 6-24a. The log uniform distributions used to bound the data appear weak in both cases, particularly in the case of uranium, where 20% of the values are much lower than the distribution. This is because sorption of uranium and neptunium on montmorillonite is highly pH dependent; however, there is no pH dependence in the model. The developed distributions endeavor to bound the highest K_d values reported. The log uniform line reflects the uncertainty in modeling sorption of these radionuclides in absence of repository specific data.

The cesium data exhibited a strong discontinuity in the CDF as shown in Figure 6-24b (and discussed in the note below it). The very high values were due to sorption reactions with tuff dominated by zeolitic phases and clays within an experimental set up that started with very dilute solutions allowing ion exchange reactions to dominate in those cases. Hence, the modeled distribution relied primarily on the other data set that used solutions with concentrations that are more like the expected conditions within the natural system, and that reflected more directly the expectation for sorption reactions with smectite clay in those solutions. Radium and cesium sorption values in DIW can be much higher than those reported in groundwater (or similarly low ionic strength solutions) where other cations will compete directly for interlayer sites. Hence, this type of data for starting solutions of DIW was excluded from direct consideration in the analysis to generate the distribution so that sorption processes were not inadvertently overestimated based on conditions that are not expected in the natural system.

In Assumption 5.1, it was pointed out that although the model assumes that the chemical behavior of Pa and Th is treated as identical to Am, experimental data tends to indicate slightly higher R_d values for Th in glass corrosion tests (Luckscheiter and Kienzler 2001 [DIRS 180831]). To account for this in the model, the Am distribution was made more conservative. In Figure 6-24c, the distribution can be seen to bound most of the reported values for Th (Bradbury and Baeyens 2005 [DIRS 179538]) and Pa (Bradbury and Baeyens 2006 [DIRS 179538]) on montmorillonite. The plutonium distribution was lowered because of the potential that the highest K_d values reported were due to precipitation oxides at the surface.

Table 6-15. K_d Values (mL/g) and Cumulative Probabilities Used for Reversible Sorption of U, Np, Sn, and Ra on Iron Oxide and Smectite Type Colloids in TSPA-LA Calculations

Radionuclide	Colloid	K_d Value Range (mL/g) with pH	K_d Value Intervals (mL/g)	K_d Value Cumulative Probabilities
Pu [(a)]	FeCP	10^4 to 10^6	1×10^4 to 5×10^4 5×10^4 to 1×10^5 1×10^5 to 5×10^5 5×10^5 to 1×10^6	0.4 0.7 0.9 1.0
	Smectite	10^3 to 10^5	1×10^3 to 5×10^3 5×10^3 to 1×10^4 1×10^4 to 5×10^4 5×10^4 to 1×10^5	0.45 0.80 0.95 1.00
Am (Th, Pa) [(a)]	FeCP	10^5 to 10^7	1×10^5 to 5×10^5 5×10^5 to 1×10^6 1×10^6 to 5×10^6 5×10^6 to 1×10^7	0.15 0.35 0.90 1.00
	Smectite	10^4 to 10^7	1×10^4 to 5×10^4 5×10^4 to 1×10^5 1×10^5 to 5×10^5 5×10^5 to 1×10^6 1×10^6 to 5×10^6 5×10^6 to 1×10^7	0.07 0.17 0.40 0.60 0.92 1.00
Cs [(a)]	FeCP	10^0 to 10^1	1×10^0 to 5×10^0 5×10^0 to 1×10^1	0.27 1.00
	Smectite	5×10^1 to 5×10^3	5×10^1 to 1×10^2 1×10^2 to 5×10^2 5×10^2 to 1×10^3 1×10^3 to 5×10^3	0.05 0.40 0.70 1.00
Np [(b)]	FeCP	10^4 to 10^6	10^4 to 10^6	Log Uniform
	Smectite	1×10^1 to 5×10^2	1×10^1 to 5×10^2	Log Uniform
U [(b)]	FeCP	10^0 to 10^4	10^0 to 10^4	Log Uniform
	Smectite	5×10^2 to 5×10^4	5×10^2 to 5×10^4	Log Uniform
Sn [(b)]	FeCP	10^2 to 10^6	10^2 to 10^6	Log Uniform
	Smectite	10^5 to 10^6	10^5 to 10^6	Log Uniform
Ra [(b)]	FeCP	10^2 to 10^4	10^2 to 10^4	Log Uniform
	Smectite	1×10^2 to 5×10^3	1×10^2 to 5×10^3	Log Uniform

Source: [(a)] Output DTN: MO0701PASORPTN.000.
[(b)] Output DTN: MO0701PAKDSUNP.000.

NOTE: Values and distributions derived from data sources are indicated in Figures 6-24a, 6-24b, and 6-24c. See text for discussion and interpretation of data. Sorption coefficients for iron oxide corrosion products are included for information purposes only. A competitive sorption model has been used to address sorption of radionuclides onto iron oxides (see SNL 2007 [DIRS 177407]).

Table 6-16. Cesium Sorption Coefficients on Yucca Mountain Tuffs

Rock Sample	Sample Identification	Temperature (°C)	Material	K_d (mL/g)
G4-270	J-13 G4 -270-C.967-20	20.0	Devitrified Tuff	1.24E+02
G4-270	J-13 G4-270-C.968-20	20.0	Devitrified Tuff	1.25E+02
G4-270	J-13 G4-270-C.962-20	20.0	Devitrified Tuff	1.26E+02
G4-270	J-13 G4-270-C.1029-80	80.0	Devitrified Tuff	1.66E+02
G4-270	J-13 G4-270-C.1030-80	80.0	Devitrified Tuff	1.71E+02
G4-270	J-13 G4-270-C.956-20	20.0	Devitrified Tuff	2.13E+02
G4-270	J-13 G4 -270-C.961-20	20.0	Devitrified Tuff	2.16E+02
G4-270	J-13 G4 -270-C.955-20	20.0	Devitrified Tuff	2.20E+02
G4-270	J-13 G4-270-C.1021-60	60.0	Devitrified Tuff	2.39E+02
G4-270	J-13 G4-270-C.1022-60	60.0	Devitrified Tuff	2.45E+02
GU3-1407	J-13 GU3-1407-C.966-20	20.0	Vitric Tuff	5.17E+02
GU3-1407	J-13 GU3-1407-C.965-20	20.0	Vitric Tuff	5.26E+02
GU3-1407	J-13 GU3-1407-C.1031-80	80.0	Vitric Tuff	6.72E+02
GU3-1407	J-13 GU3-1407-C.959-20	20.0	Vitric Tuff	7.67E+02
GU3-1407	J-13 GU3-1407-C.1032-80	80.0	Vitric Tuff	7.68E+02
GU3-1407	J-13 GU3-1407-C.960-20	20.0	Vitric Tuff	9.50E+02
GU3-1407	J-13 GU3-1407-C.1024-60	60.0	Vitric Tuff	1.03E+03
GU3-1407	J-13 GU3-1407-C.972-20	20.0	Vitric Tuff	1.04E+03
GU3-1407	J-13 GU3-1407-C.971-20	20.0	Vitric Tuff	1.05E+03
GU3-1407	J-13 GU3-1407-C.1023-60	60.0	Vitric Tuff	1.06E+03
G4-1506	J-13 G4-1506-C.957-20	20.0	Zeolitic Tuff	7.38E+03
G4-1506	J-13 G4-1506-C.964-20	20.0	Zeolitic Tuff	8.27E+03
G4-1506	J-13 G4-1506-C.963-20	20.0	Zeolitic Tuff	1.02E+04
G4-1506	J-13 G4-1506-C.1027-80	80.0	Zeolitic Tuff	1.65E+04
G4-1506	J-13 G4-1507-C.1028-80	80.0	Zeolitic Tuff	1.75E+04
G4-1506	J-13 G4-1506-C.1019-60	60.0	Zeolitic Tuff	1.96E+04
G4-1506	J-13 G4-1506-C.970-20	20.0	Zeolitic Tuff	2.97E+04
G4-1506	J-13 G4-1506-C.1020-60	60.0	Zeolitic Tuff	3.52E+04
G4-1506	J-13 G4-1506-C.969-20	20.0	Zeolitic Tuff	3.64E+04
G4-1506	J-13 G4-1506-C.958-20	20.0	Zeolitic Tuff	4.23E+04

Source: DTN: LA0407AM831341.002 [DIRS 170621].

Within the models for radionuclide transport within the engineered system, kinetic and competitive sorption models have been developed to assess sorption and retardation processes (SNL 2007 [DIRS 177407]) on both stationary steel corrosion products and on steel corrosion product colloids. Using a linear K_d, the reversibly attached radionuclide uptake onto waste package corrosion products and Fe-oxide corrosion product colloids is handled by a competitive sorption model with competition among the actinides (U, Np, Pu, Am, and Th) and Ni for a limited number of surface sites. Even though Ni is not transported within the TSPA, it is a major potential sorbing ion from the steel and its competition for sorption sites is accounted for to more accurately estimate the sorption of the radionuclides. The competitive sorption model contains both equilibrium representations (i.e., reversible sorption) for U, Np, and Th onto HFO and goethite, as well as kinetic sorption-desorption for Pu and Am, where the slow desorption is

applied to the stationary corrosion products. These models are all discussed in *EBS Radionuclide Transport Abstraction* (SNL 2007 [DIRS 177407]) (see Section 6.3.12.3).

6.3.12.2 Irreversible Attachment of Plutonium and Americium to Iron Oxyhydroxide Colloids and Stationary Phases

Evidence from sorption experiments with plutonium and americium (Lu et al. 2000 [DIRS 166315]) with colloidal hematite and montmorillonite suggest that the rates of desorption of plutonium and americium (i.e., rates of release of these radioelements from the colloid surface) are slower than the rates of sorption (forward rate). Thus, plutonium and americium are assumed to be either so strongly sorbed to the colloids, or to have been reacted via reduction at the colloid surface, that these radioelements are considered irreversibly attached (note that this general term "attached" is used to cover various process mechanisms and is not meant to imply any one specific mechanism) and are modeled as such within the EBS (SNL 2007 [DIRS 177407]). Laboratory studies and field investigations at the NTS by Kersting and Reimus (2003 [DIRS 162421]) show that Pu(V) undergoes rapid reduction on the surface of metal oxide minerals. Transport of colloidal plutonium has been observed 1.3 km from a specific underground nuclear explosion that was conducted at the Nevada Test Site (Kersting et al. 1999 [DIRS 103282]). Laboratory experiments of plutonium sorption onto iron oxides have shown that only ~1% of the initially sorbed plutonium can be desorbed into solution, even after months of time have elapsed (Lu et al. 2000 [DIRS 166315]), which is broadly consistent with field observations.

Although not relevant to the anticipated conditions at the proposed repository, plutonium behavior in soils at the Rocky Flats site in Colorado illustrates some of the complexity of predicting the environmental fate of plutonium. In these soils, plutonium was largely associated with the negatively charged organic macromolecular fraction and not with the more abundant iron oxides and clays (Ibrahim and Salazar 2000 [DIRS 170882]). Litaor and Ibrahim (1996 [DIRS 161667]) used 0.01M $CaCl_2$ as an extractant and measured plutonium in Rocky Flats soil to be 0.04% to 0.08% exchangeable. The absence of organics in the Yucca Mountain environment (Minai et al. 1992 [DIRS 100801]) makes these studies of minor relevance to this report.

The TSPA-LA model calculates irreversible attachment of plutonium and americium as functions of specific surface area (S_A), mass of corrosion colloids, dissolved concentration of plutonium and americium, target-flux out ratio (F_{RN}), and other parameters (such as flow and diffusion rate) internal to the TSPA-LA model. This is done in such a way that a majority (90% to 99%) of plutonium and americium are irreversibly attached, due to incorporation of parameter uncertainties (see SNL 2007 [DIRS 177407]). In Table 6-24, the target-flux out ratio is described as having a log-uniform distribution ranging from 0.90 to 0.99. The reversibly attached radionuclide uptake onto waste package corrosion products and Fe-oxide corrosion product colloids is handled by a competitive sorption model that is discussed in *EBS Radionuclide Transport Abstraction* (SNL 2007 [DIRS 177407]) (see also Section 6.3.12.3 below).

Specific Surface Area (S_A)—Values for specific surface area (S_A) for three different iron oxyhydroxides—goethite, hematite, and ferrihydrite (or hydrous ferric oxide, HFO)—as

tabulated from the literature, are listed in Table 6-17 for some general context (i.e., for reference use only) regarding the nature of the surface areas of these materials. Such information is used within models of sorption developed within *EBS Radionuclide Transport Abstraction* (SNL 2007 [DIRS 177407]), wherein the specific values for goethite and HFO that are used for those models are developed, and the detailed rationale for those values is provided. Note that the models in *EBS Radionuclide Transport Abstraction* (SNL 2007 [DIRS 177407]) are for sorption onto both mobile iron oxide corrosion product colloids, as well as for the sorption onto the stationary corrosion products that represent the bulk of the mass of corroded materials.

Surface area measurements on similar materials may sometimes differ by up to an order of magnitude depending on the method used and the detail in the characterization of the sample materials (see range in Table 6-17); however, the maximum values shown in Table 6-17 are conservative for assessing transport of radionuclide-associated waste-form and in-drift mobile colloids. Values reported by Roden and Zachara (1996 [DIRS 171518]) and Poulton et al. (2004 [DIRS 171519]) (Table 6-17) were obtained by N_2 gas-adsorption measurements. Nitrogen gas adsorption measurements may underestimate surface areas because of microporosity (Davis and Kent 1990 [DIRS 143280]). Surface areas of iron oxide corrosion products for use in TSPA are discussed in *EBS Radionuclide Transport Abstraction* (SNL 2007 [DIRS 177407]; see Tables 4.1-12 and 4.1-14 in that document, which have lists of literature sources that are much more extensive that the short sampling given here in Table 6-17).

Table 6-17. Selected Published Values for Specific Surface Area (S_A) for Iron Phases

Mineral/Phase	S_A (m^2/g)	
	Min	Max
Goethite (FeOOH)	31.0	153.3
Hematite (Fe_2O_3)	2.5	5.4
Ferrihydrite ($5Fe_2O_3 \cdot 9H_2O$)	240.8	600

Source: Roden and Zachara 1996 [DIRS 171518], Table 1, p. 1,621; Langmuir 1997 [DIRS 100051], p. 345, Table 10.2; Poulton et al. 2004 [DIRS 171519], p. 3,705.

Forward Rate Constant for Irreversible Attachment (*k*)—A mechanistic model for irreversible attachment of plutonium and americium on iron oxyhydroxide colloids and corrosion products for TSPA is developed and described in *EBS Radionuclide Transport Abstraction* (SNL 2007 [DIRS 177407]). The forward rate constant for irreversible attachment is computed as a function of flow rate, colloid suspension stability, and other system parameters. However, under certain chemical and hydrologic scenarios modeled in TSPA, such as under zero advective flux conditions, unstable colloid conditions, or low flow rates, the mechanistic model fails to compute reasonable values for the forward rate constant of radionuclide attachment onto waste package corrosion product colloids (designated FeO_x colloids in this report). For these scenarios, it is necessary that the forward rate constant for attachment be determined independently of flow and transport parameters. It is more appropriate to use a rate constant determined from the analysis of time-dependent sorption experiments that demonstrate that the detachment rate is much slower than the attachment rate. Note that this, as defined below more explicitly, is the definition of irreversible attachment (i.e., the attachment is *not reversible* in the true

thermodynamic sense of being at a dynamic instantaneous equilibrium, such that rates are more directly applicable to assessing the state of the system).

A series of YMP-specific sorption experiments performed by Lu et al. (2000 [DIRS 166315]; see also Lu et al. 1998 [DIRS 100946] and Lu et al. 2003 [DIRS 170883]) provides useful information on the uptake and release rates of Pu(IV), Pu(V), and Am(III) on colloidal dispersions of hematite and montmorillonite. Since the forward rate constant for irreversible sorption to iron oxyhydroxide colloids is of interest, the sorption data for hematite and goethite colloids is considered. Because the properties of these phases are similar to those for HFO, usage of this information for attachment behavior within the models in *EBS Radionuclide Transport Abstraction* (SNL 2007 [DIRS 177407]) is appropriate because it is used in a bounding manner for colloidal transport, but models for sorption onto stationary corrosion products within the drift are also evaluated using a detachment rate approach to allow radionuclides to be released over time. The sorption data for plutonium (Table 6-18) used to develop the *k* values is given in DTN: LA0004NL831352.001 [DIRS 150272]. A total of eight experiments were performed, four each for Pu(V) and Pu(IV), using J-13 well water and synthetic J-13 well water on colloids of hematite (Fe_2O_3) and goethite (FeOOH).

A first order reaction in which the sorption rate depends upon the plutonium concentration in the water is considered for calculating the reaction rate constant from the available data sets. This is expressed as:

$$\frac{df_{solution}}{dt} = -Rf_{solution} \qquad \text{(Eq. 6-16)}$$

where $f_{solution}$ is the time-dependent fraction in solution (complement of fraction sorbed), R is the linear rate constant, and t is the time duration.

The solution of the rate equation is:

$$f_{solution}(t) = f_{solution}(0)\exp(-Rt) \qquad \text{(Eq. 6-17)}$$

where the initial fraction in solution is one, $f_{solution}(0) = 1$.

Upon evaluation of the data presented in Table 6-18 and reported in DTN: LA0004NL831352.001 [DIRS 150272], it was observed that a high sorption rate occurred at early times (duration less than one hour) with a gradual decline in sorption rate at later times. Since the intent is to provide an estimate for a first order rate describing the irreversible sorption of plutonium onto iron oxide/oxyhydroxide colloids (and stationary corrosion products) over a period ranging from tens of years to several hundred years, the data at initial time and the end of experimental time have been used to estimate the average linear rate constant.

In Table 6-18, an exponential fit is performed on each of the eight datasets using the initial condition, $f_{solution}(0) = 1$, and the end condition of the experiment measurement, $f_{solution}(5{,}760)$. Equation 6-18 was solved for R using the experimental values of f(t) for t = 0 and t = 5,760 minutes. Values of R [yr^{-1}] are listed in the last column of Table 6-18. The computed values of R range from a minimum of 105 (yr^{-1}) to a maximum of 2,523 (yr^{-1}).

Table 6-18. Time-Dependent FeO_x Colloid Sorption Fraction for Plutonium and Rate Constant Calculation

Time (min)	Fraction Pu Sorbed	Fraction Pu in Solution	Computed Rate, R [yr^{-1}]
Sample: Fe_2O_3.J13.PuV			
0	0	1	473
10	0.539	0.461	
30	0.565	0.435	
60	0.594	0.406	
240	0.674	0.326	
360	0.74	0.26	
1,440	0.907	0.093	
2,880	0.948	0.052	
5,760	0.994	0.006	
Sample: Fe_2O_3.SYNJ13.PuV			
0	0	1	2,523
10	0.933	0.067	
30	0.966	0.034	
60	0.957	0.043	
240	0.996	0.004	
360	0.998	0.002	
1,440	0.999	0.001	
2,880	1	0	
5,760	0.999	0[a]	
Sample: FeOOH.J13.PuV			
0	0	1	210
10	0.303	0.697	
30	0.328	0.672	
60	0.36	0.64	
240	0.515	0.485	
360	0.595	0.405	
1,440	0.793	0.207	
2,880	0.869	0.131	
5,760	0.902	0.098	
Sample: FeOOH.SYNJ13.PuV			
0	0	1	420
10	0.831	0.169	
30	0.831	0.169	
60	0.837	0.163	
240	0.911	0.089	
360	0.932	0.068	
1,440	0.987	0.013	
5,760	0.991	0.009	
Sample: Fe_2O_3.J13.PuIV			
0	0	1	1,261
10	0.941	0.059	
30	0.982	0.018	
60	0.992	0.008	
240	0.993	0.007	
360	0.997	0.003	
1,440	0.994	0.006	
2,880	0.999	0.001	
5,760	1	0	

Table 6-18. Time-Dependent FeO_x Colloid Sorption Fraction for Plutonium and Rate Constant Calculation (Continued)

Time (min)	Fraction Pu Sorbed	Fraction Pu in Solution	Computed Rate, R [yr^{-1}]
Sample: Fe_2O_3.SYNJ13.PuIV			
0	0	1	2,523
10	0.995	0.005	
30	0.997	0.003	
60	0.997	0.003	
240	0.993	0.007	
360	0.996	0.004	
1,440	0.999	0.001	
2,880	1	0	
5,760	0.999	0[a]	
Sample: FeOOH.J13.PuIV			
0	0	1	105
10	0.496	0.504	
30	0.558	0.442	
60	0.834	0.166	
240	0.733	0.267	
360	0.703	0.297	
1,440	0.648	0.352	
2,880	0.689	0.311	
5,760	0.621	0.379	
Sample: FeOOH.SYNJ13.PuIV			
0	0	1	263
10	0.523	0.477	
30	0.627	0.373	
60	0.832	0.168	
240	0.834	0.166	
360	0.921	0.079	
1,440	0.918	0.082	
2,880	0.861	0.139	
5,760	0.929	0.071	

Source: DTN: LA0004NL831352.001 [DIRS 150272].

[a] These values were given as 0.001, but were changed to zero (0) due to consideration of irreversible attachment processes (i.e., once complete sorption occurs no desorption would be permitted).

Evaluation of the data in Table 6-18 indicates that sorption of plutonium onto the iron oxyhydroxide colloids was lower in natural groundwater samples ("J13") than in synthetic groundwater ("SYNJ13") (i.e., the fraction of plutonium in solution appears to be consistently higher in the natural groundwater experiments). Lu et al. (2000 [DIRS 166315]) reported that these differences might be due to the adsorption of dissolved organic carbon present in the natural groundwater, thereby reducing the amount of plutonium adsorbed. Additionally, differences in the quantities of multivalent cations in the two experimental waters may have also influenced adsorption. However, given that data at initial time and the end of experimental time were used to estimate the average linear rate constant, these differences between the two experimental waters do not impact the computed rate (R). The calculated rate (R) is most applicable at pH values of approximately 7.2 to 8.4. The experiments by Lu et al. (2000 [DIRS 166315]) had a starting solution pH of 8.2 to 8.4 with a 0.5 to 1 pH unit drop during the experiments.

The rate computed above needs to be converted to a per unit surface area basis in order to be applied to other mineral–water systems. The rate can be expressed as:

$$R = \hat{S}_{FeOx_c} c_{FeOx_c} k \quad \text{(Eq. 6-18)}$$

where

$\hat{S}_{FeOx_c}$ = specific surface area of FeO_x colloids [area FeO_x colloids/mass FeO_x colloids]

c_{FeOx_c} = FeO_x colloid concentration [mass FeO_x colloid/water volume]

k = forward rate constant per unit mineral surface area [water volume/area FeO_x colloids/time].

Equation 6-18 is solved for forward rate constant, k, as:

$$k = \frac{R}{\hat{S}_{FeOx_c} c_{FeOx_c}} \quad \text{(Eq. 6-19)}$$

Lu et al. (2000 [DIRS 166315]) provide the values for $\hat{S}_{FeOx_c}$ = 53.5 m^2/g, and c_{FeOx_c} = 1,000 mg/L for the experimental design and these parameters are used as direct input to these analyses. These experiments were conducted under a specific set of conditions that are different from the specific values developed for iron oxyhydroxide colloid concentrations (Section 6.3.8) and for the specific surface area (S_A) values of these colloids in the EBS. The concentration reported by Lu et al. (2000 [DIRS 166315]) was specifically prepared in the laboratory for their experiments, and the specific surface reported by those authors was unique to their experiments. The range of values referred to in Section 6.3.8 are based on values reported in the literature so they are more generally applicable than simply for that specific set of experiments.

Substituting the experimental fixed values for these two parameters in Equation 6-19 and using the values of R listed in Table 6-18, the values for k are calculated to range from 0.002 ($m^3\ m^{-2}\ yr^{-1}$) to 0.048 ($m^3\ m^{-2}\ yr^{-1}$). Therefore, based on the dataset (DTN: LA0004NL831352.001 [DIRS 150272]), a log uniform distribution is recommended for sampling the value of k in the TSPA-LA model with a minimum of 0.002 ($m^3\ m^{-2}\ yr^{-1}$) and a maximum of 0.05 ($m^3\ m^{-2}\ yr^{-1}$) when the linear rate is determined independently of flow and transport parameters.

6.3.12.3 Sorption Capacity Model

This simplified competitive reversible sorption capacity model begins with the assumption that the available sorption sites can be partitioned linearly amongst the radionuclides based on their sampled K_d values and their concentrations in solution. This model is necessarily a recursive model as implemented in GoldSim, i.e., there will be a one time-step delay, as shown below, in the sorption capacity calculation. The detailed conceptualization for this option follows.

At each time-step, partition the total molar density of sorption sites, $\overline{c}_{\max_T}$, into an allowable molar density of sorption sites for each species, $\overline{c}^{n}_{\max_i}$, according to the following equation (the model assumes that all sites are available for reversible sorption:

$$\overline{c}^{n-1}_{\max_i} = \overline{c}_{\max_T} \left(\frac{\overline{K}_{d,i} \frac{c_i^{n-1}}{M_{W_i}}}{\sum_j \overline{K}_{d,j} \frac{c_j^{n-1}}{M_{W_j}}} \right) \qquad \text{(Eq. 6-20)}$$

where

$\overline{K}_{d,i}$ = sampled K_d for the ith species (different for each realization), [=] m^3 solution per kg smectite or uranophane colloids

$\overline{c}^{n}_{\max_i}$ = molar density of sites for the ith species at the $(n-1)^{th}$ time-step, [=] kg-moles sorbed of ith species per kg colloid mass. This will be a function of surface area.

$\overline{c}_{\max_T}$ = molar density of sites (could potentially be a function of pH or reduced by the amount of H^+ sorption), [=] kg-moles of sites per kg colloid mass. The value is a function of surface area.

c_i^{n-1} = aqueous concentration of the ith species at the $(n-1)^{th}$ time-step, [=] kg i^{th} species per m^3 solution

M_{W_i} = molecular weight of ith species, [=] kg of ith species per kg-mole.

Next, each side of Equation 6-20 is divided by $\frac{c_i^{n-1}}{M_{w_i}}$:

$$\frac{\overline{c}^{n-1}_{\max_i}}{c_i^{n-1} / M_{W_i}} = \overline{c}_{\max_T} \left(\frac{\overline{K}_{d,i}}{\sum_j \overline{K}_{d,j} \frac{c_j^{n-1}}{M_{W_j}}} \right) \qquad \text{(Eq. 6-21)}$$

The left-hand side of the equation is defined to be the maximum allowable sorption partition coefficient, $K_{d,i}^{\max,n}$, for the ith species at the nth time-step:

$$K_{d,i}^{\max,n} \equiv \frac{\overline{c}_{\max_i}^{n-1}}{c_i^{n-1} \Big/ M_{W_i}} = \overline{c}_{\max_T} \left(\frac{\overline{K}_{d,i}}{\sum_j \overline{K}_{d,j} \dfrac{c_j^{n-1}}{M_{W_j}}} \right) \qquad \text{(Eq. 6-22)}$$

At the nth time-step, the sorption partition coefficient, $K_{d,i}^{n}$, that is used for the ith species is given by the following (i.e., it is the minimum of the competitive K_d computed in Equation 6-22 and the sampled K_d from the Latin Hypercube sampling):

$$K_{d,i}^{n} = \min\left(\overline{K}_{d,i}, K_{d,i}^{\max,n}\right) \qquad \text{(Eq. 6-23)}$$

6.3.13 Potential Effects of Microbes and Organic Compounds

Microbes and organic compounds will not affect the generation of inorganic colloids. Any interactions will tend to destabilize colloids, possibly decreasing the mobility of associated radionuclides.

The effects of microbes in colloid-facilitated transport in the repository can include:

- Microbial oxidation of metallic iron can produce iron-oxide colloids and aggregates (Minai et al. 1992 [DIRS 100801]).
- Microorganisms may decrease the concentration of stable colloid suspensions by aggregating colloidal material that they use as a food source. This has been shown to result in a decrease in colloid concentrations of up to 91% (Hersman 1995 [DIRS 100750]).

Natural organic matter, such as fulvic compounds from soils, will stabilize inorganic colloids in natural waters (Buffle et al. 1998 [DIRS 161653]). However, certain types of natural organic matter have been shown to have a tendency to destabilize colloids (Wilkinson et al. 1997 [DIRS 161732]).

6.3.13.1 Potential Microbial Communities within the Engineered Barrier System

Qualitative analyses and bounding calculations address microbial growth in *Evaluation of Potential Impacts of Microbial Activities on Drift Chemistry* (BSC 2004 [DIRS 169991], Section 7.1). That study recommends that TSPA use 90% relative humidity as a threshold for microbial-induced corrosion, but states that the potential impact of microbial activity on drift chemistry does not warrant a direct feed to TSPA-LA (BSC 2004 [DIRS 169991], Section 7.1).

In assessing the potential effects on microbial populations within the EBS, *Evaluation of Potential Impacts of Microbial Activities on Drift Chemistry* (BSC 2004 [DIRS 169991]) considered the drift mineralogy, drift physical parameters, metals used in EBS components, waste dissolution rates and quantities, groundwater compositions and infiltration rates, and compositions and fluxes of gases (e.g., CO_2, water vapor). Environmental limits on microbial activity considered include redox conditions, temperature, radiation, hydrostatic pressure, water activity, pH, salinity, available nutrients, and others.

The study evaluated the potential for radionuclide transport facilitated by suspended microbial cells, or biocolloids (BSC 2004 [DIRS 169991], Section 6.5.4). The study concluded that the potential affect of radionuclide bearing colloids is negligible, and the presence of microbial cells and their by-products may even help immobilization of radionuclides. The transport and facilitated radionuclide migration are expected to be limited due to low liquid saturation, high ionic strength and low microbial activity.

6.3.13.2 Discussion

The presence of organic polymers such as those produced by microbes and their byproducts will generally reduce the stability of inorganic colloid suspensions and result in enlargement of particles through heteroaggregation (Wilkinson et al. 1997 [DIRS 161732]).

It is currently anticipated that the repository invert, comprised of crushed volcanic tuff with intergranular void spaces, will remain undersaturated with respect to groundwater. The adhesion of microbes to unsaturated porous media, like the invert, can be controlled by the level of fluid saturation and the extent of the air–water interface network within the medium. Since microbes tend to adhere strongly to the air–water interface, lower saturations would result in increased microbe retention and reduced transport (BSC 2004 [DIRS 169991], Section 6.5.4).

Considerable uncertainty surrounds the role that microbes may play in the repository system. Thus, given the current knowledge, it is difficult to estimate their effects on the colloid source term, in particular the effect of microbes on colloid concentration and suspension stability. However, it is understood that microbial action will tend to increase the sizes of inorganic colloids, which promotes gravitational settling and filtration. Thus, not including the effects of microbes in colloid source term and transport analysis is considered reasonable, and it follows that neglect of the effects of microbes is reasonable with respect to TSPA dose assessments.

6.4 CONSIDERATION OF ALTERNATIVE MODELS

The following sections describe three models considered as alternatives to the base-case model. The first considers a two-site sorption kinetic model as an alternative to the assumption of irreversible attachment used in the base-case model, the second considers waste form corrosion rate for bounding colloid formation, and the third model considers release of particles from a weathered waste form surface under unsaturated flow conditions where attachment to air–water interfaces may limit colloid movement. These alternative conceptual models (ACMs) are listed in Table 6-19, along with the principal bases and screening assessments.

Table 6-19. Alternative Conceptual Models Considered

ACM	Basis for Model	Screening Assessment
Kinetic Sorption Model	Instead of assuming irreversible attachment, this model provides a method for predicting sorption behavior beyond laboratory time-scales. Allows interpretation of data from different time scales. Based on model developed by Painter et al. (2002 [DIRS 174071]) and extended two- and three-site model developed by Wittman et al. (2005 [DIRS 174895])	This ACM is screened out for the following reasons: – Slow kinetic sorption rates are difficult to determine in laboratory tests that have been run for <150 days. – The lack of sufficient sorption data on colloids for sufficient time periods causes uncertainty in the extrapolation beyond the experimental times.
Rate of Colloid Generation	Method for using markers for DHLWG corrosion for estimating colloid production	This ACM is screened out for the following reason: – The model may overestimate colloid formation by not accounting for significant retention of actinides to the immobilized phase, as has been observed in waste form corrosion experiments.
Mechanisms of Colloid Generation	Mobile colloid generation will require large perturbations to the system that may not occur within the waste package. Furthermore, attachment of particles to air-water interfaces may limit mobile colloid generation.	This ACM is screened out for the following reasons: – Data for Yucca Mountain-related conditions are unavailable. – The process of attachment to air–water interfaces will depend on the degree of particle hydrophobicity. Smectite clays and iron oxyhydroxides in general will not attach to air–water interfaces, but various oxides and U(VI) oxides phases may. – For flow rates similar to those anticipated in the repository waste package environment, there is no literature evidence to indicate mobile colloid generation.

6.4.1 Kinetic Sorption Model: An Alternative to Irreversible Attachment

Painter et al. (2002 [DIRS 174071]) presented a two-site sorption kinetics model that allows evaluation of sorption data; in particular, the model permits analysis of adsorption on long time scales as compared to times for experimentally measured adsorption. The two-site model is probably the simplest dynamical linear model that can represent both a fast adsorption (or desorption) for a near-term equilibrium distribution [$(K_{ci})_{fast}$] and a delayed adsorption for a long term $(K_{ci})_{slow}$ that may be much larger. Both reversible sorption and irreversible attachment for colloids can be represented by the full analytical solution to the rate equations for a flow-through or batch reactor. The solutions are offered as guidance for interpreting sorption data and for predicting the long-term discharge concentrations through an aquifer. This model was applied by Wittman et al. (2005 [DIRS 174895]) to plutonium sorption data reported for smectite, montmorillonite, and hematite as discussed in the study by Lu et al. (1998 [DIRS 100946]; 2000 [DIRS 166315]). In Figure 6-25a, three site simulations of sorption data are shown that demonstrate the importance of a slowly reversible nonzero desorption term, $k_{R3} = 0.0017\ h^{-1}$ (red lines) versus $k_{R3} = 0$ (blue lines). Figure 6-25b shows the fit of the three-site model to the data.

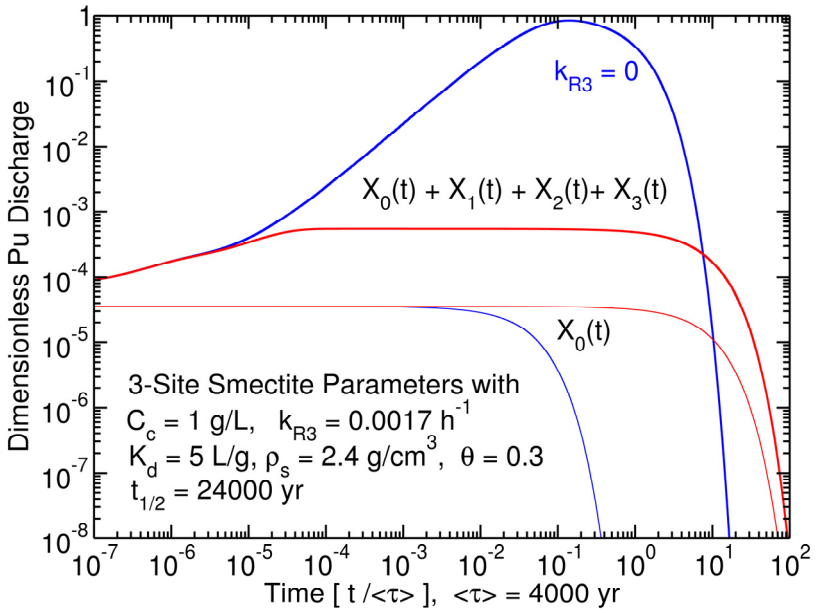

Source: Wittman et al. 2005 [DIRS 174895], Figure 5.1, p. 5.2.

NOTE: Values above were used to fit data from Lu et al. (2000 [DIRS 166315]) with (i) irreversible attachment (i.e., $k_{R3} = 0$), wherein plutonium association with colloids is only reduced through ^{239}Pu decay; and (ii) a small reversible factor, wherein the peak dose for plutonium-sorbed colloids decreases. For details of the analysis and fit of the data, see the source (Wittman et al. 2005 [DIRS 174895]).

Figure 6-25a. Kinetic Sorption Model Predictions for Plutonium Sorption onto Colloids

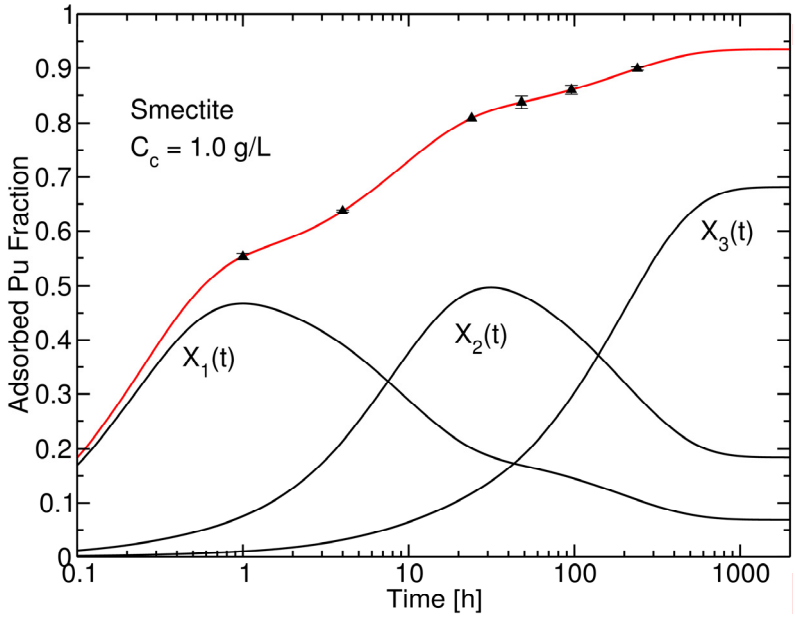

Source: Wittman 2005 [DIRS 174895], Figure 4.3, p. 4.4.

NOTE: Model was used for fitting data reported for plutonium sorption onto iron oxide with exponential fit used to derive rate constant from Table 6-18.

Figure 6-25b. Three-Site Sorption Model

Painter et al. (2002 [DIRS 174071]) demonstrated a simple way to gauge the impact of the reversible rate constant, β (called k_{Ri} in Wittman et al. 2005 [DIRS 174895]). The qualitative behavior of the aquifer can be represented as a flow-through reactor. Figure 6-25 shows the long-term presence of mobile contaminant (dimensionless Pu discharge) in a system as a function of time for colloid sorption assuming a possible mean flow-through residence time of 4,000 years by Wittman et al. (2005 [DIRS 174895]). X_o is the fraction of Pu in solution, X_i are the fractions of Pu present in i independent forms on the mobile colloid. At t = 0, the contaminant is assumed to be entirely distributed between the liquid and the immobile surface. In the case of irreversible sorption, adsorption onto the colloid continues to increase the mobile fraction of the contaminant until the "source" contribution from the immobile phase and liquid (X_o) drops to low concentrations from dilution. For reversible sorption, adsorption onto the colloid reaches an equilibrium maximum long before dilution effects purge the contaminant from the system. A greater fraction remains in the immobile phase during most of the flow history. The irreversible case of Figure 6-25a assumes that k_{R3} is zero; in the reversible case, β is assumed to be the value obtained from fitting the colloid sorption data (red lines). Even though the total mobile concentration would possibly be low in both reversible and irreversible cases, the peak concentration for the reversible case is about 1,000 times lower. Additionally, in the reversible case, the equilibrium behavior over most of the flow history supports the use of a distribution coefficient K_d (called K_{ci} for colloids, not to be confused with K_c used in the transport model) for representing sorption in colloid assisted transport models. For the two-site model by Painter et al. (2002 [DIRS 174071]), K_{ci} is the sum of K_{ci}(fast) and K_{ci}(slow) representing equilibrium for fast and slow sorption processes, respectively.

Exact analytical solutions of the minimal sorption kinetics equations were used by Wittman et al. (2005 [DIRS 174895]) in the analysis. Analytical solution offered a huge advantage in computing speed because the model could be evaluated at an arbitrary time-step. Best fits to the data were obtained by performing a least-squares fit for the rate constants. A multidimensional secant method was used to search for a local least squares fit with resulting rate constants allowing the determination of distribution coefficients (Wittman et al. 2005 [DIRS 174895]).

Painter et al. (2002 [DIRS 174071]) show that uncertainty in the value of the reverse rate causes large uncertainty in the peak plutonium and americium discharge because no sorption experiment has been run for sufficient time to allow an accurate determination of the reversible process and some extrapolation is necessary. In Table 6-20, the developed sorption coefficients for clay and hematite colloids are listed. In both cases, the developed values are at the low range for the distributions in Table 6-15.

Table 6-20. Plutonium Sorption Coefficients Developed from Kinetic Sorption Model

	Colloid Concentration	Sorption Coefficients, K_{ci} (mL/g)			
Mineral	C_c (mg/L)	K_{c1}	K_{c2}	K_{c3}	K_{ci} (total)
Hematite	200	9.16×10^3	1.245×10^5	0	1.336×10^5
Smectite	1,000	1.046×10^3	2.81×10^3	1.04×10^4	1.43×10^4
Montmorillonite	200	2.0×10^2	7.96×10^3	0	8.16×10^3

Source: Wittman et al. 2005 [DIRS 174895], Table 5.1, p. 5.1, with units converted from L/g to mL/g.

Alternative Model Description and Data Needs—Important data requirements for this model are longer-term sorption experiments and improved characterization of the surface area, morphology, and composition of the starting materials. For example, the sorption results reported by Lu et al. (1998 [DIRS 100946]) for smectite and the results reported for montmorillonite are vastly different despite few differences in the nature of these phases. This suggests that small differences in the composition and morphology of these two materials led to large differences in the sorption characteristics. Painter et al. (2002 [DIRS 174071]) has suggested the need for a better understanding of the microscopic exchange mechanisms of plutonium on colloids at different time scales.

Assessment of Alternative Model—The kinetic model represents a useful tool for examining sorption data and examining the evidence for slow reversible sorption of plutonium on colloids. The model clearly demonstrates that the data from Lu et al. (2000 [DIRS 166315]) can be fit with reversible components, suggesting that irreversible sorption is conservative. The kinetic model has not been adopted because it is immature and the base model is conservative and bounding.

6.4.2 Rate of Colloid Generation Model

The following subsections describe an approach to estimating the rate of release of colloidal plutonium from degraded waste, based on the rate of waste degradation. This modeling approach is preliminary and is provided here as an alternative model for prediction of colloid release and transport in the waste package and drift and as a basis for potential subsequent discussion and project planning. It is based on a colloid generation rate model presented in *Colloid-Associated Radionuclide Concentration Limits: ANL* (CRWMS M&O 2001 [DIRS 154071]).

Rate of Colloid Formation from DHLWG—The normalized mass loss of plutonium, NL(Pu), was compared to the normalized mass loss of boron, NL(B), to indicate the amount of plutonium released relative to the amount of boron released, which is directly proportional to the amount of DHLWG corroded. The NL(Pu) was consistently lower than the NL(B) by at least one order of magnitude. NL(Pu)/NL(B) decreases for the longer duration tests at higher S_A/V, up to about 10^{-3} for stable colloid-inhibiting conditions.

Under low-ionic strength conditions, the colloid suspensions are stable in the fluid and the rate of formation of plutonium-bearing colloids, $dm_{Pu\text{-}coll}/dt$, is proportional to the amount of altered glass, M_{alt}. As the glass alters, the rate of radionuclide-bearing colloids production decreases, initially following a power law, attributed to their sorption by the fixed clay alteration layer (CRWMS M&O 2001 [DIRS 154071], Section 6.4.2). The rate of colloid formation can be described by the relationship in Equation 6-24:

$$\frac{dm_{Pucoll}}{dt} = a\left(M_{alt}\right)^{-b} \qquad \text{(Eq. 6-24)}$$

The constants, a and b, derived for the various glasses may be a function of the S_A/V, leachate composition (ionic strength, etc.), colloid composition, or other parameters. Table 6-21 summarizes the ranges and bounding values for a and b.

Table 6-21. Ranges and Bounds for Constants, *a* and *b*, in Equation 6-24

Constant	Static-Saturated Tests		Drip Tests		Bounding Values
	Low	High	Low	High	
a	8×10^{-12}	4×10^{-6}	2×10^{-6}	5×10^{-6}	10^{-4}
b	3	8	0.3	1.7	1

Source: CRWMS M&O 2001 [DIRS 154071], Section 6.4.2.

At the high-ionic strengths encountered in certain static tests, there was no correlation observed between plutonium and boron production rates since the quantity of colloids was low. In the drip tests, ionic strength remained low because EJ-13 well water was periodically injected.

Once the cumulative boron release is greater than approximately 1 to 3 g m^{-2}, the radionuclide release is controlled by spallation of the clay layer. Thus, radionuclide release is a two-step process: (1) alteration of the glass waste form and precipitation of colloids, and (2) erosion of colloid-sized fragments from the alteration products.

Release of colloids due to spallation is given by the derived relationship:

$$\frac{dm_{Pu_{coll}}}{dt} = \kappa M_{alt} \qquad \text{(Eq. 6-25)}$$

where $dm_{Pu_{coll}}/dt$ is the mass release of plutonium suspended per time as colloidal particulates and κ is a parameter that depends on, among other things, the mechanical condition of the altered waste form, the water flow rate over the waste form, and the water chemistry (CRWMS M&O 2001 [DIRS 154071], Section 6.4.2). An empirical bound for κ is 10^{-4} d^{-1}.

Calculation of Quantity and Rate of Production of Irreversibly Attached Radionuclides—Parameters used to calculate mobilized radionuclide quantities and rates of production are listed in Table 6-22. After the quantities of total mobilized radionuclides are calculated, they are distributed between radionuclides irreversibly attached to colloids, dissolved (aqueous) radionuclides, and radionuclides coprecipitated in immobile secondary phases. Since the experimental evidence indicates that most waste form colloids are radionuclides, radionuclide-bearing phases, or both, irreversibly associated with smectite colloids, this fraction is given as the difference between the dissolved radionuclides and the total radionuclides mobilized by the waste degradation time step:

$$RN_{coll,irrev} + RN_{layer,irrev} = RN_{mob} - RN_{diss} - RN_{secondaryphase} \qquad \text{(Eq. 6-26)}$$

where RN = radionuclide.

The irreversibly attached radionuclides are in turn distributed between the clay layers on altered DHLWG and clay colloids produced from DHLWG and SNF; the aqueous radionuclides are available for reversible sorption onto colloids.

If the cumulative release of boron is less than 1 g m^{-2}, then the following relationship is invoked to calculate the quantity of radionuclides irreversibly attached to colloids produced for that time step.

The equation for calculating the mass of radionuclides is:

$$\text{Mass of irreversibly attached RN} = a * (B_{cum})^{-b} \quad \text{(Eq. 6-27)}$$

where B_{cum} represents the mass of DHLWG degraded and *a* and *b* are empirically derived constants, and RN = radionuclide.

Table 6-22. Parameters Used in Description of Alternative Model

Parameter	Description	Value /Range/ Distribution	Source
B_{inv}, Tc_{inv}, Pu_{inv}, Am_{inv}	Masses of B and radionuclides in unaltered waste form during time step	—	Would be calculated by TSPA-LA model
B_{mob}, Tc_{mob}, Pu_{mob}, Am_{mob}	Masses of B and radionuclides "mobilized" in WF_{deg} during time step	—	Would be calculated by TSPA-LA model
B_{cum}	Cumulative mass of B "mobilized" in WF_{deg} for all previous time steps	—	Would be calculated by TSPA-LA model
M_{alt}	Amount of altered glass	—	CRWMS M&O 2001 [DIRS 154071]
a	Empirically derived constant used in expression for precipitated smectite colloids	10^{-4} (bound)	CRWMS M&O 2001 [DIRS 154071]
b	Empirically derived constant used in expression for precipitated smectite colloids	1 (bound)	CRWMS M&O 2001 [DIRS 154071]
κ	Empirically derived constant used in expression for spalled smectite colloids	10^{-4} (bound)	CRWMS M&O 2001 [DIRS 154071]

NOTE: WF = waste form.

If B_{cum} is greater than 3 g m^{-2}, then the second model is invoked to calculate the quantity of radionuclides irreversibly attached to colloids formed from spallation of the alteration clay layer. The equation for calculating radionuclide mass mobilized due to spallation is:

$$\text{Mass of irreversibly attached spalled RN} = \kappa * B_{cum} \quad \text{(Eq. 6-28)}$$

where

κ is an empirically derived constant

RN = radionuclide

If B_{cum} is between 1 and 3, then either the first or second is chosen randomly (0.5 probability).

Assessment of Rate-of-Colloid-Generation Model—This alternative model takes into account many of the results from waste form corrosion testing programs, as well as models derived from them. It incorporates an analytical approach that would couple the waste form degradation

calculations by the TSPA-LA model more closely to the process model derived from the experiments (CRWMS M&O 2001 [DIRS 154071]).

While it takes advantage of the most complete information available on waste form corrosion, at the same time it is tailored closely to the experimental conditions and configurations. There are aspects of the experiments that may make them inappropriate to apply to a more general case. A possible example is the rate of spallation of the clay layer from altered DHLWG, which may be due to the specific dynamics surrounding the impacts of the drips falling on the sample in the DHLWG drip tests (CRWMS M&O 2001 [DIRS 154071], Section 6.2.1). If the corroded contents of a failed waste canister assume a geometry that does not allow dripping of water onto the alteration products, spallation may not occur. If dripping does occur, of course, spallation may be a viable process, and an analysis of colloid production and transport would have to consider it.

6.4.3 Mechanisms of Colloid Generation

This alternative model, described by Buck et al. (2004 [DIRS 171479]), investigates the processes whereby colloid generation at, and mobilization from, the surface of degrading waste is primarily related to flow rate at the waste surface and the attachment of colloids to air–water interfaces. The supporting concepts and data from the peer-reviewed literature that support this alternative model were developed in the context of deposition and remobilization of existing colloids under conditions of moderate to high fluid flow. The model suggests that unless high flows are present, mobile colloid generation would be negligible owing to the strong and irreversible attachment of hydrophobic colloids to air bubbles on the surface of waste package components.

Under specific experimental environments, a flow rate dependence on colloid release has been observed (Ryan and Gschwend 1994 [DIRS 180525]), although a full explanation for these empirical relationships has not yet been developed. For flow rates similar to those anticipated in the repository waste package environment, there is no literature evidence to indicate mobile colloid generation. In this alternative model, flow-rate dependence of the entrainment and mobilization of waste form colloids would be determined. In addition, the influences of fluid chemistry and of the actual phases formed and their physical association in a model waste form system would be investigated. This model will allow quantification of changes in particle release under different flow rates, fluid chemistries, and particle–particle interaction scenarios.

In tests performed by Buck et al. (2004 [DIRS 171479]), metaschoepite formed during the weathering of UO_2 powder was demonstrated to be hydrophobic. The particles were stabilized at polar–nonpolar interfaces (i.e., air–water or oil–water interfaces), similar to observations in many other mineral oxide colloidal systems where hydrophobic colloids become irreversibly attached to air bubbles (Abdel-Fattah et al. 1998 [DIRS 158692]).

Assessment of the Colloid Generation Mechanisms Model—For flow rates similar to those anticipated in the repository waste package environment, there is no literature evidence to indicate mobile colloid generation due to water flow. Omission of colloid partitioning to the air–water interface is conservative because this effect would likely curtail colloid transport.

6.5 MODEL FORMULATION FOR BASE-CASE ASSESSMENT

This section describes in detail the methodology used to incorporate the various model elements formulated in this model analysis into a colloids source term abstraction (i.e., a simplified model intended to retain the important principles and features of the analyses) for implementation in the TSPA-LA model. The logic and parameters implemented in the TSPA-LA model are provided, although specific programming details are not.

Figures 6-26 and 6-27 provide an overview of the model methodology with cross-references to the underlying model elements developed in Section 6. Figure 6-26 illustrates how colloids are modeled in the waste package (Section 6.5.1), and Figure 6-27 in the drift (Section 6.5.2). Parameters used in the abstraction are described in Table 6-24. Sections 6.5.1 and 6.5.2 present the details of the abstraction, describing the logic and flow of the abstraction approach.

At each time step executed in the TSPA-LA calculations, the colloid model uses the characteristics of the water in the waste package (ionic strength, pH, and dissolved radionuclide concentrations) to describe the formation and behavior of colloids and the distribution of the radionuclides in the waste package. The elements considered and incorporated into the calculations are Pu, Am, Th, Pa, U, Np, Cs, Sn, and Ra. Three groups of colloids are considered in the model: waste form derived colloids (DHLWG, CSNF, and DSNF), waste package corrosion product (iron oxyhydroxides) colloids, and seepage water/groundwater colloids. Colloids formed from the DHLWG and the naturally occurring groundwater colloids are modeled as montmorillonite. In the irreversible case, CSNF-derived colloids are modeled as ZrO_2 particles; and, as U(VI) phases (conceptually considered to be uranophane) and modeled as meta-autunite with reversibly sorbed radionuclides. DSNF-derived colloids are modeled only with reversible sorption onto U(VI) phases (conceptually considered as uranophane) and modeled as meta-autunite. The iron oxyhydroxide colloids formed during corrosion of steel waste package materials are modeled as hematite for stability calculations, and as HFO and goethite for the reversible sorption of radionuclides. Furthermore, irreversible sorption of Pu and Am onto iron oxyhydroxides colloids is also included.

The stability of colloid suspensions is defined by DLVO theory and literature data, with separate relationships for montmorillonite colloids, irreversible SNF colloids (defined by ZrO_2 particles), reversible SNF colloids (meta-autunite), and waste package corrosion product colloids (hematite). At each time step, the ionic strength threshold above which the colloids are unstable is defined by a simple function of pH of the waste package/in-drift solution. For montmorillonite colloid suspensions (DHLWG and seepage/groundwater colloids), Equation 6-9 defines the ionic strength threshold above which the colloid suspensions will be unstable. For irreversible SNF colloids (ZrO_2), Equations 6-10a and 6-10b define the ionic strength threshold above which the colloids are considered unstable. For reversible SNF colloids, modeled as meta-autunite, Equation 6-11 defines the ionic strength threshold above which the colloids are unstable. For waste package corrosion product colloid suspensions that are modeled as hematite, Equations 6-8a and 6-8b define the ionic strength threshold above which the colloids are considered unstable. When colloids are unstable, a low (nonzero) limit of colloid concentration is used for modeling purposes. This value varies depending on the system and is listed in Table 6-24.

Reversible sorption onto the smectite colloids for each of the considered radionuclides is discussed and the recommended values for implementation are listed in Table 6-15. Reversible sorption on uranophane colloids is addressed in Section 6.3.2.6. For waste package corrosion product colloids, irreversible sorption of plutonium and americium is also included (Section 6.3.12.2). Irreversibly attached (or embedded) plutonium and americium on DHLWG-derived (see Section 6.3.2.2) and SNF (ZrO_2) colloids (see Section 6.3.2.4) are also included.

The dissolved radionuclide concentration is calculated by TSPA and is an input to the colloid model. The colloid model determines the concentration of plutonium and americium irreversibly attached ("embedded") in DHLWG smectite and ZrO_2-SNF colloids, the concentration of radionuclides sorbed reversibly onto colloids, and the mass concentration of each colloid type (Figure 6-26).

The colloid and radionuclide concentration values along with the pH of solution serve as source term for the invert. Based on the pH in the seepage water in the invert and comparison of the calculated ionic strength threshold with the invert ionic strength, the model determines colloid stabilities and redistributes the reversibly sorbed radionuclides and dissolved radionuclides based on the distribution coefficients and the total mass of each type of colloid (Figure 6-27). Colloids flow unimpeded through the invert to the unsaturated zone. The irreversibly sorbed radionuclides are not redistributed.

6.5.1 Waste Form Abstraction Implementation in TSPA–LA

The abstraction requires parameters calculated by the TSPA-LA model as output from in-package chemistry, solubility limits, and near-field chemical environment calculations: $C_{RN,diss}$, $I_{wp,\ inv}$, and $pH_{wp,\ inv}$.

The concentrations of colloids and colloid-associated radionuclides were calculated on the basis of abstractions of the laboratory and field observations and chemical principles described in Section 6.3. A stepwise approach was taken in the abstraction, and each step is set out below with a flow diagram and logic statements that describe the abstraction step. Parameters are defined in Table 6-24.

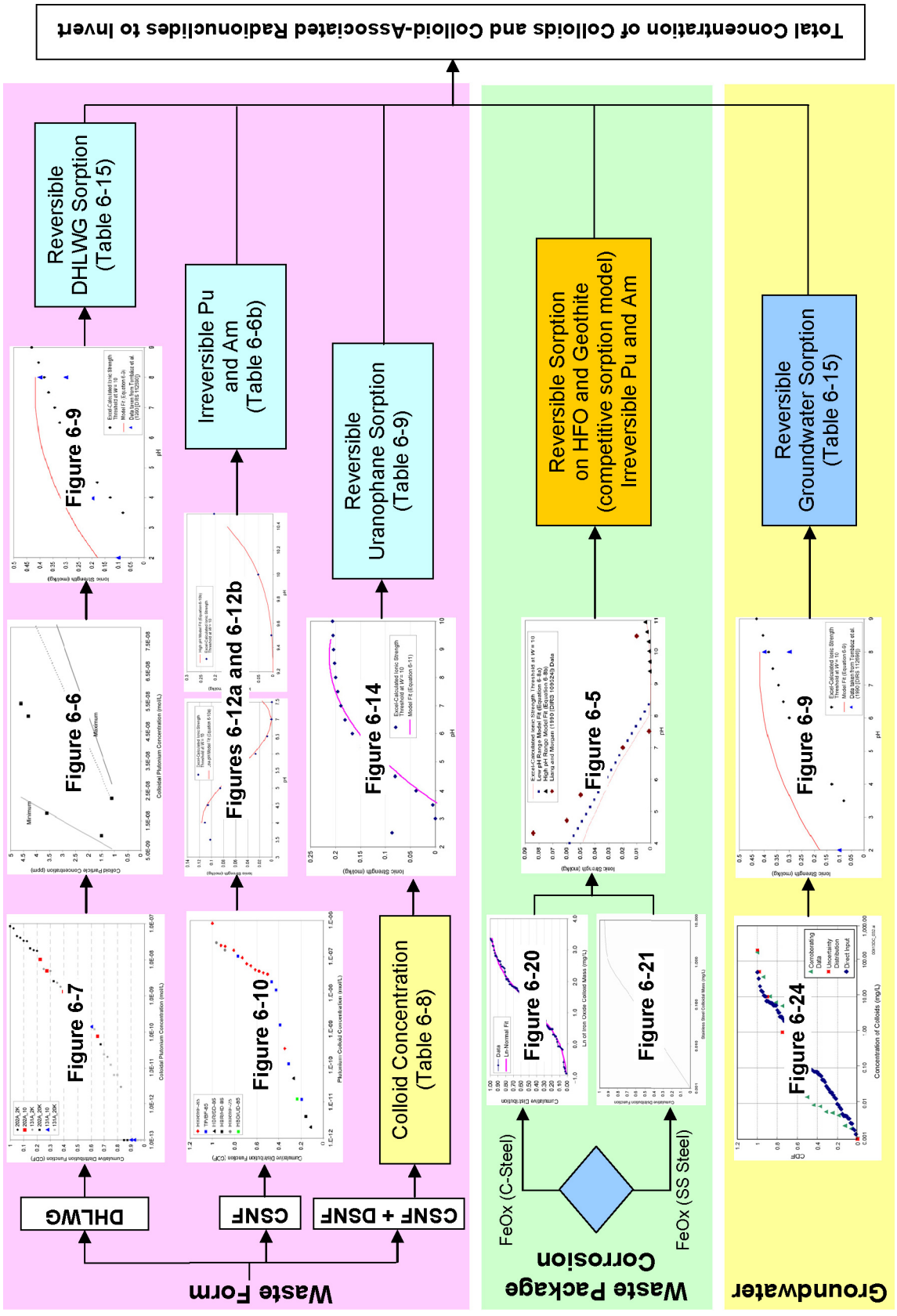

Figure 6-26. Processes within the Waste Package

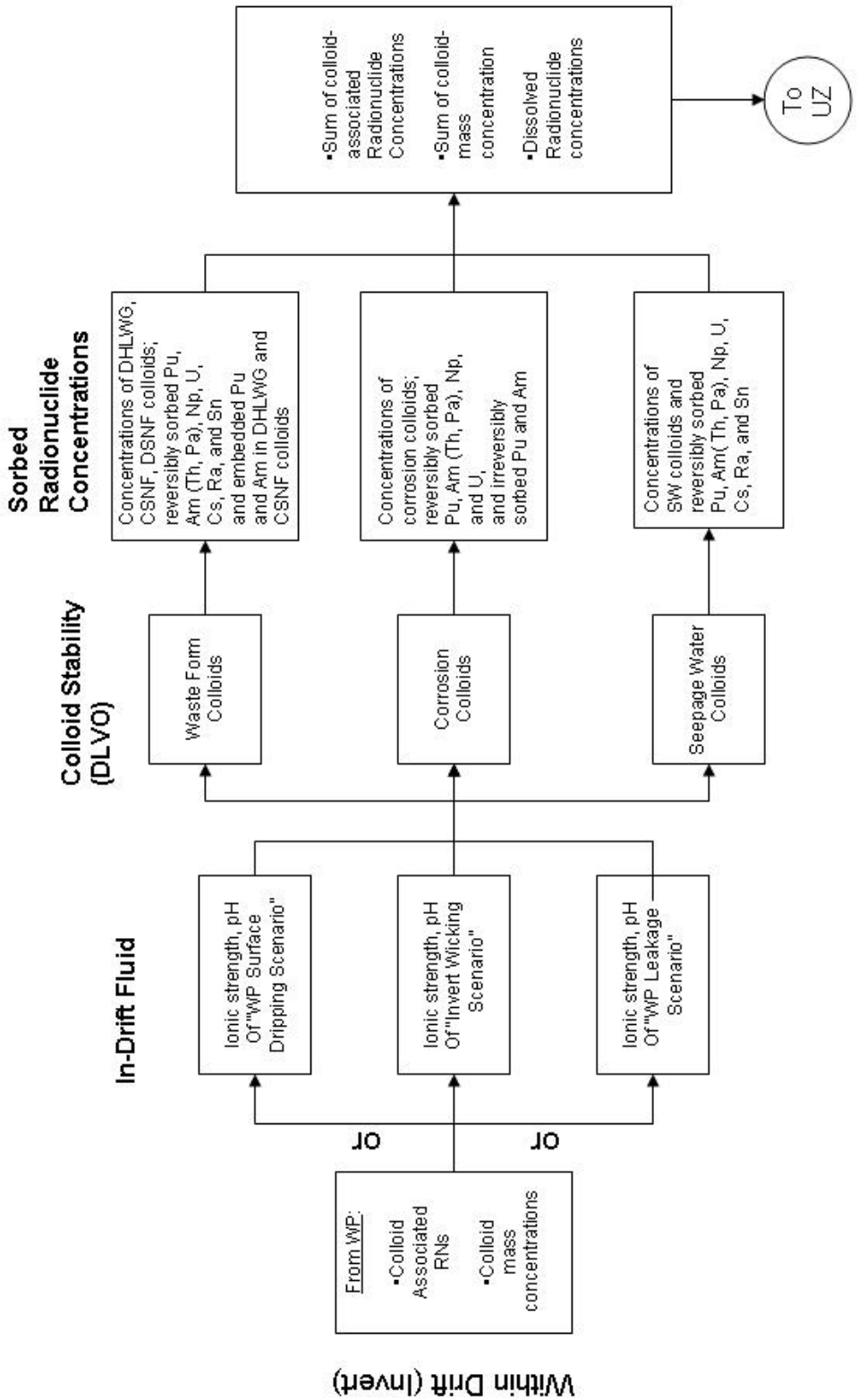

NOTE: WP = waste package; RN = radionuclide; SW = seepage water; HLW = high-level waste.

Figure 6-27. Processes within the Drift (invert)

6.5.1.1 Irreversible Waste Form Colloids (DHLWG)

Step 1a. The radionuclides Pu and Am are modeled as irreversibly sorbed within DHLWG colloids. The first part of the process uses the waste package inputs, pH_{wp} and I_{wp}, to determine if the colloids will be stable. If I_{wp} is less than the value ($I_{threshold}$) calculated from input pH_{wp} using the quadratic relationship below, the smectite DHLWG colloids will be stable.

Input $pH_{wp,\,inv}$ $I_{wp,\,inv}$

$I_{threshold} = (-0.008 \times pH^2) + (0.12 \times pH) - 0.03$

IF $I_{wp,\,inv} > I_{threshold}$

THEN

$C_{RNcoll,DHLWG.embed} = C_{RNcoll,DHLWG,embed,min}$

ELSE

$C_{RNcoll,DHLWG.embed} = C_{RNcoll,DHLWG,embed,\,sampled}$

Step 1b. The colloid mass concentration (mg/L) is related to the irreversibly sorbed plutonium concentration through the following:

$$M_{coll,DHLWG} = 1 \text{ (mg/L)} \times C_{RNcoll,DHLWG,embed,\,sampled} \div C_{RNcoll,DHLWG,embed,\,triangular}$$

Concentration of irreversibly sorbed Am, should be computed determining the fraction of this element present compared to plutonium in the inventory.

Calculation of the mass concentration of waste form colloids (mg/L) from DHLWG is done by sampling a cumulative distribution based on experimental data (Table 6-5) and dividing by the scaling factor represented as a triangular distribution in Table 6-4 (minimum, mode, maximum).

Step 1c. The calculation of the concentration of radionuclides (U, Np, Th, Pa, Ra, Sn, and Cs) reversibly sorbed on waste form colloids from DHLWG is based on the mass concentration of waste form colloids, K_d values describing the distribution of radionuclides between the fluid and smectite colloids, and the dissolved concentration of radionuclides as calculated by the TSPA-LA model. The sorption capacity model described in Section 6.3.12.3 is used to provide a reasonable bound on the sorption of radionuclides onto the DHLWG colloids:

$$C_{RNcoll,DHLWG,rev} = C_{RNdiss} \times K_{d,RN,coll,DHLWG} \times M_{coll,DHLWG}$$

The C_{RNdiss} is the concentration of radionuclide "RN," determined by the TSPA-LA model as constrained by the solubility limits model, which is used as an input to the colloid abstraction. $K_{d,RN,DHLWG}$ is obtained from Table 6-15 (K_d table).

6.5.1.2 Irreversible SNF Colloids (SNF)

Step 2a. The radionuclides Pu and Am are modeled as irreversibly sorbed within SNF ("ZrO_2") colloids. The first part of the process uses the waste package inputs, pH_{wp} and I_{wp}, to determine if the colloids will be stable. If I_{wp} is less than the value ($I_{threshold}$) calculated from input pH_{wp} using the quadratic relationship below, the irreversible SNF colloids will be stable.

Input $pH_{wp,\ inv}$ $I_{wp,\ inv}$
IF $4 < pH_{wp,\ inv} < 7$
THEN $I_{threshold} = (0.0089 \times pH^3) - (0.1466 \times pH^2) + (0.7462 \times pH) - 1.092$
IF $I_{wp,\ inv} > I_{threshold}$
THEN $C_{RNcoll,SNF.embed} = C_{RNcoll,SNF,embed,min}$
ELSE
$C_{RNcoll,SNF.embed} = C_{RNcoll,SNF,embed,sampled}$
IF $pH_{wp,\ inv} > 9.3$
THEN $I_{threshold} = (0.087362 \times pH^3) - (2.4078 \times pH^2) + (22.126 \times pH) - 67.791$
IF $I_{wp,\ inv} > I_{threshold}$
THEN $C_{RNcoll,SNF.embed} = C_{RNcoll,SNF,embed,min}$
ELSE
$C_{RNcoll,SNF.embed} = C_{RNcoll,SNF,embed,sampled}$

ELSE $C_{RNcoll,SNF.embed} = C_{RNcoll,SNF,embed,min}$

(If the pH is <4.0 use the $I_{threshold}$ value calculated at pH 4.0 and if the pH > 10.6 use the $I_{threshold}$ value calculated at pH 10.6.)

Step 2b. Calculation of the mass concentration (mg/L) of waste form colloids from SNF is done by sampling a cumulative distribution based on experimental data (Table 6-10) and scaling to 1 ppm.

$$M_{coll,SNF} = 1\ (mg/L) \times C_{RNcoll,SNF,embed,\ sampled} \div C_{RNcoll,SNF,embed,uniform}$$

Concentration of irreversibly sorbed Am should be computed determining the fraction of this element present compared to plutonium in the inventory.

Step 2c. Reversible sorption of radionuclides onto the irreversible SNF colloids is excluded.

6.5.1.3 Reversible CSNF and DSNF Colloids

Step 3a. The stability and mass concentration of uranium (VI) colloids from corroded CSNF and DSNF is determined on the basis of the fluid ionic strength and pH.

Input $pH_{wp,}$ I_{wp}
$I_{threshold} = -(0.008 \times pH^2) + (0.14 \times pH) - 0.4$
IF $I_{threshold} > I_{wp,\ inv}$
THEN
$C_{Rncoll,uranophane} = C_{Rncoll,uranophane,min}$
ELSE

(If $pH_{wp,inv} < 4$ colloids are unstable and at pH > 9 use $I_{threshold}$ calculated at pH 9.)

Step 3b. In this step, reversible sorption is calculated from the sampled mass concentration of uranophane colloids, K_d values describing the distribution of radionuclides (Pu, Np, Am (Th, Pa), Ra, Cs, and Sn) between the fluid and the U(VI) phase (uranophane) colloids, and the dissolved concentration of radionuclides as calculated by the TSPA-LA model. The sorption

capacity model described in Section 6.3.12.3 is used to provide a reasonable bound on the sorption of radionuclides onto the uranophane colloids:

$$C_{RNcoll,uranophane} = C_{RNdiss} \times K_{d,RN,uranophane} \times C_{coll,uranophane,sampled}$$

$K_{d,RN,uranophane}$ is a parameter obtained from Table 6-9 and is an equilibrium sorption coefficient used to approximate the partitioning of dissolved radionuclide between colloids and fluid.

6.5.1.4 Waste Package Corrosion-Generated Colloids

Step 4a. The stability and mass concentration of waste package corrosion colloid (modeled as hematite and labeled as FeO_x below) is determined on the basis of the fluid ionic strength and pH (Figure 6-5).

Input $pH_{wp,\ inv,}\ I_{wp,inv}$
IF $4.5 < pH_{inv,wp} < 8.4$
THEN $I_{threshold} = -0.013 \times pH + 0.11$
IF $I_{wp,\ inv} > I_{threshold}$
THEN $M_{coll,FeOx} = M_{Coll,FeOx,min}$
ELSE
$M_{coll,FeOx} = M_{coll,FeOx,sampled}$

IF $10.4 > pH_{inv,wp} > 9.4$
THEN $I_{threshold} = (0.0017 \times pH^2) - (0.0327 \times pH) + 0.158$
IF $I_{wp,\ inv} > I_{threshold}$
THEN $M_{coll,FeOx} = M_{Coll,FeOx,min}$
ELSE
$M_{coll,FeOx} = M_{coll,FeOx,sampled}$

ELSE $M_{coll,FeOx} = M_{Coll,FeOx,min}$

(If the pH is <4.5 use the $I_{threshold}$ value calculated at pH 4.5 and if the pH > 10.4 use the $I_{threshold}$ value calculated at pH 10.4.)

Step 4b. The K_d values reported in Table 6-15 for iron oxides and hydroxides in this report are supplied for information purposes only. A competitive sorption model reported in *EBS Radionuclide Transport Abstraction* (SNL 2007 [DIRS 177407]) has been developed for modeling radionuclide sorption onto HFO and goethite (for discussion of that model that is applied to stationary corrosion products, as well as to the iron oxide/hydroxide corrosion product colloids see Sections 6.3.12.1, 6.3.12.2, and 6.3.12.3).

Step 4c. In this step two types of sorption are modeled: kinetically determined irreversible sorption of plutonium and americium onto iron oxyhydroxide corrosion colloids, and reversible sorption of Th, Pa, Np, and U, onto colloids modeled as HFO and goethite. The distribution of irreversibly sorbed Pu and Am onto colloidal substrates is performed in the TSPA-LA model. It is a kinetic model that is described in *EBS Radionuclide Transport Abstraction* (SNL 2007 [DIRS 177407]). Parameters used include specific surface area (S_A), the sampled corrosion

colloid mass concentration ($M_{coll,FeOx,sampled}$), concentration of dissolved radionuclides (C_{RNdiss}), and experimentally-based forward rate constant (k) applicable under certain scenarios such as unstable colloidal suspension conditions, low flow rates, etc. The forward rate constant for irreversible sorption is used only for sorption of Pu and Am. The backward rate constants, calculated from the forward rate constants and the K_d values, are used for reversible Pu, Am desorption from FeO_x fixed corrosion products.

Reversible sorption is determined using the competitive sorption model reported in *EBS Radionuclide Transport Abstraction* (SNL 2007 [DIRS 177407]) from the sampled mass concentration of corrosion colloids. The amount of waste package colloids depends on the presence of carbon steel and stainless steel.

$$C_{RNcoll,FeOx} = C_{RNdiss} \times K_{d,RN,FeOx} \times M_{coll,FeOx,\ sampled}$$

In Step 4b, the irreversibly sorbed Pu and Am are determined, along with reversibly sorbed radionuclides. The C_{RNdiss} is the concentration of radionuclide "RN," determined by the TSPA-LA model as constrained by the solubility concentration model, which is used as an input to the colloid abstraction.

6.5.1.5 Seepage Water (Smectite) Colloids

Seepage water/groundwater colloid-related input parameters used in the abstraction are listed, as well as information used to develop the parameters, in Table 6-24.

Step 5a. The mass concentration of seepage water colloids is calculated on the basis of fluid ionic strength in Step 5a. The first step checks whether the colloids will be stable and then assigns a mass concentration based on the CDF.

Only applies if liquid flux water exists:

Input $pH_{wp,\ inv}$, $I_{wp,\ inv}$

$I_{threshold} = (-0.008 \times pH^2) + 0.12 \times (pH - 0.03)$

IF $I_{wp,inv} > I_{threshold}$

THEN $M_{coll,gw} = M_{coll,gw,min}$ (1×10^{-6} mg/L)

ELSE

$M_{coll,gw} = M_{coll,gw,sampled}$

The groundwater colloid concentration range (and distribution) is an intermediate parameter derived from several sources containing groundwater concentration data versus ionic strength from the Yucca Mountain vicinity and elsewhere.

Step 5b. The concentrations of radionuclides (Pu, U, Np, Am (Th, Pa), Cs, Ra, and Sn) reversibly sorbed on groundwater colloids are calculated based on the mass of groundwater colloids, K_d values describing the distribution of radionuclides between the fluid and montmorillonite, and the dissolved concentration of radionuclides within the waste package as calculated by the TSPA-LA model. The sorption capacity model described in Section 6.3.12.3 is

used to provide a reasonable bound on the sorption of radionuclides onto the montmorillonite (seepage) colloids:

$$C_{RNcoll,gw} = C_{RNdiss} \times K_{d,RN,coll,gw} \times M_{coll,gw}$$

The C_{RNdiss} is the concentration of radionuclide "RN," determined by the TSPA-LA model as output from the solubility concentration model that is used as an input to the colloid abstraction. $K_{d,RNcoll,gw}$ is a parameter derived from several sources (Table 6-15) and is an equilibrium sorption coefficient used to approximate the partitioning of dissolved radionuclide between colloids and fluid. The 1×10^{-6} portion of the relationship designates a correction factor to accommodate differences in units among the various parameters.

6.5.1.6 Outputs from the Waste Package to the Drift

In Steps 1 through 4, the total colloid-associated radionuclide concentrations, total colloid mass concentrations, and the remaining radionuclide concentrations in the fluid were calculated for waste form colloids derived from DHLWG, CSNF, and DSNF (Steps 1, 2, and 3), colloids derived from the corrosion of the waste package interior (Step 4), and seepage water/groundwater colloids that entered the waste package (Step 5). In Step 6 these quantities are passed from the waste package interior to the drift environment.

Step 6. Outputs from the waste package, which are also inputs to the drift, are colloid-associated radionuclide concentrations and colloid mass concentration.

The colloid-associated radionuclide source term is calculated in Step 6 by passing to the invert the contributions to the source term from Steps 1 through 5 (Figure 6-28).

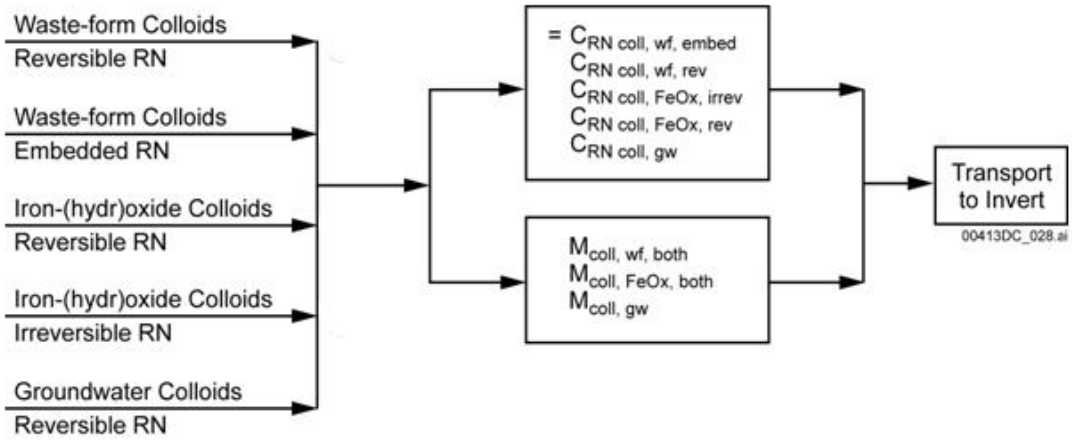

NOTE: $C_{RN\ coll,\ wf,\ embed}$ refers to irreversible DHLWG and CSNF ("ZrO2") colloids; $C_{RN\ coll,wf,\ rev}$ refers to reversibly sorbed DHLWG colloids and uranophane colloids from CSNF and DSNF.

Figure 6-28. Flow Chart and Logic Statements: Transfer of Colloid-Associated Radionuclide Source Term to Invert

The radionuclide component of the source term is made up of individual radionuclide mass concentrations irreversibly sorbed in and reversibly attached to DHLWG (modeled as montmorillonite) colloids ($C_{RNcoll,DHLWG,embed}$ and $C_{RN,DHLWG,rev}$), irreversibly attached to CSNF (modeled as ZrO_2) colloids ($C_{RNcoll,SNF,embed}$), reversibly sorbed to CSNF and DSNF colloids ($C_{RNcoll,uranophane,rev}$), irreversibly and reversibly attached to corrosion-generated iron oxyhydroxide colloids ($C_{RNcoll,FeOx,irrev}$ and $C_{RNcoll,FeOx,rev}$), and reversibly attached to groundwater (smectite) colloids ($C_{RNcoll,gw}$).

The colloid component of the source term is the sum of the mass concentrations of the waste form colloids ($M_{coll,wf,both}$; "both" signifies the inclusion of smectite (montmorillonite) waste form colloids from DHLWG and CSNF (modeled ZrO_2) colloids with irreversibly sorbed radionuclides (Pu and Am), or reversibly associated with radionuclides, or both (only in the case of DHLWG)); the iron oxyhydroxide corrosion-generated colloids ($M_{coll,FeOx,both}$; "both" signifies that corrosion-generated iron oxyhydroxide colloids irreversibly or reversibly associated with radionuclides, or both, are included); and the smectite groundwater colloids.

6.5.2 In-Drift Abstraction Implementation in TSPA–LA

6.5.2.1 In-Drift Colloid Stability and Mass Concentrations

Step 7 incorporates the outputs from the waste package in Step 6 with the invert fluid properties, ionic strength (I_{inv}) and pH (pH_{inv}), from TSPA-LA calculations.

Step 7. The primary function of Step 7 is incorporation of the invert fluid chemical properties and the calculation of resulting colloid stabilities using the DLVO model and mass concentrations of colloids entering the invert fluid from the waste package as shown in Figure 6-29.

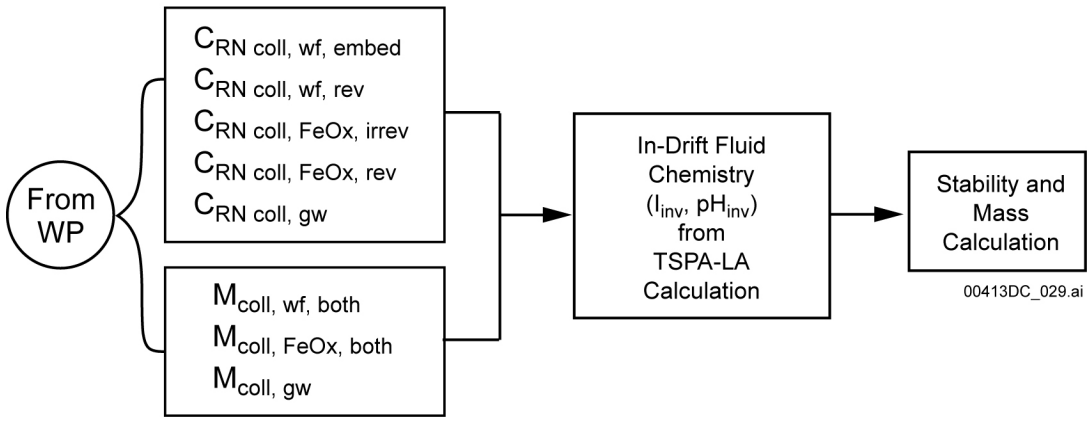

NOTE: $C_{RN\ coll,\ wf,\ embed}$ refers to irreversible DHLWG and CSNF ("ZrO2") colloids; $C_{RN\ coll,\ wf,\ rev}$ refers to reversibly sorbed DHLWG colloids and uranophane colloids from CSNF and DSNF.

Figure 6-29. Inputs to Drift from Waste Package

The concentrations of colloids and colloid-associated radionuclides within the drift are calculated on the basis of abstractions of the laboratory and field observations and chemical principles described in Section 6.3, with methods similar to those used to determine radionuclide and colloid concentrations within the waste package. A stepwise approach was taken in the abstraction, and each step is set out below with a flow diagram and logic statements that describe the abstraction step. Parameters are defined in Table 6-24.

In the TSPA-LA model calculations, the colloids with reversibly and irreversibly sorbed radionuclides leave the failed waste package and enter the drift geochemical environment. The colloids exit in-package chemical conditions and enter invert chemical conditions, which are potentially different from in-package conditions. Once the colloids are subject to the invert chemical conditions, the stability and concentration of the colloid suspensions are recalculated based on pH_{inv} to determine the $I_{threshold}$ value. Stability of the particles is based on comparison with I_{inv}. Therefore, if the colloid mass concentrations change (due to loss of colloid stability), the concentrations of sorbed radionuclides are recalculated as shown in Figure 6-27.

6.5.2.2 Recalculation of Colloid-Associated Radionuclides Concentrations in Drift

Step 8. In Step 8, the concentrations of radionuclides sorbed to colloids exiting the waste package are recalculated because of different chemical conditions in the invert. The new concentrations of dissolved radionuclides sorbed onto the colloids are determined. This step is illustrated by the flow chart in Figure 6-30 and by the logic statements that follow:

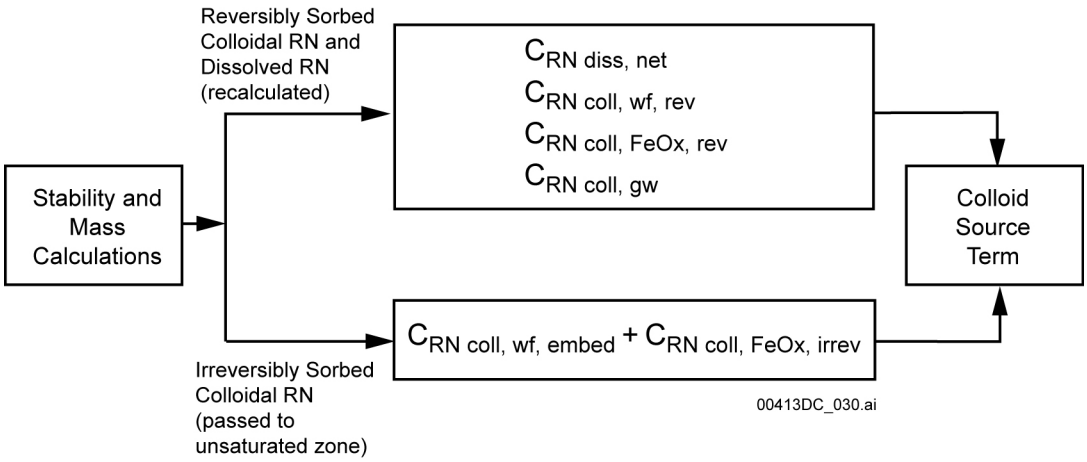

NOTE: $C_{RN\ coll,\ wf,\ embed}$ refers to irreversible DHLWG and CSNF ("ZrO_2") colloids; $C_{RN\ coll,\ wf,\ rev}$ refers to reversibly sorbed DHLWG colloids and uranophane colloids from CSNF and DSNF. $C_{RN\ coll,\ FeOx,\ rev}$ is determined in *EBS Radionuclide Transport Abstraction* (SNL 2007 [DIRS 177407]).

Figure 6-30. Recalculation of Colloid-Associated Radionuclides in Drift

$C_{RNdiss,net}$ is the net concentration of dissolved radionuclides after removal of radionuclides from fluid by sorption onto waste form, corrosion, and seepage water colloids.

Calculation of radionuclide sorption on colloids:

$$C_{RNcoll,DHLWG,rev} = C_{RNdiss} \times K_{d,RN,DHLWG} \times M_{coll,DHLWG,both}$$

$$C_{RNcoll,uranophane,rev} = C_{RNdiss} \times K_{d,RN,uranophane}$$

$$C_{RNcoll,FeOx,rev} = C_{RNdiss} \times K_{d,RN,FeOx} \times M_{coll,FeOx,both}$$

$$C_{RNcoll,gw} = C_{RNdiss} \times K_{d,RN,gw} \times M_{coll,gw}$$

6.5.2.3 Calculation of Colloid Source Term for Radionuclide Element (RN)

Step 9. The colloid source term is calculated by summing the determined concentrations of waste form, iron oxyhydroxide, and seepage water or groundwater colloids and the concentrations of the radionuclides associated with the colloids, as shown in Figure 6-31.

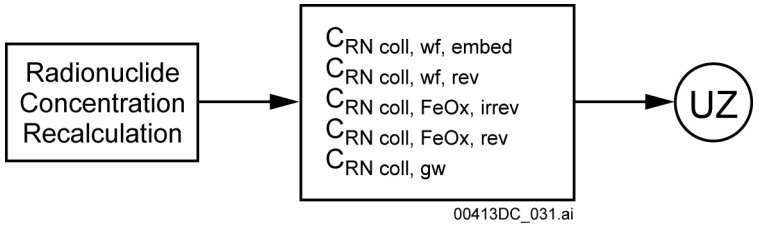

NOTE: $C_{RN\ coll,\ wf,\ embed}$ refers to irreversible DHLWG and CSNF (modeled as "ZrO_2") colloids; $C_{RN\ coll,\ wf,\ rev}$ refers to reversibly sorbed DHLWG colloids and uranophane (modeled as meta-autunite) colloids from CSNF and DSNF.

Figure 6-31. Source Term Summation for Colloid-Associated Radionuclide Concentrations in Drift

The sum of the radionuclides sorbed to colloids (reversibly sorbed and irreversibly sorbed) and net dissolved radionuclides (those remaining after sorption) is passed to the UZ for disposition in TSPA-LA calculations.

6.5.3 Implementation of Colloid-Facilitated Transport in the Natural Barrier System

The maximum groundwater colloid concentration used in the UZ and SZ colloid transport models (SNL 2007 [DIRS 181006]; BSC 2004 [DIRS 170006]) is a sampled value based on the data presented in Section 6.3.11 and in Figures 6-23 and 6-24. The groundwater colloids are modeled as montmorillonite; smectite (montmorillonite) colloids are available to form pseudocolloids through sorption of dissolved radionuclides. The radionuclides Sn, Pu, Am (Th, Pa), and Cs are considered explicitly in the UZ and SZ models for colloid-facilitated transport. See the end of Section 6.6.8 in this report for discussion of additional radionuclides that are not necessary for explicit treatment within UZ and SZ transport models as sorbed colloids.

Within the EBS colloid models, the montmorillonite waste form colloids, which originate from alteration of DHLWG, contain (1) plutonium and americium that is assumed to be irreversibly attached (i.e., non-detachable or embedded) and reversibly sorbed radionuclides. Corrosion-product colloids also contain reversibly sorbed and non-detachable radionuclides. All of these colloids and associated radionuclides are available as output for the UZ transport model

from the EBS. For non-detachable colloids, they are combined and transported as non-detachable (i.e., irreversible) colloids in the UZ transport model. Those reversibly sorbed radionuclides associated with colloids from the corrosion of CSNF and DSNF are re-cast as montmorillonite (smectite) colloids when transferred from the EBS to the UZ portion of the models.

Colloid transport in the UZ (SNL 2007 [DIRS 181006]) and SZ (BSC 2004 [DIRS 170006]) occurs by advective transport; colloid diffusion is considered negligible because colloids have free diffusion coefficients that are 2 to 4 orders of magnitude smaller than solutes. Colloids will transport wherever water flows, which in the unsaturated zone is a combination of fractures and the matrix, and in the saturated zone it is almost exclusively in fractures or through advective flow pathways in alluvium. The YMP has no site-specific data on colloid transport under unsaturated conditions, so colloid transport parameters developed from tests conducted in saturated fractured volcanic tuffs are applied to the UZ (SNL 2007 [DIRS 181006]). This approach is considered conservative, as it is widely recognized that colloids tend to be more retarded under unsaturated conditions than under saturated conditions in media that are otherwise similar. This greater retardation in the UZ occurs because: (1) immobile air–water interfaces serve as additional surfaces to trap colloids, and (2) UZ pore waters tend to have higher ionic strengths than SZ pore waters, resulting in a greater tendency for colloids to attach to rock surfaces.

Some of the plutonium and americium leaving the EBS is modeled as irreversibly attached to colloids. The irreversibly attached fractions of these radionuclides travel through the UZ and SZ at the same rate as the associated colloids. Irreversibly attached radionuclides on colloids leaving the EBS are split into two fractions: one retarded by colloid filtration and detachment processes and the other assumed to be completely unretarded. The fraction that travels unretarded depends on the groundwater travel time through the natural barrier system (UZ and SZ combined), with greater travel times resulting in smaller fractions. However, the unretarded fraction is <0.01, so the vast majority of the colloids experience filtration processes in the natural barriers that result in colloid retardation. The fraction of unretarded colloids is determined by a procedure described in *Saturated Zone Colloid Transport* (BSC 2004 [DIRS 170006]). The rationale for assuming that a small colloid mass fraction may travel unretarded through the natural barriers is that there have been observations of small mass fractions of plutonium migrating over 1.3 km within 30 years on silica-based colloids at the Nevada Test Site (Kersting et al. 1999 [DIRS 103282], p. 59) and about 4 km in 55 years associated with iron oxide (ferrihydrite) colloids at the Mayak facility in Russia (Novikov et al. 2006 [DIRS 179554]).

For colloids that experience filtration in the natural barrier system, colloid retardation factors (R_c) are randomly sampled from cumulative distribution functions developed separately for the fractured volcanics and the alluvium. These cumulative distribution functions are constructed using retardation factors derived from laboratory and field colloid transport tests conducted under varying geochemical conditions with different colloid types and sizes. The value of R_c is dependent on several factors such as colloid size, colloid type, and geochemical conditions (e.g., pH, Eh, and ionic strength). For any TSPA simulation, the cumulative distribution functions are sampled independently for the volcanics and alluvium. However, the distribution sampled for the volcanics is used for both the UZ and the volcanic portion of the SZ flow system, but the ranges are sampled independently. No correlation is assumed between

retardation factors in the volcanics and alluvium. The cumulative distribution functions in the volcanics and the alluvium are truncated at the lower end so that the minimum retardation factor in the volcanics is 6 and the minimum in the alluvium is 8. These truncations result in the vast majority of colloids (with the exception of the small unretarded fraction) experiencing retardation in the natural barrier system.

The transport of radionuclides that are reversibly sorbed to colloids is governed by equilibrium partitioning of the radionuclides between the solution phase, the immobile rock matrix, and mobile colloids. Plutonium radioisotopes are transported as one group; Am, Pa, and Th, radioisotopes as a second group; Cs radioisotopes as a third group; and Sn radioisotopes as a fourth group. Groundwater travel times through the natural barriers are slow enough that equilibrium sorption can be assumed even for slow radionuclide sorption and desorption rates. Any radionuclide mass that desorbs from colloids at rates slow enough to be comparable to travel times through the system is inherently considered part of the irreversibly sorbed radionuclide mass fraction. Colloid-facilitated transport of reversibly sorbed radionuclides depends on colloid transport parameters, the mobile colloid mass concentrations, and radionuclide sorption partition coefficients onto colloids and the immobile rock matrix. High colloid concentrations and large radionuclide sorption partition coefficients onto colloids (relative to the rock matrix) favor colloid-facilitated radionuclide transport at rates that can exceed transport rates in the absence of colloids. Because reversibly sorbed radionuclides will readily desorb from retarded colloids to resume partitioning between the solution phase, mobile colloids, and the immobile rock matrix, the retardation of colloids works to counterbalance the otherwise enhanced mobility of the radionuclide. However, because the sorption of this fraction is assumed to be reversible, colloids still serve to facilitate transport, even if they are retarded due to filtration processes.

6.6 BASE-CASE MODEL RESULTS

This section provides an overview of the model abstraction results, with a general discussion of the range of results, important couplings among processes and their impact on performance measures, and data uncertainty and propagation of the uncertainties through the model. As discussed in Section 6.1, colloid suspensions may affect repository performance if they are generated, and are stable within the waste package, EBS, and UZ and SZ. In the absence of filtration and thin-film straining, radionuclide-bearing colloids may readily transport from the EBS to the UZ and SZ and beyond. Output quantities from the waste form and engineered barrier system colloids models to downstream natural barrier system models and/or analyses include waste form colloid source terms, including DHLWG and CSNF colloid concentrations with irreversibly attached radionuclides and uranophane colloids with reversibly associated radionuclides. Also, the waste form and EBS colloid models determine the concentration of natural seepage water/groundwater colloids and corrosion product (iron oxyhydroxide) colloids that are released from the EBS.

6.6.1 Uncertainty Associated with the Model Analysis

The parameters discussed in this report and reported in the DTNs are based on data that may not be specific to Yucca Mountain repository conditions. The value ranges, probability distributions, and bounding assumptions for various parameters need to be assessed for uncertainty to facilitate

their appropriate representation in the TSPA calculations. The three types of parameter range-related issues relate to: (1) "temporal scaling," (2) "spatial scaling," and (3) extrapolation from the physical and chemical conditions of data acquisition.

6.6.1.1 Temporal Scaling

Experimental data obtained over short time periods is being used to address issues for the regulatory compliance period and beyond. These include waste form and waste package corrosion tests and sorption studies. These are discussed in greater detail with respect to each colloid type below.

Decreasing colloid concentrations in waste form corrosion tests with time where solution conditions (i.e., pH and ionic strength) have not changed may indicate a low stability ratio value. The decrease in particle concentration can be determined from the initial particle concentration, n_0, at time t_0 and k_f rate. The particle concentration, n_1, at time t_1 is determined from the following second order relationship:

$$\frac{1}{n_1} = \frac{1}{n_0} + \left(k_f \left(t_1 - t_0\right)\right) \qquad \text{(Eq. 6-29)}$$

Understanding the effect of the stability ratio on colloid populations helps in the interpretation of experimental results. A data set showing a decrease in particle concentration with time can be used to establish the stability ratio, W, for the system, as long as the system remains chemically stable (i.e., no significant changes in pH and ionic strength). As an example of this, Figure 6-32 shows experimental data from Mertz et al. (2003 [DIRS 162032]) on uranyl oxide hydrate colloids. Based on fitting curves, the stability ratio was determined to be ~10^5. If the initial particle concentration is high, colloids will destabilize rapidly as the opportunity for collisions increases (i.e., $t_{1/2} \approx 2 \times 10^{11}/n_o$). The stability ratio defines the ability of the electrostatic repulsion between the colloidal particles to make collisions less likely. However, given enough time, unless that stability ratio is infinite, the particle system will collapse.

It can be assumed that a corroding waste form will produce colloids continuously. At the corroded surface, the colloid concentration might be high as particles are constantly produced. However, at a distance from the waste form, the change in the colloid concentration will depend on the initial concentration and the stability ratio for that system and not on the condition of the waste form. If the time taken for the colloids to migrate from the waste package/in-drift to the invert is greater than 10 years, for example, determining the possible colloid stabilities might be useful in the model in providing more realistic assessments of colloid concentrations. However, W is not calculated directly in the model and a potentially more reasonable approach has been taken to set $W = 10$ for the ionic strength threshold as discussed below. This method is recommended, though it may over-predict colloid stability in some instances, as it bounds colloid behavior.

The relationships described in this section suggest that low concentrations can be stable. In other words, a contaminant may travel a long distance because it was present at a low concentration. Increasing the colloid concentration at the source may not necessarily increase the concentration transported.

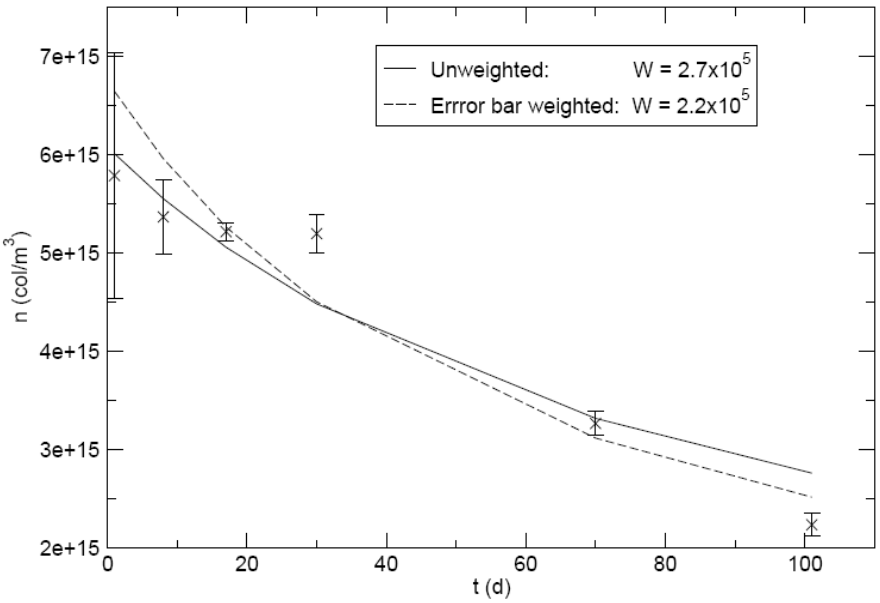

Source: Output DTN: MO0705CSIONSTH.000.

Figure 6-32. Stability Ratio (*W*) of Colloids Calculated from Particle Concentrations Reported by Mertz et al. (2003 [DIRS 162032], Table A3-1)

6.6.1.2 Spatial Scaling

Spatial scaling refers to the extrapolation or application of a process occurring at laboratory scale to the scale of the repository setting. Small-scale laboratory tests may not duplicate the environment of the waste package; however, the sequence of alteration and secondary mineralization observed in waste form corrosion tests has been shown to be accurate when compared to natural analogue weathering. Corrosion tests that endeavor to mimic the potential repository environment have many uncontrollable variables which makes these types of tests difficult to interpret. In particular, filtration and thin-film straining are not included in the model analysis but will be processes that occur in experiments. This makes the model conservative with respect to colloid stability and radionuclide-associated colloid concentrations.

6.6.1.3 Extrapolation from Physical and Chemical Conditions of Data Acquisition

Laboratory and field experiments may yield potentially useful data for TSPA models, but these may have employed several solution conditions that may not be directly relevant to repository conditions. For instance, Novikov et al. (2006 [DIRS 179554]) have stated that, as any potential nuclear waste repository site has unique physicochemical characteristics, site-specific investigations of actinide colloids are required for accurate predictions. However, as there will be uncertainty in the ionic strength and pH of the waste package environment, major factors affecting colloid stability, repository specific tests may be elusive. The approach used in this model of developing uncertainty distributions for radionuclide associations and colloid concentrations and using DLVO theory for estimating colloid stability allows the model to be useful under a variety of potential conditions.

6.6.2 Uncertainty Associated with DHLWG Colloid Formation

DHLWG corrosion tests have been used to establish the range of colloidal plutonium concentrations in the model. Tests with powdered samples were considered less relevant than those using monoliths specimens and experiments that were simple batch tests were favored over those that had more uncontrolled variables, such as unsaturated intermittent flow tests.

If all the data in Figure 6-7 was equally applicable to the Pu colloid concentrations in the repository for 1 million years, then a log-uniform distribution from about 1×10^{-12} to 1×10^{-7} mol/L would be indicated. However, the data from powdered samples could overestimate the colloid concentrations that arise from the fragmented logs of glass emplaced at the repository because the rapid degradation of the powdered glass promotes the homogeneous nucleation of Pu colloids. Because the ionic strength rises rapidly in these experiments causing coagulation, the data from powdered samples could underestimate the colloid concentrations. The experiments with the monoliths of glass do not have these limitations, and provide a narrower range from 1×10^{-11} to 1×10^{-8} mol/L (DTN: LL991109751021.094 [DIRS 142910] (MOL.20000124.0207, p. 27); DTN: LL000905312241.018 [DIRS 152621] (MOL.20001130.0021, pp. 29 and 70)). The monolith tests may overemphasize the low range because very little glass degradation has occurred in these tests compared to that which will occur over 1 million years. Given the uncertainty in these data sets, it is recommended that the range of 1×10^{-11} to 1×10^{-8} mol/L be sampled uniformly.

6.6.2.1 Temporal Scaling Issues with DHLWG Colloids

DHLWG corrosion tests that were used to establish plutonium concentrations were obtained over 7 to 720 days (DTN: LL991109751021.094 [DIRS 142910] (MOL.20000124.0207, p.27); DTN: LL000905312241.018 [DIRS 152621] (MOL.20001130.0021, pp. 29, 30, and 70)). Waste glass corrosion rates were accelerated by running tests at high temperatures and optimizing the waste form surface area-to-leachate volume so that the precipitation of secondary minerals became thermodynamically favorable. These types of tests are known to mimic the natural alteration of glass that has taken place over millions of years in humid and saturated environments, including in the Yucca Mountain tuff rock. Accelerated testing may result in changes in particle size and shape which in turn would influence colloidal properties.

In the case of DHLWG tests, colloids under the 2,000 m^{-1} SRL202 glass condition had steady colloid concentrations for the duration of the test. Based on solution analyses of these tests, the glass dissolution rate was minimal for the duration of the tests after the first few days (DTN: LL000123351021.117 [DIRS 143308]). Modeling the stability ratio from these tests is uncertain. The plot in Figure 6-33 shows three curves that predict the future stability of the system. High stability ratios of $W = 1 \times 10^{8}$ and $W = 1 \times 10^{10}$ both fit the early data for the SRL202 test, and the $W = 270{,}000$ fits the data from the SRL131 test where the ionic strength is known to have been increasing. In the $W = 1 \times 10^{8}$ case, this results in loss of significant colloid concentrations within 1,000 years; however, with the highest stability case, the colloid concentrations would remain significant for 10,000 years. Hence, the short-term tests indicate that plutonium concentrations associated with DHLWG colloids will remain constant, if solution conditions remain constant.

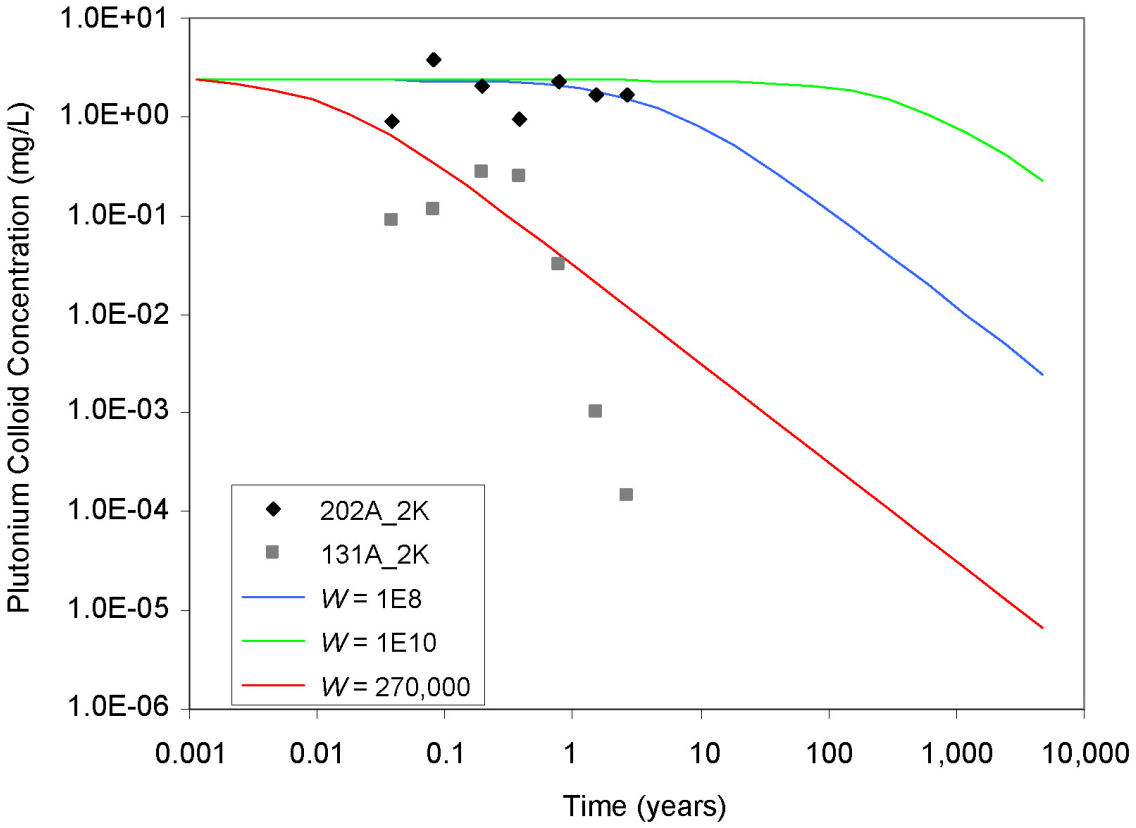

Source: Data points taken from Table 6-5 and fits for *W* taken using Equations 6-29 and 7-1 and following text.

NOTE: The *W* values represent degrees of stability. The scaling factor of 1 ppm is equivalent to 2×10^{-8} mol/L plutonium was used in the calculation. The fit is the second order rate equation where $dn/dt = -k_{smo}\, n^2_i/W$.

Figure 6-33. Predicted Change in Glass Colloid Concentration Based on DHLWG Tests

6.6.2.2 Spatial Scaling Issues with DHLWG Colloids

The small-scale laboratory product consistency DHLWG tests do not duplicate the environment of the waste package. Hence, the range of plutonium concentrations associated with DHLWG colloids were based on monolith tests that are better approximations to production glasses.

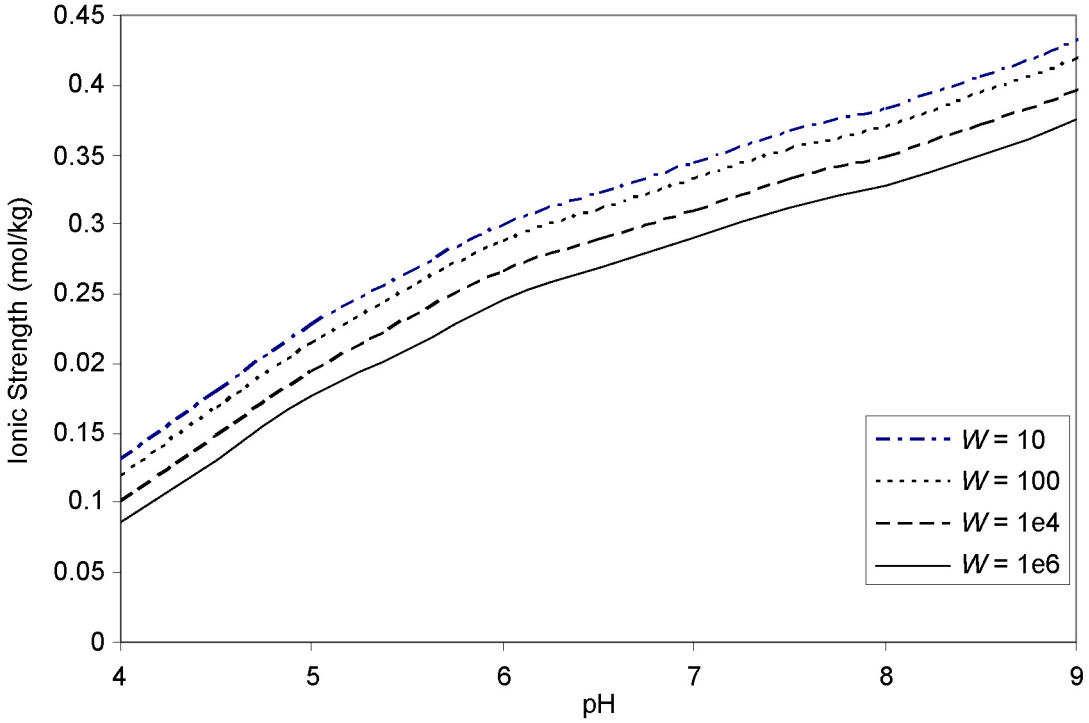

Source: Output DTN: MO0705CSIONSTH.000.

NOTE: Calculations were performed with a particle radius = 300 nm. With an initial concentration of 3 mg/L and $W = 10$ and 1×10^6, the half-lives are 35 hours and 400 years, respectively.

Figure 6-34. Stability of Montmorillonite Colloids with pH and a Series of *W* Values

Smectite colloids are predicted to be highly stable under in-package chemistry conditions (see Figure 6-34). The stability of these particles indicates that they may be stable in groundwater from the Yucca Mountain environment. Indeed, clay particles have been observed in sampled groundwaters from the NTS (Kersting et al. 1999 [DIRS 103282]).

6.6.2.3 Extrapolation from Physical and Chemical Conditions of Data Acquisition

The equations describing particle stability can be used under a range of conditions. The stability of clay colloids is remarkably constant over a large pH range; hence, there is little uncertainty that clay colloids once formed will remain stable unless subject to physical filtration. This is in agreement with the observations of long-range radionuclide transport associated with silicate (clay and zeolite) minerals at the Nevada Test Site (Kersting et al. 1999 [DIRS 103282], Figure 4, p. 58).

6.6.3 Uncertainty Associated with Irreversible CSNF Colloid Formation

Wilson (1990 [DIRS 100793]) conducted tests on five in-rod segments of spent nuclear fuel that represented a range of potential degrees of cladding failure. This data set was used because there is uncertainty in the fraction of Zircaloy-clad fuel rods that initially failed. Tests on bare fuel fragments (~13 cm pieces ~80 g each) exhibited the highest plutonium colloid release rates, while all tests on undefected, slit-defect, and hole-defect samples exhibited releases of plutonium

colloids that were approximately 10,000 times lower. The concentration of colloidal plutonium peaked at 1×10^{-6} M in the uncanistered fuel tests but remained above 1×10^{-8} M at 25°C for the duration of the test. The distribution observed in these studies used in model development are partially corroborated by Grambow et al. (1996 [DIRS 113253], Figure IV.8, p. 123), who reported plutonium colloid concentrations from 5×10^{-12} mol/L to 1×10^{-7} mol/L under non-oxidizing conditions. Hence, it is reasonable to assume that these CSNF plutonium colloid concentrations will persist for 1 Ma, if CSNF is still present and undergoing weathering, and the solution conditions are suitable for stable colloids. It is conservative to assume that these colloids persist at late times after all waste forms are degraded and the initially suspended colloids are washed away.

6.6.3.1 Temporal Scaling Issues with CSNF Colloids

CSNF corrosion tests that were used to establish plutonium concentrations were obtained over 1 to 174 days. The alteration products from these tests closely resemble secondary minerals found at natural uraninite deposits that have been contacted by silica-bearing solutions, such as uranophane and boltwoodite. The growth pattern of the secondary minerals under accelerated conditions may alter the colloidal behavior of the particles, as slow growth might result in the formation of large crystals that would be unlikely to become colloidal. In Figure 6-35, CSNF colloid data from Wilson (1990 [DIRS 100793]) have been used to determine stability ratios. The rapid decrease in colloids with time suggested a W value ~1×10^{6}. Under these conditions, the colloids would be predicted to remain stable for one year.

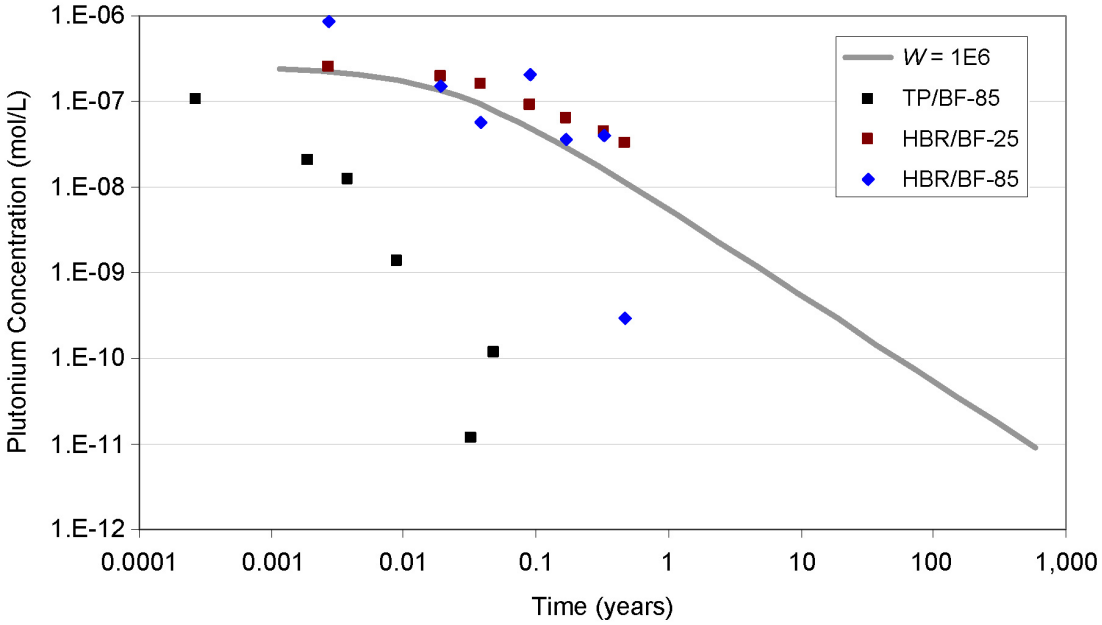

Source: Data taken from Table 6-6a and Equations 6-29 and 7-1 and following text.

NOTE: The fit is a second order rate equation with $dn/dt = -k_{smo}\, n^2_i/W$, where n is the plutonium colloid concentration.

Figure 6-35. Predicted Stability of Plutonium Colloids from CSNF based on Data from Wilson (1990 [DIRS 100793]) with $W = 1 \times 10^{6}$

These calculations suggest that high colloid concentrations may be unsustainable unless the stability ratio is extremely high (see Figure 6-36). These relationships may explain the colloid concentrations in short-term experiments, such as the saturated batch CSNF tests (Wilson 1990 [DIRS 100793]) and unsaturated intermittent flow CSNF tests (Mertz et al. 2003 [DIRS 162032]).

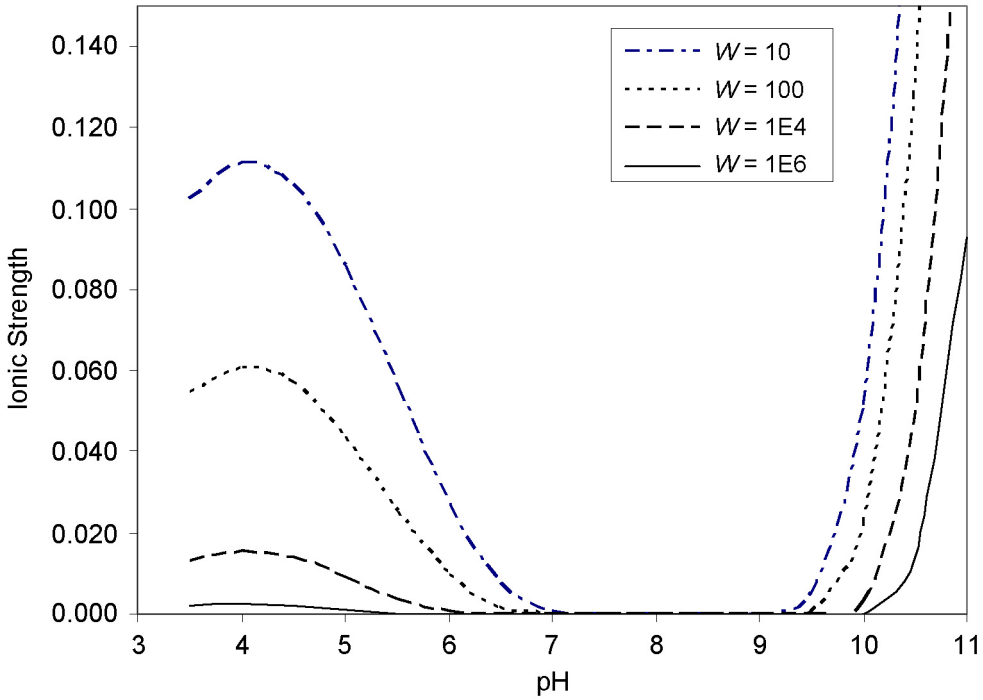

Source: Output DTN: MO0705CSIONSTH.000.

NOTE: At stability ratios (W) of 10, 100, 1×10^4, and 1×10^6. The calculations were performed in Excel using the "Solver" function to obtain the ionic strength threshold. The particle diameter was set at 60 nm.

Figure 6-36. Stability of CSNF Irreversible Colloid (ZrO_2) with pH and Ionic Strength

6.6.3.2 Spatial Scaling Issues with CSNF Colloids

Spatial scaling refers to the extrapolation or application of a process occurring at laboratory scale to the scale of the repository setting. Small-scale laboratory tests may not duplicate the environment of the waste package; however, by treating plutonium colloid concentration from waste forms separately from colloid stability, this uncertainty has been captured. The tests used in model development were conducted with fragments of CSNF solids (see Wilson 1990 [DIRS 100793]). Other tests, notably those by Mertz et al. (2003 [DIRS 162032]), were also conducted with fragments of CSNF solids, which though very useful for understanding CSNF behavior, may have been prone to physical filtration owing to the tortuous path from specimen surface to the collection vessel. Because the plutonium colloid concentration distributions developed from DHLWG tests were from experiments that had minimal physical filtration of potential colloids, similar experiments were selected for the development of the colloidal plutonium distributions from CSNF. Likewise, data using crushed or powdered CSNF (see McNamara et al. 2005 [DIRS 174068]) were not utilized as the conditions in these tests do not

represent directly the condition expected of fuel in the repository system and may overestimate colloid plutonium concentrations.

Physical filtration and thin-film straining of particles will undoubtedly occur in the repository owning to the tortuous paths between the in-package environment and the invert and the limited amounts of water in the system. These processes would serve to retard or reduce the transport of colloids through the engineered barrier system and representation of these should be handled meticulously so as to not inadvertently convolve such transport processes with the processes for colloid abundance and stability or radionuclide attachment onto colloids. For discussion of the transport processes in the EBS, see *EBS Radionuclide Transport Abstraction* (SNL 2007 [DIRS 177407]). It should be noted that leaving such processes out of the model would serve to over-estimate the transport of radionuclides on colloids and therefore it would bound the expected results.

6.6.3.3 Extrapolation from Physical and Chemical Conditions of Data Acquisition

By employing DLVO theory to describe particle stability, it has been possible to develop a model that addresses changes in pH and ionic strength. Therefore, the CSNF colloid model can be applied to conditions outside the bounds of any test and within the constraints provided in *In-Package Chemistry Abstraction* (2007 [DIRS 180506]) and *Engineered Barrier System: Physical and Chemical Environment* (SNL 2007 [DIRS 177412]). As stated previously, under very high ionic strength conditions (i.e., >1 mol/kg), the DLVO theory may not be suitable; however, these conditions are not anticipated in the repository environment when advective flow is significant.

6.6.4 Uncertainty Associated with Reversible Colloid Formation from DSNF and CSNF

Uranium (VI) colloidal phases have been observed in many corrosion tests. However, the total concentration of these particles has not been well established. Results reported by Wronkiewicz et al. (1996 [DIRS 102047]) had concentrations exceeding 50 mg/L; however, it is likely that a few large fragments may be biasing the results. To estimate the uncertainty, it is recommended that the uranophane colloids have a distribution identical to that of the groundwater colloids because the dominant interfacial phase in the groundwater (smectite clay) has surface electrical properties that are similar to uranophane. As the K_d values for the uranophane are low, the probability of radionuclide transport, other than uranium, associated with these colloids is low. Furthermore, under some conditions (e.g. lower silica and uranium concentrations), uranophane may become thermodynamically unstable and will dissolve.

6.6.4.1 Temporal Scaling Issues with Uranophane Colloids

Experimental data obtained over short time periods are being used to address issues for the regulatory compliance period and beyond. These include waste form and waste package corrosion tests and sorption studies. Accelerated testing can result in changes in particle size and shape, which in turn would influence colloidal properties. According to predictions presented in Figure 6-37, uranophane-type colloids would be expected to be stable under a wide range of pH similar to the case of smectite colloids. However, unlike smectite colloids, the rigid often acicular nature of uranophane particles might result in physical filtration and entrapment.

Natural uranophane crystals may grow to a few millimeters in length (McKinley et al. 2006 [DIRS 179552]); however, in the presence of trace elements within the system, such as neptunium, growth may be severely limited to the colloidal size range (Douglas et al. 2005 [DIRS 173086], Figure 2, p. 269).

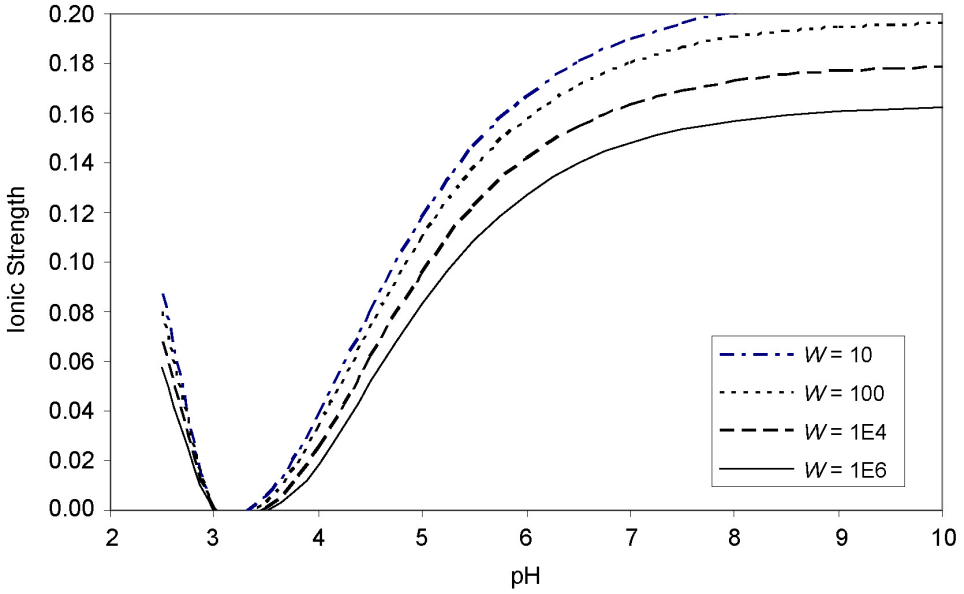

Source: Output DTN: MO0705CSIONSTH.000.

NOTE: Half-lives at $W = 10$ and 1×10^6 are 20 hours and 230 years, respectively. Calculations were with performed using the "Solver" function in Excel with particles with a = 250 nm and an initial concentration of 3 mg/L.

Figure 6-37. Stability of U(VI) Phase with pH and Ionic Strength

Scanning electron microscopy images of the uranophane particles reported by Douglas et al. (2005 [DIRS 173086]) indicate that the Np phases were much more fine grained. The model indicates that uranophane particles should be stable, yet they are not typically observed in nature, although they can exist with colloidal-sized dimensions. One possible reason for their absence in natural systems is filtration of these often needle-like particles. Because filtration is not included in this model, usage of the experimental results does not underestimate the possible transport of the finer, more equant particles observed in some short term tests. That is, if the uranophase colloids that form are acicular they would be expected to be filtered more easily, or the model would be bounding if it did not include the filtration. Also, if the uranophane colloids that are forming with some Np around form more equant colloids, then these would not be expected to be filtered.

6.6.4.2 Spatial Scaling Issues with Uranophane Colloids

Small-scale laboratory tests may not duplicate the environment of the waste package; however, the experiments conducted by Wronkiewicz et al. (1996 [102047]) on UO_2 alteration were run for 10 years and the sequence of secondary phase formation and alteration was found to be very similar to that observed on natural uraninite analogues. This observation of the same general

alteration sequences of secondary mineral formation within small-scale tests on uranium phase alteration compared to the largest natural systems indicated that the chemical processes controlling mineral formation are generally independent of spatial scale. In terms of the abundance of colloids, there may be some spatial scale effects related to the physical filtration of colloids and it is therefore a focus when evaluating test data to evaluate how much physical filtration may have played a role at these small scales. These tests had fewer impediments to physical filtration than similar long term corrosion/alteration tests conducted with CSNF. The presence of colloid U(VI) phases in these experiments after ~10 years supports the DLVO model that would predict high colloid stability of these types of phases. Maintaining separation from inadvertent incorporation of filtration effects into colloid stability or sorption constraints should minimize the spatial scale effects of the model. For uranophane colloids, these effects are even less of a focus because they relatively unimportant to the colloidal transport of radionuclides and therefore to the overall radionuclide transport in the system.

A good indicator of the importance of colloids is the K_c, the ratio of colloid-carried radionuclide to the dissolved radionuclide. The K_c is obtained by multiplying the groundwater colloid concentration by the colloid K_d. For Pu and Am (Th, Pa), the maximum sorption coefficients onto the U(VI) colloids were 10^4 mL/g (Table 6-9). In comparison, sorption onto either iron oxides or smectite clay is far greater (see Table 6-15). Additionally, for Pu and Am, irreversible colloids are represented as ZrO_2 particles generated from CSNF with Pu and Am embedded within them. This treatment of Pu and Am as irreversibly attached will make them relatively more important for transport of these radionuclides. In Figure 6-38, the relative unimportance of colloidal uranophane with reversibly sorbed radionuclides is considered using the K_c ratio (see discussion below). The plot demonstrates that little effect is expected from these colloids on overall transport of radionuclides. In conclusion, the uranophane colloids will be relatively unimportant for transport within the colloid subsystem model, and therefore negligible within the transport subsystem overall.

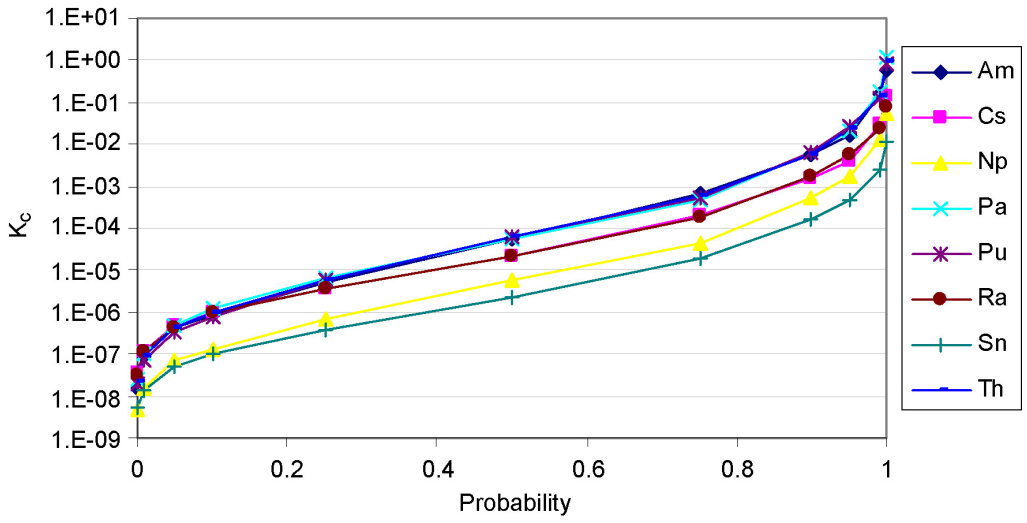

Source: Output DTN: MO0705DSCSCUSS.000.

Figure 6-38. Distribution of Radionuclide-Associated Colloid Partitioning between the Fluid and the Colloid

6.6.4.3 Extrapolation from Physical and Chemical Conditions of Data Acquisition

The uranophane colloid submodel is based on experimental data from a related U(VI) phase with a different composition and structure. There is considerable uncertainty on whether the meta-autunite data set reflects the surface electrical properties of a uranophane colloid. The rationale for using meta-autunite is discussed in Sections 4.1 and 5.6.

Using meta-autunite as a model colloid, the DLVO theory results indicate that uranophane colloids would be stable over the range of conditions anticipated in the repository because of the high permanent negative surface charge. There is clear experimental evidence for the occurrence of colloid uranophane in the tests reported by Wronkiewicz et al. (1996 [DIRS 102047]). However, the fact that large-scale migration of uranophane or other U(VI) colloids has not been observed in nature suggests that other factors must limit the transport of this type of phase as a colloid. Pearcy et al. (1995 [DIRS 110223]) discuss the occurrence of U(VI) alteration phases in silica-bearing uranium deposits at Peña Blanca, but do not describe any evidence that might imply colloidal transport. One potential mechanism for retardation of uranophane colloids might be physical filtration as the uranophane and related structures tend to have acicular forms. This fact might make them less amenable to transport in pores and fractures than smectite particles despite both phases possessing high surface charges.

The model is therefore conservative in considering the stability of uranophane colloids in the system.

6.6.5 Uncertainty Associated with Corrosion Product Colloid Formation

There is limited information in the literature concerning the quantity of corrosion product colloids that could potentially form during the degradation of waste package materials and the corrosion of other steel components in the EBS. Significant quantities of iron oxyhydroxide corrosion products were observed in scaled-down miniature waste package degradation experiments (DTN: MO0312UCC034JC.008 [DIRS 166367]). However, this occurred for only a short time (4 weeks) after which there was no outflow due to clogging. Observations reported by Bates et al. (1995 [DIRS 170880]) on DHLWG unsaturated flow tests using sensitized (i.e., heat treated) Stainless Steel Type 304L components indicated rust proportional to the test duration on components that were in contact with the radioactive glass and little corrosion in areas only contacted with dripping water. The heaviest corrosion was observed at weld points. The colloids released from these tests contained high concentrations of iron; however, these tests could not be used to establish steel corrosion colloid concentrations. The colloid concentration distribution for Stainless Steel Type 316 used in the model was based on assessment of likely colloid concentrations based on scientific judgment (Section 6.3.8).

6.6.5.1 Temporal Scaling Issues with Iron Oxide Colloids

Tests with miniature waste packages that were used to establish iron oxide concentrations for the model were obtained over a one- to four-week period (DTN: MO0312UCC034JC.008 [DIRS 166367]). The weathering products were consistent with the phases observed during long-term corrosion of iron and steel. If the iron oxide colloid concentration is set between 30 to 0.03 mg/L (Section 6.3.8) and assumed to possess a high stability ratio, the particle concentration

would not remain at 1 mg/L for longer than 1 year (see Figure 6-39). This is in partial agreement with the experimental results, which indicated no detectable colloids after 4 weeks; however, the lack of colloids was due to clogging (i.e., filtration) that is not included in the model.

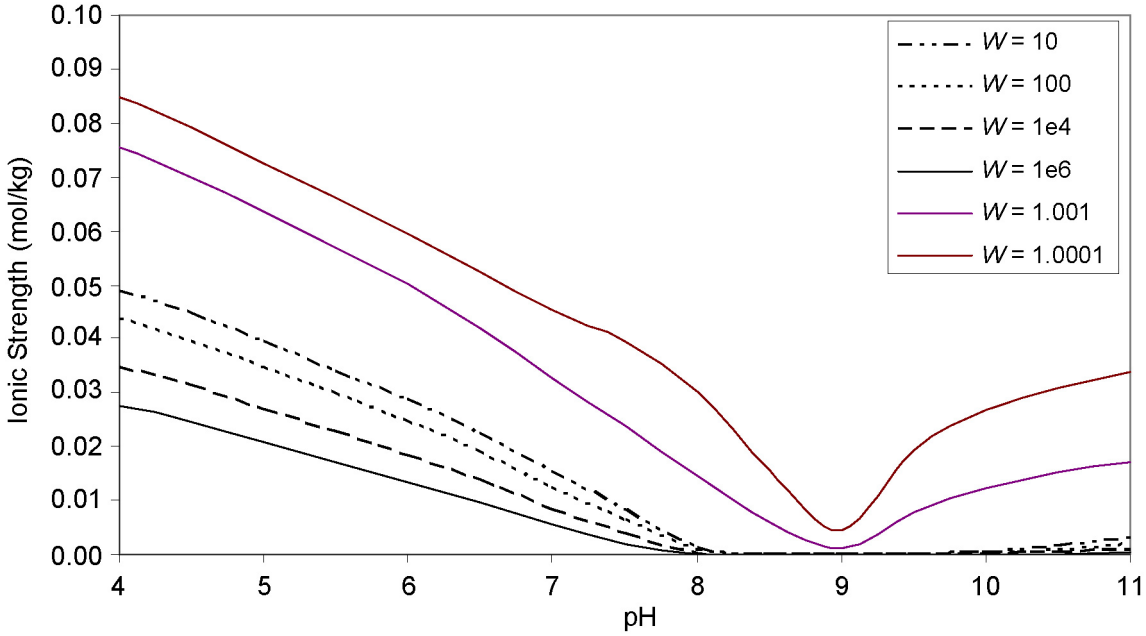

Source: Output DTN: MO0705CSIONSTH.000.

NOTE: The calculation used a diameter of 60 nm and an initial concentration of 3 mg/L. At $W = 10$, the particles are stable for 1,000 seconds and at $W = 1 \times 10^6$, the particles are stable for 3.2 years, whereas at $W = 1 \times 10^{15}$, particles would be predicted to be stable indefinitely.

Figure 6-39. Variation in Stability Ratio with pH and Ionic Strength

6.6.5.2 Spatial Scaling Issues with Iron Oxide Colloids

The tests used to obtain data on the probable concentrations of iron oxide–oxyhydroxide colloids that might be expected within the EBS were based on scaled-down waste packages (DTN: MO0312UCC034JC.008 [DIRS 166367]). Within those tests the spatial scaling of the containers was based on scaling the surface areas of the steel to be appropriate. However, the flow rate of the fluid was not scaled and this led to both spatial-scale effects (i.e., the volume and flux of water relative to the steel surface areas and masses were much too large) and temporal scale effects (i.e., the flush rate was much higher than would be expected for repository conditions). Such effects create highly disequilibrium reaction conditions (not expected for the repository system), as well as material transport conditions that are more substantial than would be expected. Some of the experiments were conducted under chemical conditions not relevant directly to the repository because of the relative masses of such extreme fluid compositions compared to the steel masses, and in some of these instances colloidal re-stabilization, particle entrainment, and incorporation of other solids (e.g., salt crystals) may have occurred. Hence, the data from these tests tend to overestimate equilibrium colloid formation and their use in the model development provides a bounding (conservative) constraint on that.

6.6.5.3 Extrapolation from Physical and Chemical Conditions of Data Acquisition

The results from Zarrabi et al. (2003 [DIRS 171238]) that were used to establish particle concentrations from corroded waste package materials are highly conservative; however, the DLVO approach used in this model would have not predicted colloids under two of the conditions, as shown in Table 6-23.

Table 6-23. Conditions from Experiments by Zarrabi et al. (2003 [DIRS 171238]) and Predicted Outcome Based on DLVO Model

Test	Conditions		Prediction from DLVO Based Model
	Ionic Strength (M)	pH Range	
High saline	1.3705	8.8 to 9.5	Unstable
Low pH	0.00223	2.0 to 4.8	Highly stable
High saline-high nitrate	1.3953	8.8 to 9.5	Unstable
J-13 well water	0.00249	7.4 to 8.5	Stable to pH 8.5

At very high ionic strengths, colloid behavior can no longer be modeled using simple DLVO theory. A phenomenon known as colloid re-stabilization can occur above an ionic strength of 1.0 mol/kg due to the development of an ion layer on the surface of the colloid together with polarization of the medium between particles. This leads to an additional repulsive energy term that results in re-stabilization. The phenomenon has been observed in laponite (Huang and Berg 2006 [DIRS 179549]) and rutile. The behavior may explain the colloid concentrations observed in the high saline tests reported in DTN: MO0312UCC034JC.008 [DIRS 166367]. Ruckenstein and Huang (2003 [DIRS 179556]) have developed a model to describe this behavior, but it has not been implemented in the current abstraction because the model is not well established in the scientific community. It is also possible that the presence of small amounts of silica, such as in J-13 well water, can coat iron oxides and change the zeta potential characteristics with pH. This might lead to a shift in the zero point of charge to low pH and a high overall surface potential and higher stability (Jara et al. 2005 [DIRS 180834]). However, the use of a conservative stability ratio value ($W = 10$) has captured the potential uncertainty in surface charge in more complex systems.

Ryan and Gschwend (1994 [DIRS 180525]) have described a simple relationship between flow and particle detachment and developed an empirical rate of colloid release, defined as:

$$k_{exp} = 10^{1.01 \pm 0.1} \nu^{0.84 \pm 0.02} \quad \text{(Eq. 6-30)}$$

This equation suggests that there is a surface attachment energy for release that is not accounted for in the DLVO theory. High flow rates may account for the occurrence of iron oxide suspensions in the miniature waste package tests.

As discussed above in Section 6.6.5.2, the colloid concentrations obtained from the experiments by Zarrabi et al. (2003 [DIRS 171238]) represent a bound on carbon steel colloidal corrosion products.

6.6.6 Uncertainty Associated with the Measurement of Seepage Water/Groundwater Colloids

Several factors contribute to uncertainty in the concentrations of colloids in the groundwater samples used to establish parameters for use in the TSPA analysis, including (1) field sampling techniques, including differences in pumping rates at each well during extraction of the water samples, (2) other unknown factors affecting the quantities of particles suspended in the water samples, including the types of additives introduced in the wells during the drilling process itself, and (3) errors inherent to the laboratory methods used to measure the quantities of colloids suspended in the water samples (e.g., filter ripening, interference and detection limitations for dynamic light scattering measurement techniques). A cumulative distribution function was developed to accommodate the variable colloid concentrations and the uncertainty in groundwater sample collection. This allowed for stochastic sampling, including high concentrations (i.e., ~100 mg/L) in at least 2% of the model iterations, while probabilistically allowing for the selection of lower mass concentrations (0.001 mg/L to 1.0 mg/L) 75% of the time.

6.6.7 Uncertainty Associated with the Determination of Colloid Stability

The DLVO predictions show that particle size has a significant effect on particle–particle collisions. This is a result of the linear dependence of the van der Waals and electrical double layer interaction forces on particle size.

The stability model calculates the ionic strength at which a colloid would be unstable. The model is based on experimental zeta potential data, a fixed Hamaker constant, and fixed particle size. The relationships were compared to other experimental data for validation, including data from Liang and Morgan (1990 [DIRS 109524]) (see Figure 6-5). However, the uncertainties in the calculation are: the surface potential of the colloids in the repository environment that may be influenced by the presence of other species such as silica or carbonate; the Hamaker constant, which may range between 10^{-19} and 10^{-20} J; and the heterogeneous nature of the colloids in terms of composition, surface charge, size, and shape.

By using a low colloid stability threshold, the model has bounded possible behavior.

6.6.8 Uncertainty Associated with Radionuclide Sorption onto Colloids

With proper data selection and application to appropriate conditions, the linear adsorption model (K_d model) may yield adequate predictions. Depending on the rate of alteration and weathering in the waste package and in-drift environment, there may be changes in the reactivity of radionuclides with surfaces and consequently large changes in K_d values. Changes in K_d values are dependent upon changes in pH, Eh, sodium ion concentration, and radionuclide concentration (Cantrell et al. 2002 [DIRS 179540]), although the pH range of interest in the repository environment is narrow (pH 4.5 to 8). For instance, a high concentration of radionuclides may lead to saturation of adsorption sites. An inherent assumption of the linear adsorption model approach is that the adsorption sites never become saturated. With respect to colloid transport, errors in the low K_d values for poorly sorbing radionuclides are less important as these radionuclides will not be associated significantly with colloids. Also, because transport in the

natural system relies on an approach that combines the values for sorption coefficients (K_d) with the concentrations of the colloidal particles to constrain the K_c value, these convolved parameters are discussed below to provide context for the natural system usage of the sorption information presented in this model.

In contrast to iron oxides, the surfaces of alumino-silicate minerals are more complex in terms of site types. In a smectite clay mineral there will be >Si-OH groups and pH-dependent >Al-OH groups, as well as interlayer sites. Reported experimental studies have sometimes been conducted under high ionic strength conditions that prevent ion exchange and will therefore conclude that edge sites dominate sorption behavior. Pabalan and Turner (1997 [DIRS 179555]) and Bradbury and Baeyens (2005 [DIRS 179538]; 2006 [DIRS 179541]) have developed surface complexation models for montmorillonite (smectite) clays that provide good predictions for the sorption of radionuclides.

Sorption of uranium and neptunium onto smectite both do exhibit pH dependence (see Figure 6-40). As the model does not include an explicit pH dependency, the distributions have been set to bound potential behavior by capturing the data for their sorption over a range of pH conditions. The uranium sorption experiment was conducted in equilibrium with atmospheric pCO_2, whereas the neptunium experiment was conducted under carbonate-free conditions. In the case of Np data, this would serve to enhance the sorption onto the colloid at chemical conditions where aqueous carbonate complexes would have dominated (e.g., high pH) if there had been dissolved carbonate in the solution. Without the carbonate complexing in the aqueous phase, the surface complexes can "compete" more effectively for the dissolved Np. Lu et al. (2000 [DIRS 166315]) discussed K_d values for Np on montmorillonite and silica colloids in natural groundwater and synthetic J-13 between 1.1×10^1 mL/g and 5.5×10^2 mL/g between pH 8.2 and 8.3 after 240 days, which is consistent with the data shown in Figure 6-40b.

Iron oxides also exhibit pH dependent sorption behavior; however, as these radionuclides are being considered within the competitive surface complexation model (see SNL 2007 [DIRS 177407]), the details for this were not provided in the model.

Because the specific surface area of a colloidal phase may be larger than that of the mineral phase from which the K_d value is determined, the K_d distributions have been adjusted to account for this effect by providing higher conservative upper bounds. High redox potentials will have an effect on actinide sorption and chemical state but were not considered in development of the K_d values. In most groundwaters, this is not an issue; however, the redox potential at the surface of a nuclear waste form may be high (i.e., >500 meV) (Runde et al. 2002 [DIRS 168432]). Within this range, small changes in the redox potential can cause large changes in overall radionuclide behavior and will consequently affect colloid formation and adsorption.

Figure 6-41 shows the CDF of the K_c values obtained using the in-drift colloid K_d values for sorption onto smectite, for the radioelements under consideration in the model. The distribution of K_c values for neptunium is low enough that smectite colloids will not transport neptunium significantly. For radium, 99% of the realizations show no significant colloid-facilitated transport, but for uranium, only 90% of the realizations show no significant colloid-facilitated transport. At the 99.9 percentile, ignoring colloids overestimates the effective rock U K_d by a factor of about 6.

The recently considered radionuclides for reversibly sorbed smectite colloids of the EBS colloid model are U, Np, Ra, and Sn. Of these, only Sn definitively exhibits significant potential for colloid-facilitated transport in the natural system. This is based on examining the cumulative distribution functions for the K_c parameter that would be used for each of these radionuclides in the UZ and SZ models for smectite colloids (see Figure 6-41). The K_c parameter is the ratio of the radionuclide concentration within the colloidal suspension to the concentration of the dissolved species. This parameter is equivalent to the product of the distribution coefficient (K_d) of the radionuclide onto the colloid and the colloid particle concentration. The cumulative distributions defined above for these two smectite colloid parameters were convolved within GoldSim V. 9.60.1 and the results are plotted (using Excel 2003) in Figure 6-41.

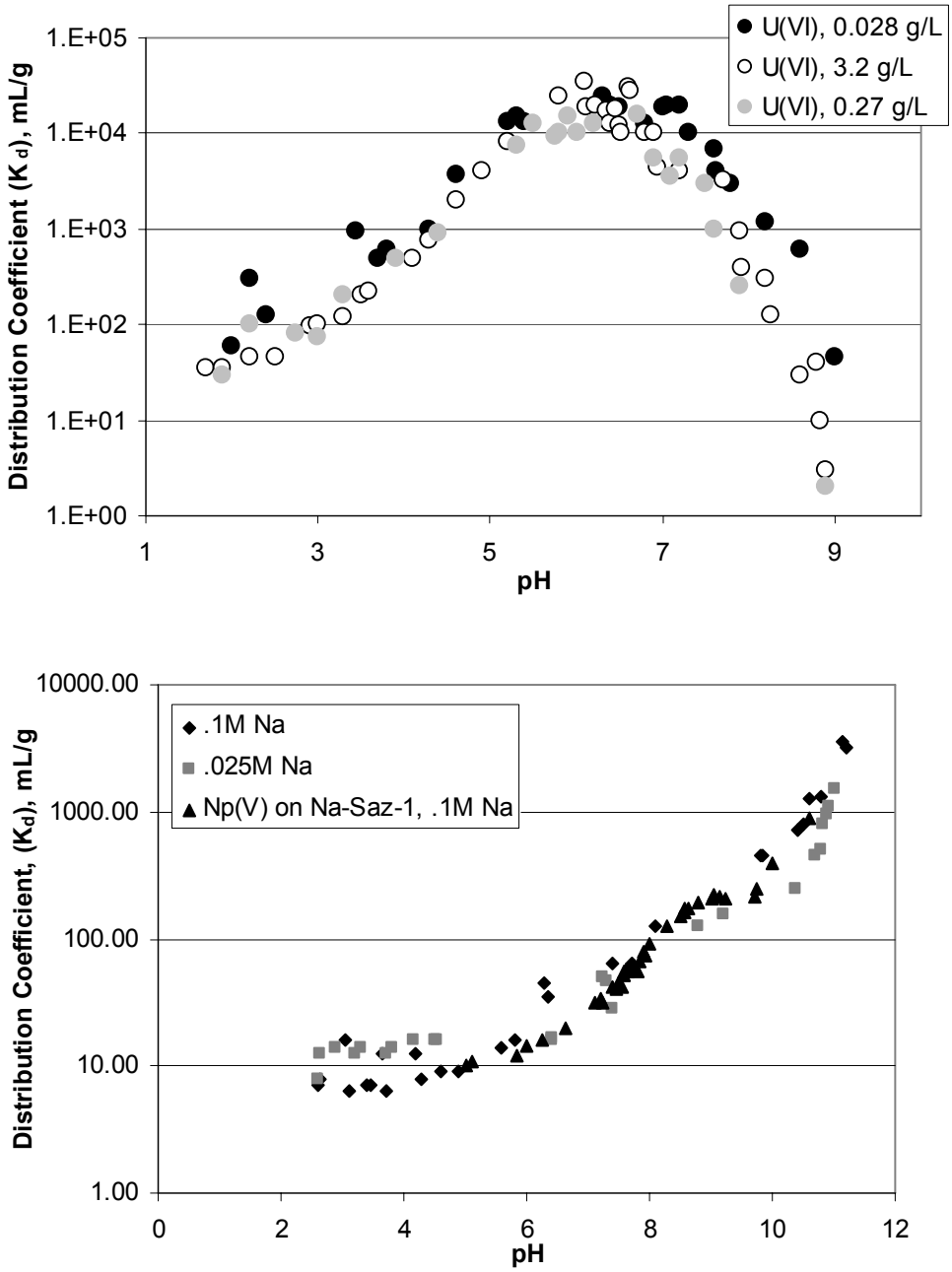

Source: Data taken from Pabalan and Turner (1997 [DIRS 179555], Figure 4, p. 211) and Bradbury and Baeyens (2005 [DIRS 179538], Figure A-4 (c and d), p. 889).

NOTE: Uranium sorption experiments performed in atmospheric CO_2 (Pabalan and Turner 1997 [DIRS 179555]). Neptunium sorption experiments were performed in carbonate-free conditions (Bradbury and Baeyens 2006 [DIRS 179541]).

Figure 6-40. Plots Showing pH Dependent Sorption of (a) U(VI) and (b) Np(V) on Montmorillonite

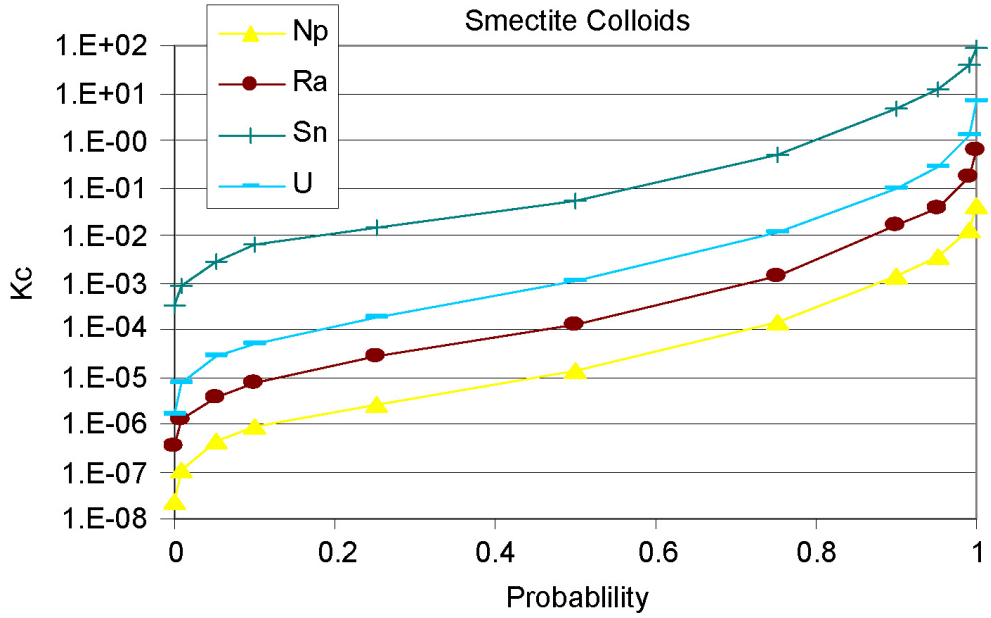

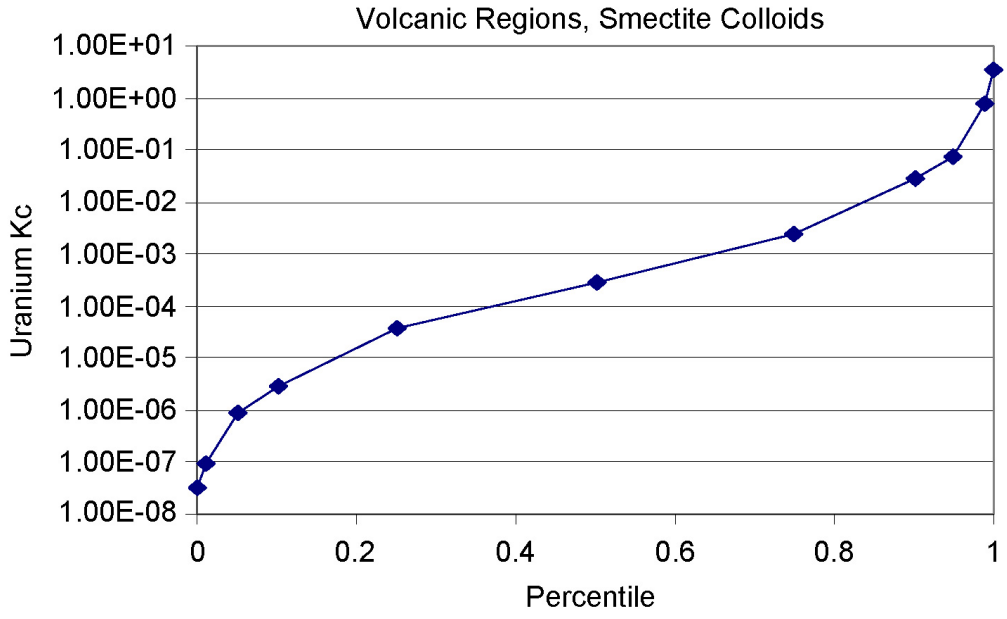

Source: Output DTN: MO0705DSCSCUSS.000.

Figure 6-41. (a) Cumulative Distribution Functions for the K_c of Smectite Colloids Using Transport Parameters Defined for the Conditions within the EBS; (b) Cumulative Distribution Functions for Uranium K_c for Smectite Colloids in the Yucca Mountain Volcanic Regions

In the colloid-facilitated radionuclide transport model used in the UZ and SZ transport models, the retardation of a radionuclide in the fracture system is reduced by transport on colloids, thus increasing the speed of transport. If the distribution of K_c does not have a significant probability (i.e., above about 10% of the cumulative probability) for K_c values above 0.1, colloids will not significantly facilitate radionuclide transport. (Because of the other bounding aspects of these transport models, this is probably also the case for K_c values of 1.0.) As can be seen in Figure 6-41, the distribution for K_c for Sn crosses the K_c = 0.1 line at slightly above the 50th percentile, so smectite colloids clearly have the potential for a significant role in Sn transport. At the other extreme, the K_c for Np does not exceed 0.1 even at the 99.9th percentile, so smectite colloids do not play a significant role in Np transport. U and Ra show only a limited probability that their K_c will go above 0.1, about 10% and 1%, respectively, so that Ra transport on smectite colloids also does not appear to be necessary to represent explicitly.

Note that the above analysis assumes that the radionuclide-smectite colloid K_d values assigned for EBS chemical conditions are applicable in the UZ and SZ environment. However, the values of K_d can be quite pH dependent (see Figure 6-40), and the distribution of pH values is different in the UZ and SZ compared to that within the EBS. In particular, the K_d value of uranium is quite pH dependent (see Figure 6-40, after Figure 4 of Pabalan and Turner 1997 [DIRS 179555]), so the K_c of uranium on smectite of the UZ and SZ volcanic regions was further evaluated.

The 23 pH values from *Saturated Zone Site-Scale Flow Model* (SNL 2007 [DIRS 177391], Table A6-1) for Yucca Mountain Crest, Central and Southeast regions, were assumed to be equally probable and indicative of the UZ and SZ volcanics. These values were used with an empirical pH-K_d correlation derived from the Pabalan and Turner (1997 [DIRS 179555]) data to develop a distribution of K_c for uranium on smectite colloids that would be more representative of the natural system conditions (Output DTN: MO0705DSCSCUSS.000; also shown in Figure 6-41b). Based on this information, the uranium K_c exceeds the value of 0.1 only at above the 95th percentile; therefore, only about 5% of the values appear to have any potential to contribute to the transport of uranium. Given that the transport of uranium as uranophane colloids does not even appear to be a significant contribution relative to the dissolved transport (see Section 7), transport of reversibly sorbed uranium on smectite colloids does not appear to be an essential consideration within a risk-informed approach.

6.6.8.1 Temporal Scaling with Sorption Coefficients

Sorption experimental data has been obtained over short time periods but is being used to address issues for the regulatory compliance period and beyond. To accelerate reactions on the laboratory time-scale, conditions other than those anticipated in the waste package and in-drift environment may have been imposed. For example, experiments may employ high concentrations, rapid flow rates, and elevated temperatures. If the chemical conditions do not change significantly, the application of the K_d values for long time periods will be adequate for modeling purposes. There is no reason that sorption coefficients will alter over time.

6.6.8.2 Spatial Scaling with Sorption Coefficients

By scaling down systems of interest (the repository environment) to the laboratory size, certain physical conditions must be altered. For example, the water/solid mass ratio in most repository systems is <1; however, to perform analyses, the ratio may need to be increased. Nevertheless, for a water/colloid system, the laboratory data may be a better representation of repository systems than for modeling sorption on the stationary phase environment, as the defined water/colloid mass ratio in this model is high. For strongly sorbing radionuclides, such as Pu and Am, the performance assessment model may be uncertain because site-specific sorption isotherms are not available. To overcome this situation, a pedotransfer function relating parameters relevant for the description of sorption to the known waste package and in-drift environmental properties might need to be applied. An advantage of using a pedotransfer function is that the spatial variability of the sorption-relevant properties on the repository scale may easily be incorporated in the risk assessment.

One important source of uncertainty is the limited accuracy of the applied linear sorption relationships when predicting solute concentrations in the solid or liquid phase. In addition, radionuclide sorption varies in space because of the spatial variability of the repository environment. Spatial variability will be an intrinsic feature of the waste package, EBS, and the tuff rock environment. The characterization of this variability will be an additional source of uncertainty because quality, availability, and amount of site-specific information is heterogeneous.

Implementation of the uncertainties associated with the sorption parameters established during this model analysis is accomplished through the use of parameter ranges and distributions, rather than single, deterministic parameter values.

6.6.8.3 Extrapolation from Physical and Chemical Conditions of Data Acquisition

The K_d sorption model incorporates wide ranges to account for solution chemistry changes. The issues concerning changes in Eh and carbonate on radionuclide speciation and sorption are discussed in *Site-Scale Saturated Zone Transport* (SNL 2007 [DIRS 177392], Appendix A).

Table 6-24. Parameters Used in Model

New TSPA Name	Report Name	Description	Form	Parameter Values	Output DTN
Conc_Col_FeOx_Min	$M_{coll,FeOx,min}$	Lowest observed or expected mass of iron oxyhydroxide colloids per unit volume or mass of water	Fixed value	1×10^{-6} mg/L	MO0701PAIRONCO.000
Conc_Col_GW_Sampled_a	$M_{coll,GW,sampled}$	Sampled groundwater colloid mass per unit volume or mass of water when colloids are stable	CDF	See Table 6-13	MO0701PAGROUND.000
Conc_Col_GW_Minimum	$M_{coll,GW,Min}$	Expected mass per unit volume or mass of water of ground water colloids when colloids are unstable	Fixed Value	1×10^{-6} mg/L	MO0701PAGROUND.000
Target_Flux_Out_Ratio_a	F_{RN}	Concentration of Pu on Colloids / (Concentration of Pu on colloids + Concentration of Pu dissolved in water)	Uniform	0.9 to 0.99	MO0701PAIRONCO.000
CPu_Col_WF_Embed_Sampled	$C_{RNcoll,DHLWG, embed, sampled}$	Concentration of irreversibly attached plutonium, associated with DHLWG colloids	Uniform	See Table 6-4	MO0701PAGLASWF.000
CPu_Col_WF_Embed_Min	$C_{RNcoll,DHLWG, embed, Min}$	Lowest observed or expected concentration of irreversibly attached plutonium associated with DHLWG colloids	Fixed value	1×10^{-13} mol/L	MO0701PAGLASWF.000
CPu_Per_WF_Embed_Col_a	$C_{coll,DHLWG, triangular}$	Concentration of irreversibly attached plutonium per concentration of colloids	Triangular distribution	See Table 6-3	MO0701PAGLASWF.000
Smectite _ZPC		Smectite zero point of charge, pH below which the smectite does not sorb	Fixed value	1.5	MO0701PAGLASWF.000
Smectite_pH_hi		High pH for smectite ionic strength threshold fit	Fixed value	9	MO0701PAGLASWF.000
Coeff_pH_Sq_Smectite		Coefficient of pH squared term for fit of ionic strength threshold for smectite colloid stability	Fixed value	−0.008	MO0701PAGLASWF.000
Coeff_pH_Smectite		Coefficient of pH term for fit of ionic strength threshold for smectite colloid stability	Fixed value	0.12	MO0701PAGLASWF.000
Coeff_inter_Smectite		Intercept term for fit of ionic strength threshold for smectite colloid stability	Fixed value	0.03	MO0701PAGLASWF.000
Kd_Pu_Rev_Smectite_a	$K_{d,Pucoll,wf}$	Distribution coefficient for reversible sorption of plutonium onto smectite colloids	CDF	See Table 6-15	MO0701PASORPTN.000
Kd_Am_Rev_Smectite_a	$K_{d,Amcoll,wf}$	Distribution coefficient for reversible sorption of americium onto smectite colloids	CDF	See Table 6-15	MO0701PASORPTN.000

Table 6-24. Parameters Used in Model (Continued)

New TSPA Name	Report Name	Description	Form	Parameter Values	Output DTN
Kd_Th_Rev_Smectite_a	$K_{d,Thcoll,wf}$	Distribution coefficient for reversible sorption of thorium onto smectite colloids (same as Am)	CDF	See Table 6-15	MO0701PASORPTN.000
Kd_Pa_Rev_Smectite_a	$K_{d,Pacoll,wf}$	Distribution coefficient for reversible sorption of protactinium onto smectite colloids (same as Am)	CDF	See Table 6-15	MO0701PASORPTN.000
Kd_Cs_Rev_Smectite_a	$K_{d,Cscoll,wf}$	Distribution coefficient for reversible sorption of cesium onto smectite colloids	CDF	See Table 6-15	MO0701PASORPTN.000
Kd_Pu_Rev_FeOx_Col_a	$K_{d,Pucoll,FeOx}$	Distribution coefficient for reversible sorption of plutonium onto corrosion-generated (iron oxyhydroxide) colloids	CDF	See Table 6-15	MO0701PASORPTN.000
Kd_Am_Rev_FeOx_Col_a	$K_{d,Amcoll,FeOx}$	Distribution coefficient for reversible sorption of americium onto corrosion-generated (iron oxyhydroxide) colloids	CDF	See Table 6-15	MO0701PASORPTN.000
Kd_Th_Rev_FeOx_Col_a	$K_{d,Thcoll,FeOx}$	Distribution coefficient for reversible sorption of thorium onto corrosion-generated (iron oxyhydroxide) colloids (same as Am)	CDF	See Table 6-15	MO0701PASORPTN.000
Kd_Pa_Rev_FeOx_Col_a	$K_{d,Pacoll,FeOx}$	Distribution coefficient for reversible sorption of protactinium onto corrosion-generated (iron oxyhydroxide) colloids (same as Am)	CDF	See Table 6-15	MO0701PASORPTN.000
Kd_Cs_Rev_FeOx_Col_a	$K_{d,Cscoll,FeOx}$	Distribution coefficient for reversible sorption of cesium onto corrosion-generated (iron oxyhydroxide) colloids	CDF	See Table 6-15	MO0701PASORPTN.000
Conc_Col_FeOx_Min		Minimum concentration of FeOx colloids	Fixed value	1e-6 mg/l	MO0701PAIRONCO.000
Conc_Col_FeOx_CS_Samplea	$M_{coll,FeOx,sampled}$	Sampled FeOx colloid concentration when carbon steel is degrading	Natural log uniform	0.03 to 30 mg/L	MO0701PAIRONCO.000
Conc_Col_FeOx_SS_Sampled_a		Sampled FeOx colloid concentration for locations containing degraded stainless steel	CDF	See Figure 6-11	MO0701PAIRONCO.000
Min_Default_Fwd_Rate_Const Max_Default_Fwd_Rate_Const	k	Forward rate constant for plutonium and americium for irreversible sorption onto iron oxyhydroxide colloids and stationary corrosion products in the waste package for zero advective flux conditions or where colloids are unstable	Log uniform	0.002 to 0.05 $m^3m^{-2}yr^{-1}$	MO0701PAIRONCO.000
FeOx_pH_lo		Low pH for FeOx colloid ionic strength threshold fit	Fixed value	4.5	MO0701PAIRONCO.000

Table 6-24. Parameters Used in Model (Continued)

New TSPA Name	Report Name	Description	Form	Parameter Values	Output DTN
FeOx_ZPC_lo		Low end of zero point of charge range	Fixed value	8.4	MO0701PAIRONCO.000
FeOx_ZPC_hi		Low end of zero point of charge range	Fixed value	9.4	MO0701PAIRONCO.000
FeOx_pH_hi		Low pH for FeOx colloid ionic strength threshold fit	Fixed value	10.4	MO0701PAIRONCO.000
Coeff_pH_lo_FeOx		Coefficient of pH term for fit of ionic strength threshold for FeOx colloid stability at low pH	Fixed value	−0.013	MO0701PAIRONCO.000
Coeff_Inter_pH_lo_FeOx		Intercept term for fit of ionic strength threshold for FeOx colloid stability at low pH	Fixed value	0.11	MO0701PAIRONCO.000
Coeff_pH_sq_hi_FeOx		Coefficient of pH squared term for fit of ionic strength threshold for FeOx colloid stability at high pH	Fixed value	0.0017	MO0701PAIRONCO.000
Coeff_pH_hi_FeOx		Coefficient of pH term for fit of ionic strength threshold for FeOx colloid stability at high pH	Fixed value	−0.0327	MO0701PAIRONCO.000
Coeff_inter_pH_hi_FeOx		Intercept term for fit of ionic strength threshold for FeOx colloid stability at high pH	Fixed value	0.158	MO0701PAIRONCO.000
Kd_U_Rev_Smectite_a	$K_{d,Ucoll,Smectite}$	Distribution coefficient for reversible sorption of uranium onto smectite colloids	Log uniform	See Table 6-15	MO0701PAKDSUNP.000
Kd_Np_Rev_Smectite_a	$K_{d,Npcoll,Smectite}$	Distribution coefficient for reversible sorption of neptunium onto smectite colloids	Log uniform	See Table 6-15	MO0701PAKDSUNP.000
Kd_Sn_Rev_Smectite_a	$K_{d,Sncoll,Smectite}$	Distribution coefficient for reversible sorption of tin onto smectite colloids	Log uniform	See Table 6-15	MO0701PAKDSUNP.000
Kd_Ra_Rev_Smectite_a	$K_{d,Racoll,Smectite}$	Distribution coefficient for reversible sorption of radium onto smectite colloids	Log uniform	See Table 6-15	MO0701PAKDSUNP.000
Kd_U_Rev_FeOx_Col_a	$K_{d,Ucoll,FeOx}$	Distribution coefficient for reversible sorption of uranium onto corrosion-generated (iron oxyhydroxide) colloids	Log uniform	See Table 6-15	MO0701PAKDSUNP.000
Kd_Np_Rev_FeOx_Col_a	$K_{d,Npcoll,FeOx}$	Distribution coefficient for reversible sorption of neptunium onto corrosion-generated (iron oxyhydroxide) colloids	Log uniform	See Table 6-15	MO0701PAKDSUNP.000
Kd_Sn_Rev_FeOx_Col_a	$K_{d,Sncoll,FeOx}$	Distribution coefficient for reversible sorption of tin onto corrosion-generated (iron oxyhydroxide) colloids	Log uniform	See Table 6-15	MO0701PAKDSUNP.000
Kd_Ra_Rev_FeOx_Col_a	$K_{d,Racoll,FeOx}$	Distribution coefficient for reversible sorption of radium onto corrosion-generated (iron oxyhydroxide) colloids	Log uniform	See Table 6-15	MO0701PAKDSUNP.000

Table 6-24. Parameters Used in Model (Continued)

New TSPA Name	Report Name	Description	Form	Parameter Values	Output DTN
CPu_Col_CSNF_Embed_Sampled	$C_{RNcoll,SNF,embed,sampled}$	Concentration of irreversibly attached radionuclide element RN (plutonium, americium) associated with SNF colloids	CDF	See Table 6-6b	MO0701PACSNFCP.000
CPu_Per_CSNF_Embed_Col_a	$C_{coll,SNF,uniform}$	Concentration of irreversibly attached plutonium per concentration of CSNF colloids	Uniform	5e-7 to 1e-6 Mol/L Pu per ppm colloid	MO0701PACSNFCP.000
CPu_Col_CSNF_Min	$C_{coll,SNF,min}$	Minimum observed or expected concentration of Pu on CSNF colloids	Fixed value	1×10^{-13} mol/L	MO0701PACSNFCP.000
CSNF_pH_lo		Lower limit of pH range for CSNF colloid stability data	Fixed value	4	MO0701PACSNFCP.000
CSNF_ZPC_lo		Lower limit of pH range for zero point of charge for CSNF colloid stability data	Fixed value	7	MO0701PACSNFCP.000
CSNF_ZPC_hi		Upper limit of pH range for zero point of charge for CSNF colloid stability data	Fixed value	9.3	MO0701PACSNFCP.000
CSNF_pH_hi		Upper limit of pH range for CSNF colloid stability data	Fixed value	10.6	MO0701PACSNFCP.000
Coeff_pH_Cube_lo_CSNF		Coefficient of pH cubed term for fit of ionic strength threshold for CSNF colloid stability at low pH	Fixed value	0.0089	MO0701PACSNFCP.000
Coeff_pH_Sq_lo_CSNF		Coefficient of pH squared term for fit of ionic strength threshold for CSNF colloid stability at low pH	Fixed value	−0.1466	MO0701PACSNFCP.000
Coeff_pH_lo_CSNF		Coefficient of pH term for fit of ionic strength threshold for CSNF colloid stability at low pH	Fixed value	0.7462	MO0701PACSNFCP.000
Coeff_inter_pH_lo_CSNF		Coefficient of intercept term for fit of ionic strength threshold for CSNF colloid stability at low pH	Fixed value	−1.092	MO0701PACSNFCP.000
Coeff_pH_Cube_hi_CSNF		Coefficient of pH cubed term for fit of ionic strength threshold for CSNF colloid stability at high pH	Fixed value	0.087362	MO0701PACSNFCP.000
Coeff_pH_Sq_hi_CSNF		Coefficient of pH squared term for fit of ionic strength threshold for CSNF colloid stability at high pH	Fixed value	−2.4078	MO0701PACSNFCP.000
Coeff_pH_hi_CSNF		Coefficient of pH term for fit of ionic strength threshold for CSNF colloid stability at high pH	Fixed value	22.126	MO0701PACSNFCP.000

Table 6-24. Parameters Used in Model (Continued)

New TSPA Name	Report Name	Description	Form	Parameter Values	Output DTN
Coeff_inter_pH_hi_CSNF		Coefficient of intercept term for fit of ionic strength threshold for CSNF colloid stability at high pH	Fixed value	−67.791	MO0701PACSNFCP.000
Conc_Col_U_Sampled	$M_{coll,uranophane,\ sampled}$	Expected mass of uranophane colloids per unit volume or mass of water	CDF	See Figure 6-8	MO0701PACSNFCP.000
Conc_Col_U_Min	$M_{coll,uranophane,\ min}$	Lowest observed or expected mass of uranophane colloids per unit volume or mass of water	Fixed value	1×10^{-6} mg/L	MO0701PACSNFCP.000
U_pH_lo		Lower limit of pH range for U colloid stability data	Fixed value	4	MO0701PACSNFCP.000
U_pH_hi		Upper limit of pH range for U colloid stability data	Fixed value	9	MO0701PACSNFCP.000
Coeff_pH_Sq_U		Coefficient of pH squared term for fit of ionic strength threshold for U colloid stability	Fixed value	−0.008	MO0701PACSNFCP.000
Coeff_pH_U		Coefficient of pH term for fit of ionic strength threshold for U colloid stability	Fixed value	0.14	MO0701PACSNFCP.000
Coeff_inter_U		Coefficient of intercept term for fit of ionic strength threshold for U colloid stability	Fixed value	0.4	MO0701PACSNFCP.000
Kd_Pu_Rev_U_a	$K_{d,Pucoll,uranophane}$	Distribution coefficient for reversible sorption of plutonium onto uranophane colloids	Log uniform	5×10^{0} to 1×10^{4} mL/g	MO0701PACSNFCP.000
Kd_Am_Rev_U_a	$K_{d,Amcoll,uranophane}$	Distribution coefficient for reversible sorption of americium onto uranophane colloids	Log uniform	5×10^{0} to 1×10^{4} mL/g	MO0701PACSNFCP.000
Kd_Th_Rev_U_a	$K_{d,Thcoll,uranophane}$	Distribution coefficient for reversible sorption of thorium onto uranophane colloids	Log uniform	5×10^{0} to 1×10^{4} mL/g	MO0701PACSNFCP.000
Kd_Pa_Rev_U_a	$K_{d,Pacoll,uranophane}$	Distribution coefficient for reversible sorption of Pa onto uranophane colloids	Log uniform	5×10^{0} to 1×10^{4} mL/g	MO0701PACSNFCP.000
Kd_Cs_Rev_U_a	$K_{d,Cscoll,uranophane}$	Distribution coefficient for reversible sorption of cesium onto uranophane colloids	Log uniform	1×10^{1} to 1×10^{3} mL/g	MO0701PACSNFCP.000
Kd_Np_Rev_U_a	$K_{d,Npcoll,uranophane}$	Distribution coefficient for reversible sorption of neptunium onto uranophane colloids	Log uniform	1×10^{1} to 5×10^{2} mL/g	MO0701PACSNFCP.000
Kd_Ra_Rev_U_a	$K_{d,Racoll,uranophane}$	Distribution coefficient for reversible sorption of radium onto uranophane colloids	Log uniform	1×10^{1} to 1×10^{3} mL/g	MO0701PACSNFCP.000
Kd_Sn_Rev_U_a	$K_{d,Sncoll,uranophane}$	Distribution coefficient for reversible sorption of tin onto uranophane colloids	Log uniform	1×10^{0} to 1×10^{2} mL/g	MO0701PACSNFCP.000

Table 6-24. Parameters Used in Model (Continued)

New TSPA Name	Report Name	Description	Form	Parameter Values	Output DTN
Specific_SA_U_Col	$S_{A,\ uranophane,\ coll}$	Specific Surface Area for uranophane	Fixed Value	30 m^2/g	MO0701PACSNFCP.000
U_Site_Density	$N_{S,uranophane,\ coll}$	Site density for uranophane particle colloid	Fixed value	2 sites/nm^2	MO0701PACSNFCP.000
Specific _SA_Smectite_Col_a	$S_{A,\ Smectite,\ coll}$	Specific surface area for DHLWG (smectite) colloid	Uniform	10 to 100 m^2/g	MO0701PAGLASWF.000
Smectite_Site_Density	$N_{S,\ Smectite,\ coll}$	Site density for DHLWG (smectite) colloid	Fixed value	2.3 sites/nm^2	MO0701PAGLASWF.000

NOTE: Competitive sorption model is being used for Pu, Am, Np, U, Pa, and Th sorption on iron oxides (see SNL 2007 [DIRS 177407]). Values for Cs, Ra, and Sn sorption onto iron oxides are included for completeness; however, these radionuclides cannot be modeled at present. Iron oxide surface area and site densities are not outputs from this model.

6.7 DESCRIPTION AND ANALYSES OF THE BARRIER CAPABILITY

As discussed in Section 1, the abstraction of the process models reported in this document is intended to capture the most important characteristics of radionuclide–colloid behavior for use in predicting the potential impact of colloid-facilitated radionuclide transport on repository performance. As modeled in TSPA, colloids may act to facilitate transport of radionuclides from the waste package to the surrounding EBS and beyond to the underlying UZ component of the natural barrier system of the repository.

6.8 EVALUATION OF ALTERNATIVE MODELS

The alternative models described in Section 6.4 provide an alternative method for including kinetic-based sorption that allows for slowly reversible processes, an alternative model for waste form colloid generation, and a method for introducing thin-film filtration. The latter two models were considered to be of less practical use within the existing model structure.

A kinetic-based sorption model similar to the one described in Section 6.4 has been included in *EBS Radionuclide Transport Abstraction* (SNL 2007 [DIRS 177407]).

INTENTIONALLY LEFT BLANK

7. VALIDATION

The waste form and in-drift colloids abstraction model is used to describe the possible consequences of colloid-facilitated radionuclide transport during postclosure. The types and characteristics (including stability and concentration) of colloids formed from the degradation of the waste forms as used in the abstraction is based on DLVO theory, observations of colloids from testing programs, and natural groundwaters.

Confidence-Building during Model Development to Establish Scientific Basis and Accuracy for Intended Use—Section 2.2.2 of the TWP (BSC 2006 DIRS 177389]) lists six steps for confidence building during model development. These are reproduced here with pointers to where in the document each is addressed.

> *Each model will contain documentation of decisions and activities implemented during model development to build confidence and verify a reasonable, corroborative, and credible technical approach using scientific and engineering principles was taken to:*
>
> *A. Evaluate and select input parameters or data, or both.*

The bases for selecting the input data used to determine and develop the colloid model are documented Section 4.1. The input data are obtained from controlled sources. When possible, site-specific data were used for establishing radionuclide concentrations, sorption properties, groundwater colloid concentrations, and waste package-derived colloid concentrations. This builds confidence that the developed model is appropriate for its intended use. The theoretical DLVO model was developed using literature values and is designed to be applicable for a range of conditions. Model assumptions have been described in Section 5. Detailed discussion about model concepts can be found in Section 6. Thus, this requirement is met.

> *B. Formulate defensible assumptions and simplifications.*

Discussion of assumptions and simplifications and their rationale is provided in Sections 5 and 6. The major simplification in the model concerns the use of well-defined colloid particles to describe a complex repository environment. The reasons for this and the justification are discussed in Section 6 and throughout the assumptions in Section 5. Thus, this requirement is met.

> *C. Ensure consistency with physical principles, such as conservation of mass, energy, and momentum.*

The colloid model is consistent with the physical behavior of colloids. The classical DLVO theory (van Olphen 1977 [DIRS 114428]) contends that colloid mobilization is activated by physical or chemical perturbations, which can change the forces between the colloid and surfaces. Colloid mobilization requires that the changes in solution chemistry or changes in the hydrodynamic shear forces produce repulsive forces between the attached colloids and the surface that exceed the attractive forces. However, large discrepancies will exist between predicted and observed detachment of particles under natural conditions, mainly because of the heterogeneous properties of the colloids and surfaces (both in chemical composition and geometries), nonuniform flow velocity, and chemical heterogeneity of the infiltrating solution.

The waste package is a heterogeneous system and has been simplified through the model to represent well defined colloid particles to represent the variety of particle types that would be expected in a complex repository environment; however, the application of the DLVO theory within the model provides a physically reasonable, bounding, and conservative case for colloid behavior in the waste package. Thus, this requirement is met.

D. Represent important future state (aleatoric), parameter, and alternative model uncertainties.

Uncertainties associated with the model analysis are discussed in Section 6.6. Alternative model uncertainties are discussed in Section 6.4. Thus, this requirement is met.

E. Ensure simulation conditions have been set up to span the range of intended use and avoid inconsistent outputs.

Waste form corrosion data were limited to only certain chemical conditions. In the case of DHLWG, this was due to the effect of the glass dissolution on the chemistry of the leachate. In other cases, including spent nuclear fuel experiments, tests were conducted in J-13 well water or other similar composition solutions. However, data on the characteristics of the types of model colloids (montmorillonite, hematite, ZrO_2, and meta-autunite) is presented in the model abstraction over a wide range of pH and ionic strength. As high ionic strength and extreme pH values will reduce sorption, the model is bounding by using sorption values obtained in J-13 well water. The sorption coefficients were measured using dilute radionuclide concentrations to avoid the confounding process of precipitation. When these coefficients are applied under conditions where solubility is high (extreme pH values) they may overestimate the amount of sorption. The colloid concentration model spans the expected ranges of ionic strength and pH. Thus, this requirement is met.

F. Ensure model predictions (performance parameters) adequately represent the range of possible outcomes consistent with important uncertainties.

Uncertainties associated with the model analysis are discussed in Section 6.6. Thus, this requirement is met. Thus, all six steps for confidence building during model development have been met.

Confidence-Building after Model Development to Support the Scientific Basis of the Model—Post-development model validation is required by procedure. For confidence building after model development, the TWP (BSC 2006 [DIRS 177389], Table 2-3) specifies this model as Level II, which requires two post-development validation activities for each model and specifies a validation criterion for data comparisons that states, "corroborating data must match qualitatively or must be bounded by model predictions."

The post-development validation has been accomplished through corroboration of model results with data acquired from the laboratory and analogue studies and through corroboration with information published in refereed journals. The following four general questions from *Technical Work Plan for Waste Form Testing and Modeling* (BSC 2006 DIRS 177389]) are used to validate the model via critical review (previously referred to as criteria VA5 via independent technical review in BSC 2006 [DIRS 177389]), which serves as the second post-development

method needed to establish the appropriate level of confidence in most (see below for exception for the uranyl colloids model) of the colloid source term models.

H. Do the models of corrosion product colloid stability and attachment of radionuclides adequately cover the range of possible behavior or bound the behavior of corrosion product colloids in facilitating radionuclide transport within the drift?

I. Do the models of waste form colloid stability and attachment of radionuclides adequately cover the range of possible behavior or bound the behavior of waste form colloids (DHLWG, CSNF and DSNF) in facilitating radionuclide transport within the drift?

J. Do the models of ground water colloid stability and attachment of radionuclides adequately cover the range of possible behavior or bound the behavior of groundwater colloids in facilitating radionuclide transport within the drift?

K. Are the models adequate and appropriate for intended use?

See Appendix IV for the additional details of the critical review, as well as to see the results of this post-development validation activity. For the uranyl colloids model (and submodels), this single post-development validation activity serves to provide appropriate confidence at validation level I (see below for discussion/justification).

Because a number of additional colloid models have been added to this work to more extensively cover the conceptual range of possible colloids for transport, there are some models for types of colloids that are relatively unimportant aspects of the colloid subsystem model, and as a result are not important to radionuclide transport. The uranyl colloid model (and submodels) is the primary example of this. As such, an exception is taken with the need for Validation Level II as specified in the TWP (BSC 2006 [DIRS 177389], Table 2-3). The rationale and justification for this exception for the uranyl colloid model (and submodels) is given below.

SCI-PRO-002 states:

> All models used to support the LA submittal, the determination of compliance, and the subsequent defense of the License Application shall be validated to at least Level I. No justification is required for assigning Level II validation to a given model because this level is the most stringent one. For those models that provide a direct input to the TSPA Model the use of a risk-informed technical basis is recommended, but not required, to support the decision of Level I validation for a given model. *However, written justification by the principal investigators (PIs) and respective technical group lead responsible for each model is required if Level I validation is assigned to a model. Note that a risk-informed technical basis may come from relevant and defensible sub-system or total system analyses. If sub-system analyses are used to establish the level of importance of a model, the relationship and importance of the subsystem analysis to the total system analysis shall be established.*

The rationale for Level I validation of the uranyl colloid model and its submodels is based on a risk-informed technical basis that is applied to specifically the uranyl colloid model (and its submodels) because they constitute a relatively unimportant aspect of the colloid subsystem model. The colloid subsystem model consists of multiple colloid models (with both reversible and irreversible/kinetic radionuclide attachment behavior) and provides an additional transportable form of radionuclides to the dissolved concentrations of those same radionuclides. The colloid subsystem model and the aqueous radionuclide transport subsystem model represent the radionuclide transport subsystem. Within the previous TSPA analyses, colloids have only ever been the dominant form of release for a small number of radionuclides (e.g., Pu) and only for a limited number of scenarios. As such, radionuclides that are relatively less effectively adsorbed/attached, and/or types of colloids that are relatively less abundant in the solutions/suspensions, will only play a minor to insignificant role in the radionuclide transport subsystem. Below is a discussion regarding the uranyl colloid model (and its submodels) that concludes that only Level I validation is needed because the model is a relatively unimportant contributor to the full set of colloid subsystem models, which itself is generally a minor contributor to the radionuclide transport subsystem.

Sections 6.3.2.5 through 6.3.2.7 describe the basis for the U(VI)-phase, reversible (i.e., uranyl) colloid model for commercial and defense spent nuclear fuels. The information in these sections indicates that the colloid particles could be uranyl hydrates (e.g., metaschoepite) or uranyl silicates (e.g., uranophane) depending on the composition of the aqueous system. Because the colloidal component (which also contained particles larger than colloidal size; Figure 6-15, note) represents only a small fraction (about 1% to 12%; Section 6.3.2.6) of the amount of uranium dissolved in the solution, it is a minor contributor to the overall transport of uranium. This would be even more the case if the uranyl colloids themselves dissolve as they transport. The radionuclides assessed for transport as reversibly attached to these uranyl colloids are Pu, Am, Th, Pa, Ra, Cs, Np, and Sn, and these are listed in Table 6-9 with the distributions of the sorption coefficients onto these colloids. The distributions are log uniform and Table 6-9 lists the minimum and maximum values of the distributions. In general, the rationale below relies on comparison of the maximum sorption coefficients for each radioelement onto uranyl colloids to the range of sorption coefficients for that radioelement onto other colloids, because the latter generally exceeds or equals the former and indicates that the uranyl colloids should be much less important relatively.

For Pu and Am, the maximum sorption coefficients for each of these radioelements onto uranyl colloids are 10^4 mL/g (Table 6-9). For Pu, sorption coefficients for hematite colloids range up to 7×10^5 mL/g (Table 6-14), and up to 10^5 and 10^6 mL/g for smectite and Fe-corrosion products, respectively (Table 6-15). For Am, sorption coefficients for montmorrillonite and hematite range up to 10^5 and 10^7 mL/g (Table 6-14), respectively, and up to 10^7 mL/g for both Fe-corrosion products and smectite (Table 6-15). Additionally, for Pu and Am, irreversible colloids are represented as ZrO_2 particles generated from CSNF with Pu and Am embedded within them. This treatment of Pu and Am as irreversibly attached will make these relatively more important for transport of these radionuclides. Therefore, uranyl colloids will be a relatively unimportant component for transport of Pu and Am within the colloid subsystem model, and therefore within the transport subsystem overall.

For Th, Pa, Np, and Sn, the comparison of sorption coefficient values onto Fe-corrosion products and smectite colloids (Table 6-15) provides the same indication as that for Pu and Am discussed above. That is, uranyl colloids will be a relatively unimportant component for transport of Th, Pa, Np, and Sn within the colloid subsystem model, and therefore within the radionuclide transport subsystem overall. The maximum value for Ra sorption coefficients onto Fe-corrosion products (for a log uniform distribution) exceeds its maximum sorption coefficient onto uranyl colloids by an order of magnitude, and therefore the same conclusion can be drawn. Although the relative contribution of uranyl colloids to Ra transport would be larger than for the other radioelements listed above, it will still be minor within the full set of colloid subsystem models, and therefore relatively unimportant within the transport subsystem overall.

For Cs, the basis for needing only Level I validation for the uranyl colloid model (and its submodels) is multifaceted. First, the uranyl colloid submodels for particle concentration and for sorption coefficients of Cs onto uranyl colloids are both directly taken from the smectite colloid model using arguments by analogy that the behavior would be approximately the same given uranyl colloids that are predominantly phases such as uranophone or Na-boltwoodite (Section 6.3.2.6). Therefore, the uranyl colloid submodels for Cs are identical to those for smectite colloid submodels for Cs, and it can therefore at most contribute similarly to the Cs transport. The smectite colloid submodels have had Level II validation applied; therefore, it is only the analogy being made that needs to be validated for the uranyl colloid submodels for Cs transport. In addition, the submodel for the surface area of the uranyl colloids (Section 6.3.2.7) indicates that they are assigned a value of 30 m^2/g versus the distribution for smectite colloid surface area that ranges up to 100 m^2/g (Section 6.3.2.3.1). Therefore, it is expected that, all other aspects being equal, uranyl colloids will be a minor contributor to colloidal Cs transport relative to the smectite colloids. Lastly, the sorption of Cs onto the zeolitic tuff is quite strong with sorption coefficients ranging to $\sim 4 \times 10^4$ mL/g (Table 6-16), such that for reversible sorption the tuff is expected to take Cs away from the uranyl colloids (and the smectite colloids as well) such that the uranyl colloids will be a relatively unimportant contributor to Cs transport within the full set of colloid subsystem models and within the radionuclide transport subsystem overall.

Given the above discussions, it is concluded that Level I validation for the uranyl colloid models (and submodels) is sufficient and justified.

As Section 6.3 of SCI-PRO-006 lists validation activities (VAs), this model report will refer to the TWP (BSC 2006 [DIRS 177389]) "activities" as those methods for addressing the "questions" to be answered to validate the model. The seven questions specified in the TWP (BSC 2006 [DIRS 177389]) are listed below, along with examples of the applicable types of post-development methods that can be applied. The TWP (BSC 2006 [DIRS 177389]) defines "VA 1" and "VA 3" in Table 2-1, and refers to them as examples for the questions in Table 2-3, where they are appropriate for meeting procedurally required post-development validation. These correspond to the first and third bulleted items within the current SCI-PRO-006 (Section 6.3.2). The statements from the TWP (BSC 2006 [DIRS 177389]) are repeated here for completeness.

In addition, there are two questions (B and G below) for which the TWP indicates "VA N/A." The TWP (BSC 2006 [DIRS 177389]) defines "VA N/A" in Table 2-1 as "Not required per

LP-SIII.10Q-BSC but … performed to increase confidence in important parameters and/or analyses." The activities performed to address these two questions (B and G as noted below) are not procedurally required post-development model validation activities; rather, they are additional efforts to provide enhanced confidence in parameter values or analyses results.

Validation Activity 1: (VA 1) Corroboration of model results with data acquired from the laboratory, field experiments, analog studies, or other relevant observations, not previously used to develop or calibrate the model.

Validation Activity 3: (VA 3) Corroboration with information published in refereed journals or literature.

The following questions from the TWP (BSC 2006 [DIRS 177389]) are to be answered through validation activities.

Validation of Mathematical Form of Model

Question A. *Is the use of the stability criterion based upon ionic strength and pH corroborated in the literature and is the dependence of colloid stability on pH and ionic strength consistent with Project and industry literature data (VA 1 and/or VA 3)?*

Question B. *(VA N/A) To increase confidence with colloid concentration parameters, is the use of colloid concentration derived from waste form degradation reasonable?*

NOTE: The activities performed to address this question B are not procedurally required post-development model validation activities; rather they are additional efforts to provide enhanced confidence in parameter values or analyses results.

Question C. *Is the reversible sorption of radionuclides corroborated by industry literature (VA 1 and/or VA 3)?*

Validation of Model Results for Colloid and Plutonium Concentrations

Question D. *Are the concentrations of colloids and plutonium consistent with scientific principles and corroborated by observed colloid concentrations in the Project- and peer-reviewed literature (VA 1 and/or VA 3)?*

Question E. *Are the commercial and DOE-owned SNF models approaches corroborated by commercial and DOE-owned SNF-specific test results and peer-reviewed literature on field observations near uranium deposits (VA 1 and/or VA 3)?*

Question F. *Are the ranges of corrosion product and groundwater colloid concentrations reasonable (VA 1 and/or VA 3)?*

Question G. *(VA N/A) Are the distribution coefficient parameters for sorption of radionuclides onto colloids (K_d values) corroborated by peer-reviewed literature and analytical modeling results?*

NOTE: The activities performed to address this question G are not procedurally required post-development model validation activities, rather they are additional efforts to provide enhanced confidence in parameter values or analyses results.

Corroborating or supporting data and information used to develop and validate the models (or optionally to provide additional confidence in parameter values or analyses results) are listed in Table 7-1. The table is divided into the major submodels: DLVO stability theory, waste form colloids, radionuclide sorption, and groundwater colloids. Within these major categories, the sections are further sub-divided. For each sub-category and validation question, two sources are named (i.e., (i) for the primary validation source and (ii) for the secondary validation source. In instances where this validation method has not be possible, a description of the reasons is provided in the text.

Table 7-1. Supporting (Corroborating) Information Used to Validate the Colloid Model and/or Provide Additional Confidence in Parameter Values and Analyses Results

TWP Question	Supporting (Corroborating) Information Source	Data/Information
DLVO Theory and Stability Model		
A (i)	Smectite: Tombácz et al. 1990 [DIRS 112690], Figure 3, p. 77; Sondi et al. 1996 [DIRS 170928], Figure 6, p. 518	Montmorillonite stability data as function of ionic strength and pH
	Iron Oxide: Liang and Morgan 1990 [DIRS 109524], Figure 1, p. 40	Experimental stability data for Iron oxide colloids
	U(VI) Phase: Mertz et al. 2000 [DIRS 162161]	Uranium (VI) phases
	CSNF Irreversible: Hsu et al. 1988 [DIRS 174350]	Characteristics of ZrO_2 (SNF) analogues
A (ii)	Smectite: Jara et al. 2005 [DIRS 180834], Figure 7, p. 168; Kraepiel et al. 1999 [DIRS 180997], Figure 5, p. 50	Surface charge of aluminosilicates, variation in zeta potential with pH
	Iron Oxide: Madden et al. 2006 [DIRS 180995]	Surface Charge on iron oxide colloids
	U(VI) Phase: Schindler et al. 2004 [DIRS 174507], Equations 11 and 12, p. 1642	Surface characteristics of U(VI) phases
Plutonium Colloid Concentrations Models from Borosilicate Waste Glasses and Spent Fuel		
B, D, E(i)	Glass: Ménard et al. 1998 [DIRS 171053]; Pirlet 2001 [DIRS 174351]; Vernaz and Gordon 1992 [DIRS 174503]; Fowler 2003 [DIRS 164361]	Corroborative information regarding the association of plutonium/americium with colloids during waste glass corrosion
	SNF: Mertz et al. 2003 [DIRS 162032], Figure 11, p. 41; Kaminski et al. 2005 [DIRS 179550], Section 3.3, pp. 82 and 83; Wronkiewicz et al. 1996 [DIRS 102047], Table 1, p. 80	Corroborative data supporting colloid concentrations with SNF and UO_2 corrosion
B, D, E (ii)	Glass: Luckscheiter and Kienzler 2001 [DIRS 180831], Figure 2, p. 157	Corroborative information regarding the association of plutonium/americium with colloids during waste glass corrosion
	SNF: Grambow et al. 1996 [DIRS 113253], Figure IV.8, p. 123	Corroborative data supporting colloid concentrations with SNF corrosion

Table 7-1. Supporting (Corroborating) Information Used to Validate the Colloid Model and/or Provide Additional Confidence in Parameter Values and Analyses Results (Continued)

TWP Question	Supporting (Corroborating) Information Source	Data/Information
Plutonium Colloid Concentrations Models from CSNF and DSNF Comparison with Uranium Deposits		
E (ii)	Murakami et al. 2005 [DIRS 175700], Figure 4, p. 122; McKinley et al. 2006 [DIRS 179552], Figure 6, p. 1881; Wang et al. 2006 [DIRS 179563], Figure 3, p. 168	Corroborative information and data regarding colloid-associated uranium concentrations in the vicinity of uranium deposits
E (ii)	Pearcy et al. 1995 [DIRS 110223]; van Middlesworth and Wood 1998 [DIRS 170927]	Validation through natural analogues and uranium deposits
Colloid Concentrations Models from Waste Package Materials		
F(i)	Dietz 2005 [DIRS 179542], Section 2.3, pp. 22 to 24	Corrosion of stainless steel under hydrothermal conditions
F(ii)	Ziemniak and Hanson 2001 [DIRS 179566], Abstract, p. 3; Smailos et al. 2003 [DIRS 179559], Table 11, p. 32; Section 2.2, p. 11	Corrosion of stainless steel
Groundwater Colloid Concentrations Model		
F (i)	Nuttall 1986 [DIRS 121867]; Kingston and Whitbeck 1991 [DIRS 113930]; Novikov et al. 2006 [DIRS 179554], Table 1, p. 639	Colloid concentrations in groundwater
F (ii)	DTN: LA0002SK831352.003 [DIRS 161771]; DTN: LA0002SK831352.004 [DIRS 161579]; Widerlund et al. 2004 [DIRS 180833], Figure 4, p. 1544	Corroborative data for groundwater colloids concentrations
Reversible Sorption Model		
C (i)	EPA 1999 [DIRS 147475], Vol. 2, Appendices D, G, I, and J; EPA 2004 [DIRS 172215]; Serne and Relyea (1982 [DIRS 147681]; Beckman et al. (1988 [DIRS 144956])	Data for reversible sorption and modeling results for partitioning of radionuclides between colloids and stationary phases
C (ii)	Honeyman and Ranville 2002 [DIRS 161657]; Stenhouse 1995 [DIRS 147477]; Atun et al. 1996 [DIRS 164865]	Data for reversible sorption and modeling results for partitioning of radionuclides between colloids and stationary phases
Radionuclide Sorption Parameters		
G (i)	EPA 1999 [DIRS 147475], Vol. 2, Appendices D, G, I, and J; EPA 2004 [DIRS 172215]; Serne and Relyea 1982 [DIRS 147681]; Beckman et al. 1988 [DIRS 144956]	Distribution coefficients (K_d values) for radionuclides onto colloids; modeling results for partitioning of radionuclides between colloids and stationary phases
	Powell et al. 2004 [DIRS 180836], Table 2, p. 6020; Powell et al. 2005 [DIRS 174726], Table 1, p. 2110, and Table 2, p. 2112.	Rate of Pu uptake onto iron oxides
G (ii)	Honeyman and Ranville 2002 [DIRS 161657]; Stenhouse 1995 [DIRS 147477]; Atun et al. 1996 [DIRS 164865]	Distribution coefficients (K_d values) for radionuclides onto colloids; modeling results for partitioning of radionuclides between colloids and stationary phases

NOTES: Two sets of post-development model validation sources have been included for each question, as well as for questions B and G, that provide additional confidence for parameter values or analyses results. These are labeled as (i) and (ii).

The study by Tombácz et al. (1990 [DIRS 112690]) was used as a direct source for determination of the surface charge with pH and the Hamaker constant. However, in this section, other experimental data on the stability of montmorillonite from Tombácz et al. (1990 [DIRS 112690]) are being used to validate the DLVO stability model.

7.1 VALIDATION OF MODEL

The colloid model consists of: (a) a stability model/criterion based upon DLVO theory with inputs from ionic strength and pH, (b) concentration models of plutonium and americium within the DHLWG and CSNF degradation colloids, (c) rate parameters of radionuclide sorption onto iron oxide colloids, and (d) parameters for reversible sorption onto selected colloids. Each of the model components has required post-development validation in this section, and sorption parameters have some additional confidence developed via optional post-development activities.

7.1.1 Validation of Mathematical Form of Model

The mathematical form of the colloid model consists of a stability criterion based upon DLVO theory with inputs from ionic strength and pH. These model components are validated below.

Question A. *Is the use of the stability criterion based upon ionic strength and pH corroborated in the literature and is the dependence of colloid stability on pH and ionic strength consistent with Project and industry literature data (VA 1 and/or VA 3)?*

The first degree validation of the DLVO approach has been accomplished by corroborating experimental data from Tombácz et al. (1990 [DIRS 112690]) (see Figure 6-9) and Liang and Morgan (1990 [DIRS 109524]) (see Figure 6-5) with predicted mathematical stability model for smectite clay and iron oxide, respectively. The DLVO theory as applied in this model represents an appropriate method for describing colloid stability. The theoretical method was applied to determine the stability of colloids with changes in pH and ionic strength, allowing the model to be applied to conditions not described in experiments. However, there are parameters used in the calculation which remain uncertain: for instance, the Hamaker constant and the distribution of particle sizes. Furthermore, the pH_{pzc} for the types of colloids considered in the model may vary depending on particle morphology, phase, and the occurrence of other species in solution. For instance, the pH_{pzc} values for iron oxides can range from 6.8 to 9.3 depending on the phase (Table 7-2).

Jara et al. (2005 [DIRS 180834]) provide second degree validation of the smectite stability model. They have shown that synthetic amorphous aluminosilicates, typical of the phases that initially form following natural glass or borosilicate glass weathering, have a pzc between pH 3.9 and 4.4. This is significantly higher than that observed for well-crystallized montmorillonite. Furthermore, between pH 5 and pH 7, only a moderate negative charge was observed, which would suggest that these particles would be unstable. The current model is bounded by the behavior of the system investigated by Jara et al. (2005 [DIRS 180834]). Hence, the smectite model has been validated by two corroborative methods.

The second method for validating the iron oxide colloid stability model was with data from Madden et al. (2006 [DIRS 180995], Figure 5, p. 4099). The zeta potential versus pH plot corroborates qualitatively with data from Gunnarsson et al. (2001 [DIRS 179547]). Madden et al. (2006 DIRS 180995]) used 7-nm and 25-nm hematite particles. The smaller particles had the highest overall surface potential below the pzc. The values and ranges compared favorably with the ones used in model development.

Data from Mertz et al. (2000 [DIRS 162161]) was used to validate the zeta potential data from Zheng et al. (2006 [DIRS 179565]) that was used to develop the reversible U(VI) phases. As the zeta potential curve to pH reported by Mertz et al. (2000 [DIRS 162161]) was qualitatively similar to results from Zheng et al. (2006 [DIRS 179565]), the U(VI) colloid phase stability model has been corroborated. An additional source for validation is available from Schindler et al. (2004 [DIRS 174507], Equations 11 and 12, p. 1642), where calculated surface potential models agree qualitatively with the data used to establish the U(VI) colloid phase submodel.

Hsu et al. (1988 [DIRS 174350], Figure 7, p. 36) published electro-mobility data for various forms of cerium oxide. Cerium oxide is another reasonable analogue for the Pu-Zr colloid phase from corroded CSNF under consideration in this model. These agree qualitatively with the values published by Bitea et al. (2003 [DIRS 174504], Figure 3, p. 59) for the ζ-potential of ZrO_2 colloids that were used to develop the irreversible CSNF ("ZrO_2") model. The pzc for ZrO_2 was at pH 8.4, and for CeO_2 between 5.5 and 6.5, depending on particle shape. By selecting ZrO_2 as the modeled colloid, that model is conservative as the particles are relatively stable below pH 8, whereas, if CeO_2 had been selected, the particles would have been described as unstable for most of the pH range of interest to the waste package and in-drift environment. Hence, this sub-component of the model has been validated.

The DLVO theory can be used to predict the behavior of colloids in simple electrolyte solutions. The model treats the coulombic interaction between like-charged colloids in an aqueous solution as only repulsive, and treats the attractive forces as governed solely by van der Waals forces. However, van der Waals attractive forces can only exceed thermal energies (k_BT) when the particles are separated by only a few nanometers. At very small separations (~3 nm), repulsive hydration forces dominate, which means that DLVO cannot predict the behavior of aggregated colloids. In addition, DLVO does not explain long range attractive forces, as the van der Waals forces are negligible at long distances. Another criticism of the DLVO theory is that it only considers two particles, and so may only be appropriate under very dilute conditions. Hence, the application of DLVO theory to explain colloidal interactions in the Hanford waste tanks, for instance, would be inappropriate; however, the application of DLVO to the repository environment is reasonable, because ionic strengths are anticipated to be low and predicted colloid concentrations are expected to be low. It is for these reasons that the current model cannot readily explain the presence of suspended aggregates of particles in the experiments performed by Zarrabi et al. (2003 [DIRS 171238]), because these experiments represent conditions that are not expected to occur in the waste package and in-drift environment (i.e., highly saline conditions).

There is uncertainty in the Hamaker constant and in the particle size distribution; hence, to provide a bounding model for particle stability, a stability ratio criteria of $W = 10$ was selected. This is discussed in greater detail below.

Table 7-2. pH_{pzc} of Iron Oxides

Mineral	pH
α-Fe_2O_3 (hematite)	8.5
α-FeOOH (goethite)	7.3
α-Fe_3O_4 (magnetite)	6.6

Source: Davis and Kent [DIRS 143280], Table 4, p. 210.

Selection of Colloid Stability Threshold ($W = 10$)

In the stability model, a stability ratio boundary was determined to divide the pH vs. ionic strength plane into regions where the colloid should be considered stable or unstable with respect to aggregation and gravity settling. Colloid aggregation kinetics can be approximated by considering only binary collisions represented by a second-order rate equation:

$$\frac{dn}{dt} = -k_f\, n^2 \qquad \text{(Eq. 7-1)}$$

where n is the colloid number density and $k_f = k_{smol}/W$. The Smoluchowski rate constant, k_{smol}, is set to 6.16×10^{-18} m^3s^{-1} at room temperature.[2] The solution of Equation 7-1 shows that larger values of W effectively inhibit aggregation and increase the stability half-life. The characteristic stability time is then seen to be proportional to the stability ratio and inversely proportional to the initial concentration. Therefore, given a fixed initial concentration, the value of the stability ratio W is selected to best represent the stability boundary. Because the probability of collision is inhibited exponentially by electrostatic repulsion, it is possible to determine a region in the pH vs. ionic strength plane where W begins to change very rapidly (see for example Figure 6-39 for hematite). It is in this region where colloid stability transitions from rapid aggregation (a few seconds) to very stable over geological time. A value of $W = 10$ was selected for the stability boundary; this region for $W < 10$ will be unstable to aggregation. While it is true that all $W > 10$ cannot be considered stable over geological time, the rapid variation in W makes $W = 10$ a satisfactory boundary for specifying where the rapid variation to a very stable condition will occur.

The $W = 10$ boundary is not only a satisfactory one, but utilizing this value is conservative and captures the potential uncertainties in the particle size and Hamaker constant.

Conclusion: The application of stability ratios to describe colloid behavior is a standard scientific practice within the literature as discussed in Sections 6.3.2. The dependence of colloid suspension stability upon pH and ionic strength is reasonably consistent with YMP data and literature data. Therefore, this component is validated through corroboration with literature and YMP data (VA 1 and 3).

[2] $k_{smol} = 4k_BT/3\eta$, where viscosity, η, is ~0.0009 Pa-s for water, k_B is the Boltzmann constant, T is the temperature in Kelvin. Therefore, $4k_BT/3\eta = 1.33 \times 1.38 \times 10^{-23} / 0.0009 = 6.16 \times 10^{-18}$ m^3s^{-1} (Lide et al. 1991 [DIRS 131202]).

Question B. (VA N/A) To increase confidence with colloid concentration parameters, is the use of colloid concentration derived from waste form degradation reasonable?

NOTE: The activities performed to address this question are not procedurally required post-development model validation activities, rather they are additional efforts to provide enhanced confidence in parameter values or analyses results.

The model provides parameters to account for colloids derived from waste form degradation. Immersion corrosion tests on crushed or powdered waste forms are run to allow observation of changes within experimental time frames that under disposal conditions will be many orders of magnitude slower. In more repository-relevant tests that contained a mixture of materials (e.g., stainless steel holders) and low flow rates, filtration or reduced water contact can lower colloid formation. There is also a difference between the theoretical colloidal size range and the achievable experimentally measured colloid range and population. It is important to consider the testing conditions and analysis techniques when evaluating colloid formation from waste form corrosion tests. The use of product consistency test data for DHLWG-derived colloids is conservative because these can produce copious amounts of colloids; therefore, this conservatism was eliminated by obtaining plutonium-associated colloid concentrations from monolith immersion tests. Likewise, in the case of CSNF, plutonium concentrations were obtained from fragment immersion tests. The use of parameters for this purpose is reasonable and does not require validation. The validation of the model output is contained in Sections 7.1.2 and 7.1.3.

Question C. Is the reversible sorption of radionuclides corroborated by industry literature (VA 1 and/or VA 3)?

Conclusion—K_d values are frequently used with the assumption that adsorption and desorption reactions are reversible. This assumption is contrary to most experimental observations that show that the desorption process is appreciably slower than the adsorption process, a phenomenon referred to as hysteresis. Good examples of this hysteresis would be the observation of plutonium transport at the NTS (Kersting et al. 1999 [DIRS 103282]) and at the Mayak facility (Novikov et al. 2006 [DIRS 179554]). The rate of desorption may even go to zero, yet a significant mass of the contaminant remains sorbed on the transported particles. Thus, use of K_d values determined from batch adsorption tests in contaminant transport models is generally considered to provide estimates of contaminant remobilization (release) from the solid phase that are too large (i.e., estimates of contaminant retention that are too low).

In many instances, an R_d is quoted to account for the fact that experimental systems have not attained equilibrium. However, for modeling purposes, reported R_d values have been used as K_d values in several instances. Therefore, this component is validated through corroboration with literature (i.e., VA 3; see also Table 7-1 above). Additionally, see Appendix IV for the Critical Review of the colloid models, including this aspect. The appropriateness of the distribution coefficient parameters is discussed in Section 7.1.5.

7.1.2 Validation of Model Results for Colloid and Plutonium Concentrations

Question D: Are the concentrations of colloids and plutonium consistent with scientific principles and corroborated by observed colloid concentrations in the Project and peer-reviewed literature? (VA 1 and 3)

DHLWG-Derived Colloids

The DHLWG test data set used in the model can be validated by comparison with published data generated from other testing programs using similar alkali borosilicate glass. Corrosion tests on the plutonium-, americium-, and thorium-doped alkali-borosilicate waste glasses (Ménard et al. 1998 [DIRS 171053]; Pirlet 2001 [DIRS 174351]; Vernaz and Gordon 1992 [DIRS 174503]) suggest that plutonium was strongly bonded to all colloidal particles in the leachate. Furthermore, 70% to 100% of lanthanides and thorium were associated with colloids (on 0.45-μm and 1.8-nm filters), while uranium and neptunium retention varies from 40% in a 5×10^{-3} carbonate medium to 95% in a 5×10^{-3} M phosphate solution. The R7T7 glasses were doped with different quantities of actinides for testing (Ménard et al. 1998 [DIRS 171053]). The actinide level in the alpha-doped glasses was 0.85% and is much higher than those used in the SRL glass static tests (Bates et al. 1995 [DIRS 170880]) or anticipated in current U.S. high-level waste production glasses and the R7T7 French production waste glasses (Table 7-3; Advocat et al. 2001 [DIRS 163198]). DHLWG with LaBS plutonium-bearing glass will result in a higher total plutonium content for the borosilicate glasses that will be closer to that used in corrosion tests reported by Pirlet (2001 [DIRS 174351]) and Ménard et al. (1998 [DIRS 171053]). Nevertheless, small quantities of phosphate in the glass can have a profound effect on the behavior of actinides during glass weathering.

Tests reported by Pirlet (2001 [DIRS 174351]) on ^{239}Pu-doped R7T7 glass are comparable to the static tests on SRL glasses used in model development and exhibited similar long-term behavior. However, the tests were performed with a glass surface area-to-leachate volume (S_A/V) of 50/m, which may result in less overall reaction. The actinides were initially released congruently with other glass matrix elements; however, as the corrosion progressed, an amorphous "gel" layer formed on the glass surface and retained most of the actinides despite further glass reaction. Over 80% of the plutonium and 99% of the americium were found as particulates rather than solution species. Actinide retention factors were found to increase with increasing temperature, which would be consistent with decreasing plutonium-colloid stability with temperature.

In spite of the large plutonium loading, Ménard et al. (1998 [DIRS 171053]) were unable to provide supporting evidence for precipitated actinides associated with phyllosilicate (montmorillonite) colloids because examination of microscopic characterization of the leachates was limited in scope. Plutonium concentrations in static leach tests conducted for one year in distilled water with an S_A/V of 50/m resulted in peak plutonium concentrations of 1.5×10^{-7} M with ^{239}Pu-doped R7T7 glasses (Pirlet 2001 [DIRS 174351]) (see Figure 7-1); however, results from the ^{238}Pu-doped glass tests did not appear to reach a saturation level after one year of reaction. The ^{238}Pu glass reaction is dominated by the radiolytic field and is not relevant to long-term DHLWG disposal.

Table 7-3. Actinide Levels in Borosilicate Glasses Used for Testing

Oxide (wt %)	R7T7 α-Doped[a]	SRL-202A[b]	SRL-131A[b]	R7T7 Production[c]	DWPF Production[d]
PuO_2	0.85	1.3×10^{-2}	1.2×10^{-2}	~0.74	2.2×10^{-4} to 5.8×10^{-2}
ThO_2	0	0.28	0.01	N/A	0.011 to 0.55
AmO_2	0.85	4.4×10^{-4}	4.5×10^{-4}	N/A	N/A
NpO_2	0.85	1.4×10^{-2}	1.3×10^{-2}	N/A	N/A
UO_2	0	2.0	3.0	0.12	1.01 to 2.88

[a] Ménard et al. 1998 [DIRS 171053], Table 1; Vernaz and Gordon 1992 [DIRS 174503], p. 39, Table 1.
[b] Bates et al. 1995 [DIRS 170880], Table 1b.
[c] Advocat et al. 2001 [DIRS 163198], Table 1 and Table 2. The PuO_2 value (A) was calculated from the total Pu activity of 1.54×10^5 Bq/g (B) by scaling to 0.2 wt % Pu oxide (C) equivalent to 4.17×10^6 Bq/g (D). That is, A = (C/D) × B.
[d] Fowler 2003 [DIRS 164361], Table 3, p. 12.

NOTE: N/A = not available. The levels of plutonium, uranium, and thorium anticipated to be present in HLW production glasses is similar to that used in glass corrosion tests used in the model development.

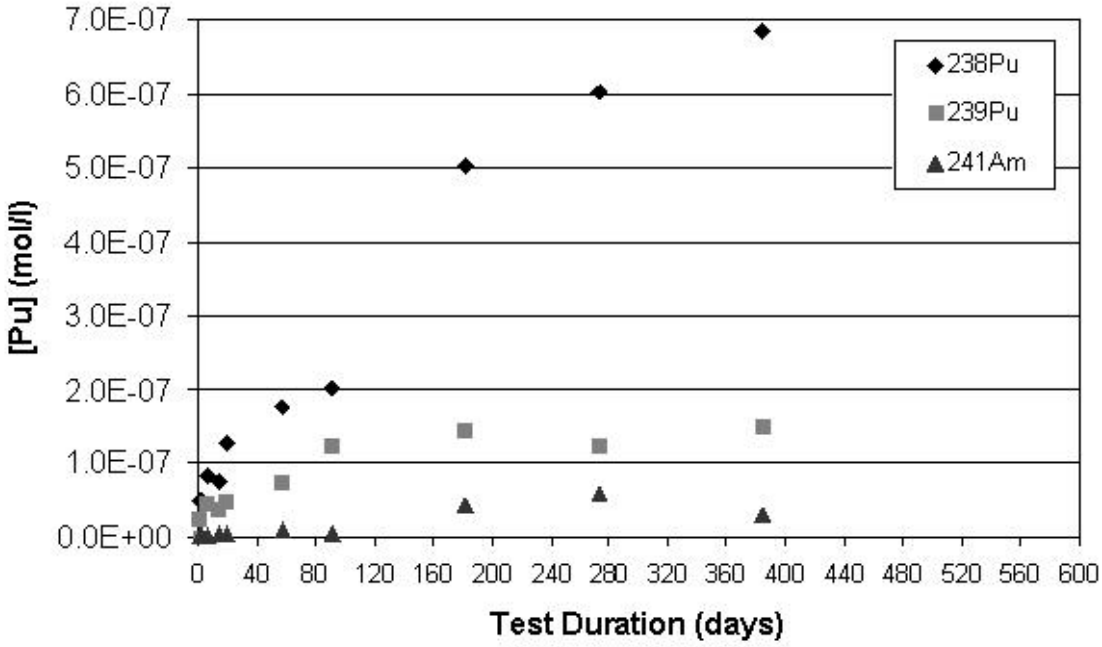

Source: Pirlet et al. 2001 [DIRS 174351], p. 48, Figure 1; Vernaz and Gordon 1992 [DIRS 174503], p. 43, Table 3.

Figure 7-1. Total Plutonium and Americium Concentration from Static Tests on Actinide-Doped R7T7 Borosilicate Glass Conducted at 90°C with an S_A/V of 50/m

Spent Nuclear Fuel-Derived Colloids

Direct comparison of plutonium colloid data from SNF tests by Grambow et al. (1996 [DIRS 113253]), Wilson (1990 [DIRS 100793]), McNamara et al. (2005 [DIRS 174068]), and Mertz et al. (2003 [DIRS 162032]) is difficult because of experimental differences. Values reported by Grambow et al. (1996 [DIRS 113253]) for plutonium colloids ranged from 5×10^{-12} mol/L to 1×10^{-7} mol/L between pH values 6 and 8.5 for SNF tests. These values are similar to those reported by Wilson (1990 [DIRS 100793]) for tests with cladding and by Mertz et al. (2003 [DIRS 162032]) for intermittent drip tests. It is possible that the intermittent drip tests under-reported the levels of actinide colloids because of filtration by the Zircaloy holder; however, in immersion tests by Wilson (1990 [DIRS 100793]), the presence of any Zircaloy cladding (including defected cladding) reduced the observed plutonium concentrations by three to four orders of magnitude. A change in the design of the holder for the intermittent drip tests on SNF (Mertz et al. 2003 [DIRS 162032]) increased the release of plutonium. However, in all tests it is also possible that the spent fuel dissolution process slowed down. In summary, the data from Grambow et al. (1996 [DIRS 113253]) and Mertz et al. (2003 [DIRS 162032]) bound the data reported by Wilson (1990 [DIRS 100793]) and used in the model development.

Data on a mixed UO_{2+x} and meta-schoepite test was used to estimate a stability ratio (W) as Mertz et al. (2005 [DIRS 162032]) reported a decrease in particle concentrations with time. Using Equations 6-4 and 6-5 in Section 6.3.2, it is possible to derive the stability ratio. The value calculated indicated that the colloids were stable. In a silica-bearing water, these particles would not be the solubility controlling phase for uranium; however, uranium silicate phases might remain stable.

Conclusion—The concentration of plutonium associated with DHLWG colloids may depend on the initial concentration of plutonium in the glass. The concentration of plutonium colloids from ^{239}Pu-doped R7T7, SRL131A, and SRL-202A tests did not exceed 5×10^{-7} M. Application of a distribution has provided a more reasonable estimate of colloid concentrations generated from DHLWG. The concentration of plutonium colloids from SNF was obtained from a distribution of results. The results from both waste forms may be conservative, as in the presence of Zircaloy materials or iron materials colloid concentration can be lower.

7.1.3 Validation of CSNF and DSNF Model Results

Question E: Are the commercial and DOE-owned SNF model approaches corroborated by commercial and DOE-owned SNF-specific test results and peer-reviewed literature on field observations near uranium deposits? (VA 3)

Wronkiewicz et al. (1996 [DIRS 102047]) observed suspended particles of uranophane ($Ca(UO_2)_2(SiO_3OH)_2 \cdot 5H_2O$) and uraninite ($UO_2$) within the leachates of drip tests on unirradiated UO_2; however, similar uranophane suspended particles were not observed on the two high drip-rate tests on SNF (Mertz et al. 2003 [DIRS 162032]). This may have been due to the design differences between these intermittent flow tests, which resulted in holdup of particles on the Zircaloy holder used in the SNF intermittent drip tests.

Unsaturated drip tests on spent nuclear fuels ATM-103 and ATM-106 were performed for over eight years (see Figure 7-2). Fuel fragments were contained in a Zircaloy holder (Zircaloy-4). The holder consists of a Zircaloy tube sitting atop a Zircaloy retainer with fifty 7-µm-diameter holes. The Zircaloy retainers in the high-drip tests on ATM-103 and ATM-106 were replaced with new Zircaloy retainers (with 10-µm-diameter holes) at the end of the 7.3-year sampling interval; and these were subsequently replaced by gold retainers with 200-µm-diameter mesh size at the end of the 7.7-year sampling interval. Fuel holders and fuel fragments were set on a ledge inside each Stainless Steel Type 304L reaction vessel. At the start of each testing interval, about 5 mL of equilibrated J-13 water was placed inside each vessel. Each reaction vessel was sealed with a copper gasket and placed into a 90°C oven. Each reaction vessel was injected with equilibrated J-13 well water. The average concentration of uranium in equilibrated J-13 well water entering the unsaturated drip test system was 6.7×10^{-9} mol/L (Thomas 2003 [DIRS 163048], Table 2, p. 18). The release characteristics of selected actinides from the ATM-103 and ATM-106 "drip" tests is shown in Figure 7-2.

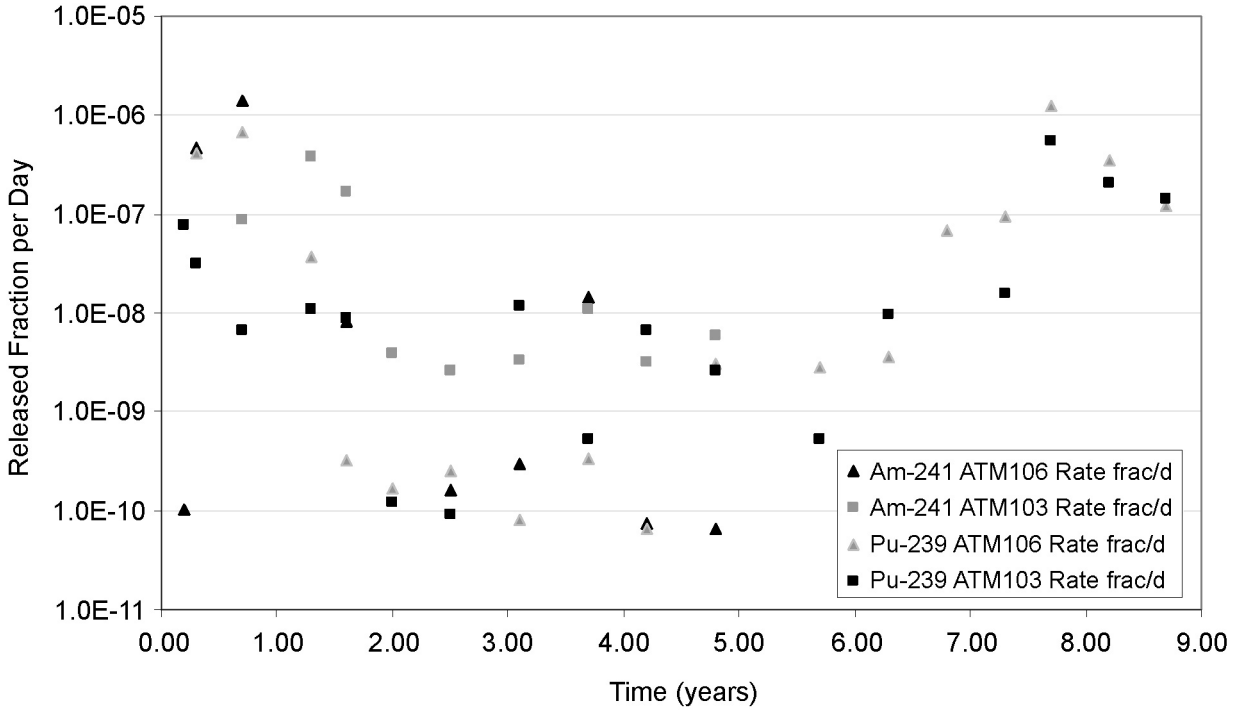

Source: Developed from: CRWMS M&O 2000 [DIRS 131861], Table 4 (ATM-103 HDR) and Table 5 (ATM-106 HDR), between 0 and 4.8 years of reaction; Thomas 2003 [DIRS 163048], Table 18 (ATM-103 and ATM-106 HDR), between 5.7 and 8.7 years of reaction.

NOTES: The Zircaloy holder was replaced at 7.3 years and replaced with a gold mesh at 7.7 years. In the ATM-103 HDR test, 33% of the expected volume was recovered in the 5.2-year sample and the vessel was run dry at 6.8 years (Mertz et al. 2003 [DIRS 162032]). In the ATM-106 HDR tests, water loss occurred for the 5.2-year and 6.8-year samples, with 33% and 10% of the expected water volume recovered (Mertz et al. 2003 [DIRS 162032]). Values represent the total concentration measured. The reasons for the increased release at later times may be related to the change in experimental design after 6.3 years.

Figure 7-2. Released Fraction per Day of ^{239}Pu and ^{241}Am as a Function of Test Duration for the CSNF High Drip-Rate Tests

The Zircaloy retainer (with 50 drilled holes 7 μm in diameter) was replaced twice, once at 7.3 years with a similar type of material and then at ~7.7 years with a gold mesh, which had a much larger open area. This may have had two effects: (a) reduce the total contact time of the water with the fuel and (b) allow larger particles to fall through. Evidence from examination of the retainers indicates that they are coated with particles of corroded fuel and alteration products (Finn et al. 1998 [DIRS 100392]). Therefore, the retainer may have filtered out many particles that would have otherwise reached the collection vessel. In 5.2-year and 6.8-year samplings, the testing system had lost water, which may have reduced the release of colloidal particles (Mertz et al. 2003 [DIRS 162032]). The results from the unsaturated drip test appear to validate the model with very low concentrations of colloids. However, there are unknown factors in these experiments which make it difficult to draw direct relationships.

DSNF constitutes <3% of the total repository waste inventory and the N-Reactor fuel comprises approximately 85% of the DSNF inventory (DOE 2002 [DIRS 158405]) and is the surrogate for DSNF in the TSPA-LA model. Uranium metal is unstable in water and will rapidly oxidize depending on the temperature. Kaminski et al. (2005 [DIRS 179550]) have examined colloid formation from corroded N-reactor metal in the presence of J-13 groundwater. They observed the formation of uranium silicates and clay phases in the leachate. These results are similar to that observed during the corrosion of CSNF. Hence, the use of uranophane colloids to represent the major particle type produced from the corrosion of DSNF is reasonable.

Studies by van Middlesworth and Wood (1998 [DIRS 170927]) at the Cretaceous Idaho batholith represent possibly the most intriguing natural analogue site for colloids derived from waste forms. At this deposit, hydrothermal alteration of the Casto granite containing allanite {(Ca, Mn, Ce, La, Y)$_2$($Fe^{2+}Fe^{3+}$,Al)$_3$O·OH(Si_2O_7)(SiO_4)} to phosphate phases, such as monazite {(La, Ce)PO_4} and rhabdophane {(La,Ce)PO_4·2H_2O}, is almost directly analogous to the laboratory weathering experiments with alkali borosilicate glasses (Buck and Bates 1999 [DIRS 109494]; DTN: MO0407ANLGNN02.608 [DIRS 171277]). This qualitative evidence corroborates the approach adopted in the model for considering the behavior of Pu and Am in weather waste forms. Many of these rare earth-containing phosphate minerals have been found to be associated with silicates, including clays (Taunton et al. 2000 [DIRS 170891]; van Middlesworth and Wood 1998 [DIRS 170927]). The analysis of filtered and unfiltered samples from the Idaho batholith groundwater indicated that a majority of the rare earths and thorium was associated with colloids, while most of the uranium was soluble (Table 7-4). An important aspect of the study by van Middlesworth and Wood (1998 [DIRS 170927]) was the application of ferric hydroxide coprecipitation for the quantitative analysis of trace levels of uranium, thorium, and rare earths in their solutions, which supports the contention that attenuation of actinides in the waste package will occur by reaction with iron corrosion products.

Table 7-4. Colloid Data on Rare Earths and Actinides from Locations in the Cretaceous Idaho Batholith

	Total (Rare Earths) (mol/L)	Thorium (mol/L)	Uranium (mol/L)
Weir Creek			
Unfiltered	3.9×10^{-9}	1.4×10^{-10}	4.2×10^{-11}
Filtered	1.1×10^{-9}	$<4 \times 10^{-11}$	1.4×10^{-8}
Horse Creek			
Unfiltered	8.2×10^{-9}	9.2×10^{-10}	8.4×10^{-9}
Filtered	3.3×10^{-9}	2.0×10^{-10}	8.0×10^{-9}
Big Creek			
Unfiltered	1.0×10^{-8}	6.3×10^{-10}	2.1×10^{-10}
Filtered	5.6×10^{-9}	2.7×10^{-10}	1.4×10^{-10}
Sharkey			
Unfiltered	1.5×10^{-8}	5.5×10^{-10}	7.6×10^{-11}
Filtered	1.1×10^{-9}	$<4 \times 10^{-11}$	6.3×10^{-11}

Source: van Middlesworth and Wood 1998 [DIRS 170927] (units converted from Table 2, p. 870).

Various colloidal phases (e.g., rare earth element-bearing phases) were detected in CSNF tests leachates at early times (Finn et al. 1994 [DIRS 100746]); but, at later times, colloids were not observed and colloid release may have stopped, possibly due to experimental conditions (see discussion Section 6.3.4). Microscopy evidence for U(VI) colloids has been reported by Buck et al. (2004 [DIRS 171479]), Kaminski et al. (2005 [DIRS 179550]), Wronkiewicz et al. (1996 [DIRS 102047]), and Finn et al. (1994 [DIRS 100746]). Evidence for CSNF and CSNF-analogue particles has been reported by Finn et al. (1994 [DIRS 100746]), Wang et al. (2006 [DIRS 179563]), and Bitea et al. (2003 [DIRS 173041]). These data sources corroborate the model for considering the occurrence of colloids from CSNF and DSNF corrosion.

Evidence from natural analogue sites does not indicate long-range transport of U(VI) phases, although the formation of nano-precipitates of U(VI) is observed. Nanocrystals of U(VI) phosphates have been reported by Murakami et al. (1997 [DIRS 113272]) in Koongarra groundwaters that were under-saturated with respect to saléeite $\{Mg[(UO_2)(PO_4)]_2(H_2O)_{10}\}$ and meta-torbernite $\{Cu[(UO_2)(PO_4)]_2(H_2O)_8\}$. At the Hanford site, McKinley et al. (2006 [DIRS 179552]) have shown that U(VI) precipitates (uranophane) formed from the reaction of uranyl ion bearing contaminant solutions and the Hanford sediments. However, there is no clear evidence for the migration of these colloidal-sized U(VI) phases. Uranophane is the predominant long-term phase in the uranium deposit at Nopal site, Peña Blanca, a close natural analogue of the Yucca Mountain repository environment (Wronkiewicz et al. 1996 [DIRS 102047]). These observations suggest that the model is conservative in allowing the formation of stable uranophane colloids. In Figure 7-3, several examples of uranium nano-particles and analogues of potential CSNF colloids are shown.

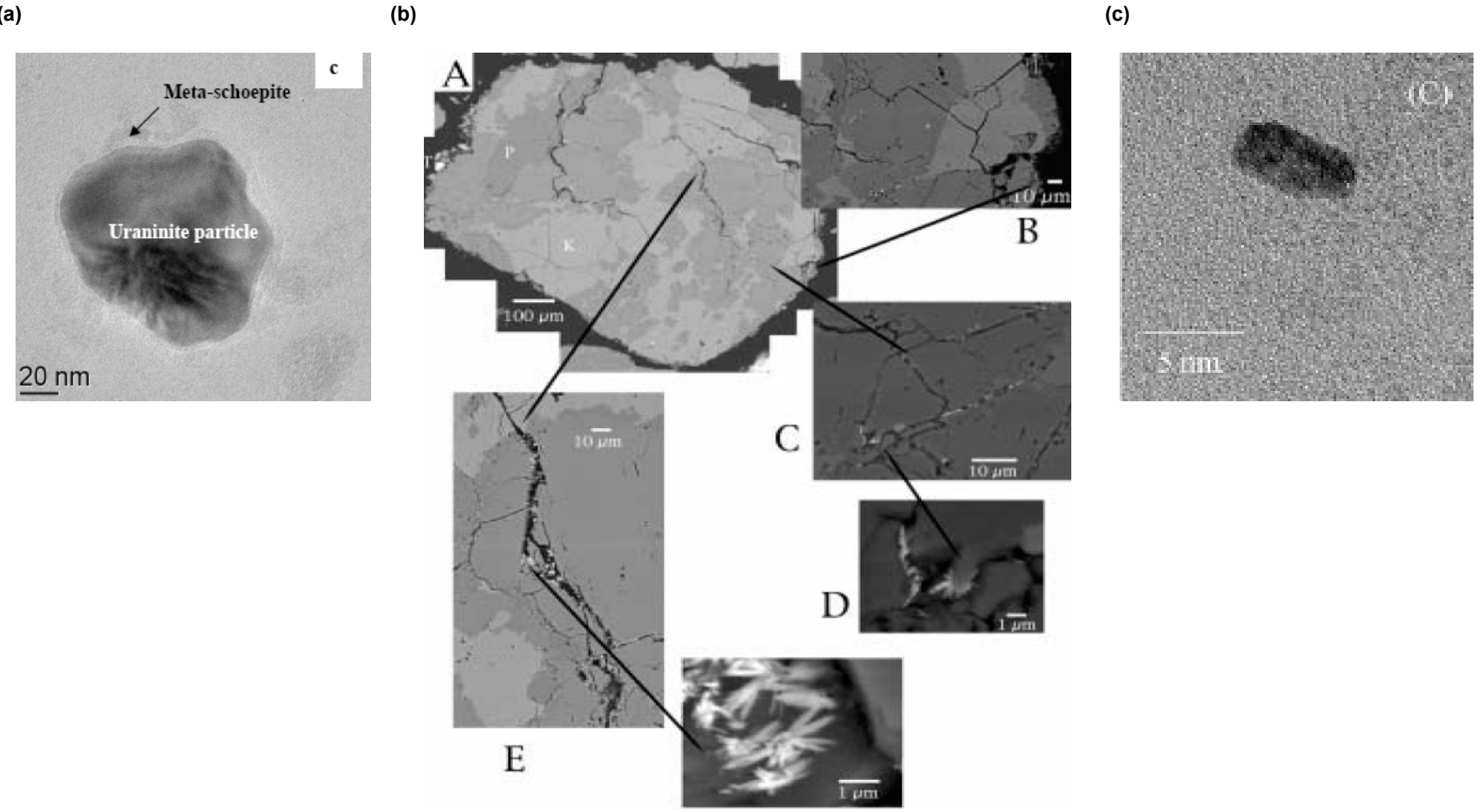

NOTE: (a) U(VI) oxide (meta-schoepite) phase observed in corrosion test with UO_2 (Buck et al. 2004 [DIRS 171479]). (b) Precipitated U(VI) Nano-precipitates in grain fractures of quartz and feldspar in BX-102 Sediment 61 from the Hanford site (McKinley et al. 2006 [DIRS 179552], Figure 4, p. 1879). (c) Small europium oxide colloidal particle in test analogous to possible CSNF irreversible particles (Wang et al. 2006 [DIRS 179563]).

Figure 7-3. Microscopic Images of Colloidal U(VI) Phases and Analogues of Possible CSNF Irreversible Colloids

Conclusion—The corroborating data match qualitatively with CSNF- and DSNF-specific test results and peer-reviewed literature on field observations near uranium deposits and are in agreement with model predictions.

7.1.4 Validation of Corrosion Product and Groundwater Colloid Concentration Model Results

Question F: Are the ranges of corrosion product and groundwater colloid concentrations reasonable? (VA 1, 3)

Honeyman and Ranville (2002 [DIRS 161657]) point out that although most systems of interest for radioactive waste disposal exhibit low colloid concentrations (less than 10 mg/L), concentrations exceeding 100 mg/L are not uncommonly reported. Based on a review by Triay et al. (1995 [DIRS 100789]), high reported colloid concentrations in groundwaters may be the result of colloid sampling techniques. Hence, colloid concentrations between 50 mg/L and 200 mg/L have been assigned only a sampling probability of 2% when the ionic strength of the solution suggests instability of colloids within the waste form and EBS components of the TSPA-LA model calculations.

There is little currently available data that would allow verification of waste package corrosion product colloid concentrations. Validation of the concentrations used in the model has been obtained by examining the concentrations of iron oxides reported in the literature in natural environments and studies on the corrosion of steels. Smailos et al. (2003 [DIRS 179559]) have examined the long-term performance of carbon steel and stainless steels with respect to the European nuclear waste management program. These studies are relevant to non-oxidizing saturated environments, and so may have limited applicability to the Yucca Mountain environment. Zeimniak and Hanson (2001 [DIRS 179566], abstract, p. 3) investigated the corrosion of Stainless Steel Type 304L in high temperature water and observed a parabolic rate of 1.16 $mg \bullet dm^{-2} \bullet hr^{-1/2}$. Most of the iron in solution was associated with colloids, but colloid concentrations were not provided. Studies by Smailos et al. (2003 [DIRS 179559], Table 11, p. 32) on TstE355 carbon steel in a high concentration $MgCl_2$ brine at 90°C yielded a mass of colloids ranging from 3.7 ± 2.5 mg/L (Fe_3O_4) at 460 days of testing.

Figure 7-4 shows data extracted from Novikov et al. (2006 [DIRS 179554], Table 1, p. 639) that demonstrates that colloidal plutonium was not observed above pH ~8 in agreement with the current model. The plutonium was shown by micro-analysis to be associated only with iron oxyhydroxides. If the reported ratio of iron to plutonium was a constant, the iron oxyhydroxide colloid concentration distribution would be log-uniform between 0.5 and 50 mg/L. Widerlund et al. (2004 [DIRS 180833], Figure 4, p. 1544) reported total iron oxyhydroxide colloid concentration of ~0.25 mg/L in flooded mine tailing ponds. Both manganese and aluminum appeared to be truly dissolved species in contrast to the iron.

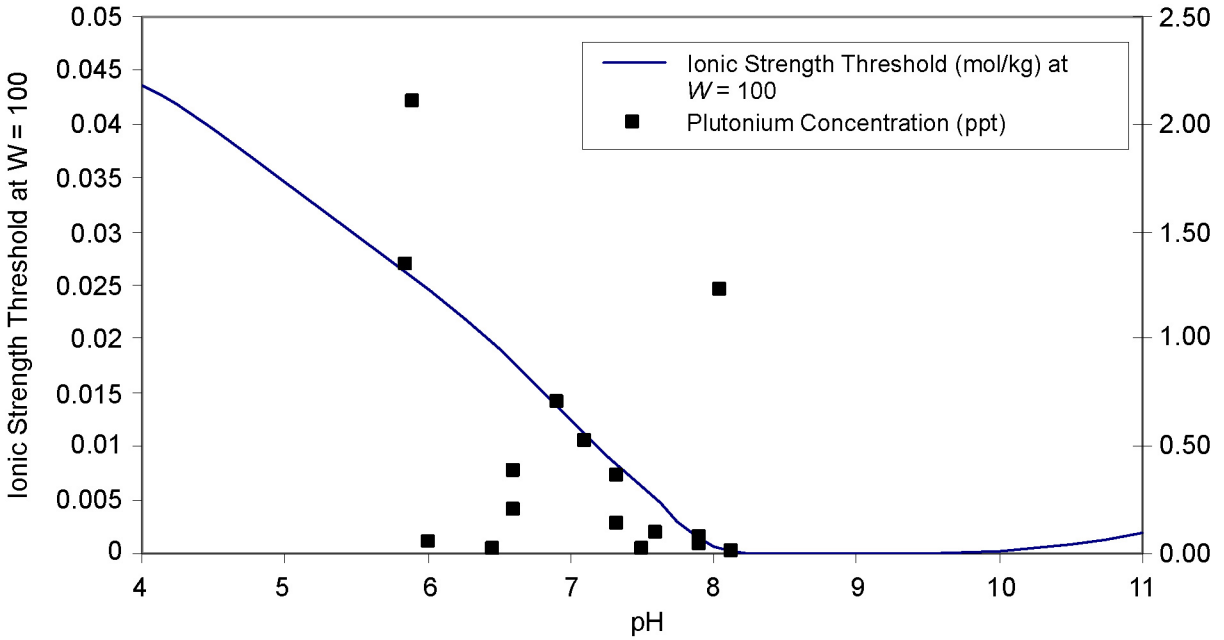

Source: Iron oxide stability curve from Output DTN: MO0705CSIONSTH.000 and Novikov et al. (2006 [DIRS 179554], Table 1, p. 639).

NOTE: Ionic strength can be estimated from the reported nitrate concentrations, which in several instances were between 0.4 and 0.72 mol/kg; however, the plutonium concentration has only been plotted against pH. Nevertheless, the plot demonstrates that no colloidal plutonium was observed above pH ~8 and the highest Pu colloid concentrations were observed at pH ~6.

Figure 7-4. Comparison of Plutonium Concentration with pH Reported on Iron Oxide Colloids at the Mayak Facility in Russia and DLVO-Predicted Stability of Iron Oxides from Current Model with $W = 100$

The range of values for maximum iron oxide–oxyhydroxide colloids concentration (0.3 mg/L to 30 mg/L) was chosen so that it was substantially greater than iron oxyhydroxide colloid levels found in groundwater, but high enough to reflect the masses of corroded ferrous metal anticipated in the repository. Additionally, the value acknowledges the high end of the range of colloids in general reported in groundwaters.

Experiments examining the corrosion of scaled waste packages indicated that abundant suspended material was produced. However, all releases ceased after four weeks of testing because of clogging in the system (DTN: MO0312UCC034JC.008 [DIRS 166367]).

The distribution of colloid concentrations from corroded Stainless Steel Type 316 was set at a lower range as these materials are significantly more corrosion resistant. There is no data on colloids from 316 steels; however, vapor hydration and immersion tests[3] conducted by Dietz (2005 [DIRS 179542]) on a series of 304 and 316 stainless steels containing Zircaloy indicate that even after aggressive conditions (immersion tests at 90°C for 700 days and vapor hydration

[3] Vapor hydration and immersion tests were similar to those that have been conducted on nuclear waste forms.

tests at 200°C for 365 days), the corrosion rind was on the order of 40 to 100 nm thick and release of iron was minimal or below detection limits (see Figure 7-5). Hence, the colloid concentrations from stainless steel will be much less than those from carbon steel. The distribution used in the model for corroded stainless steel colloid concentration was compared to the data presented by Dietz (2005 [DIRS 179542]).

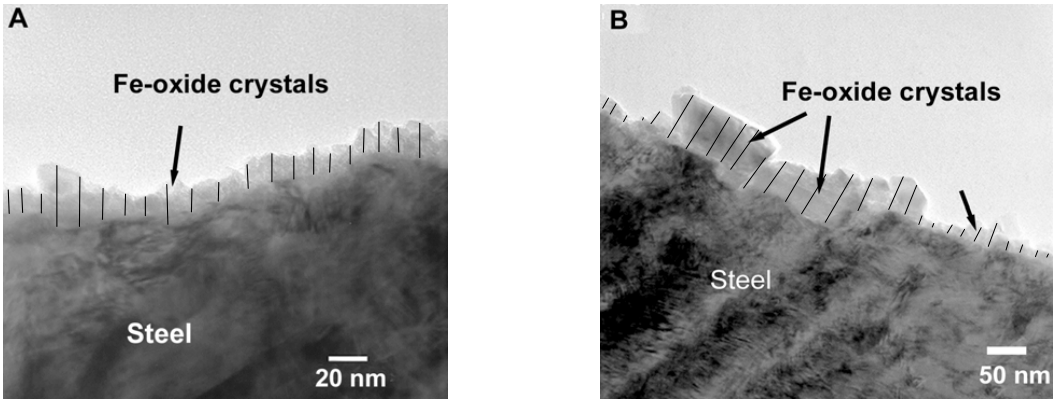

Source: Dietz 2005 [DIRS 179542], Figures 14A and 14B.

NOTE: The corrosion layer was not continuous but occurred only in isolated regions. The black lines are measurements of the layer thickness used in the comparative analysis (see Output DTN: MO0705COLCONCS.000).

Figure 7-5. Transmission Electron Micrograph of Corroded Stainless Steel Showing Iron Oxide Surface

Assuming that spallation is the principal method for releasing colloids from a corroded material, and only a very small fraction of the layer contributes to colloids (between 1% and 0.1%), it is possible to estimate the range of colloid concentrations that may be present. The release range was estimated from tests on DHLWG. In the glass corrosion experiments, the alteration rinds ranged in thickness from 100 to 300 nm in the 2,000/m tests (SA = 0.02 m^2 and leachant volume = 10 mL) and colloid concentrations ranged from 1 to 4.5 ppm (CRWMS M&O 2001 [DIRS 154071]; DTN: LL000123351021.117 [DIRS 143308]). Assuming the colloid density is 2.7 g/cm^3, the percentage released as colloids based on layer thickness (100 to 300 nm) is 0.05% to <1%. This same range was used to estimate a possible proportion of the iron oxide surface that might become colloidal. In Figure 7-6, the distribution used in the model matches reasonably with the estimated values based on the two electron micrographs shown in Figure 7-5 using the assumptions described above.

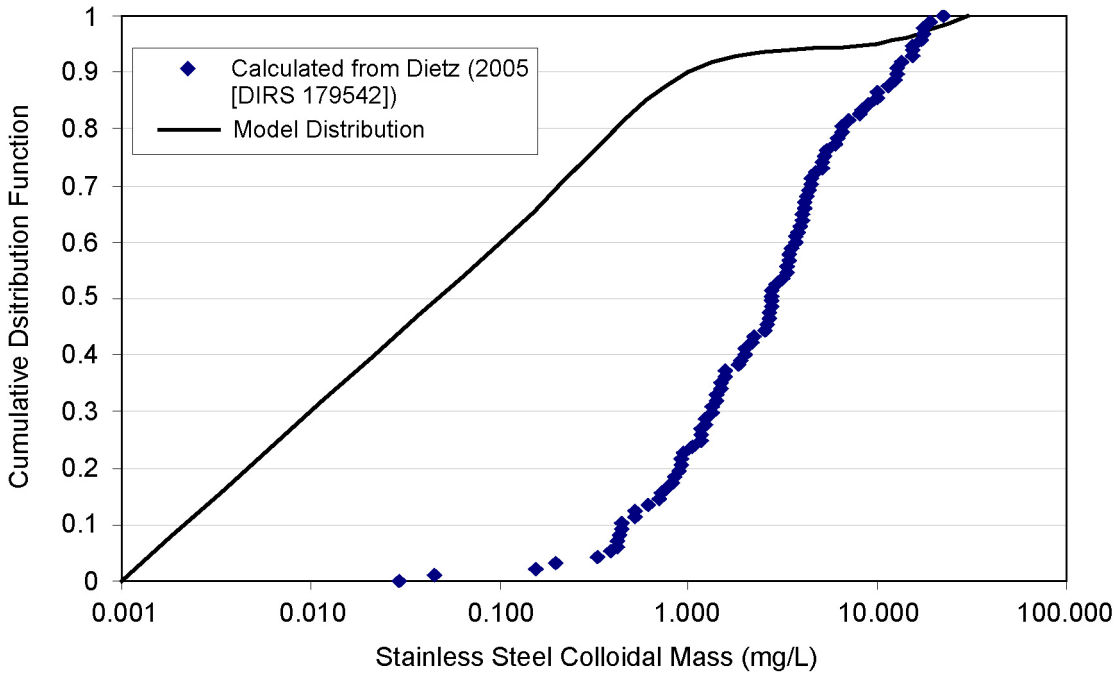

Source: Dietz 2005 [DIRS 179542]; Output DTN: MO0705COLCONCS.000.

NOTE: Total solid surface area in 1 L solution assumed to be 1 m^2. A random release value between 1% and 0.1% of the corrosion rind was calculated to contribute to colloid formation. Density assumed to be 4.5 g/cm^3 with 80% porosity.

Figure 7-6. Cumulative Distribution Plot of Values Calculated from Results Reported by Dietz (2005 [DIRS 179542]; see Output DTN: MO0705COLCONCS.000) Compared to the Stainless Steel Corrosion Product Colloid Distribution Used in the Model

Conclusion—The conceptual view that continuous production and outflow of iron oxide–oxyhydroxide colloids in the waste package would continue unimpeded is highly conservative, and by examining the data collection methods and the nature of particle stability, the range was reduced to a more defensible one. The ranges of corrosion product and groundwater colloid concentrations in the corroborating data match qualitatively and are bounded by model predictions. Therefore, the model is validated through corroboration (VA 1 and VA 3).

7.1.5 Optional Additional Confidence Building for Distribution Coefficient Values

Question G: (VA N/A) Are the distribution coefficient parameters for sorption of radionuclides onto colloids (K_d values) corroborated by peer-reviewed literature and analytical modeling results?

NOTE: The activities performed to address this question are not procedurally required post-development model validation activities; rather they are additional efforts to provide enhanced confidence in parameter values or analyses results.

The K_d value ranges chosen for reversibly attached radionuclides are based on laboratory results and peer-reviewed literature, which are described in detail in Section 6.3.12. Building additional confidence for K_d distributions developed for several radionuclides from published literature was accomplished by considering alternative calculations for determining effective K_d values. Beckman et al. (1988 [DIRS 144956]) reported sorption studies for cesium on zeolites and silicate phases (Figure 7-7 and Table 7-5). These are similar to those reported in Section 6. Table 6-15 lists the radionuclides to which K_d values have been assigned in this report for montmorillonite (smectite) clay. Table 7-8 lists K_d values that are the result of modeling described by Honeyman and Ranville (2002 [DIRS 161657], Figure 8-6). As described in Section 6.3.11, Yucca Mountain vicinity-specific colloid concentrations and groundwater chemistry from Kingston and Whitbeck (1991 [DIRS 113930]) were used as input to a mechanistic sorption model and surface complexation calculations. The K_d ranges vary in part as a function of colloid concentration, which ranged from 0.1 mg/L to 100 mg/L.

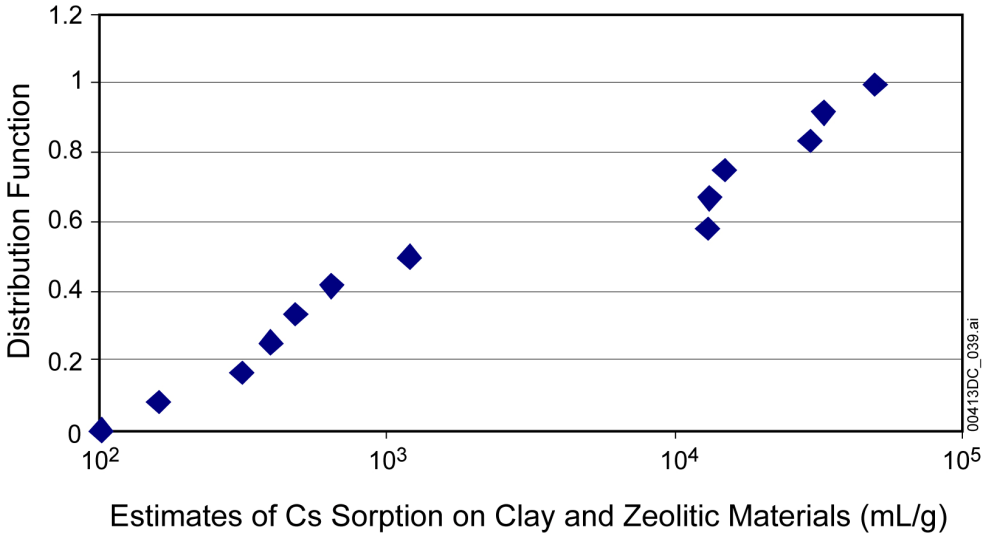

Source: Adapted from data reported by Beckman et al. 1988 [DIRS 144956].

NOTE: The distribution of K_d values for cesium on smectite is bound within this data obtained for related silicate mineral phases.

Figure 7-7. Cumulative Distribution Function Showing the Distribution of Cesium Sorption Coefficients Obtained on Clay, Zeolite, and Glass

Table 7-5. Cesium Sorption with 95% Lower- and Upper-Confidence Bounds (mL/g)

Type/ID	Lower	Estimate	Upper
D G1-1883	1.25E+02	1.85E+02	2.75E+02
D G1-1882	6.87E+02	1.20E+03	2.10E+03
D G1-2363	2.66E+02	3.95E+02	5.86E+02
D JA-32	8.40E+01	1.01E+02	1.23E+02
D JA-37	5.24E+02	6.39E+02	7.80E+02
D YM-22	2.12E+02	3.14E+02	4.66E+02
D YM-45	2.75E+02	4.80E+02	8.39E+02
D YM-54	1.16E+02	1.61E+02	2.22E+02

Table 7-5. Cesium Sorption with 95% Lower- and Upper-Confidence Bounds (mL/g) (Continued)

Type/ID	Lower	Estimate	Upper
D JA-18	1.06E+04	1.30E+04	1.60E+04
D YM-49	2.21E+04	3.28E+04	4.86E+04
D G1-2289	1.98E+04	2.94E+04	4.36E+04
D YM-38	9.64E+03	1.33E+04	1.84E+04
D YM-48	8.58E+03	1.50E+04	2.62E+04
D G1-3658	3.34E+04	4.95E+04	7.35E+04

Source: Beckman et al. 1988 [DIRS 144956].

Sorption of cesium onto montmorillonite was investigated by Serne and Relyea (1982 [DIRS 147681]) over a range of pH values and ionic strengths (see Figure 7-8). The results demonstrate the effect of salt concentration on the sorption capacity of clays owing to ion exchange reactions and no pH dependence on sorption. Clay formed during DHLWG reaction would also result in a large quantity of sodium, which would block sites in the smectite clays and reduce overall sorption of cesium.

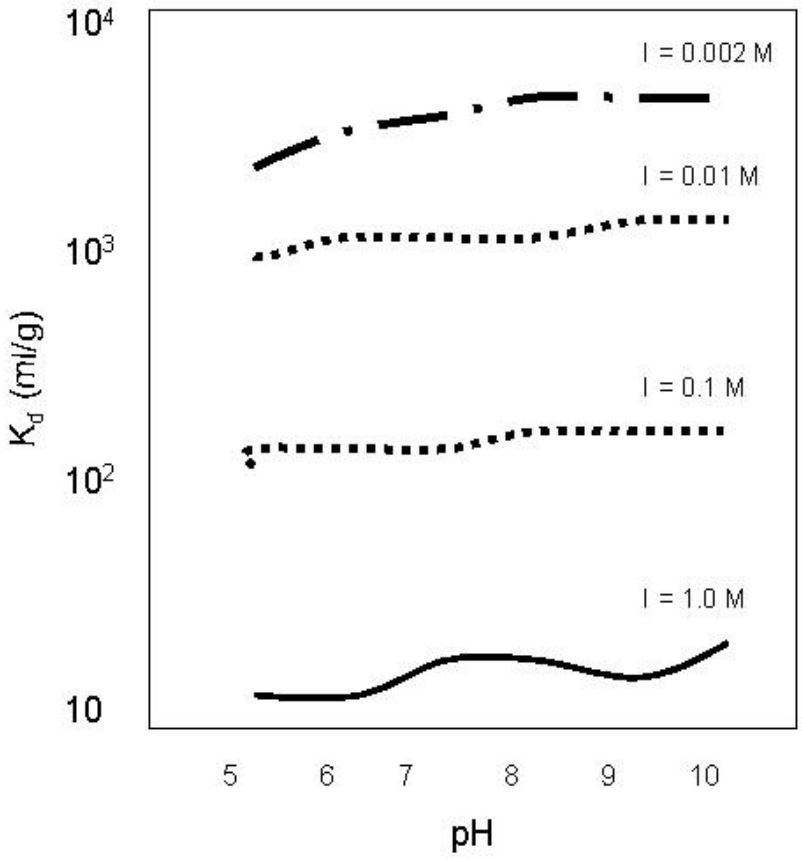

Source: Serne and Relyea 1982 [DIRS 147681], p. 45, Figure 6.

Figure 7-8. Schematic Plot Adapted from Data Reported for Cesium Sorption on Montmorillonite with pH and NaCl Concentration

Two compendia of sorption data are available. The National Cooperative for the Disposal of Radioactive Waste (NAGRA) (Stenhouse 1995 [DIRS 147477]) developed one to compile a set of K_d values useful for evaluation of waste disposal in hypothetical sites in Switzerland. The sorbents considered were crystalline rock, marl, and bentonite with reducing groundwaters (or pore water, in the case of bentonite). Ionic strengths are similar to (or greater than) J-13 well water. The information compiled by Stenhouse (1995 [DIRS 147477]) needs to be applied carefully to the YMP because K_d values are only applicable to a single set of environmental conditions.

Stenhouse (1995 [DIRS 147477]) has proposed "realistic values" and "conservative values" to account for uncertainty in oxidation states (composite K_d values were reduced by an order of magnitude). With respect to the oxidation state, the conservative values may be more relevant to Yucca Mountain. However, the realistic values are useful to compensate for the use of a mass-based K_d approach on colloids. In Table 7-6, the rock composite K_d values and individual K_d values for smectite and oxides or quartz are compiled. The individual mineral values are probably more suitable to consider for Yucca Mountain colloid K_d values.

Table 7-6. Summary of Sorption Data Developed by National Cooperative for the Disposal of Radioactive Waste for Bentonite, Crystalline Rock, and Marl

Radionuclide and Oxidation State(s)	Database	NAGRA Rock K_d (mL/g) (page)	NAGRA Mineral K_d (mL/g)
Th(IV)	79 entries; 22 references	5,000 (p. Th-7)	Smectite = 2,000; Oxides, Quartz = 1,000
Pa(V)	21 entries; 12 references	1,000 (p. Pa-3)	NAGRA uses Zr(IV) as analogue for Pa(IV); use Np(V) for Pa(V) for YMP.
U(VI)	382 entries; 32 references	5,000 (p. U-7)	Smectite = 100; Oxides, Quartz = 20
Np(V)	389 entries; 53 references	5,000 (p. Np-8)	Smectite = 100; Oxides, Quartz = 20
Pu(IV, V, VI)	298 entries; 25 references	5,000 (p. Pu-10)	Smectite = 1,000; Oxides, Quartz = 200
Am(III)	198 entries; 34 references	5,000 (p. Am-9)	Smectite = 10,000; Oxides, Quartz = 1,000
Cesium	516 entries; 41 references	1,000 (p. Cs-11)	Smectite = 2,000; Iron oxide = 40
Ra (II)	13 entries 2 references	1000-16,000 (p. Ra-15)	Montmorillonite, nontronite

Source: Stenhouse 1995 [DIRS 147477].

A second useful compendium was developed for the U.S. Environmental Protection Agency (EPA 1999 [DIRS 147475]), which compiles information on radionuclides including thorium, uranium, and plutonium, with information on neptunium and americium reported in its third volume (EPA 2004 [DIRS 172215]). The assembled data are interpreted to predict ranges of K_d values for soils in shallow subsurface environments. Redox conditions for that system are oxidizing, which makes it useful for the redox-sensitive radionuclides at the YMP.

The U.S. Environmental Protection Agency studies (EPA 1999 [DIRS 147475]; EPA 2004 [DIRS 172215]) reviewed published literature to determine the predominant aqueous chemical conditions affecting sorption in soils for thorium, uranium, plutonium, neptunium, americium,

and cesium. For thorium, pH and sorbate concentration are important. At concentrations close to its solubility limit, K_ds tend to increase. For uranium and neptunium, the pH was important, especially above pH 9. For plutonium, carbonate complexation has a strong influence on sorption, so carbonate concentration, as well as clay content, must be considered as criteria to select a relevant K_d. In Table 7-7, K_d values have been expressed in a minimum to maximum format, with no indication of distribution. Some ranges, for example uranium, span almost six orders of magnitude. To narrow the range, the geometric means were calculated below and reported in column 4 of Table 7-7.

Table 7-7. Summary of Sorption Data Developed by U.S. Environmental Protection Agency

Radionuclide and Oxidation State(s)	Database	Soil and pH Categories 20 wt % to 60 wt % Clay ("high clay") <4 wt % ("low clay")	K_d (mL/g) Range of Geometric Means
Th(IV)	17 entries	pH 8 to 10; [Th] $<10^{-9}$ mol/L (pH and Th concentration important)	20 to 2,000 (200)
U(VI)	20 references	pH 8 (pH important)	0.4 to 250,000 (316)
Pu(IV, V, VI)	2 references	High clay (51 wt % to 70 wt %); 3 to 4 meq/L CO_3^{2-}; Low clay (<4 wt %); 3 to 4 meq/L CO_3^{2-}	1,860 to 2,550 (2,178); 80 to 470 (194)
Np(V)	8 references	Clay (pH important)	0.4 to 2,575 (55)
Am(III)	11 observations	Clay (pH important)	25 to 400,000 (8,400)
Cesium	11 references	High clay (20 wt % to 60 wt %) Low clay (<4 wt %)	80 to 26,700 (1,500); 10 to 3,500 (200)

Source: EPA 1999 [DIRS 147475]; EPA 2004 [DIRS 172215].

Honeyman and Ranville (2002 [DIRS 161657]) reviewed aspects of colloid-facilitated radionuclide transport, including reduction of effective retardation of radionuclides by colloids and the effectiveness of colloids with respect to radionuclide mobility in the presence of stationary phases available for radionuclide sorption. Contardi et al. (2001 [DIRS 162732]) developed models using Yucca Mountain groundwater chemistry and colloid size and concentration data from Kingston and Whitbeck (1991 [DIRS 113930]). The K_d values were calculated with the use of a diffuse layer model and based on three principles: (1) the system is symmetrical (i.e., the colloids and stationary phases are similar with respect to mineralogy); (2) the colloids are stable; and (3) the system is in sorptive equilibrium. The ratio of stationary phase to colloid surface areas ranged up to roughly two orders of magnitude (3.2 to 63). Colloid concentrations of up to about 100 mg/L were included. In the system analyzed, approximate K_d value ranges (mL/g) for the radionuclides under consideration were given (Table 7-8).

Table 7-8. Modeled K_d Values for Plutonium, Americium, Thorium, Neptunium, and Uranium Sorption onto Yucca Mountain-Vicinity Colloids

Radionuclide Sorbate and Oxidation State(s) at YMP	K_d Values (mL/g)
U(VI)	1×10^0 to 6×10^2
Np(V)	1×10^1 to 1×10^2
Pu(V)	1×10^3 to 1×10^4
Th(IV)	2×10^3 to 9×10^4
Am(III)	1×10^4 to 1×10^7

Source: Honeyman and Ranville 2002 [DIRS 161657] (extracted from Figure 7-5 in reference).

Powell et al. (2004 [DIRS 180836]; 2005 [DIRS 174726]) have investigated the uptake of plutonium on iron oxides and have developed rate expressions for describing the adsorption and reduction of Pu(V) on various iron oxides. Data from these studies is presented in Table 7-9 and plotted in Figure 7-9.

Table 7-9. Rate of Plutonium Uptake on Iron Oxide Phases

Hematite	pH	Rate/yr	k ($m^3\ m^{-2}\ yr^{-1}$)
	4.6	2.75E+01	0.002746
	4.9	7.26E+01	0.007332
	6.09	2.74E+02	0.026824
	7.24	6.94E+02	0.070128
	7.76	3.41E+04	0.688529
	7.9	1.36E+05	1.366543
Goethite	**pH**	**Rate/yr**	k ($m^3\ m^{-2}\ yr^{-1}$)
	5.69	2.68E+03	0.026428
	6.47	2.87E+03	0.140085
	6.47	2.84E+03	0.058803
	6.66	2.56E+03	0.025284
	6.54	6.31E+04	0.210034
	6.56	9.47E+04	0.188516
	8.09	7.89E+03	0.377483
	7.96	3.16E+04	0.618776
	7.75	1.58E+06	15.7788
Magnetite	**pH**	**Rate/yr**	k ($m^3\ m^{-2}\ yr^{-1}$)
	2.85	9.15E-01	0.00000
	2.98	3.79E+01	0.00004
	3.04	9.47E+01	0.00011
	5.33	1.04E+02	0.00012
	5.14	7.57E+01	0.00009
	6.45	2.27E+03	0.00268

Table 7-9. Rate of Plutonium Uptake on Iron Oxide Phases (Continued)

Magnetite (cont.)	pH	Rate/yr	k (m^3 m^{-2} yr^{-1})
	7.93	7.26E+03	0.00857
	7.94	3.47E+04	0.04100
	7.98	6.94E+04	0.08200

Source: Powell et al. 2004 [DIRS 180836], Table 2, p. 6020; Powell et al. 2005 [DIRS 174726], Table 1, p. 2110, and Table 2, p. 2112.

NOTE: Magnetite SA = 25.4 m^2/g (0.5 g solid in 15 mL) C_{FeO} = 33333.3 g/m^3.

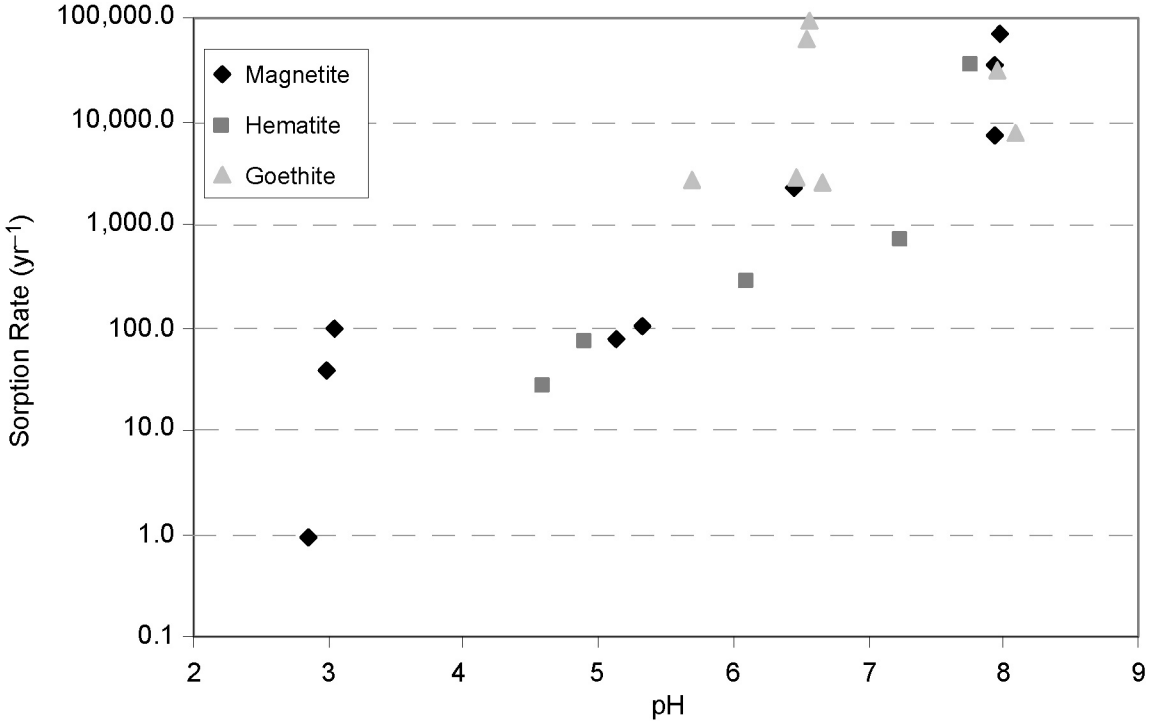

Source: Table 7-9 (in this report), adapted from Powell et al. 2004 [DIRS 180836] and Powell et al. 2005 [DIRS 174726].

NOTE: The rate values obtained from Table 6-18, were calculated to range from 0.002 (m^3 m^{-2} yr^{-1}) to 0.048 (m^3 m^{-2} yr^{-1}). These values are corroborated by the rates reported in Table 7-9.

Figure 7-9. Plot Showing Sorption Rate for Plutonium on Iron Oxides

For sorption coefficients of radionuclides onto uranyl colloids, no experimental data were found to be available for independently evaluating additional confidence in these parameter values. The discussion above in Section 7 indicates that the uranyl colloid model is unimportant to the radionuclide transport subsystem and relatively unimportant to the overall set of colloid models. Therefore, the critical review documented in Appendix IV is sufficient in scope to cover this aspect of the model at the appropriate level of confidence needed. In addition, some general observations from natural systems are discussed here regarding uranyl colloid importance within geologic systems. In nature, U(VI) minerals tend to be extremely pure. Elements such as lead can be present but will have grown in through radioactive decay. Elements that ion exchange,

such as barium and calcium, can be readily incorporated into a U(VI) mineral; likewise, elements that can form part of the anionic framework, such as silicon (uranyl silicates), arsenic (uranyl arsenates), or vanadium (uranyl vanadates), are readily incorporated. There is little evidence in the natural system for incorporation of other actinides, such as thorium. Hence, these general observations tend to support the sorption coefficients distributions used in the model (see Table 6-9) and the anticipated colloid concentration probability distribution (see Table 6-8). As such, this model would be unlikely to result in significant radionuclide-associated colloid transport.

Conclusion—The distribution coefficients for radionuclides onto colloids (K_d values) in Tables 7-5 through 7-8 are bounded by the model values in Table 6-6a. The data in the model has been shown to be corroborated by peer-reviewed literature and analytical modeling results. Corroborating data match qualitatively and are bounded by model predictions. Therefore, the model is validated through corroboration (VA 1 and VA 3).

7.1.6 Post-Model Development Validation Conclusion

The preceding sections have met the validation criteria set forth in the TWP (BSC 2006 [DIRS 177389], Table 2-3) that the "corroborating data must match qualitatively or must be bound by model predictions."

7.2 PROCESSES NOT INCORPORATED INTO THE ABSTRACTION

Sorption to the air–water interfaces in unsaturated environments was not included. Attachment of colloids to air–water interfaces depends on the hydrophobicity of the colloidal particles, which is generally low in smectites. Because partitioning to immobile air–water interfaces will tend to retard colloid transport, exclusion of this process in modeling colloid transport in the EBS is conservative.

The role of minor phases in the colloid-assisted radionuclide transport is not included in the model. In particular, the small amount of manganese present in waste package materials could lead to sorption of plutonium at lower pH than for iron oxides. Sorption of Pu(IV) on to manganese oxide minerals has been shown to be fast and reversible (Duff et al. 1999 [DIRS 170925]). Sorption on manganese phases increased at pH 3 and reached a maximum value of 100% at pH 8 and then decreased over the pH range from 8 to 10. The plutonium sorption appeared to occur via a reduction mechanism on the mineral surface and was consistent with the formation of an inner-sphere complex (Duff et al. 1999 [DIRS 170925]). No evidence of PuO_2 precipitation was detected. Although manganese minerals are excluded, by applying a conservative K_d distribution, the potential effect of the minor quantity of manganese oxide minerals that may be present is bounded.

Sorption of metals to organic matter can be greater than sorption to oxide phases (Ramsey 1988 [DIRS 144603]). Organic films on colloids will modify uptake of plutonium and other actinides. Organics may result from thermal decomposition of grease and paint. Microbial activity was discussed in the report but is not addressed within the model analysis. Microbes can bind metals, secrete metal-solubilizing compounds, and transform metal ions to altered speciation states. Owing to a lack of suitable data, predicting the fate of radionuclide transport processes

associated with biocolloids is limited. However, the quantities of organic matter and microbes either emplaced or generated (through microbial growth processes) in the waste emplacement drifts are sufficiently small that they are unlikely to be of significance.

The potential effect of radiolysis has been ignored and there is little data on the subject. Radiolysis can result in more-soluble states for the actinides, which might otherwise form colloids. Other effects include degradation of organic materials.

Sorption coefficients are dependent on pH with a sharp sorption edge observed near pH values 8 and 4 for plutonium and americium sorption onto hematite, respectively. However, J-13 well water was used in most sorption tests upon which the model was based. The range of anticipated pH is such that pH-dependent sorption may not be significant.

Conclusion—Processes not included in the model would reduce the impact of colloids in TSPA-LA; hence, the model bounds processes that were not incorporated into the abstraction.

7.3 VALIDATION ACTIVITIES EXTENDING BEYOND THE CURRENT DOCUMENTATION OF THE MODEL

The disposition of the various validation criteria described in Section 7.1 is that the level of confidence required for validation of the various components considered in this model analysis has been achieved. No further validation activities are needed to complete the model validation for its intended use.

INTENTIONALLY LEFT BLANK

8. CONCLUSIONS

8.1 MODEL SUMMARY AND IMPLEMENTATION

The model describes the types and concentrations of colloids that could be: (1) generated in the waste package from degradation of the waste forms and the corrosion of the waste package materials, (2) produced from the steel components of the repository and their potential role in radionuclide transport, and (3) present in natural waters in the vicinity of Yucca Mountain. In addition, sorption and desorption characteristics and mechanisms of colloids anticipated in the repository are addressed. The model predicts radionuclide–colloid behavior and radionuclide-sorption by creating four conceptual colloids in the waste package that bound all the potential colloids that might be present. The model uses theoretical calculations and laboratory data to determine the stability of modeled colloids with ionic strength and pH. The true nature of colloid composition and heterogeneity, generation, and flocculation in the waste package will be extremely complex, involving the formation of numerous types of phases, often depending on the composition of the various waste forms and waste package materials. This model strives to capture the uncertainty of the real system using models of four representative colloids to capture the behavior of the colloid types most likely to influence dose.

To develop a functioning model, the waste package/in-drift colloidal system needed to be subdivided into idealized colloidal particles for which there exists fundamental property data in the literature. Four conceptual particles were selected for modeling: (1) montmorillonite, (2) hematite, (3) zirconium oxide, and (4) meta-autunite to represent (1) smectite clay, (2) iron oxyhydroxides, (3) Pu-Zr oxide particles, and (4) uranophane, respectively. These phases capture the major potential particle types in the waste package and in-drift environment through evaluation of the likely long-term alteration of the waste forms and waste package materials and the secondary phases most capable of forming viable colloids. Literature data provided the relationship between zeta potential and pH and the Hamaker constants from these phases, which allowed the development of a DLVO-based stability model.

The sorption of americium and plutonium on iron oxides is modeled using a competitive sorption model which is discussed in *EBS Radionuclide Transport Abstraction* (SNL 2007 [DIRS 177407]). The target-flux out ratio, F_{RN}, parameter, defines the ratio of plutonium and americium mass attached to colloids (irreversibly) to the total plutonium and americium mass leaving the waste package (attached to colloids plus dissolved) for advective conditions. This ratio is defined as a log uniform distribution between 0.9 and 0.99. The experimentally based forward rate constant (k) defines the irreversible sorption rate of plutonium and americium onto iron oxyhydroxide colloids for zero or near-zero advective flux conditions or where colloids are unstable.

In the TSPA-LA model, natural seepage water/groundwater colloids are modeled to come in contact with and enter breached waste packages and subsequently sorb radionuclides. The resulting pseudocolloid (radionuclide complexes) will subsequently be subjected to transport from the engineered barrier system to the downstream unsaturated and saturated zones.

Recent experimental work on the corrosion of miniature carbon steel waste packages has provided needed data on the possible concentrations of iron oxide–oxyhydroxide colloids that

bound the values that might be expected from degrading carbon steel within the EBS upon contact of seepage water and subsequent corrosion of the waste packages (see Figure 6-20). The recommended values for Stainless Steel Type 316 are significantly lower with a distribution as described in Table 6-11. The distribution was developed based on an assessment of the differences between carbon steel and stainless steel corrosion. These values represent a reasonable maximum for iron oxide–oxyhydroxide colloid releases from a waste package containing both stainless and carbon steels following a potential breach (Section 6.3.8).

There are several sources of uncertainty attached to this abstraction. The representation of the waste package colloid environment with four major types of particles was done to capture the major contributors given the complexity of the system and modeling constraints. However, the surface electrical heterogeneity in the corroded waste package environment may not be represented fully by using measurements of surface potentials from modeled conceptual phases. For instance, the presence of manganese in the corroding metal components may have a strong influence on plutonium chemistry (Duff et al. 1999 [DIRS 170925]). The heterogeneity of the waste package and in-drift environment creates a variable stability field (W) where the probability that a passing colloid will be captured will be proportional to its rate of transport and the amount of surface with a low stability ratio.

These uncertainties have been bounded through the application of conservative values for (1) colloid stability ranges (i.e., application of $W = 10$ stability criteria), (2) colloid concentrations, and (3) sorption coefficients (extended K_d ranges) for this model. The abstraction is considered valid and usable in TSPA-LA calculations for any time after the temperature in the repository has decreased to below boiling after the thermal pulse.

8.2 MODEL OUTPUTS

Developed data for use directly by the TSPA-LA calculations or other submodel components in the TSPA-LA model calculations include intermediate parameters (see Table 6-24 for parameter listing and associated DTNs) and model output parameters (Table 8-1).

Table 8-1. Summary of Model Output Parameters

Parameter Name	Parameter Description	Units	Basis for Value/ Source	Value / Range / Distribution
$C_{Rncoll,DHLWG,embed}$ $C_{Rncoll,DHLWG,rev}$ $C_{Rncoll,SNF,embed}$ $C_{Rncoll,uranophane}$ $C_{Rncoll,FeOx,irrev}$ $C_{Rncoll,FeOx,rev}$ $C_{Rncoll,gw}$	Concentration of mobile colloidal radionuclide element radionuclides per unit volume or mass of water	mol/L	Determined in performance assessment calculation; Figure 6-30	Calculated at each time step; uncertainty propagated through the TSPA-LA model calculations

Additionally, parameters developed in this analysis for use elsewhere in the TSPA-LA model are listed in Table 6-24. These include waste form colloid mass concentrations (derived from DHLWG, CSNF, and DSNF), corrosion product colloid mass concentrations, K_d values for selected radionuclides onto colloids, specific surface area on colloids from a corroded waste package, and ionic strength ranges for colloid stability for the various colloid types. Output DTNs include:

- MO0701PASORPTN.000 (Colloidal sorption coefficients for Pu, Am, Th, Cs, and Pa)
- MO0701PACSNFCP.000 (CSNF Colloid Parameters)
- MO0701PAGLASWF.000 (Glass Waste Form Colloid Parameters)
- MO0701PAGROUND.000 (Groundwater Colloid Concentration Parameters)
- MO0701PAIRONCO.000 (Colloidal Iron Corrosion Products Parameters)
- MO0701PAKDSUNP.000 (Colloidal Kds for U, Np, Ra, and Sn)
- MO0705COLCONCS.000 (Colloid Concentrations from Corroded Steels)
- MO0705CSIONSTH.000 (Colloid Stability Ionic Strength Thresholds)
- MO0705DSCSCUSS.000 (Radionuclide Sorption Distributions for Smectite and Uranophane Colloids).

8.3 YUCCA MOUNTAIN REVIEW PLAN ACCEPTANCE CRITERIA

Yucca Mountain Review Plan, Final Report (NRC 2003 [DIRS 163274]) contains acceptance criteria intended to establish the basis for the review of the material contained in the license application. As this report serves, in part, as the basis for the license application, it is important to show how the information contained herein addresses each of the applicable acceptance criteria.

The acceptance criteria applicable to this report are identified in *Technical Work Plan for Waste Form Testing and Modeling* (BSC 2006 [DIRS 177389], Table 3-1). For each applicable criterion, the criterion is quoted in italics, followed by pointers to where within the model report the information addressing the criterion can be found. In some cases, the criterion is only partially addressed in this report. A demonstration of full compliance requires a review of multiple reports.

Radionuclide Release Rates and Solubility Limits (NRC 2003 [DIRS 163274], Section 2.2.1.3.4.3)

Acceptance Criterion 1—System Description and Model Integration Are Adequate

> *(1) Total system performance assessment adequately incorporates important design features, physical phenomena, and couplings, and uses consistent and appropriate assumptions throughout the radionuclide release rates and solubility limits abstraction process.*

The colloid model developed in this report is consistent with the design features relevant to models from which input is taken, and models to which output is provided. The values (or ranges of values) of parameters used in the colloid model are either developed within the model

or obtained from project or literature sources. Implementation of the colloid model requires definition of variables for solution pH and ionic strength that will be obtained from other models.

> *(2) The abstraction of radionuclide release rates and solubility limits uses assumptions, technical bases, data, and models that are appropriate and consistent with other related U.S. Department of Energy abstractions. For example, the assumptions used for this model abstraction are consistent with the abstractions of "Degradation of Engineered Barriers" (Section 2.2.1.3.1); "Mechanical Disruption of Waste Packages" (Section 2.2.1.3.2); "Quantity and Chemistry of Water Contacting Waste Packages and Waste Forms" (Section 2.2.1.3.3); "Climate and Infiltration" (Section 2.2.1.3.5); and "Flow Paths in the Unsaturated Zone" (Section 2.2.1.3.6). The descriptions and technical bases provide transparent and traceable support for the abstraction of radionuclide release rates and solubility limits.*

Coordination in modeling of colloids within the repository and natural system is discussed in Section 6.5.3.

> *(3) The abstraction of radionuclide release rates and solubility limits provides sufficient, consistent design information on waste packages and engineered barrier systems. For example, inventory calculations and selected radionuclides are based on the detailed information provided on the distribution (both spatially and by compositional phase) of the radionuclide inventory, within the various types of high-level radioactive waste.*

Design information on the in-package materials and waste forms was used in determining which colloid types to model.

> *(4) The U.S. Department of Energy reasonably accounts for the range of environmental conditions expected inside breached waste packages and in the engineered barrier environment surrounding the waste package. For example, the U.S. Department of Energy should provide a description and sufficient technical bases for its abstraction of changes in hydrologic properties in the near field, caused by coupled thermal-hydrologic-mechanical-chemical processes.*

The colloid models account for the range of environmental conditions expected (pH, temperature, and ionic strength), as described in Section 6.5.

> *(5) ...*

Not applicable (applies to thermal-hydrologic processes).

> *(6) Technical bases for inclusion of any thermal-hydrologic-mechanical-chemical couplings and features, events, and processes in the radionuclide release rates and solubility limits model abstraction are adequate. For example, technical bases may include activities, such as independent modeling, laboratory or field data, or sensitivity studies.*

The technical bases for inclusion of features, events, and processes in the colloid model are discussed in Section 6.

(7) ...

Not applicable (applies to criticality).

(8) Guidance in NUREG-1297 and NUREG-1298 or other acceptable approaches for peer reviews and data qualification is followed.

Section 4.1 and Appendix II address data inputs to the model and qualification of data.

Acceptance Criterion 2—Data Are Sufficient for Model Justification

(1) Geological, hydrological, and geochemical values used in the license application are adequately justified. Adequate description of how the data were used, interpreted, and appropriately synthesized into the parameters is provided.

The inputs are discussed in Section 4.1. Section 6 discusses how these inputs were developed into parameters.

(2) Sufficient data have been collected on the characteristics of the natural system and engineered materials to establish initial and boundary conditions for conceptual models and simulations of thermal-hydrologic-chemical coupled processes. For example, sufficient data should be provided on design features, such as the type, quantity, and reactivity of materials, that may affect radionuclide release for this abstraction.

Section 6 describes the data on the characteristics of the natural system and engineered materials that are important to the formation and stability of colloid suspensions, and the attachment of radionuclides to colloids.

(3) ...

Not applicable (applies to solubility rather than colloids).

(4) The corrosion and radionuclide release testing program for high-level radioactive waste forms intended for disposal provides consistent, sufficient, and suitable data for the in-package and in-drift chemistry used in the abstraction of radionuclide release rates and solubility limits. For expected environmental conditions, the U.S. Department of Energy provides sufficient justification for the use of test results, not specifically collected from the Yucca Mountain site, for engineered barrier components, such as high-level radioactive waste forms, drip shield, and backfill.

The corrosion and radionuclide release-testing program for high-level radioactive waste forms has provided chemistry and colloid data as well. These data, augmented, by literature data, form the basis for the colloid model as discussed in Section 6.

Acceptance Criterion 3—Data Uncertainty Is Characterized and Propagated through the Model Abstraction

(1) Models use parameter values, assumed ranges, probability distributions, and bounding assumptions that are technically defensible, reasonably account for uncertainties and variabilities, and do not result in an under-representation of the risk estimate.

Parameter values, assumed ranges, probability distributions, and bounding assumptions are discussed in Sections 5 and 6.

(2) Parameter values, assumed ranges, probability distributions, and bounding assumptions used in the abstractions of radionuclide release rates and solubility limits in the total system performance assessment are technically defensible and reasonable based on data from the Yucca Mountain region, laboratory tests, and natural analogs. For example, parameter values, assumed ranges, probability distributions, and bounding assumptions adequately reflect the range of environmental conditions expected inside breached waste packages.

Parameter values and uncertainty are discussed in Sections 4.1 and 6.6.2 and throughout the document.

(3) ...

Not applicable (applies to thermal-hydrologic-chemical coupled processes).

(4) Uncertainty is adequately represented in parameter development for conceptual models, process models, and alternative conceptual models considered in developing the abstraction of radionuclide release rates and solubility limits, either through sensitivity analyses or use of bounding analyses.

Uncertainty is addressed in Section 6.6.2 and throughout the document.

(5-6) ...

Not applicable (applies to water flow and criticality).

(7) The U.S. Department of Energy uses as appropriate range of time-history of temperature, humidity, and dripping to constrain the probability for microbial effects, such as production of organic by-products that act as complexing ligands for actinides and microbially enhanced dissolution of the high-level radioactive waste glass form.

The effects of microbes are discussed in Section 6.3.4.

(8) The U.S. Department of Energy adequately considers the uncertainties, in the characteristics of the natural system and engineered materials, such as the type, quantity, and reactivity of material, in establishing initial and boundary conditions for conceptual

models and simulations of thermal-hydrologic-chemical coupled processes that affect radionuclide release.

Uncertainty is addressed in Section 6.6.2 and throughout the document.

(9) ...

Not applicable (applies only when insufficient data exists).

Acceptance Criterion 4—Model Uncertainty Is Characterized and Propagated through the Model Abstraction

(1) Alternative modeling approaches of features, events, and processes are considered and are consistent with available data and current scientific understanding, and the results and limitations are appropriately considered in the abstraction.

Alternative modeling approaches are discussed in Section 6.4.

(2) In considering alternative conceptual models for radionuclide release rates and solubility limits, the U.S. Department of Energy uses appropriate models, tests, and analyses that are sensitive to the processes modeled for both natural and engineering systems. Conceptual model uncertainties are adequately defined and documented, and effects on conclusions regarding performance are properly assessed. For example, in modeling flow and radionuclide release from the drifts, the U.S. Department of Energy represents significant discrete features, such as fault zones, separately, or demonstrates that their inclusion in the equivalent continuum model produces a conservative effect on calculated performance.

Alternative modeling approaches are discussed in Section 6.4.

(3) Consideration of conceptual model uncertainty is consistent with available site characterization data, laboratory experiments, field measurements, natural analog information and process-level modeling studies; and the treatment of conceptual model uncertainty does not result in an under-representation of the risk estimate.

Alternative modeling approaches are discussed in Section 6.4.

(4) ...

Not applicable (applies to thermal-hydrologic-chemical coupled processes).

Acceptance Criterion 5—Model Abstraction Output Is Supported by Objective Comparisons

(1) The models implemented in this total system performance assessment abstraction provide results consistent with output from detailed process-level models and/or empirical observations (laboratory and field testing and/or natural analogs).

As discussed in Section 7, the colloid model is consistent with empirical observations.

(2) ...

Not applicable (applies to thermal hydrologic models).

(3) ...

Not applicable (applies to thermal-hydrologic-chemical coupled processes).

(4) ...

Not applicable (applies to the performance confirmation program).

9. INPUTS AND REFERENCES

9.1 DOCUMENTS CITED

158692 Abdel-Fattah, A.I. and El-Genk, M.S. 1998. "On Colloidal Particle Sorption onto a Stagnant Air–Water Interface." *Advances in Colloid and Interface Science, 78,* (3), 237-266. New York, New York: Elsevier. TIC: 253147.

156927 Abramowitz, M. and Stegun, I.A., eds. 1972. *Handbook of Mathematical Functions with Formulas, Graphs, and Mathematical Tables.* New York, New York: Dover Publications. TIC: 240610.

163198 Advocat, T.; Jollivet, P.; Crovisier, J.L.; and del Nero, M. 2001. "Long-Term Alteration Mechanisms in Water for SON68 Radioactive Borosilicate Glass." *Journal of Nuclear Materials, 298,* (1-2), 55-62. New York, New York: North-Holland. TIC: 254332.

161648 Aguilar, R.; Papenguth, H.W.; and Rigby, F. 1999. "Retardation of Colloidal Actinides through Filtration in Intrusion Borehole Backfill at the Waste Isolation Pilot Plant (WIPP)." *Actinide Speciation in High Ionic Strength Media, Experimental and Modeling Approaches to Predicting Actinide Speciation and Migration in the Subsurface, Proceedings of an American Chemical Society Symposium on Experimental and Modeling Studies of Actinide Speciation in Non-Ideal Systems, held August 26-28, 1996, in Orlando, Florida.* Reed, D.T.; Clark, S.B.; and Rao, L., eds. Pages 215-225. New York, New York: Kluwer Academic/Plenum Publishers. TIC: 253961.

134303 Atkins, P.W. 1994. *Physical Chemistry.* 5th Edition. New York, New York: W.H. Freeman and Company. TIC: 246986.

164865 Atun, G.; Bilgin, B.; and Mardinli, A. 1996. "Sorption of Cesium on Montmorillonite and Effects of Salt Concentration." *Journal of Radioanalytical and Nuclear Chemistry, 211,* (2), 435-442. New York, New York: Elsevier. TIC: 255302.

100704 Bates, J.K.; Bradley, J.P.; Teetsov, A.; Bradley, C.R.; and Buchholtz ten Brink, M. 1992. "Colloid Formation During Waste Form Reaction: Implications for Nuclear Waste Disposal." *Science, 256,* 649-651. Washington, D.C.: American Association for the Advancement of Science. TIC: 239138.

170880 Bates, J.K.; Brown, N.R.; Buck, E.C.; Dietz, N.L.; DiSanto, T.; Ebert, W.L.; Ellison, A.J.G.; Emery, J.W.; Fortner, J.A.; Hafenrichter, L.D.; Hoh, J.C.; Mazer, J.J.; Surchik, M.T.; Wolf, S.F.; and Wronkiewicz, D.J. 1995. *ANL Technical Support Program for DOE Environmental Restoration and Waste Management. Annual Report, October 1993 - September 1994.* ANL 95/20. Argonne, Illinois: Argonne National Laboratory, Chemical Technology Division. ACC: MOL.20011011.0022.

144956 Beckman, R.; Thomas, K.; and Crowe, B. 1988. *Preliminary Report on the Statistical Evaluation of Sorption Data: Sorption as a Function of Mineralogy, Temperature, Time, and Particle Size.* LA-11246-MS. Los Alamos, New Mexico: Los Alamos National Laboratory. ACC: NNA.19890918.0500.

173041 Bitea, C.; Müller, R.; Neck, V.; Walther, C.; and Kim, J.I. 2003. "Study of the Generation and Stability of Thorium(IV) Colloids by LIBD Combined with Ultrafiltration." *Colloids and Surfaces A: Physicochemical and Engineering Aspects, 217,* 63-70. New York, New York: Elsevier. TIC: 257099.

174504 Bitea, C.; Walther, C.; Kim, J.I.; Geckeis, H.; Rabung, T.; Scherbaum, F.J.; and Cacuci, D.G. 2003. "Time-Resolved Observation of ZrO_2-Colloid Agglomeration." *Colloids and Surfaces A: Physicochemical and Engineering Aspects, 215,* 55-66. New York, New York: Elsevier. TIC: 257515.

179538 Bradbury, M.H. and Baeyens, B. 2005. "Modeling the Sorption of Mn(II), Co(II), Ni(II), Zn(II), Cd(II), Eu(III), Am(III), Sn(IV), Th(IV), Np(V) and U(VI) on Montmorillonite: Linear Free Energy Relationships and Estimates of Surface Binding Constants for Some Selected Heavy Metals and Actinides." *Geochimica et Cosmoschimica Acta, 69,* (4), 875-892. New York, New York: Elsevier. TIC: 259202.

179541 Bradbury, M.H. and Baeyens, B. 2006. "Modelling Sorption Data for the Actinides Am(III), Np(V) and Pa(V) on Montmorillonite." *Radiochimica Acta, 94,* 619-625. München, Germany: Oldenbourg Wissenschaftsverlag. TIC: 259214.

169991 BSC (Bechtel SAIC Company) 2004. *Evaluation of Potential Impacts of Microbial Activity on Drift Chemistry.* ANL-EBS-MD-000038 REV 01. Las Vegas, Nevada: Bechtel SAIC Company. ACC: DOC.20041118.0005; DOC.20050505.0001; DOC.20050609.0001.

170006 BSC 2004. *Saturated Zone Colloid Transport.* ANL-NBS-HS-000031 REV 02. Las Vegas, Nevada: Bechtel SAIC Company. ACC: DOC.20041008.0007; DOC.20051215.0005.

175539 BSC 2005. *Q-List.* 000-30R-MGR0-00500-000-003. Las Vegas, Nevada: Bechtel SAIC Company. ACC: ENG.20050929.0008.

177389 BSC 2006. *Technical Work Plan for Waste Form Testing and Modeling.* TWP-WIS-MD-000018 REV 01. Las Vegas, Nevada: Bechtel SAIC Company. ACC: DOC.20060817.0001.

109494 Buck, E.C. and Bates, J.K. 1999. "Microanalysis of Colloids and Suspended Particles from Nuclear Waste Glass Alteration." *Applied Geochemistry, 14,* 635-653. New York, New York: Elsevier. TIC: 245946.

172668 Buck, E.C.; Hanson, B.D.; and McNamara, B.K. 2004. "The Geochemical Behaviour of Tc, Np, and Pu in Spent Nuclear Fuel in an Oxidizing Environment." *Energy, Waste, and the Environment: A Geochemical Perspective.* Giere, R. and Stille, P.; eds. Geological Society of London Special Publications, 236. Pages 65-88. London, England: Geological Society of London. TIC: 256910.

171479 Buck, E.C.; McNamara, B.K.; and Hanson, B.D. 2004. *Alternative Conceptual Model for Colloid Generation from Commercial Spent Nuclear Fuel.* PNNL-14306. Richland, Washington: Pacific Northwest National Laboratory. ACC: MOL.20040901.0242.

112904 Buck, E.C.; Wronkiewicz, D.J.; Finn, P.A.; and Bates, J.K. 1997. "A New Uranyl Oxide Hydrate Phase Derived from Spent Fuel Alteration." *Journal of Nuclear Materials, 249,* (1), 70-76. Amsterdam, The Netherlands: Elsevier. TIC: 234844.

161653 Buffle, J.; Wilkinson, K.J.; Stoll, S.; Filella, M.; and Zhang, J. 1998. "A Generalized Description of Aquatic Colloidal Interactions: The Three-Colloidal Component Approach." *Environmental Science & Technology, 32,* (19), 2887-2899. Washington, D.C.: American Chemical Society. TIC: 253710.

110975 Burns, P.C. 1999. "Cs Boltwoodite Obtained by Ion Exchange from Single Crystals: Implications for Radionuclide Release in a Nuclear Repository." *Journal of Nuclear Materials, 265,* 218-223. Amsterdam, The Netherlands: Elsevier. TIC: 246432.

166275 Canori, G.F. and Leitner, M.M. 2003. *Project Requirements Document.* TER-MGR-MD-000001 REV 02. Las Vegas, Nevada: Bechtel SAIC Company. ACC: DOC.20031222.0006.

179540 Cantrell, K.J.; Serne, R.J.; and Last, G.V. 2002. *Hanford Contaminant Distribution Coefficient Database and Users Guide.* PNNL-13895. Richland, Washington: Pacific Northwest National Laboratory. ACC: LLR.20070323.0003.

162732 Contardi, J.S.; Turner, D.R.; and Ahn, T.M. 2001. "Modeling Colloid Transport for Performance Assessment." *Journal of Contaminant Hydrology, 47,* (2-4), 323-333. New York, New York: Elsevier. TIC: 253918.

131861 CRWMS (Civilian Radioactive Waste Management System) M&O (Management and Operating Contractor) 2000. *Commercial Spent Nuclear Fuel Degradation in Unsaturated Drip Tests.* Input Transmittal WP-WP-99432.T. Las Vegas, Nevada: CRWMS M&O. ACC: MOL.20000107.0209.

154071 CRWMS M&O 2001. *Colloid-Associated Radionuclide Concentration Limits: ANL.* ANL-EBS-MD-000020 REV 00 ICN 01. Las Vegas, Nevada: CRWMS M&O. ACC: MOL.20010216.0003.

154818 Cunnane, J.C. 2001. ANL Waste Form Task Progress Report for November and December 2000. Letter from J.C. Cunnane (ANL) to Dr. C. Stockman (SNL), January 24, 2001. ACC: MOL.20010508.0127.

143280 Davis, J.A. and Kent, D.B. 1990. "Surface Complexation Modeling in Aqueous Geochemistry." *Mineral-Water Interface Geochemistry.* Hochella, M.F., Jr. and White, A.F., eds. Reviews in Mineralogy Volume 23. Pages 177-260. Washington, D.C.: Mineralogical Society of America. TIC: 224085.

153651 Degueldre, C.; Triay, I.; Kim, J-I; Vilks, P.; Laaksoharju, M.; and Miekeley, N. 2000. "Groundwater Colloid Properties: A Global Approach." *Applied Geochemistry, 15,* (7), 1043-1051. New York, New York: Pergamon Press. TIC: 249340.

174069 Degueldre, C.; Ulrich, H.J.; and Silby, H. 1994. "Sorption of ^{241}Am onto Montmorillonite, Illite and Hematite Colloids." *Radiochimica Acta, 65,* 173-179. München, Germany: R. Oldenbourg Verlag. TIC: 257440.

164019 Dehaudt, P. 2001. "Physical and Chemical State of the Nuclear Spent Fuel After Irradiation." Section 5.2 of *Synthesis on the Long Term Behavior of the Spent Nuclear Fuel.* Poinssot, C., ed. CEA-R-5958(E). Volume I. Paris, France: Commissariat à l'Énergie Atomique. TIC: 253976.

164037 Dehaudt, P. 2001. "State of the Art of the Oxidation of Spent Nuclear Fuel." Section 7.2 of *Synthesis on the Long Term Behavior of the Spent Nuclear Fuel.* Poinssot, C., ed. CEA-R-5958(E). Volume II. Paris, France: Commissariat à l'Énergie Atomique. TIC: 253976.

179542 Dietz, N.L. 2005. *Transmission Electron Microscopy Analysis of Corroded EBR II Metallic Waste Forms.* ANL-05/09. Argonne, Illinois: Argonne National Laboratory, Chemical Engineering Division. ACC: LLR.20070323.0007.

158405 DOE (U.S. Department of Energy) 2002. *DOE Spent Nuclear Fuel Information in Support of TSPA-SR.* DOE/SNF/REP-047, Rev. 2. Idaho Falls, Idaho: U.S. Department of Energy, Idaho Operations Office. TIC: 252089.

166268 DOE 2003. *Review of DOE Spent Nuclear Fuel Release Rate Test Results.* DOE/SNF/REP-073, Rev. 0. Idaho Falls, Idaho: U.S. Department of Energy, Idaho Operations Office. ACC: DOC.20030905.0010.

182051 DOE 2007. *Quality Assurance Requirements and Description.* DOE/RW-0333P, Rev. 19. Washington, D. C.: U.S. Department of Energy, Office of Civilian Radioactive Waste Management. ACC: DOC.20070717.0006.

173086 Douglas, M.; Clark, S.B.; Friese, J.I.; Arey, B.W.; Buck, E.C.; Hanson, B.D.; Utsunomiya, S.; and Ewing, R.C. 2005. "Microscale Characterization of Uranium(VI) Silicate Solids and Associated Neptunium(V)." *Radiochimica Acta, 93,* 265-272. München, Germany: Oldenbourg Wissenschaftsverlag. TIC: 257469.

179546 Douglas, M.; Clark, S.B.; Utsunomiya, S.; and Ewing, R.C. 2002. "Cesium and Strontium Incorporation into Uranophane, $Ca[(UO_2)(SiO_3OH)]_2 \cdot 5H_2O$]." *Journal of Nuclear Science and Technology, Supplement 3,* 504-507. Tokyo, Japan: Atomic Energy Society of Japan. TIC: 259213.

170925 Duff, M.C.; Hunter, D.B.; Triay, I.R.; Bertsch, P.M.; Reed, D.T.; Sutton, S.R.; Shea-McCarthy, G.; Kitten, J.; Eng, P.; Chipera, S.J.; and Vaniman, D.T. 1999. "Mineral Associations and Average Oxidation States of Sorbed Pu on Tuff." *Environmental Science & Technology, 33,* (13), 2163-2168. Washington, D.C.: American Chemical Society. TIC: 256464.

147475 EPA (U.S. Environmental Protection Agency) 1999. *Understanding Variation in Partition Coefficient, Kd, Values.* EPA 402-R-99-004A&B Two volumes. Washington, D.C.: U.S. Environmental Protection Agency. TIC: 249201.

172215 EPA 2004. "Review of Geochemistry and Available K_d Values for Americium, Arsenic, Curium, Iodine, Neptunium, Radium, and Technetium." Volume III of *Understanding the Variation in Partition Coefficient, K_d, Values.* EPA 402-R-04-002C. Washington, D.C.: U.S. Environmental Protection Agency. ACC: MOL.20041102.0060.

101611 Feng, X.; Buck, E.C.; Mertz, C.; Bates, J.K.; Cunnane, J.C.; and Chaiko, D.J. 1994. "Characteristics of Colloids Generated during the Corrosion of Nuclear Waste Glasses in Groundwater." *Radiochimica Acta, 66/67,* 197-205. München, Germany: R. Oldenbourg Verlag. TIC: 238720.

113030 Finch, R.J. and Ewing, R.C. 1992. "The Corrosion of Uraninite Under Oxidizing Conditions." *Journal of Nuclear Materials, 190,* 133-156. Amsterdam, The Netherlands: Elsevier. TIC: 246369.

100746 Finn, P.A.; Buck, E.C.; Gong, M.; Hoh, J.C.; Emery, J.W.; Hafenrichter, L.D.; and Bates, J.K. 1994. "Colloidal Products and Actinide Species in Leachate from Spent Nuclear Fuel." *Radiochimica Acta, 66/67,* 197-203. München, Germany: R. Oldenbourg Verlag. TIC: 238493.

100392 Finn, P.A.; Wronkiewicz, D.J.; Finch, R.J.; Hoh, J.C.; Mertz, C.; Emery, J.W.; Buck, E.C.; Fortner, J.; Wolf, S.F.; Neimark, L.A.; and Bates, J.K. 1998. *Yucca Mountain Project — Argonne National Laboratory, Annual Progress Report, FY 1997 for Activity WP1221 Unsaturated Drip Condition Testing of Spent Fuel and Unsaturated Dissolution Tests of Glass.* ANL-98/12. Argonne, Illinois: Argonne National Laboratory. ACC: MOL.19980818.0230.

114452 Fortner, J.A.; Bates, J.K.; and Gerding, T.J. 1997. *Analysis of Components from Drip Tests with ATM-10 Glass.* ANL-96/16. Argonne, Illinois: Argonne National Laboratory. TIC: 246306.

164361 Fowler, J.R. 2003. *Projected Glass Composition and Curie Content of Canisters from the Savannah River Site (U).* JKLW-SRS-2003-002, Rev. 1. Aiken, South Carolina: Westinghouse Savannah River Company, Savannah River Site. ACC: MOL.20030722.0096.

113253 Grambow, B.; Loida, A.; Dressler, P.; Geckeis, H.; Gago, J.; Casas, I.; de Pablo, J.; Giménez, J.; and Torrero, M.E. 1996. *Long-term Safety of Radioactive Waste Disposal: Chemical Reaction of Fabricated and High Burnup Spent UO2 Fuel with Saline Brines.* FZKA 5702. Final Report. Karlsruhe, Germany: Forschungszentrum Karlsruhe GmbH. TIC: 246887.

179547 Gunnarsson, M.; Rasmusson, M.; Wall, S.; Ahlberg, E.; and Ennis, J. 2001. "Electroacoustic and Potentiometric Studies of the Hematite/Water Interface." *Journal of Colloid and Interface Science, 240,* 448-458. New York, New York: Academic Press. TIC: 259215.

101672 Hanson, B.D. 1998. *The Burnup Dependence of Light Water Reactor Spent Fuel Oxidation.* PNNL-11929. Richland, Washington: Pacific Northwest National Laboratory. TIC: 238459.

100123 Hardin, E.L. 1998. *Near-Field/Altered-Zone Models Report.* UCRL-ID-129179. Livermore, California: Lawrence Livermore National Laboratory.ACC: MOL.19980630.0560.

174075 Haschke, J.M. 1998. "Corrosion of Uranium in Air and Water Vapor: Consequences for Environmental Dispersal." *Journal of Alloys and Compounds, 278,* 149-160. New York, New York: Elsevier. TIC: 257449.

100750 Hersman, L. 1995. *Microbial Effects on Colloidal Agglomeration.* LA-12972-MS. Los Alamos, New Mexico: Los Alamos National Laboratory. ACC: MOL.19971210.0253.

161657 Honeyman, B.D. and Ranville, J.F. 2002. "Colloid Properties and their Effects on Radionuclide Transport through Soils and Groundwaters." Chapter 7 of *Geochemistry of Soil Radionuclides.* Zhang, P-C. and Brady, P.V., eds. SSSA Special Publication Number 59. Madison, Wisconsin: Soil Science Society of America. TIC: 253952.

179548 Honig, E.P.; Roebersen, G.J.; and Wiersema, P.H. 1971. "Effect of Hydrodynamic Interaction on the Coagulation Rate of Hydrophobic Colloids." *Journal of Colloid and Interface Science, 36,* (1), 97-109. New York, New York: Elsevier. TIC: 259212.

174350 Hsu, W.P.; Rönnquist, L.; and Matijevic, E. 1988. "Preparation and Properties of Monodispersed Colloidal Particles of Lanthanide Compounds. 2. Cerium (IV)." *Langmuir, 4,* (1), 31-37. Washington, D.C.: American Chemical Society. TIC: 257454.

179549 Huang, A.Y. and Berg, J.C. 2006. "High-Salt Stabilization of Laponite Clay Particles." *Journal of Colloid and Interface Science, 296,* 159-164. New York, New York: Elsevier. TIC: 259211.

170882 Ibrahim, S.A. and Salazar, W.R. 2000. "Physicochemical Speciation of Americium in Soils from Rocky Flats, Colorado, USA." *Journal of Radioanalytical and Nuclear Chemistry, 243,* (2), 347-351. Dordrecht, The Netherlands: Kluwer Academic Publishers. TIC: 256466.

178810 Ilton, E.S.; Liu, C.; Yantasee, W.; Wang, Z.; Moore, D.A.; Felmy, A.R.; and Zachara, J.M. 2006. "The Dissolution of Synthetic Na-Boltwoodite in Sodium Carbonate Solutions." *Geochimica et Cosmochimica Acta, 70,* 4836-4849. New York, New York: Elsevier. TIC: 259016.

172518 Iwasaki, M.; Sakurai, T.; Ishikawa, N.; and Kobayashi, Y. 1968. "Oxidation of UO2 Pellets in Airm Effect of Heat-Treatment of Pellet on Particle Size Distribution of Powders Produced." *Journal of Nuclear Science and Technology, 5,* (12), 652-653. Tokyo, Japan: Atomic Energy Society of Japan. TIC: 255938.

180834 Jara, A.A.; Goldberg, S.; and Mora, M.L. 2005. "Studies of the Surface Charge of Amorphous Aluminosilicates Using Surface Complexation Models." *Journal of Colloid and Interface Science, 292,* 160-170. New York, New York: Elsevier. TIC: 259358.

179550 Kaminski, M.D.; Dimitrijevic, N.M.; Mertz, C.J.; and Goldberg, M.M. 2005. "Colloids from the Aqueous Corrosion of Uranium Nuclear Fuel." *Journal of Nuclear Materials, 347,* 77-87. New York, New York: Elsevier. TIC: 259210.

103282 Kersting, A.B.; Efurd, D.W.; Finnegan, D.L.; Rokop, D.J.; Smith, D.K.; and Thompson, J.L. 1999. "Migration of Plutonium in Ground Water at the Nevada Test Site." *Nature, 397,* (6714), 56-59. London, England: Macmillan Journals. TIC: 243597.

162421 Kersting, A.P. and Reimus, P.W., eds. 2003. *Colloid-Facilitated Transport of Low-Solubility Radionuclides: A Field, Experimental, and Modeling Investigation.* UCRL-ID-149688. Livermore, California: Lawrence Livermore National Laboratory. TIC: 254176.

179551 Kim, C-W.; Wronkiewicz, D.J.; Finch, R.J.; and Buck, E.C. 2006. "Incorporation of Cerium and Neodymium in Uranyl Phases." *Journal of Nuclear Materials, 353,* 147-157. New York, New York: Elsevier. TIC: 259209.

109521 Kim, J.I. 1994. "Actinide Colloids in Natural Aquifer Systems." *MRS Bulletin, 19,* (12), 47-53. Pittsburgh, Pennsylvania: Materials Research Society. TIC: 246128.

113930 Kingston, W.L. and Whitbeck, M. 1991. *Characterization of Colloids Found in Various Groundwater Environments in Central and Southern Nevada.* DOE/NV/10384-36. Las Vegas, Nevada: Desert Research Institute, Water Resources Center. ACC: NNA.19930607.0073.

180997 Kraepiel, A.M.L.; Keller, K.; and Morel, F.M.M. 1999. "A Model for Metal Adsorption on Montmorillonite." *Journal of Colloid and Interface Science, 210,* (1999), 43-54. New York, New York: Academic Press. TIC: 259419.

179654 Krupka, K.M.; Schaef, H.T.; Arey, B.W.; Heald, S.M.; Deutsch, W.J.; Lindberg, M.J.; and Cantrell, K.J. 2006. "Residual Waste from Hanford Tanks 241-C-203 and 241-C-204. 1. Solids Characterization." *Environmental Science & Technology, 40,* (12), 3749-3754. Washington, D.C.: American Chemical Society. TIC: 259229.

100051 Langmuir, D. 1997. *Aqueous Environmental Geochemistry.* Upper Saddle River, New Jersey: Prentice Hall. TIC: 237107.

168991 Leenaers, A.; Sannen, L.; Van den Berghe, S.; and Verwerft, M. 2003. "Oxidation of Spent UO_2 Fuel Stored in Moist Environment." *Journal of Nuclear Materials, 317,* (2-3), 226-233. New York, New York: Elsevier. TIC: 256014.

109524 Liang, L. and Morgan, J.J. 1990. "Chemical Aspects of Iron Oxide Coagulation in Water: Laboratory Studies and Implications for Natural Systems." *Aquatic Sciences, 52,* (1), 32-55. Basel, Switzerland: Birkhauser Verlag. TIC: 246125.

101876 Lide, D.R., ed. 1995. *CRC Handbook of Chemistry and Physics.* 76th Edition. Boca Raton, Florida: CRC Press. TIC: 216194.

131202 Lide, D.R., ed. 1991. *CRC Handbook of Chemistry and Physics.* 72nd Edition. Boca Raton, Florida: CRC Press. TIC: 3595.

161667 Litaor, M.I. and Ibrahim, S.A. 1996. "Plutonium Association with Selected Solid Phases in Soils of Rocky Flats, Colorado, Using Sequential Extraction Technique." *Journal of Environmental Quality, 25,* (5), 1144-1151. Madison, Wisconsin: American Society of Agronomy. TIC: 252783.

172864 Liu, C.; Cox, D.S.; Barrand, R.D.; and Hunt, C.E.L. 1992. "Particle Size Distributions of U_3O_3 Produced by Oxidation in Air at 300-900ºC." *Proceeding of the 13th Annual Conference, Saint John, NB, June 7-10, 1992. 1,* 1-22. Toronto, Ontario, Canada: Canadian Nuclear Society. TIC: 256950.

166315 Lu, N.; Conca, J.; Parker, G.R.; Leonard, P.A.; Moore, B.; Strietelmeier, B.; and Triay, I.R. 2000. *Adsorption of Actinides onto Colloids as a Function of Time, Temperature, Ionic Strength, and Colloid Concentration, Waste Form Colloids Report for Yucca Mountain Program (Colloid Data Summary from 1999 to 2000 Research).* LA-UR-00-5121. Los Alamos, New Mexico: Los Alamos National Laboratory. ACC: MOL.20031204.0108.

170883 Lu, N.; Reimus, P.W.; Parker, G.R.; Conca, J.L.; and Triay, I.R. 2003. "Sorption Kinetics and Impact of Temperature, Ionic Strength and Colloid Concentration on the Adsorption of Plutonium-239 by Inorganic Colloids." *Radiochimica Acta, 91,* 713-720. München, Germany: Oldenbourg Wissenschaftsverlag. TIC: 256462.

100946 Lu, N.; Triay, I.R.; Cotter, C.R.; Kitten, H.D.; and Bentley, J. 1998. *Reversibility of Sorption of Plutonium-239 onto Colloids of Hematite, Goethite, Smectite, and Silica.* LA-UR-98-3057. Los Alamos, New Mexico: Los Alamos National Laboratory. ACC: MOL.19981030.0202.

180831 Luckscheiter, B. and Kienzler, B. 2001. "Determination of Sorption Isotherms for Eu, Th, U, and Am on the Gel Layer of Corroded HLW Glass." *Journal of Nuclear Materials, 298,* 155-162. New York, New York: Elsevier. TIC: 259360.

170884 Luckscheiter, B. and Nesovic, M. 2002. "Sorption Behaviour of Am on Precorroded HLW Glass in Water and Brines." *Radiochimica Acta, 90,* 537-541. München, Germany: Oldenbourg Wissenchaftsverlag. TIC: 256461.

180995 Madden, A.S.; Hochella, M.F., Jr.; and Luxton, T.P. 2006. "Insights for Size-Dependent Reactivity of Hematite Nanomineral Surfaces through Cu^{2+} Sorption." *Geochimica et Cosmochimica Acta, 70,* 4095-4104. New York, New York: Elsevier. TIC: 259420.

108215 McCarthy, J.F. and Degueldre, C. 1993. "Sampling and Characterization of Colloids and Particles in Groundwater for Studying Their Role in Contaminant Transport." *Environmental Particles.* Buffle, J. and van Leeuwen, H.P., eds. Environmental Analytical and Physical Chemistry Series Volume 2. Pages 247-315. Boca Raton, Florida: Lewis Publishers. TIC: 245905.

100778 McCarthy, J.F. and Zachara, J.M. 1989. "Subsurface Transport of Contaminants." *Environmental Science & Technology, 23,* (5), 496-502. Easton, Pennsylvania: American Chemical Society. TIC: 224876.

113270 McEachern, R.J. and Taylor, P. 1998. "A Review of the Oxidation of Uranium Dioxide at Temperatures Below 400°C." *Journal of Nuclear Materials, 254,* 87-121. Amsterdam, The Netherlands: Elsevier. TIC: 246427.

179552 McKinley, J.P.; Zachara, J.M.; Liu, C.; Heald, S.C.; Prenitzer, B.I.; and Kempshall, B.W. 2006. "Microscale Controls on the Fate of Contaminant Uranium in the Vadose Zone, Hanford Site, Washington." *Geochimica et Cosmochimica Acta, 70,* 1873-1887. New York, New York: Elsevier. TIC: 259208.

174068 McNamara, B.; Hanson, B.; Buck, E.; and Soderquist, C. 2005. "Corrosion of Commercial Spent Nuclear Fuel. 2. Radiochemical Analyses of Metastudtite and Leachates." *Radiochimica Acta, 93,* 169-175. München, Germany: Oldenbourg Wissenschaftsverlag. TIC: 257131.

171053 Menard, O.; Advocat, T.; Ambrosi, J.P.; and Michard, A. 1998. "Behavior of Actinides (Th, U, Np and Pu) and Rare Earths (La, Ce and Nd) During Aqueous Leaching of a Nuclear Waste Glass Under Geological Disposal Conditions." *Applied Geochemistry, 13,* 105-126. New York, New York: Pergamon. TIC: 256470.

162161 Mertz, C.; Fortner, J.; Goldberg, M.; and Shelton-Davis, C. 2000. *Colloid Generation from Metallic Uranium Fuel.* Argonne, Illinois: Argonne National Laboratory. TIC: 254296.

162032 Mertz, C.J.; Finch, R.J.; Fortner, J.A.; Jerden, J.L., Jr.; Yifen, T.; Cunnane, J.C.; and Finn, P.A. 2003. *Characterization of Colloids Generated from Commercial Spent Nuclear Fuel Corrosion.* Activity Number: PAWTP30A. Argonne, Illinois: Argonne National Laboratory. ACC: MOL.20030422.0337.

100801 Minai, Y.; Choppin, G.R.; and Sisson, D.H. 1992. "Humic Material in Well Water from the Nevada Test Site." *Radiochimica Acta, 56,* 195-199. München, Germany: R. Oldenbourg Verlag. TIC: 238763.

113272 Murakami, T.; Ohnuki, T.; Isobe, H.; and Sato, T. 1997. "Mobility of Uranium During Weathering." *American Mineralogist, 82,* 888-899. Washington, D.C.: Mineralogical Society of America. TIC: 246053.

175700 Murakami, T.; Sato, T.; Ohnuki, T.; and Isobe, H. 2005. "Field Evidence for Uranium Nanocrystallization and its Implications for Uranium Transport." *Chemical Geology, 221,* 117-126. New York, New York: Elsevier. TIC: 257883.

101882 NCRP (National Council on Radiation Protection and Measurements) 1996. *Screening Models for Releases of Radionuclides to Atmosphere, Surface Water, and Ground.* NCRP Report No. 123 I. Bethesda, Maryland: National Council on Radiation Protection and Measurements. TIC: 225158.

179554 Novikov, A.P.; Kalmykov, S.N.; Utsunomiya, S.; Ewing, R.C.; Horreard, F.; Merkulov, A.; Clark, S.B.; Tkachev, V.V.; and Myasoedov, B.F. 2006. "Colloid Transport of Plutonium in the Far-Field of the Mayak Production Association, Russia." *Science, 314,* 638-641. Washington, D.C.: American Association for the Advancement of Science. TIC: 259207.

163274 NRC (U.S. Nuclear Regulatory Commission) 2003. *Yucca Mountain Review Plan, Final Report.* NUREG-1804, Rev. 2. Washington, D.C.: U.S. Nuclear Regulatory Commission, Office of Nuclear Material Safety and Safeguards. TIC: 254568.

121867 Nuttall, H.E. 1986. *Population Balance Model for Colloid Transport NNWSI Report/Milestone R318.* LA-UR 86-1914. Los Alamos, New Mexico: Los Alamos National Laboratory. ACC: NNA.19891102.0024.

179555 Pabalan, R.T. and Turner, D.R. 1997. "Uranium(6+) Sorption on Montmorillonite: Experimental and Surface Complexation Modeling Study." *Aquatic Geochemistry, 2,* 203-226. Dordrecht, The Netherlands: Kluwer Academic Publishers. TIC: 237077.

174071 Painter, S.; Cvetkovic, V.; Pickett, D.; and Turner, D.R. 2002. "Significance of Kinetics for Sorption of Inorganic Colloids: Modeling and Experiment Interpretation Issues." *Environmental Science & Technology, 36,* (24), 5369-5375. Washington, D.C.: American Chemical Society. TIC: 257438.

174361 Parks, G.A. 1964. "The Isoelectric Points of Solid Oxides, Solid Hydroxides, and Aqueous Hydroxo Complex Systems." *Chemical Reviews, 65,* (2), 177-198. Washington, D.C.: American Chemical Society. TIC: 257467.

110223 Pearcy, E.C.; Prikryl, J.D.; and Leslie, B.W. 1995. "Uranium Transport Through Fractured Silicic Tuff and Relative Retention in Areas with Distinct Fracture Characteristics." *Applied Geochemistry, 10,* 685-704. Oxford, United Kingdom: Elsevier. TIC: 246848.

174351 Pirlet, V. 2001. "Overview of Actinides (Np, Pu, Am) and Tc Release from Waste Glasses: Influence of Solution Composition." *Journal of Nuclear Materials, 298,* 47-54. New York, New York: Elsevier. TIC: 257455.

171519 Poulton, S.W.; Krom, M.D.; and Raiswell, R. 2004. "A Revised Scheme for the Reactivity of Iron (Oxyhydr)Oxide Minerals Toward Dissolved Sulfide." *Geochimica et Cosmochimica Acta, 68,* (18), 3703-3715. New York, New York: Pergamon. TIC: 256498.

180836 Powell, B.A.; Fjeld, R.A.; Kaplan, D.I.; Coates, J.T.; and Serkiz, S.M. 2004. "$Pu(V)O_2^+$ Adsorption and Reduction by Synthetic Magnetite (Fe_3O_4)." *Environmental Science & Technology, 38,* (22), 6016-6024. Washington, D. C.: American Chemical Society. TIC: 259363.

174726 Powell, B.A.; Fjeld, R.A.; Kaplan, D.I.; Coates, J.T.; and Serkiz, S.M. 2005. "$Pu(V)O_2^+$ Adsorption and Reduction by Synthetic Hematite and Goethite." *Environmental Science & Technology, 39,* (7), 2107-2114. Washington, D.C.: American Chemical Society. TIC: 257576.

144603 Ramsay, J.D.F.; Avery, R.G.; and Russell, P.J. 1988. "Physical Characteristics and Sorption Behaviour of Colloids Generated from Cementitious Systems." *Radiochimica Acta, 44/45,* 119-124. München, Germany: R. Oldenbourg Verlag. TIC: 226318.

171518 Roden, E.E. and Zachara, J.M. 1996. "Microbial Reduction of Crystalline Iron(III) Oxides: Influence of Oxide Surface Area and Potential for Cell Growth." *Environmental Science & Technology, 30,* (5), 1618-1628. Washington, D.C.: American Chemical Society. TIC: 256499.

170890 Romanovski, V.V.; Brachmann, A.; Palmer, C.E.; Shaw, H.F.; Bourcier, W.L.; and Jardine, L.J. 1999. *Characterization of Pu Colloidal and Aqueous Species in Yucca Mountain Groundwater Surrogate.* UCRL-JC-134460. Livermore, California: Lawrence Livermore National Laboratory. ACC: MOL.20040930.0291.

179556 Ruckenstein, E. and Huang, H. 2003. "Colloid Restabilization at High Electrolyte Concentrations: Effect of Ion Valency." *Langmuir, 19,* (7), 3049-3055. Washington, D.C.: American Chemical Society. TIC: 259206.

168432 Runde, W.; Conradson, S.D.; Efurd, D.W.; Lu, N.P.; VanPelt, C.E.; and Tait, C.D. 2002. "Solubility and Sorption of Redox-Sensitive Radionuclides (Np, Pu) in J-13 Water from the Yucca Mountain Site: Comparison between Experiment and Theory." *Applied Geochemistry, 17,* (6), 837-853. New York, New York: Pergamon. TIC: 254046.

180525 Ryan, J.N. and Gschwend, P.M. 1994. "Effects of Ionic Strength and Flow Rate on Colloid Release: Relating Kinetics to Intersurface Potential Energy." *Journal of Colloid and Interface Science, 164,* 21-34. New York, New York: Academic Press. TIC: 259322.

174507 Schindler, M.; Mutter, A.; Hawthorne, F.C.; and Putnis, A. 2004. "Prediction of Crystal Morphology of Complex Uranyl-Sheet Minerals. I. Theory." *The Canadian Mineralogist, 42,* (6), 1629-1649. Ottawa, Ontario, Canada: Mineralogical Association of Canada. TIC: 257517.

147681 Serne, R.J. and Relyea, J.F. 1982. *The Status of Radionuclide Sorption-Desorption Studies Performed by the WRIT Program.* PNL-3997. Richland, Washington: Pacific Norwest Laboratory. ACC: NNA.19900416.0121.

179559 Smailos, E.; Cuñado, M.Á.; Azkarate, I.; Kursten, B.; and Marx, G. 2003. *Long-Term Performance of Candidate Materials for HLW/Spent Fuel Disposal Containers.* FZKA 6809. Karlsruhe, Germany: Forschungszentrum Karlsruhe GmbH. TIC: 259248.

177418 SNL (Sandia National Laboratories) 2007. *Dissolved Concentration Limits of Elements with Radioactive Isotopes.* ANL-WIS-MD-000010 REV 06. Las Vegas, Nevada: Sandia National Laboratory. ACC: DOC.20070918.0010.

177407 SNL 2007. *EBS Radionuclide Transport Abstraction.* ANL-WIS-PA-000001 REV 03. Las Vegas, Nevada: Sandia National Laboratories. ACC: DOC.20071004.0001.

177412 SNL 2007. *Engineered Barrier System: Physical and Chemical Environment.* ANL-EBS-MD-000033 REV 06. Las Vegas, Nevada: Sandia National Laboratories. ACC: DOC.20070907.0003.

180506 SNL 2007. *In-Package Chemistry Abstraction.* ANL-EBS-MD-000037 REV 04 ADD 01. Las Vegas, Nevada: Sandia National Laboratories. ACC: DOC.20051130.0007; DOC.20070816.0004.

181006 SNL 2007. *Particle Tracking Model and Abstraction of Transport Processes.* MDL-NBS-HS-000020 REV 02 ADD 01. Las Vegas, Nevada: Sandia National Laboratories. ACC: DOC.20070823.0005.

177424 SNL 2007. *Radionuclide Screening.* ANL-WIS-MD-000006 REV 02. Las Vegas, Nevada: Sandia National Laboratories. ACC: DOC.20070326.0003.

177391 SNL 2007. *Saturated Zone Site-Scale Flow Model.* MDL-NBS-HS-000011 REV 03. Las Vegas, Nevada: Sandia National Laboratories. ACC: DOC.20070626.0004.

177392 SNL 2007. *Site-Scale Saturated Zone Transport.* MDL-NBS-HS-000010 REV 03. Las Vegas, Nevada: Sandia National Laboratories. ACC: DOC.20070822.0003.

170928 Sondi, I.; Bišcan, J.; and Pravdic, V. 1996. "Electrokinetics of Pure Clay Minerals Revisited." *Journal of Colloid and Interface Science, 178,* 514-522. New York, New York: Academic Press. TIC: 256468.

174080 Spino, J.; Vennix, K.; and Coquerelle, M. 1996. "Detailed Characterisation of the Rim Microstructure in PWR Fuels in the Burn-Up Range 40-67 GWd/tM." *Journal of Nuclear Materials, 231,* 179-190. New York, New York: Elsevier. TIC: 257447.

147477 Stenhouse, M.J. 1995. *Sorption Databases for Crystalline, Marl and Bentonite for Performance Assessment.* NAGRA Technical Report 93-06. Wettingen, Switzerland: National Cooperative for the Disposal of Radioactive Waste. TIC: 247885.

179561 Tachi, Y.; Shibutani, T.; Sato, H.; and Yui, M. 2001. "Experimental and Modeling Studies on Sorption and Diffusion of Radium in Bentonite." *Journal of Contaminant Hydrology, 47,* 171-186. New York, New York: Elsevier. TIC: 259205.

170891 Taunton, A.E.; Welch, S.A.; and Banfield, J.F. 2000. "Microbial Controls on Phosphate and Lanthanide Distributions During Granite Weathering and Soil Formation." *Chemical Geology, 169,* 371-382. New York, New York: Elsevier. TIC: 256459.

125815 Taylor, P.; Wood, D.D.; and Owen, D.G. 1995. "Microstructures of Corrosion Films on UO_2 Fuel Oxidized in Air–Steam Mixtures at 225ºC." *Journal of Nuclear Materials, 223,* (3), 316-320. New York, New York: Elsevier. TIC: 256013.

163048 Thomas, E. 2003. "Transmittal of Unsaturated Testing of Bare Spent UO_2 Fuel Fragments: Data Report, Argonne National Laboratory." Interoffice memorandum from E. Thomas (BSC) to J.C. Cunnane, July 2, 2003, 0702037939, with attachment. ACC: MOL.20030702.0116; MOL.20030311.0097.

174073 Tombácz, E. and Szekeres, M. 2004. "Colloidal Behavior of Aqueous Montmorillonite Suspensions: The Specific Role of pH in the Presence of Indifferent Electrolytes." *Applied Clay Science, 27,* 75-94. New York, New York: Elsevier. TIC: 257450.

112690 Tombácz, E.; Abraham, I.; Gilde, M.; and Szanto, F. 1990. "The pH-Dependent Colloidal Stability of Aqueous Montmorillonite Suspensions." *Colloids and Surfaces, 49,* 71-80. Amsterdam, The Netherlands: Elsevier. TIC: 246046.

171770 Torstenfelt, B.; Andersson, K.; and Allard, B. 1982. "Sorption of Strontium and Cesium on Rocks and Minerals." *Chemical Geology, 36,* 128-137. Amsterdam, The Netherlands: Elsevier. TIC: 256583.

172072 Traexler, K.A.; Utsunomiya, S.; Kersting, A.B.; and Ewing, R.C. 2004. "Colloid Transport of Radionuclides: Yucca Mountain Performance Assessment." *Scientific Basis for Nuclear Waste Management XXVII, Symposium held April 12-16, 2004, San Francisco, CA, USA. 807,* 1-6. Warrendale, Pennsylvania: Materials Research Society. TIC: 256677.

100789 Triay, I.; Simmons, A.; Levy, S.; Nelson, S.; Nuttall, H.; Robinson, B.; Steinkampf, W.; and Viani, B. 1995. *Colloid-Facilitated Radionuclide Transport at Yucca Mountain.* LA-12779-MS. Los Alamos, New Mexico: Los Alamos National Laboratory. ACC: NNA.19930628.0067.

170927 van Middlesworth, P.E. and Wood, S.A. 1998. "The Aqueous Geochemistry of the Rare Earth Elements and Yttrium. Part 7. REE, Th and U contents in Thermal Springs Associated with the Idaho Batholith." *Applied Geochemistry, 13,* (7), 861-884. New York, New York: Pergamon. TIC: 256470.

114428 van Olphen, H. 1977. *An Introduction to Clay Colloid Chemistry for Clay Technologists, Geologists, and Soil Scientists.* 2nd Edition. New York, New York: John Wiley & Sons. TIC: 208918.

174503 Vernaz, E. and Godon, N. 1992. "Leaching of Actinides from Nuclear Waste Glass: French Experience." *Scientific Basis for Nuclear Waste Management XV, Symposium held November 4-7, 1991, Strasbourg, France.* Sombret, C.G., ed. *257,* 37-48. Pittsburgh, Pennsylvania: Materials Research Society. TIC: 204618.

108285 Wan, J. and Tokunaga, T.K. 1997. "Film Straining on Colloids in Unsaturated Porous Media: Conceptual Model and Experimental Testing." *Environmental Science & Technology, 31,* (8), 2413-2420. Washington, D.C.: American Chemical Society. TIC: 234804.

179563 Wang, Z.; Felmy, A.R.; Xia, Y.; and Buck, E.C. 2006. "Observation of Aqueous Cm(III)/Eu(III) and UO_2^{2+} Nanoparticulates at Concentrations Approaching Solubility Limit by Laser-Induced Fluorescence Spectroscopy." *Journal of Alloys and Compounds, 418,* 166-170. New York, New York: Elsevier. TIC: 259204.

180833 Widerlund, A.; Shcherbakova, E.; Forsberg, J.; Holmström, H.; and Öhlander, B. 2004. "Laboratory Simulation of Flocculation Processes in a Flooded Tailings Impoundment at the Kristineberg Zn-Cu Mine, Northern Sweden." *Applied Geochemistry, 19,* 1537-1551. New York, New York: Elsevier. TIC: 259362.

161732 Wilkinson, K.J.; Nègre, J.-C.; and Buffle, J. 1997. "Coagulation of Colloidal Material in Surface Waters: The Role of Natural Organic Matter." *Journal of Contaminant Hydrology, 26,* (1-4), 229-243. New York, New York: Elsevier. TIC: 253708.

171996 Wilson, C.N. 1986. *Test Plan for Series 3 NNWSI Spent Fuel Leaching/Dissolution Tests.* HEDL-7577. Richland, Washington: Hanford Engineering Development Laboratory. ACC: NNA.19900216.0069.

102147 Wilson, C.N. 1985. *Results from NNWSI Series 1 Spent Fuel Leach Tests.* HEDL-TME 84-30. Richland, Washington: Hanford Engineering Development Laboratory. ACC: HQS.19880517.2579.

102150 Wilson, C.N. 1987. *Results from Cycles 1 and 2 of NNWSI Series 2 Spent Fuel Dissolution Tests.* HEDL-TME 85-22. Richland, Washington: Hanford Engineering Development Laboratory. ACC: HQS.19880517.2581.

121808 Wilson, C.N. 1990. "Indications for the Formation of Pu, Am, and Cm Colloids in Semi-Static Spent Fuel Dissolution Tests." *1990 Spent Fuel Workshop, Gull Harbour, Manitoba, Canada, September 3-5, 1990.* Richland, Washington: Pacific Northwest Laboratory. ACC: NNA.19920302.0064.

100793 Wilson, C.N. 1990. *Results from NNWSI Series 3 Spent Fuel Dissolution Tests.* PNL-7170. Richland, Washington: Pacific Northwest Laboratory. ACC: NNA.19900329.0142.

174895 Wittman, R.S.; Buck, E.C.; and Hanson, B.D. 2005. *Data Analysis of Plutonium Sorption on Colloids in a Minimal Kinetics Model.* PNNL-15285. Richland, Washington: Pacific Northwest National Laboratory. ACC: MOL.20050811.0087.

180970 Wood, S.A.; Gammons, C.H.; and Parker, S.R. 2006. "The Behavior of Rare Earth Elements in Naturally and Anthropogenically Acidified Waters." *Journal of Alloys and Compounds, 418,* 161-165. New York, New York: Elsevier. TIC: 259421.

102047 Wronkiewicz, D.J.; Bates, J.K.; Wolf, S.F.; and Buck, E.C. 1996. "Ten-Year Results from Unsaturated Drip Tests with UO_2 at 90°C: Implications for the Corrosion of Spent Nuclear Fuel." *Journal of Nuclear Materials, 238,* (1), 78-95. Amsterdam, The Netherlands: North-Holland. TIC: 243361.

171238 Zarrabi, K.; McMillan, S.; Elkonz, S.; and Cizdziel, J. 2003. *Corrosion and Mass Transport Processes in Carbon Steel Miniature Waste Packages.* Document TR-03-003, Rev. 0. Task 34. Las Vegas, Nevada: University of Nevada, Las Vegas. ACC: MOL.20040202.0079.

170892 Zhao, P. and Steward, S.A. 1997. *Literature Review of Intrinsic Actinide Colloids Related to Spent Fuel Waste Package Release Rates.* UCRL-ID-126039. Livermore, California: Lawrence Livermore National Laboratory. ACC: MOL.19971212.0585.

179565 Zheng, Z.; Wan, J.; Song, X.; and Tokunaga, T.K. 2006. "Sodium Meta-Autunite Colloids: Synthesis, Characterization, and Stability." *Colloids and Surfaces A: Physicochemical Engineering Aspects, 274,* 48-55. New York, New York: Elsevier. TIC: 259203.

179566 Ziemniak, S.E. and Hanson, M. 2001. *Corrosion Behavior of 304 Stainless Steel in High Temperature, Hydrogenated Water.* LM-01K046. Schenectady, New York: Lockheed Martin Corporation. ACC: LLR.20070323.0004.

9.2 CODES, STANDARDS, REGULATIONS, AND PROCEDURES

180319 10 CFR 63. 2007 Energy: Disposal of High-Level Radioactive Wastes in a Geologic Repository at Yucca Mountain, Nevada Internet Accessible.

105725 ASTM C 1174-97. 1998. *Standard Practice for Prediction of the Long-Term Behavior of Materials, Including Waste Forms, Used in Engineered Barrier Systems (EBS) for Geological Disposal of High-Level Radioactive Waste.* West Conshohocken, Pennsylvania: American Society for Testing and Materials. TIC: 246015.

IM-PRO-003, Rev 3, ICN 0. *Software Management*. Washington, D.C.: U.S. Department of Energy, Office of Civilian Radioactive Waste Management. ACC: DOC.20070918.0001.

SCI-PRO-001, Rev 4, ICN 0. *Qualification of Unqualified Data*. Washington, D.C.: U.S. Department of Energy, Office of Civilian Radioactive Waste Management. ACC: DOC.20070725.0002.

SCI-PRO-002, Rev. 2, ICN 0. *Planning for Science Activities*. Washington, D.C.: U.S. Department of Energy, Office of Civilian Radioactive Waste Management. ACC: DOC.20070320.0001.

SCI-PRO-004. Rev 5, ICN 0. *Managing Technical Product Inputs*. Washington, D.C.: U.S. Department of Energy, Office of Civilian Radioactive Waste Management. ACC: DOC.20070810.0002.

SCI-PRO-006, Rev. 5, ICN 0. *Models*. Washington, D.C.: U.S. Department of Energy, Office of Civilian Radioactive Waste Management. ACC: DOC.20070810.0004.

9.3 SOURCE DATA, LISTED BY DATA TRACKING NUMBER

149232 LA0002SK831352.001. Total Colloidal Particles Concentration and Size Distribution in Groundwaters from the Nye County Early Warning Drilling Program. Submittal date: 02/24/2000.

149194 LA0002SK831352.002. Total Colloidal Particles Concentration and Size Distribution in Groundwaters Around Yucca Mountain. Submittal date: 02/25/2000.

161771 LA0002SK831352.003. Colloid Size Distribution and Total Colloid Concentration in INEEL Groundwater Samples. Submittal date: 02/25/2000.

161579 LA0002SK831352.004. Colloid Size Distribution and Total Colloid Concentration in Groundwaters from the Nuclear Test Site. Submittal date: 02/25/2000.

148751 LA0003AM831341.001. Probability Distributions for Sorption Coefficients (Kd's). Submittal date: 03/29/2000.

149172 LA0003NL831352.001. Experimental Data on Sorption and Desorption Amounts for Plutonium Onto Clay Colloids. Submittal date: 03/16/2000.

148526 LA0003NL831352.002. The KD Values of 239Pu on Colloids of Hematite, Ca-Montmorillonite and Silica in Natural and Synthetic Groundwater. Submittal date: 03/29/2000.

150272 LA0004NL831352.001. Pu(IV) and Pu(V) Sorption on Hematite and Goethite Colloids with Natural and Synthetic J-13 Water (1997-98 Data). Submittal date: 04/04/2000.

149623 LA0005NL831352.001. The Kd Values of 243Am on Colloids of Hematite, Montmorillonite and Silica in Natural and Synthetic Groundwater. Submittal date: 05/03/2000.

161580 LA0211SK831352.001. Colloid Concentration and Size Distribution from Crater Flats Wells. Submittal date: 12/04/2002.

161581 LA0211SK831352.002. Colloid Concentration and Size Distribution from Nye County Early Warning Drilling Program, Alluvial Testing Complex (ATC) Wells. Submittal date: 12/04/2002.

161582 LA0211SK831352.003. Colloid Concentration and Size Distribution from Nellis/Desert Research Institute (DRI) Wells. Submittal date: 12/04/2002.

161458 LA0211SK831352.004. Colloid Concentration and Size Distribution from Nye County Early Warning Drilling Program, Fall 2000 Field Sampling. Submittal date: 12/04/2002.

163196 LA0304PR831232.001. Calculation of Ionic Strengths Based on Cation Concentrations in Various Groundwater Samples in Which Colloid Concentrations Were Measured. Submittal date: 05/13/2003.

163197 LA0304PR831232.002. Calculation of Ionic Strengths Based on Non-Q Cation Concentrations in Various Groundwater Samples in Which Colloid Concentrations Were Measured. Submittal date: 05/13/2003.

170621 LA0407AM831341.002. Batch Sorption Coefficient Data for Cesium on Yucca Mountain Tuffs in Representative Water Compositions. Submittal date: 07/12/2004.

144991 LA9910SK831341.005. Total Colloidal Particles Concentration and Size Distribution in NTS-ER-20-5-1, NTS-ER-20-5-3, and J-13 Groundwater. Submittal date: 12/07/1999.

143308 LL000123351021.117. ANL 94/34 - The Effects of the Glass Surface Area/Solution Volume Ratio on Glass Corrosion: A Critical Review. Submittal date: 01/28/2000.

152621 LL000905312241.018. Data Associated with the Detection and Measurement of Colloids Recorded in Scientific Notebook 1644. Submittal date: 09/29/2000.

142910 LL991109751021.094. Data Associated with the Detection and Measurement of Colloids in Scientific Notebook SN 1644. Submittal date: 01/10/2000.

162871 MO0302UCC034JC.003. Graphical X-Ray Diffractometer Data and Mineral Analysis of Filtered Solids from Effluent Solution During Miniature Waste Package Corrosion. Submittal date: 02/10/2003.

163910 MO0306ANLSF001.459. Colloids Generated from Irradiated N Reactor Fuel, Data Report. Submittal date: 06/04/2003.

166367 MO0312UCC034JC.008. Mass Transport of Solids in Effluent Solution During Miniature Waste Package Corrosion. Submittal date: 12/05/2003.

171277 MO0407ANLGNN02.608. Normalized Mass Losses of Radionuclides in N2 Tests. Submittal date: 07/27/2004.

181399 MO0705ANLGSV01.258. Results of Static Tests with SRL 131A and SRL 202A Glass. Submittal date: 05/16/2007.

162744 SNT05080598002.001. Engineered Barrier System (EBS) Transport Sorption and Colloid Parameters for the TSPA-VA (Total System Performance Assessment-Viability Assessment) Rip Calculations. Submittal date: 11/06/1998.

9.4 OUTPUT DATA, LISTED BY DATA TRACKING NUMBER

MO0701PASORPTN.000. Colloidal Sorption Coefficients For Pu, Am, Th, Cs, and Pa. Submittal date: 04/17/2007.

MO0701PACSNFCP.000. CSNF Colloid Parameters. Submittal date: 04/17/2007.

MO0701PAGLASWF.000. Glass Waste Form Colloid Parameters. Submittal date: 04/17/2007.

MO0701PAGROUND.000. Groundwater Colloid Concentration Parameters. Submittal date: 01/18/2007.

MO0701PAIRONCO.000. Colloidal Iron Corrosion Products Parameters. Submittal date: 04/17/2007.

MO0701PAKDSUNP.000. Colloidal Kds For U, Np, Ra and Sn. Submittal date: 04/17/2007.

MO0705COLCONCS.000. Colloid Concentrations from Corroded Steels. Submittal date: 5/18/2007.

MO0705CSIONSTH.000. Colloid Stability Ionic Strength Thresholds. Submittal date: 5/18/2007.

MO0705DSCSCUSS.000. Radionuclide Sorption Distributions for Smectite and Uranophane Colloids. Submittal date: 5/18/2007.

9.5 SOFTWARE CODES

181903 Goldsim V. 9.60.100. 2007. WIN 2000, 2003, XP. STN: 10344-9.60-01.

APPENDIX I
CALCULATION OF GROUNDWATER COLLOID PARAMETERS

INTENTIONALLY LEFT BLANK

I. CALCULATION OF GROUNDWATER COLLOID PARAMETERS

The groundwater colloid parameters for use in the TSPA-LA model were based on a data set including 79 groundwater samples collected in the Yucca Mountain vicinity and 11 samples collected from the Idaho National Laboratory (Table I-1). The Idaho groundwater colloid data (DTN: LA0002SK831352.003 [DIRS 161771]) were deemed appropriate for corroboration of the data used for the analysis because the area's climate (arid) and bedrock geology (volcanic fractured basalts) are similar. In addition, the five samples from the NTS wells (DTN: LA0002SK831352.004 [DIRS 161579]) were also used as corroborating data.

Colloid populations (particles/mL) in the groundwater samples were converted to mass concentrations (mg/L) (Figure 6-24, Section 6.3.11).

I.1 CONVERSION OF THE COLLOID POPULATIONS TO MASS CONCENTRATIONS

In order to derive particle size and concentrations from light-scattering instruments, particles must be modeled as spherical with uniform refractive index. The slightly higher refractive indices of the iron oxide minerals compared to silicate minerals would have resulted in an overestimation of colloid particle populations in the groundwater, if these were present.

Mass concentrations were obtained by applying a mineral density of 2.5 g/cm^3 (2.5×10^{-18} mg/nm^3). Silicate minerals might have particle densities ranging from 2 g/cm^3 to 3 g/cm^3 (e.g., 2.65 g/cm^3 for quartz). Smectite phases have densities near the low end of this range (Lide 1995 [DIRS 101876], pp. 4-132 through 4-138). The iron oxide minerals were not included in the mass determination. The densities of hematite, goethite, and lepidocrocite are 5.26, 3.3 to 4.3, and 4.05 to 4.31 g/cm^3, respectively (Lide 1995 [DIRS 101876], pp. 4-132 through 4-138). This could potentially result in an underestimation of particle mass concentrations, although these are generally a smaller component than the silicates.

The volume of a sphere (V) can be calculated from the radius (R) by the following relationship:

$$V = 4/3\ \pi\ R^3 \qquad \text{(Eq. I-1)}$$

The colloid population data for each groundwater sample consisted of population data recorded at 10-nm increments from the particle-size diameter range (50 nm to 200 nm) as reported in the DTNs. The midpoint of the particle diameter size class ranges that are reported in the groundwater datasheets was used to establish the radius for the particle-volume calculations using Equation I-1. For example, those particles with diameter ranging from 50 nm to 60 nm were assigned a size of 55 nm. Thus, the radius (R), for this particle-diameter size population was 27.5 nm.

After calculating an estimate of volume for each particle diameter size class interval, the mass concentration (mg/L) for each particle-size interval was calculated by multiplying particle volume (nm^3) by particle density (mg/nm^3); this product was then multiplied by the total number of particles in the size class interval to derive an estimate of the total colloid mass in each particle-size class interval. The total colloid mass in the water sample (Column 4 in Table I-1) was then estimated by summing the mass concentrations in each particle-size class interval. For

example, the total colloid concentration for the groundwater sample extracted from Well NC-EWDP-01s was calculated as outlined in Table I-2.

Table I-1. Groundwater Samples Used to Develop Cumulative Distribution Function Developed to Establish Colloid Concentration Sampling Frequency for TSPA-LA for Solutions with Stable Colloids

Groundwater Sample	Well ID	Colloid Population (pt/mL)	Colloid Concentration (mg/L)
Data Source DTN: LA0002SK831352.001 [DIRS 149232], Alluvium			
1	NC-EWDP-01s, Depth 170	1.07E+07	3.02E-02
2	NC-EWDP-01s, Depth 250	2.08E+07	4.62E-02
3	NC-EWDP-03s, Depth 449	3.56E+08	3.48E-01
4	NC-EWDP-03s, Depth 390	1.78E+09	1.90E+00
5	NC-EWDP-09SX, Depth 310	3.85E+07	4.49E-02
6	NC-EWDP-09SX, Depth 270	7.24E+07	8.74E-02
7	NC-EWDP-09SX, Depth 150	9.73E+07	1.62E-01
8	NC-EWDP-09SX, Depth 112	7.14E+07	8.89E-02
9	NC airport	7.95E+07	1.41E-01
Data Source DTN : LA0002SK831352.002 [DIRS 149194], Volcanics			
10	UE-25 J-13	1.19E+06	1.35E-03
11	UE-25 J-13	1.046E+06	1.75E-03
12	USW SD-6	5.07E+08	7.24E-01
13	USW SD-6	1.05E+08	1.43E-01
14	UE-25 WT #17	2.11E+09	3.49E+00
15	UE-25 WT #17	1.475E+09	2.32E+00
16	UE-25 WT #17	2.633E+07	2.69E-02
17	UE-25 WT #17	8.236E+07	1.32E-01
18	UE-25 WT #3	7.78E+06	2.02E-02
19	UE-18 WW #8	2.93E+06	2.79E-03
20	UE-18 WW #8	3.31E+06	3.70E-03
21	U-20 WW #20	5.16E+07	5.83E-02
22	U-20 WW #20	5.72E+07	7.71E-02
23	UE-29 a #1	7.45E+06	1.44E-02
24	UE-29 a #2	3.66E+07	6.73E-02
25	UE-25 c #1	4.63E+06	9.68E-03
26	UE-25 c #1	2.82E+06	4.49E-03
Data Source DTN : LA9910SK831341.005 [DIRS 144991], Volcanics			
27	NTS-ER-20-5-3	1.43E+10	1.02E+01
28	NTS-ER-20-5-1	1.25E+10	6.74E+00
29	UE-25 J-13	1.54E+06	3.72E-03
Data Source DTN: LA0211SK831352.004 [DIRS 161458], Nye Co. Phase 2 – Alluvium			
30	NC=EWDP-15P	1.34E+08	1.73E-01
31	NC-EWDP-7S	3.02E+06	9.01E-03
32	NC-EWDP-4PB	1.41E+09	2.03E+00
33	NC-EWDP-4PA	2.34E+08	3.05E-01
34	NC-EWDP-5SB	9.38E+08	2.69E+00
35	NC-EWDP-12PA	7.52E+07	1.42E-01

Table I-1. Groundwater Samples Used to Develop Cumulative Distribution Function Developed to Establish Colloid Concentration Sampling Frequency for TSPA-LA for Solutions with Stable Colloids (Continued)

Groundwater Sample	Well ID	Colloid Population (pt/mL)	Colloid Concentration (mg/L)
36	NC-EWDP-12PB	8.54E+07	1.53E-01
37	NC-EWDP-12PC	2.11E+07	6.29E-02
38	NC-EWDP-19D	8.27E+07	7.73E-02
Data Source DTN: LA0211SK831352.002 [DIRS 161581], ATC Wells			
39	ATC-IM1-A	1.01E+10	7.39E+00
40	ATC-IM1-B	9.51E+09	7.20E+00
41	NC-EWDP-19IM-2-A	1.71E+10	1.35E+01
42	NC-EWDP-19IM-2-B	1.76E+10	1.46E+01
43	NC-EWDP-19IM1-Z1	6.40E+09	5.61E+00
44	NC-EWDP-19IM1-Z2	3.23E+09	2.70E+00
45	NC-EWDP-19IM1-Z3	7.73E+09	5.67E+00
46	NC-EWDP-19IM1-Z4	8.52E+09	6.40E+00
47	NC-EWDP-19IM1-Z5	2.33E+10	1.93E+01
48	NC-EWDP-19D-Z5	1.27E+10	1.08E+01
49	ATC-19D1-011602-1350C	1.01E+10	6.57E+00
50	ATC-19D1-011702-1215C	9.28E+09	5.64E+00
51	ATC-19D1-011602-011702	7.33E+10	4.84E+01
52	ATC-19D1-012802-1500	5.19E+10	3.15E+01
53	NC-EWDP-19D, Z1	5.13E+09	4.12E+00
54	NC-EWDP-19D-Z1	8.27E+07	7.74E-02
55	NC-EWDP-19D, Z2	8.73E+07	9.75E-02
56	NC-EWDP-19D, Z2	2.29E+08	2.47E-01
57	NC-EWDP-19D, Z2	2.24E+08	2.24E-01
58	NC-EWDP-19D	9.34E+08	7.47E-01
59	NC-EWDP-19D	2.77E+08	2.52E-01
60	NC-EWDP-19D	3.51E+09	1.87E+00
Data Source DTN: LA0211SK831352.001 [DIRS 161580], USGS Wells at Crater Flat			
61	USGS-VH-1	1.33E+07	2.45E-02
62	USGS-VH-2	1.18E+06	5.03E-03
63	USGS-VH-1-A	2.17E+07	2.07E-02
64	USGS-VH-1-B	1.09E+07	1.34E-02
Data Source DTN: LA0211SK831352.003 [DIRS 161582]			
65	DRI-EH-2-091200-0800	2.17E+06	4.36E-03
66	DRI-BLM-091200-0915	3.24E+07	3.93E-02
67	DRI-TTR3B-091200-1430	4.25E+06	6.77E-03
68	DRI-Cedar Pass-091200-1325	1.01E+06	2.67E-03
69	DRI-EH-7-091200-1040	8.58E+05	1.89E-03
70	DRI-Sandia 7-091300-1030	1.05E+07	1.70E-02
71	DRI-Sandia 6-091300-0930	6.29E+07	8.29E-02
72	DRI-Tolicha Peak-091400-0745	6.98E+06	7.62E-03
73	DRI-Airforce 3A-091300-1500	1.34E+09	1.58E+00
74	DRI-Roller Coaster-091300-0930	1.12E+06	4.48E-03

Table I-1. Groundwater Samples Used to Develop Cumulative Distribution Function Developed to Establish Colloid Concentration Sampling Frequency for TSPA-LA for Solutions with Stable Colloids (Continued)

Groundwater Sample	Well ID	Colloid Population (pt/mL)	Colloid Concentration (mg/L)
Corroborative Data Source DTN: LA0002SK831352.003 [DIRS 161771], INL Wells			
75	USGS 117-1	4.23E+06	8.97E-03
76	M7S-1	1.30E+06	2.35E-03
77	USGS 120-1	3.76E+06	5.80E-03
78	USGS 119-1	8.13E+06	1.48E-02
79	M3S-1	1.24E+06	1.97E-03
80	M1S-1	3.28E+06	5.42E-03
81	USGS-87-1	2.63E+06	4.63E-03
82	M10S-1	9.37E+07	1.71E-01
83	BLR-99-1	7.73E+07	1.38E-01
84	M14S-1	4.28E+06	8.21E-03
85	USGS 92-1	8.00E+10	1.72E+02
Corroborative Data Source DTN: LA0002SK831352.004 [DIRS 161579], NTS Wells			
86	NTS-ER-20-5-1	1.25E+10	6.74E+00
87	NTS-ER-20-5-3	1.43E+10	1.02E+01
88	NTS-U20n, ~2,511 ft	2.57E+08	3.20E-01
89	NTS-U20n, lower zone	5.19E+09	5.47E+00
90	NTS-U19q	2.72E+10	3.51E+01

NOTE: INL = Idaho National Laboratory; USGS = U.S. Geological Survey.

Table I-2. Example Calculation for Total Colloid Mass in Well NC-EWDP-01s, Depth 170

Particle Diameter Size Range (nm)	Particle Diameter (nm)	Colloid Number (pt/mL)	Calculated Colloid Mass (mg/L)
50 to 60	55	9.27E+05	2.0189E-04
60 to 70	65	1.01E+06	3.6308E-04
70 to 80	75	8.64E+05	4.7713E-04
80 to 90	85	8.01E+05	6.4392E-04
90 to 100	95	8.51E+05	9.5508E-04
100 to 110	105	1.14E+06	1.7275E-03
110 to 120	115	8.01E+05	1.5947E-03
120 to 130	125	7.26E+05	1.8561E-03
130 to 140	135	5.26E+05	1.6941E-03
140 to 150	145	6.26E+05	2.4981E-03
150 to 160	155	5.76E+05	2.8077E-03
160 to 170	165	4.51E+05	2.6520E-03
170 to 180	175	4.13E+05	2.8974E-03

Table I-2. Example Calculation for Total Colloid Mass in Well NC-EWDP-01s, Depth 170 (Continued)

Particle Diameter Size Range (nm)	Particle Diameter (nm)	Colloid Number (pt/mL)	Calculated Colloid Mass (mg/L)
180 to 190	185	3.13E+05	2.5942E-03
190 to 200	195	3.63E+05	3.5233E-03
200	200	3.51E+05	3.6757E-03
Totals		**1.07E+07**	**3.02E-02**

Source: DTN: LA0002SK831352.001 [DIRS 149232].

I.2 ESTABLISHMENT OF GROUNDWATER COLLOID PARAMETERS FOR USE IN THE TSPA-LA MODEL

Mass concentrations (mg/L) of the groundwater in Table I-1 were pooled and a discrete cumulative distribution function was established to evaluate the uncertainty in colloid concentration distribution (Figure 6-24, Section 6.3.11). Filtered water samples were not considered in the development of the cumulative distribution function. Since the colloid particles were measured by dynamic light-scattering techniques, any potential error in measurement of colloid populations for the various particle size classes due to filter "ripening" (i.e., clogging of filter pores through time during the filtration process) was avoided by using only nonfiltered sample data.

The data shown in Figure 6-24, Section 6.3.11, reflect observed variability in groundwater colloid concentrations. The goal of the uncertainty distribution for groundwater colloid concentrations is to numerically capture our knowledge about uncertainty on a large scale. Based on the groundwater colloid concentration collected at the two sites (Yucca Mountain and the Idaho National Laboratory), which corroborate each other, and the uncertainty associated with the collection of groundwater colloids, a reasonable representation of the uncertainty is captured in the cumulative distribution function. Major factors that contribute to uncertainty in the concentrations of colloids in the groundwater samples include: (1) collection techniques, (2) differences in pumping rates at each well, and (3) unknown factors including the types of additives introduced in the wells during the drilling process.

INTENTIONALLY LEFT BLANK

APPENDIX II
QUALIFICATION OF UNQUALIFIED DATA USED AS DIRECT INPUTS

INTENTIONALLY LEFT BLANK

II. QUALIFICATION OF UNQUALIFIED DATA USED AS DIRECT INPUTS

The following constitutes the planning and documentation for the qualification of external source data used as direct input. The intent of the qualification process is to qualify the data for the intended use only within this report.

Data from references used as direct input to this model must meet the definition of "qualified" in accordance with SCI-PRO-004, *Managing Technical Product Inputs*. Input data that do not meet the definition of "qualified" data require qualification in accordance with the requirements in SCI-PRO-006, Section 6.2.1(K), and SCI-PRO-001, *Qualification of Unqualified Data*.

Data from the external sources listed in Table II-1a are qualified for intended use in this report in Sections II.1 through II.5, in accordance with SCI-PRO-006, Section 6.2.1(K) (bullet 2) and SCI-PRO-001. YMP participant data listed in Table II-1b are qualified for intended use in this report in Sections II.6 and II.7, in accordance with SCI-PRO-006, Section 6.2.1(K) (bullet 1) and SCI-PRO-001.

Table II-1a. Data Qualified for Direct Input Using SCI-PRO-006, Section 6.2.1(K)

DIRS	Qualification Title	Section	Brief Input Description
174504	Bitea, C.; Walther, C.; Kim, J.I.; Geckeis, H.; Rabung, T.; Scherbaum, F.J.; and Cacuci, D.G. 2003. "Time-Resolved Observation of ZrO_2-Colloid Agglomeration." *Colloids and Surfaces A: Physicochemical and Engineering Aspects, 215,* 55-66. New York, New York: Elsevier. TIC: 257515.	II.1	ZrO_2 particle characteristics
179547	Gunnarsson, M.; Rasmusson, M.; Wall, S.; Ahlberg, E.; and Ennis, J. 2001. "Electroacoustic and Potentiometric Studies of the Hematite/Water Interface." *Journal of Colloid and Interface Science, 240,* 448-458. New York, New York: Academic Press. TIC: 259215.	II.1	Hematite colloid characteristics
112690	Tombacz, E.; Abraham, I.; Gilde, M.; and Szanto, F. 1990. "The pH-Dependent Colloidal Stability of Aqueous Montmorillonite Suspensions." *Colloids and Surfaces, 49,* 71-80. Amsterdam, The Netherlands: Elsevier. TIC: 246046.	II.1	Smectite clay colloid characteristics
179565	Zheng, Z.; Wan, J.; Song, X.; and Tokunaga, T.K. 2006. "Sodium Meta-Autunite Colloids: Synthesis, Characterization, and Stability." *Colloids and Surfaces A: Physicochemical Engineering Aspects, 274,* 48-55. New York, New York: Elsevier. TIC: 259203.	II.1	Meta-autunite particle characteristics
172864	Liu, C.; Cox, D.S.; Barrand, R.D.; and Hunt, C.E.L. 1992. "Particle Size Distributions of U_3O_3 Produced by Oxidation in Air at 300-900°C." *Proceeding of the 13th Annual Conference, Saint John, NB, June 7-10, 1992. 1,* 1-22. Toronto, Ontario, Canada: Canadian Nuclear Society. TIC: 256950.	II.4	Particle-Size Distribution

Table II-1a. Data Qualified for Direct Input Using SCI-PRO-006, Section 6.2.1(K) (Continued)

DIRS	Qualification Title	Section	Brief Input Description
179538	Bradbury, M.H. and Baeyens, B. 2005. "Modeling the Sorption of Mn(II), Co(II), Ni(II), Zn(II), Cd(II), Eu(III), Am(III), Sn(IV), Th(IV), Np(V) and U(VI) on Montmorillonite: Linear Free Energy Relationships and Estimates of Surface Binding Constants for Some Selected Heavy Metals and Actinides." *Geochimica et Cosmoschimica Acta, 69,* (4), 875-892. New York, New York: Elsevier. TIC: 259202.	II.2	Radionuclide sorption onto smectite clay
179541	Bradbury, M.H. and Baeyens, B. 2006. "Modelling Sorption Data for the Actinides Am(III), Np(V) and Pa(V) on Montmorillonite." *Radiochimica Acta, 94,* 619-625. München, Germany: Oldenbourg Wissenschaftsverlag. TIC: 259214.	II.2	Radionuclide sorption onto smectite clay
179555	Pabalan, R.T. and Turner, D.R. 1997. "Uranium(6+) Sorption on Montmorillonite: Experimental and Surface Complexation Modeling Study." *Aquatic Geochemistry, 2,* 203-226. Dordrecht, The Netherlands: Kluwer Academic Publishers. TIC: 237077.	II.2	Radionuclide sorption onto smectite clay
179561	Tachi, Y.; Shibutani, T.; Sato, H.; and Yui, M. 2001. "Experimental and Modeling Studies on Sorption and Diffusion of Radium in Bentonite." *Journal of Contaminant Hydrology, 47,* 171-186. New York, New York: Elsevier. TIC: 259205.	II.2	Radionuclide sorption onto smectite clay
174068	McNamara, B.; Hanson, B.; Buck, E.; and Soderquist, C. 2005. "Corrosion of Commercial Spent Nuclear Fuel. 2. Radiochemical Analyses of Metastudtite and Leachates." *Radiochimica Acta, 93,* 169-175. München, Germany: Oldenbourg Wissenschaftsverlag. TIC: 257131.	II.3	Radionuclide sorption onto U(VI) colloidal phase
178810	Ilton, E.S.; Liu, C.; Yantasee, W.; Wang, Z.; Moore, D.A.; Felmy, A.R.; and Zachara, J.M. 2006. "The Dissolution of Synthetic Na-Boltwoodite in Sodium Carbonate Solutions." *Geochimica et Cosmochimica Acta, 70,* 4836-4849. New York, New York: Elsevier. TIC: 259016.	II.3	Specific surface area for Na-Boltwoodite
110975	Burns P.C. 1999. "Cs Boltwoodite Obtained by Ion Exchange from Single Crystals: Implications for Radionuclide Release in a Nuclear Repository." *Journal of Nuclear Materials, 265,* 218-223. Amsterdam, The Netherlands: Elsevier. TIC: 246432.	II.3	Radionuclide sorption onto U(VI) colloidal phase
179546	Douglas, M.; Clark, S.B.; Utsunomiya, S.; and Ewing, R.C. 2002. "Cesium and Strontium Incorporation into Uranophane, $[Ca(UO_2)(SiO_3OH)]_2 \cdot 5H_2O]$." *Journal of Nuclear Science and Technology, Supplement 3,* 504-507. Tokyo, Japan: Atomic Energy Society of Japan. TIC: 259213.	II.3	Radionuclide sorption onto U(VI) colloidal phase

Table II-1a. Data Qualified for Direct Input Using SCI-PRO-006, Section 6.2.1(K) (Continued)

DIRS	Qualification Title	Section	Brief Input Description
173086	Douglas, M.; Clark, S.B.; Friese, J.I.; Arey, B.W.; Buck, E.C.; Hanson, B.D.; Utsunomiya, S.; and Ewing, R.C. 2005. "Microscale Characterization of Uranium(VI) Silicate Solids and Associated Neptunium(V)." *Radiochimica Acta, 93,* 265-272. München, Germany: Oldenbourg Wissenschaftsverlag. TIC: 257469.	II.3	Radionuclide sorption onto U(VI) colloidal phase
179551	Kim, C-W.; Wronkiewicz, D.J.; Finch, R.J.; and Buck, E.C. 2006. "Incorporation of Cerium and Neodymium in Uranyl Phases." *Journal of Nuclear Materials, 353,* 147-157. New York, New York: Elsevier. TIC: 259209.	II.3	Radionuclide sorption onto U(VI) colloidal phase
181399	MO0705ANLGSV01.258. Results of Static Tests with SRL131a and SRL202a Glass. Submittal date: 05/16/2007.	II.5	Plutonium concentrations from DHLWG tests

Table II-1b. Data Qualified for Direct Input Using SCI-PRO-001

DIRS	Qualification Title	Section	Brief Input Description
166315	Lu, N.; Conca, J.; Parker, G.R.; Leonard, P.A.; Moore, B.; Strietelmeier, B.; and Triay, I.R. 2000. *Adsorption of Actinides onto Colloids as a Function of Time, Temperature, Ionic Strength, and Colloid Concentration, Waste Form Colloids Report for Yucca Mountain Program (Colloid Data Summary from 1999 to 2000 Research).* LA-UR-00-5121. Los Alamos, New Mexico: Los Alamos National Laboratory. ACC: MOL.20031204.0108.	II.6	Iron oxide surface area (53.5 m^2/g) and iron oxide colloid concentration (200 mg/L)
100793	Wilson, C.N. 1990. *Results from NNWSI Series 3 Spent Fuel Dissolution Tests.* PNL-7170. Richland, Washington: Pacific Northwest Laboratory. ACC: NNA.19900329.0142.	II.7	Spent nuclear fuel colloids

II.1 QUALIFICATION OF EXTERNAL SOURCE DATA FROM BITEA ET AL. (2003 [DIRS 174504]), GUNNARSSON ET AL. (2001 [DIRS 179547]), TOMBACZ ET AL. (1990 [DIRS 112690]), AND ZHENG ET AL. (2006 [DIRS 179565])

The data listed below contained within this report regard colloid characteristics of ZrO_2, hematite, smectite clay, and meta-autunite, which are directly applicable to the DLVO colloid stability model and, thus, represent a property of interest. Plots showing zeta potential with pH were fitted with Excel to provide an equation relating surface charge at any pH.

- Bitea, C.; Walther, C.; Kim, J.I.; Geckeis, H.; Rabung, T.; Scherbaum, F.J.; and Cacuci, D.G. 2003. "Time-Resolved Observation of ZrO_2-Colloid Agglomeration." *Colloids and Surfaces A: Physicochemical and Engineering Aspects, 215,* 55-66. New York, New York: Elsevier. TIC: 257515. [DIRS 174504]

- Gunnarsson, M.; Rasmusson, M.; Wall, S.; Ahlberg, E.; and Ennis, J. 2001. "Electroacoustic and Potentiometric Studies of the Hematite/Water Interface." *Journal of Colloid and Interface Science, 240,* 448-458. New York, New York: Academic Press. TIC: 259215. [DIRS 179547]

- Tombácz, E.; Abraham, I.; Gilde, M.; and Szanto, F. 1990. "The pH-Dependent Colloidal Stability of Aqueous Montmorillonite Suspensions." *Colloids and Surfaces*, *49*, 71-80. Amsterdam, The Netherlands: Elsevier. TIC: 246046. [DIRS 112690]

- Zheng, Z.; Wan, J.; Song, X.; and Tokunaga, T.K. 2006. "Sodium Meta-Autunite Colloids: Synthesis, Characterization, and Stability." *Colloids and Surfaces A: Physicochemical Engineering Aspects, 274,* 48-55. New York, New York: Elsevier. TIC: 259203. [DIRS 179565]

Method 5 (Technical Assessment) from Attachment 3 of SCI-PRO-001 is used for all four of the data sources in this section. The rationale for using this method for these documents is that there is no record of the QA plans under which the data were collected in the original source (i.e., scientific journal or publication). These evaluations were performed independently from the data collection or data reduction process and by a subject matter expert.

Qualification process attributes used in the technical assessment of the external sources are selected from the list provided in Attachment 4 of SCI-PRO-001 and represent the acceptance criteria used to determine if the data are qualified. Process attributes used specifically for data qualification in this report are:

- *Qualifications of personnel or organizations generating the data are comparable to qualification requirements of personnel generating similar data under an approved program that supports the YMP License Application process or post closure science.*

- *The extent to which the data demonstrate the properties of interest (e.g., physical, chemical, geologic, mechanical).*

II.1.1 Qualification of External Source Data from Bitea et al. (2003 [DIRS 174504])

The data used from this source are the ZrO_2 particle characteristics. Method 5 (Technical Assessment) from Attachment 3 of SCI-PRO-001 is used to qualify these data. The "action to be taken" is (b), determination that confidence in data acquisition or developmental results is warranted.

Justification for qualification of the data: The experimental work described by Bitea et al. (2003 [DIRS 174504]) was performed at the Forschungszentrum Karlsruhe (formerly Karlsruhe Nuclear Research Center), which is one of the largest non-commercial science and engineering research institutions in Germany. Claudia Bitea has written several papers on colloid formation. Because Zr(VI) is known for its similarity to Pu(IV) regarding colloid formation her work is intended to serve as a model for the aggregation of Pu(IV)-colloids, the stability of which may be similar to that of the irreversible CSNF colloids described in this model. Thus, these data demonstrate the properties of interest for this report. Bitea's coauthors are well-respected

scientists known for their work on colloid investigations. Co-author Jae Il Kim has written over a hundred publications from his work at the Forschungszentrum Karlsruhe, much of which is focused on colloid characterization, formation, and stability. The report by Bitea et al. (2003 [DIRS 174504]) was published in the peer-reviewed journal *Colloids and Surfaces A: Physicochemical and Engineering Aspects,* an international journal devoted to the science fundamentals, engineering fundamentals, and applications of colloidal and interfacial phenomena and processes, in publication since 1980. The quality of the investigations and the qualifications of the personnel involved provide confidence that the data from Bitea et al. (2003 [DIRS 174504]) are reliable.

II.1.2 Qualification of External Source Data from Gunnarsson et al. (2001 [DIRS 179547])

The data used from this source are the hematite colloid characteristics. Method 5 (Technical Assessment) from Attachment 3 of SCI-PRO-001 is used to qualify these data. The "action to be taken" is (b), determination that confidence in data acquisition or developmental results is warranted.

Justification for qualification of the data: The work described by Gunnarsson et al. (2001 [DIRS 179547]) was performed at Goteborg University, Department of Chemistry, in collaboration with the Commonwealth Scientific and Industrial Research Organisation, Petroleum, Australia. Magnus Gunnarsson has performed research on surface complexation and sorption studies on colloids using poteniometry and tracers. Co-author Mikael Rasmusson has numerous papers focused on the modeling of colloids, electroacoustic measurements, and electrostatic characterizations. Co-author Elisabeth Ahlberg is a professor of electrochemistry and has written extensively on electrochemical, spectroscopic, and structural investigations. Co-author Jonathan Ennis-King is a Research Scientist with Commonwealth Scientific and Industrial Research Organisation, Australia's national research organization, specializing in the modeling and simulation of underground storage of carbon dioxide, and working for a research project associated with the Australian Petroleum Cooperative Research Center. Within this project, he has been responsible for four long-term site-specific simulation studies, and his research focus has been on the mechanisms for the slow migration and dissolution of carbon dioxide underground, especially convective mixing. Göteborg University is an international university engaged in some 2,300 collaborative projects in various parts of the world. Chemistry at Göteborg University has a broad field of research significant to Environmental Science. The electrochemical research at Göteborg has produced numerous publications. The Commonwealth Scientific and Industrial Research Organization in Australia have provided research support for energy with a primary focus on oil and gas. It concentrates on exploration, field appraisal and development, production, and gas processing. Göteborg University is one of many collaborators with this Australian organization. These data were published in the *Journal of Colloid and Interface Science,* which is a peer-reviewed journal that publishes original research on fundamental principles of colloid and interface science and applications. The quality of the investigations and the qualifications of the personnel involved provide confidence that the data from Gunnarsson et al. (2001 [DIRS 179547]) are reliable.

II.1.3 Qualification of External Source Data from Tombacz et al. (1990 [DIRS 112690])

The data used from this source are the montmorillonite clay colloid characteristics Method 5 (Technical Assessment) from Attachment 3 of SCI-PRO-001 is used to qualify these data. The "action to be taken" is (b), determination that confidence in data acquisition or developmental results is warranted.

Justification for qualification of the data: Tombácz et al. (1990 [DIRS 112690]) investigated the stability of montmorillonite clay colloid suspensions as a function of pH and ionic strength in NaCl solution. In this model, DLVO theory was applied using the applicable van der Waals and repulsive energy terms for plate-like particles. The primary author, Dr. Etelka Tombácz, is from the Department of Colloid Chemistry, University of Szeged, Hungary, where she is a professor. She has over 30 journal and book chapter publications dealing with colloid chemistry. This report was published in the peer-reviewed journal *Colloids and Surfaces,* an international journal devoted to the science fundamentals, engineering fundamentals, and applications of colloidal and interfacial phenomena and processes, in publication since 1980.

II.1.4 Qualification of External Source Data from Zheng et al. (2006 [DIRS 179565])

The data used from this document are the meta-autunite particle characteristics. Method 5 (Technical Assessment) from Attachment 3 of SCI-PRO-001 is used to qualify these data. The "action to be taken" is (b), determination that confidence in data acquisition or developmental results is warranted.

Justification for qualification of the data: The paper by Zheng et al. (2006 [DIRS 179565]) reports combined experimental and theoretical work performed at Lawrence Berkeley National Laboratory. The investigation was funded by the Basic Energy Science Program of the U.S. Department of Energy. The primary author (Z. Zheng) has been at Lawrence Berkeley National Laboratory since 2002. His research interests have centered on the synthesis, characterization, and transport potential of sodium meta-autunite colloids in the subsurface. His co-authors (Jiamin Wan and Tetsu K. Tokunaga) have several publications in the fields of contaminant transport in saturated and unsaturated geologic media and the mobility of nanoparticles in the subsurface. The report by Zheng et al. (2006 [DIRS 179565]) was published in the peer-reviewed journal *Colloids and Surfaces A: Physicochemical and Engineering Aspects,* an international journal devoted to the science fundamentals, engineering fundamentals, and applications of colloidal and interfacial phenomena and processes, in publication since 1980. The quality of the investigations and the qualifications of the personnel involved provide confidence that the data from Zheng et al. (2006 [DIRS 179565]) are reliable.

II.1.5 Conclusions

The suitability of the data from reports by Bitea et al. (2003 [DIRS 174504]), Gunnarsson et al. (2001 [DIRS 179547]), Tombàcz et al. (1990 [DIRS 112690]), and Zheng et al. (2006 [DIRS 179565]) for their intended use in this report has been demonstrated in the discussions presented above. On the basis of the evidence presented relevant to the qualification criteria used, the data are therefore qualified for their intended use in this report.

II.2 QUALIFICATION OF EXTERNAL SOURCE DATA FROM BRADBURY AND BAEYENS (2005 [DIRS 179538]; 2006 [DIRS 179541]), PABALAN AND TURNER (2001 [DIRS 179555]), AND TACHI ET AL. (2001 [DIRS 179561])

The following presents planning and documentation for the qualification of external source data used as direct input. The intent of the qualification process is to qualify the data for use only within this report.

The data listed below regard sorption characteristics of radionuclides (Pu, Am, Th, Pa, Np, U, Ra, Cs, and Sn) on smectite clay, which are directly applicable to the colloid model and, thus, represent a property of interest:

- Bradbury, M.H. and Baeyens, B. 2005. "Modeling the Sorption of Mn(II), Co(II), Ni(II), Zn(II), Cd(II), Eu(III), Am(III), Sn(IV), Th(IV), Np(V) and U(VI) on Montmorillonite: Linear Free Energy Relationships and Estimates of Surface Binding Constants for Some Selected Heavy Metals and Actinides." *Geochimica et Cosmoschimica Acta, 69,* (4), 875-892. New York, New York: Elsevier. TIC: 259202. [DIRS 179538]

- Bradbury, M.H. and Baeyens, B. 2006. "Modelling Sorption Data for the Actinides Am(III), Np(V) and Pa(V) on Montmorillonite." *Radiochimica Acta, 94,* 619-625. München, Germany: Oldenbourg Wissenschaftsverlag. TIC: 259214. [DIRS179541]

- Pabalan, R.T. and Turner, D.R. 1997. "Uranium(6+) Sorption on Montmorillonite: Experimental and Surface Complexation Modeling Study." *Aquatic Geochemistry, 2,* 203-226. Dordrecht, The Netherlands: Kluwer Academic Publishers. TIC: 237077. [DIRS 179555]

- Tachi, Y.; Shibutani, T.; Sato, H.; and Yui, M. 2001. "Experimental and Modeling Studies on Sorption and Diffusion of Radium in Bentonite." *Journal of Contaminant Hydrology, 47,* 171-186. New York, New York: Elsevier. TIC: 259205. [DIRS 179561]

Method 5 (Technical Assessment) from Attachment 3 of SCI-PRO-001 is used for all four of the data sources in this section. The rationale for using this method for these documents is that there is no record of the QA plans under which the data were collected in the original source (i.e., scientific journal or publication). These evaluations were performed by a subject matter expert independently from the data collection or data reduction process.

Qualification process attributes used in the technical assessment of the external sources are selected from the list provided in Attachment 4 of SCI-PRO-001 and represent the acceptance criteria used to determine if the data are qualified. Process attributes used specifically for data qualification in this report are:

- *Qualifications of personnel or organizations generating the data are comparable to qualification requirements of personnel generating similar data under an approved program that supports the YMP License Application process or post closure science.*

- *The extent to which the data demonstrate the properties of interest (e.g., physical, chemical, geologic, mechanical).*

II.2.1 Qualification of External Source Data from Bradbury and Baeyens (2005 [DIRS 179538]; 2006 [DIRS 179541])

The data used from these sources are the radionuclide (radium) sorption data. Method 5 (Technical Assessment) from Attachment 3 of SCI-PRO-001 is used to qualify these data. The "action to be taken" is (b), determination that confidence in data acquisition or developmental results is warranted.

Justification for qualification of the data: The sorption studies of U^{6+} by Bradbury and Baeyens (2005 [DIRS 179538]; 2006 [DIRS 179541]) were part of the Febex II project, which was co-funded by the European Commission and performed as part of the Fifth Euraton framework program, key action Nuclear Fission (1998-2002). Partial financial support for these projects was provided by the world-renowned National Cooperative for the Disposal of Radioactive Waste (NAGRA). Michael Bradbury has a BSc in Materials Science (1969) and a D.Phil. in Materials Science (1974) from the University of Sussex, UK. He has worked at the Paul Scherrer Institut in Switzerland since 1987. He was deputy head of the Laboratory for Waste Management and leads the experimental studies section during the research. He is an expert in sorption mechanisms and modeling metal sorption onto rocks and near-field materials relevant to radioactive waste disposal in Switzerland. He is also responsible for the synthesis of sorption databases for repository performance assessment studies.

The data from Bradbury and Baeyens (2005 [DIRS 179538]; 2006 [DIRS 179541]) were published in the geochemistry scientific journals *Geochimica et Cosmoschimica Acta*, and *Radiochimica Acta* respectively. The data published in *Geochimica et Cosmochimica Acta*, one of the oldest (since 1950) and most respected periodicals in the field of geochemistry, are subjected to peer-review by three researchers in the field. The data published in *Radiochimica Acta*, a well-respected periodical in the field of the chemical aspects of nuclear science and technology, are also subjected to peer-review by several researchers in the field. The quality of the investigations and the qualifications of the personnel involved provide confidence that the data from Bradbury and Baeyens (2005 [DIRS 179538]; 2006 [DIRS 179541]) are reliable.

II.2.2 Qualification of External Source Data from Pabalan and Turner (2001 [DIRS 179555])

The data used from this source are the radionuclide (U^{6+}) sorption data. Method 5 (Technical Assessment) from Attachment 3 of SCI-PRO-001 is used to qualify these data. The "action to be taken" is (b), determination that confidence in data acquisition or developmental results is warranted.

Justification for qualification of the data: This study on sorption of $U^{6+}$was funded by the U.S. Nuclear Regulatory Commission from the Office of Nuclear Research, Division of Regulatory Applications, and the Office of Nuclear Material Safety and Safeguards, Division of Waste Management. Roberto T. Pabalan is an Institute Scientist at the Center for Nuclear Waste Regulatory Analyses at the Southwest Research Institute, in San Antonio, Texas. He is an

acknowledged expert in the area of sorption of radionuclides to common rock-forming minerals. He is best known for his work in the modeling the uptake of dissolved constituents onto mineral surfaces, using Monte Carlo and Molecular Dynamics simulations. David R. Turner also works for the Southwest Research Institute and is well-known for sorption studies. The quality of the investigations and the qualifications of the personnel involved provide confidence that the data from Pabalan and Turner (2001 [DIRS 179555]) are reliable.

II.2.3 Qualification of External Source Data from Tachi et al. (2001 [DIRS 179561])

The data used from this source are the radionuclide sorption data. Method 5 (Technical Assessment) from Attachment 3 of SCI-PRO-001 is used to qualify these data. The "action to be taken" is (b), determination that confidence in data acquisition or developmental results is warranted.

Justification for qualification of the data: The work by Tachi et al (2001 [DIRS 179561]) was performed at the Japan Nuclear Cycle Development Institute (JNC). The authors have been vital to work on the Barrier Performance Research Group, Waste Isolation Research Division. Lead author Y. Tachi's previous work has focused on diffusion behavior in bentonite. There are three co-authors on this report, T. Shibutani, H. Sato, and M. Yui, all of whom have considerable experience in the solubility and adsorption studies on radioactive elements. Shibutani has worked on solubility and speciation of radioactive elements of high-level radioactive disposal systems, adsorption and diffusion mechanisms of nuclides in buffer material and geosphere, diffusion behavior of plutonium and americium, and migration behavior of cesium in compacted sodium bentonite. Sato's work has focused on nuclide diffusion and adsorption and its mechanisms in buffer material. Yui is member of the DECOVALEX-THMC project (acronym for International co-operative project for the DEvelopment of COupled models and their VALidation against EXperiments in nuclear waste isolation). This project research efforts include modeling thermo-hydro-mechanical-chemical (T-H-M-C) processes in fractured rocks and buffer materials. The JNC was formed in October 1998 as a successor organization of Power Reactor and Nuclear Fuel Development Corporation; its mission is to perform the development of the advanced technology required to establish the complete nuclear fuel cycle. JNC published the report for HLW disposal in Japan. This report is important to obtain confidence in the HLW disposal system and was used to establish the implementation body. JNC has developed databases of glass dissolution and radionuclide migration for performance analysis of the engineered barrier system (EBS) and the geosphere. The databases developed are of dissolution rates of high-level radioactive vitrified waste, thermochemical data of radioactive elements (database referred to as the JNC-TDB), and sorption/diffusion data in the EBS and the geosphere. The database development has been focused on repository conditions; reducing conditions and compacted/intact system, e.g., actinide (IV)/(III), derivation of sorption coefficients from diffusion experiments rather than batch sorption experiments. The JNC-TDB and sorption database have been developed under the auspices of international experts. The quality of these databases has been checked through independent individual experiments; glass leaching, solubility, batch sorption, diffusion experiments; and through coupled leaching experiments by using the fully high-level radioactive glass and plutonium-doped glass, which were sandwiched between compacted bentonite saturated with water. Based on these studies, JNC has determined the transport parameters, dissolution rate of glass for a soluble radioactive element (Cs), solubility for insoluble radioactive elements (e.g., actinides, Tc), distribution

coefficients and effective diffusion coefficients in the EBS and the geosphere. The quality of the investigations and the qualifications of the personnel involved provide confidence that the data from Tachi et al (2001 [DIRS 179561]) are reliable.

II.2.4 Conclusions

The suitability of the data from reports by Bradbury and Baeyens (2005 [DIRS 179538]; 2006 [DIRS 179541]), Pabalan and Turner (2001 [DIRS 179555]), and Tachi et al. (2001 [DIRS 179561]) for their intended use in this report has been demonstrated in the discussions presented above. On the basis of the evidence presented relevant to the qualification criteria used, the data are therefore qualified for their intended use in this report.

II.3 QUALIFICATION OF EXTERNAL SOURCE DATA FROM MCNAMARA ET AL (2005 [DIRS 174068]), ILTON ET AL. (2006 [DIRS 178810]), BURNS (1999 [DIRS 110975]), DOUGLAS ET AL. (2002 [DIRS 179546]; 2005 [DIRS 173086]), AND KIM ET AL. (2006 [DIRS 179551])

The following presents planning and documentation for the qualification of external source data used as direct input. The intent of the qualification process is to qualify the data for use only within this report.

The data contained within this report regard sorption characteristics of radionuclides (Pu, Am, Th, Pa, Np, U, Ra, Cs, and Sn) on uranophane and surface area of uranophane, which are directly applicable to the colloid model and, thus, represent a property of interest.

- McNamara, B.; Hanson, B.; Buck, E.; and Soderquist, C. 2005. "Corrosion of Commercial Spent Nuclear Fuel. 2. Radiochemical Analyses of Metastudtite and Leachates." *Radiochimica Acta, 93,* 169-175. München, Germany: Oldenbourg Wissenschaftsverlag. TIC: 257131. [DIRS 174068]

- Ilton, E.S.; Liu, C.; Yantasee, W.; Wang, Z.; Moore, D.A.; Felmy, A.R.; and Zachara, J.M. 2006. "The Dissolution of Synthetic Na-Boltwoodite in Sodium Carbonate Solutions." *Geochimica et Cosmochimica Acta, 70,* 4836-4849. New York, New York: Elsevier. TIC: 259016. [DIRS 178810]

- Burns P.C. 1999. "Cs Boltwoodite Obtained by Ion Exchange from Single Crystals: Implications for Radionuclide Release in a Nuclear Repository." *Journal of Nuclear Materials, 265,* 218-223. Amsterdam, The Netherlands: Elsevier. TIC: 246432. [DIRS 110975]

- Douglas, M.; Clark, S.B.; Utsunomiya, S.; and Ewing, R.C. 2002. "Cesium and Strontium Incorporation into Uranophane, [Ca $(UO_2)(SiO_3OH)]_2 \bullet 5H_2O$]." *Journal of Nuclear Science and Technology, Supplement 3,* 504-507. Tokyo, Japan: Atomic Energy Society of Japan. TIC: 259213. [DIRS 179546]

- Douglas, M.; Clark, S.B.; Friese, J.I.; Arey, B.W.; Buck, E.C.; Hanson, B.D.; Utsunomiya, S.; and Ewing, R.C. 2005. "Microscale Characterization of Uranium(VI) Silicate Solids and Associated Neptunium(V)." *Radiochimica Acta, 93,* 265-272. München, Germany: Oldenbourg Wissenschaftsverlag. TIC: 257469. [DIRS 173086]

- Kim, C-W.; Wronkiewicz, D.J.; Finch, R.J.; and Buck, E.C. 2006. "Incorporation of Cerium and Neodymium in Uranyl Phases." *Journal of Nuclear Materials, 353,* 147-157. New York, New York: Elsevier. TIC: 259209. [DIRS 179551]

Method 5 (Technical Assessment) from Attachment 3 of SCI-PRO-001 is used for all six of the data sources for this section. The rationale for using this method for these documents is that there is no record of the QA plans under which the data were collected in the original source (i.e., scientific journal or publication). These evaluations were performed by a subject matter expert independently from the data collection or data reduction process.

Qualification process attributes used in the technical assessment of the external sources are selected from the list provided in Attachment 4 of SCI-PRO-001 and represent the acceptance criteria used to determine if the data are qualified. Process attributes used specifically for data qualification in this report are:

- *Qualifications of personnel or organizations generating the data are comparable to qualification requirements of personnel generating similar data under an approved program that supports the YMP License Application process or post closure science.*

- *The extent to which the data demonstrate the properties of interest (e.g., physical, chemical, geologic, mechanical).*

II.3.1 Qualification of External Source Data from McNamara et al. (2005 [DIRS 174068])

The data used from this source are the radionuclide sorption data (metastudtite). Method 5 (Technical Assessment) from Attachment 3 of SCI-PRO-001 is used to qualify these data. The "action to be taken" is (b), determination that confidence in data acquisition or developmental results is warranted.

Justification for qualification of the data: McNamara et al. (2005 [DIRS 174068]) ran a number of immersion tests on bare fragments of spent nuclear fuel and spent nuclear fuel fragments with partial cladding, and reported analyses of suspended colloidal particles from spent nuclear fuel corrosion tests run at 25°C. Data from this source have been used as direct input to this model to obtain radionuclide-associated colloid concentrations from DHLWG, CSNF, and DSNF. These data demonstrate the properties of interest for this report.

Dr. Bruce McNamara is a Senior Scientist at Pacific Northwest National Laboratory in Richland, WA. He is an expert in radiochemistry with a Ph.D. from the University of California, Berkeley, with several peer-reviewed publications concerning the long-term behavior of spent fuel. These data were published in the journal *Radiochimica Acta*, a well-respected periodical in the field of chemical aspects of nuclear science and technology, whose articles are subjected to peer-review

by several researchers in the field. The quality of the investigations and the qualifications of the personnel involved provide confidence that the data from McNamara et al. (2005 [DIRS 174068]) are reliable.

II.3.2 Qualification of External Source Data from Ilton et al. (2006 [DIRS 178810])

The data used from this source are the radionuclide sorption data onto smectite clay. Method 5 (Technical Assessment) from Attachment 3 of SCI-PRO-001 is used to qualify these data. The "action to be taken" is (b), determination that confidence in data acquisition or developmental results is warranted.

Justification for the appropriate use of the data: The specific surface area data from Ilton et al. (2006 [DIRS 178810]) were available for Na-boltwoodite. In this case, the structures of boltwoodite and uranophane are similar enough for modeling purposes. Based on BET analysis reported on boltwoodite $\{K(H_3O)[(UO_2)(SiO_4)]\bullet 0.5H_2O\}$, a value of 30 m^2/g was selected as a reasonable value for the surface area of uranophane. Micrographs of a natural uranyl carbonate specimen, čejkaite, and a uranophane specimen were examined to determine if the value selected for the model was a reasonable value. These studies were completed on uranium contamination of groundwater and soils at the DOE site at Hanford, WA. Groundwater samples were analyzed with an inductively coupled plasma-atomic emission spectrometer. Solid samples (soils) were analyzed with powder X-ray diffraction, high-resolution transmission electron microscopy, laser-induced fluorescence spectroscopy, and X-ray photoelectron spectroscopy. These analytical methods were documented in the report. Standard scientific practices were used in obtaining these data.

Dr. Eugene Ilton is a senior research scientist within the Fundamental Sciences Division at the Pacific Northwest National Laboratory in Richland, WA. Dr. Ilton has a Ph.D. in Geochemistry from the John Hopkins University and a B.A. in Geology from the University of Pennsylvania. These data were published in the geochemistry scientific journal *Geochimica et Cosmoschimica Acta*. The data published in *Geochimica et Cosmochimica Acta*, one of the oldest (since 1950) and most respected periodicals in the field of geochemistry, are subjected to peer-review by three researchers in the field. The quality of the investigations and the qualifications of the personnel involved provide confidence that the data from Ilton et al. (2006 [DIRS 178810]) are reliable.

II.3.3 Qualification of External Source Data from Burns (1999 [DIRS 110975])

The data used from this source are the radionuclide sorption data (cesium into Na-boltwoodite). Method 5 (Technical Assessment) from Attachment 3 of SCI-PRO-001 is used to qualify these data. The "action to be taken" is (b), determination that confidence in data acquisition or developmental results is warranted.

Justification for qualification of the data: Ion exchange of cesium into the interlayer sites of boltwoodite has been demonstrated by Burns (1999 [DIRS 110975], Table 4, p. 222). Burns analyzed boltwoodite crystals for ion exchange with X-ray diffraction studies. These analytical methods were documented in the report. Standard scientific practices were used in obtaining these data. These data also demonstrate the properties of interest for this report.

Prof. Peter Burns from Notre Dame University is a world-renowned expert in uranium mineralogy. He has published several articles dealing with the mechanism of radionuclide association with uranium minerals. Burns has a Ph.D. in Geology (1994) from the University of Manitoba, a M.Sc. in Geology (1990) from the University of Western Ontario, and a B.Sc. (Honours) (1988) from the University of New Brunswick. The data from Burns (1999 [DIRS 110975]) were published in the peer-reviewed *Journal of Nuclear Materials*, which publishes high-quality papers in materials research relevant to nuclear fission and fusion reactors and high power accelerator technologies, and in closely related aspects of materials science and engineering. The quality of the investigations and the qualifications of the personnel involved provide confidence that the data from Burns (1999 [DIRS 110975]) are reliable.

II.3.4 Qualification of External Source Data from Douglas et al. (2002 [DIRS 179546]; 2005 [DIRS 173086])

The data used from this source are the radionuclide sorption data (cesium, strontium, and neptunium) into uranophane. Method 5 (Technical Assessment) from Attachment 3 of SCI-PRO-001 is used to qualify these data. The "action to be taken" is (b), determination that confidence in data acquisition or developmental results is warranted.

Justification for qualification of the data: Douglas et al. (2002 [DIRS 179546]) reported an ion exchange of both cesium and strontium into uranophane. Scanning electron microscopy images of the uranophane particles reported by Douglas et al. (2005 [DIRS 173086]) indicate that the Np phases were much more fine grained. The model indicates that uranophane particles should be stable, yet they are not typically observed in nature, although they can exist with colloidal-sized dimensions. Both papers by Douglas et al. (2002 [DIRS 179546]; 2005 [DIRS 173086]) discuss the importance of boltwoodite and uranophane as secondary products due to the alteration of spent nuclear fuel. Thus, the subjects of both of these papers demonstrate the properties of interest for this report. The analytical methods for data collection were documented in each report. Standard scientific practices were used in obtaining these data.

Matt Douglas performed work on the uptake of radionuclides into uranophane as part of a Ph.D. program at Washington State University under the direction of Prof. Susan Clark. He is presently a scientist within the National Security Directorate at the Pacific Northwest National Laboratory in Richland, WA.

The first article by Douglas et al. (2002 [DIRS 179546]) was published in the peer-reviewed *Journal of Nuclear Science and Technology*, published by the Atomic Energy Society of Japan. The second article by Douglas et al. (2005 [DIRS 173086]) was published in the journal *Radiochimica Acta*, a well-respected periodical in the field of the chemical aspects of nuclear science and technology, whose articles are subjected to peer-review by several researchers in the field. The quality of the investigations and the qualifications of the personnel involved provide confidence that the data from Douglas et al. (2002 [DIRS 179546]; 2005 [DIRS 173086]) are reliable.

II.3.5 Qualification of External Source Data from Kim et al. (2006 [DIRS 179551])

The data used from this source are the radionuclide sorption data. Method 5 (Technical Assessment) from Attachment 3 of SCI-PRO-001 is used to qualify these data. The "action to be taken" is (b), determination that confidence in data acquisition or developmental results is warranted.

Justification for qualification of the data: The data from Kim et al. (2006 [DIRS 179551]) include the development of K_d values for Pu, Am, and Th on U(VI) minerals. The data values were based on analogue chemical behavior of rare earth elements for Pu, Am, and Th. The experiments were conducted on oxidized spent nuclear fuel in environmental conditions expected to exist in the Yucca Mountain repository. The analytical methods for obtaining the data were documented in the report. Standard scientific practices were used in obtaining these data. These data also demonstrate the properties of interest for this report.

Work by Dr. Cheol Kim, who is currently a scientist in South Korea, was performed under the direction of Prof. David J. Wronkiewicz. Microanalysis of samples was performed by Kim and Edgar Buck at Argonne National Laboratory. The work was presented in the well-respected, peer-reviewed *Journal of Nuclear Materials*, which publishes high-quality papers in materials research relevant to nuclear fission and fusion reactors and high power accelerator technologies, and in closely related aspects of materials science and engineering. The quality of the investigations and the qualifications of the personnel involved provide confidence that the data from Kim et al. (2006 [DIRS 179551]) are reliable.

II.3.6 Conclusions

The suitability of the data from reports by McNamara et al. (2005 [DIRS 174068]), Ilton et al. (2006 [DIRS 178810]), Burns (1999 [DIRS 110975]), Douglas et al. (2002 [DIRS 179546]; 2005 [DIRS 173086]), and Kim et al. (2006 [DIRS 179551]) for their intended use in this report has been demonstrated in the discussions presented above. On the basis of the evidence presented relevant to the qualification criteria used, the data are therefore qualified.

II.4 QUALIFICATION OF EXTERNAL SOURCE DATA FROM LIU ET AL. (1992 [DIRS 172864])

The data provided by this source concern particle size characteristics of U_3O_8 following high temperature oxidation, which are directly applicable to the colloid model and thus represent a property of interest.

- Liu, C.; Cox, D.S.; Barrand, R.D.; and Hunt, C.E.L. 1992. "Particle Size Distributions of U_3O_8 Produced by Oxidation in Air at 300-900°C." *Proceeding of the 13th Annual Conference, Saint John, NB, June 7-10, 1992. 1,* 1-22. Toronto, Ontario, Canada: Canadian Nuclear Society. TIC: 256950. [DIRS 172864]

Method 5 (Technical Assessment) from Attachment 3 of SCI-PRO-001 is used for the data source for this section. The rationale for using this method is that there is no record of the QA plans under which the data were collected in the original source (i.e., scientific journal or

publication). These evaluations were performed by a subject matter expert independently from the data collection or data reduction process.

Qualification process attributes used in the technical assessment of the external sources are selected from the list provided in Attachment 4 of SCI-PRO-001, and represent the acceptance criteria used to determine if the data are qualified. Process attributes used specifically for data qualification in this report are:

- *Qualifications of personnel or organizations generating the data are comparable to qualification requirements of personnel generating similar data under an approved program that supports the YMP License Application process or post closure science.*

- *The extent to which the data demonstrate the properties of interest (e.g., physical, chemical, geologic, mechanical).*

Justification for qualification of the data: Particle size distributions for unirradiated and irradiated UO_2 fuel following high-temperature oxidation (300°C to 900°C) have been reported by Liu et al. (1992 [DIRS 172864]). These data were obtained at the well-respected Atomic Energy Canada Laboratory, Whiteshell, Canada. This organization has performed many studies on spent nuclear fuel behavior over many years. The analytical methods for obtaining the data were documented in the report and standard scientific practices were used in obtaining these data. These data also demonstrate the properties of interest for this report.

Co-authors Hunt, Cox, and Barrand have published several papers in peer-reviewed scientific publications, including work in the *Journal of Nuclear Materials* and *Nuclear Engineering and Design* on uranium oxide oxidation and fission product release over 10 to 20 years. The article by Liu et al. (1992 [DIRS 172864]) was published as part of the 13th Annual Conference of the Canadian Nuclear Society, and also as part of the 32nd Annual Conference of the Canadian Nuclear Association.

The suitability of the data from the report by Liu et al. (1992 [DIRS 172864]) for the intended use in this report has been demonstrated in the discussions presented above. On the basis of the evidence presented relevant to the qualification criteria used, the data are therefore qualified.

II.5 QUALIFICATION OF EXTERNAL SOURCE DATA FROM DTN: MO0705ANLGSV01.258 [DIRS 181399]

The data contained within this source involve immersion corrosion tests on SRL-131A and SRL-202A glasses. These data were collected under the Environmental Management Division at Argonne National Laboratory (ANL). This data collection activity at ANL was performed under a contract with DOE; however, it was not performed under contract with the YMP, and therefore these data are treated as an external source. It should be noted that the same personnel at worked on the YMP at ANL collected this dataset, just under a different contract. Method 5 (Technical Assessment) from Attachment 3 of SCI-PRO-001 is used to qualify these data. The "action to be taken" is (b), determination that confidence in data acquisition or developmental results is warranted. A facsimile of the Data Qualification Plan (Attachment 6 of SCI-PRO-001) is presented in Appendix III.

- MO0705ANLGSV01.258. Results of Static Tests with SRL 131A and SRL 202A Glass. Submittal date: 05/16/2007. [DIRS 181399]

Method 5 (Technical Assessment) from Attachment 3 of SCI-PRO-001 is used to qualify these data. The rationale for using this method is that there is no record of the QA plans under which the data were collected in the original source (i.e., the DTN). These evaluations were performed by a subject matter expert independently from the data collection or data reduction process.

Qualification process attributes used in the technical assessment of the data are selected from the list provided in Attachment 4 of SCI-PRO-001 and represent the acceptance criteria used to determine if the data are qualified. Process attributes used specifically for data qualification in this report are:

- *Qualifications of personnel or organizations generating the data are comparable to qualification requirements of personnel generating similar data under an approved program that supports the YMP License Application process or post closure science.*

- *The extent to which the data demonstrate the properties of interest (e.g., physical, chemical, geologic, mechanical).*

- *Extent and quality of corroborating data or confirmatory testing results.*

- *The environmental conditions under which the data were obtained if germane to the quality of data.*

Justification for qualification of the data: The data contained within this source involve immersion corrosion tests on SRL-131A and SRL-202A glasses; these data are presented in Table 6-5. The data files used from DTN: MO0705ANLGSV01.258 [DIRS 181399] contain the releases of glass component cations, Pu, and Si during MCC-1 tests conducted in J-13 water at 90°C with SRL 131A and SRL 202A glasses. These data were collected by ANL from January 30, 1990, through September 30, 1994, under the Environmental Management Division, which had its own QA program. The data were collected in ANL Scientific Notebook Number 675 under ANL Technical Procedure DP-05-113. Similar data have been documented in qualified DTNs: LL000905312241.018 [DIRS 152621] and LL991109751021.094 [DIRS 142910], in which Pu, Si and cation release data were collected on the same SRL-131A and SRL-202A glasses analyzed via the same procedures. Note that DTN: MO0705ANLGSV01.258 [DIRS 181399] the DTN being qualified, as well as the two other DTNs (LL000905312241.018 [DIRS 152621] and LL991109751021.094 [DIRS 142910]) are presented in Table 6-5, all with similar results. The environmental conditions under which the data archived in DTN: MO0705ANLGSV01.258 [DIRS 181399] were collected are the same as the conditions under which the data in DTNs: LL000905312241.018 [DIRS 152621] and LL991109751021.094 [DIRS 142910] were collected. The only difference was the contract under which the work was completed.

The suitability of the data from DTN: MO0705ANLGSV01.258 [DIRS 181399] for the intended use in this report has been demonstrated in the discussions presented above. On the basis of the evidence presented relevant to the qualification criteria used, the data are therefore qualified.

II.6 QUALIFICATION OF YMP PROJECT SOURCE DATA FROM LU ET AL. (2000 [DIRS 166315])

The data contained within this source regard the surface area of iron oxides and colloid concentration, which are directly applicable to the colloid model and thus represent a property of interest. These data were collected by YMP personnel and are being qualified in accordance with SCI-PRO-001 (consistent with SCI-PRO-006, Section 6.2.1(K), bullet 1). Method 5 (Technical Assessment) from Attachment 3 of SCI-PRO-001 is used to qualify these data. For Method 5, the "action to be taken" is (b), determination that confidence in data acquisition or developmental results is warranted. A facsimile of the Data Qualification Plan (Attachment 6 of SCI-PRO-001) is presented in Appendix III.

- Lu, N.; Conca, J.; Parker, G.R.; Leonard, P.A.; Moore, B.; Strietelmeier, B.; and Triay, I.R. 2000. *Adsorption of Actinides onto Colloids as a Function of Time, Temperature, Ionic Strength, and Colloid Concentration, Waste Form Colloids Report for Yucca Mountain Program (Colloid Data Summary from 1999 to 2000 Research).* LA-UR-00-5121. Los Alamos, New Mexico: Los Alamos National Laboratory. ACC: MOL.20031204.0108. [DIRS 166315]

Method 5 (Technical Assessment) from Attachment 3 of SCI-PRO-001 is used to qualify this data. The rationale for using this method is that there is no record of the QA plans under which the data were collected in the original source (i.e., scientific journal or publication). These evaluations were performed by a subject matter expert independently from the data collection or data reduction process.

Qualification process attributes used in the technical assessment of the data are selected from the list provided in Attachment 4 of SCI-PRO-001 and represent the acceptance criteria used to determine if the data are qualified. Process attributes used specifically for data qualification in this report are:

- *Qualifications of personnel or organizations generating the data are comparable to qualification requirements of personnel generating similar data under an approved program that supports the YMP License Application process or post closure science.*

- *The extent to which the data demonstrate the properties of interest (e.g., physical, chemical, geologic, mechanical).*

- *Extent and quality of corroborating data or confirmatory testing results.*

*Justification for qualification of the data***:** The surface area and colloid concentration data from Lu et al. (2000 [DIRS 166315], Table 1) are being qualified for use as direct input to this document.

Data from Table 1 of the report by Lu et al. (2000 [DIRS 166315]), which displays surface areas for iron oxides and mass of colloids (Lu et al. 2000 [DIRS 166315]), are being qualified in accordance with SCI-PRO-001. These data demonstrate the properties of interest for use in this report. The qualification process used for these data is necessary because the documentation of

proof of proper data acquisition is unavailable for review. This qualification process is designed to provide the desired level of confidence for the data in their intended use for this modeling report. The measurements of the surface area of iron oxides were performed using ethylene glycol monoethyl ether sorption. This method is typically used for soil surface area determinations, particularly for clays. Its application to iron oxides (i.e., hematite) is reasonable and the values obtained are comparable to the results of Roden and Zachara (1996 [DIRS 171518]) and Poulton et al. (2004 [DIRS 171519]) on similar iron oxide particles. The concentration of colloids was obtained through standard weighing and dilution. Eight grams of ground Fe_2O_3 powder were added to 500 mL of J-13 or SYN.J-13 water and shaken vigorously. After leaving to stand for one hour, the 2/3 of the upper portion of the suspension was diluted with 500 mL of J-13 or SYN.J-13 water. The mass of colloids was determined by weight difference of the colloid suspension before and after drying. The J-13 solution had been passed through a 50-nm membrane filter under ~2 atmospheres, and the SYN.J-13 solution was prepared using 0.028g Na_2CO_3 and 1.92g $NaHCO_3$ to 10 L of nanopure deionized water (Lu et al. 2000 [DIRS 166315]). The data are considered suitable for modeling purposes. Los Alamos National Laboratory (LANL) is, and has been for years, one of the few resources in the U.S. with the ability to perform complex laboratory investigations with radioactive materials. The results of the investigations are generally published as LANL reports and eventually are published in peer-reviewed literature. The experimental investigations were performed under the auspices of the Yucca Mountain Project. Ningping Lu has been senior author or a coauthor on 11 LANL reports related to radioactive elements and isotopes and their behavior in the environment. She has published in peer-reviewed journals, including *AIP Journal*, *Applied Radiation and Isotopes*, *Applied Geochemistry*, *Radiation Physics and Chemistry*, and *Radiochimica Acta*.

Conclusion: The conclusion from this report is that the input data being considered here is qualified only for the purposes of this model report.

II.7 QUALIFICATION OF YMP PROJECT DATA FROM WILSON (1990 [DIRS 100793])

The data contained within in Tables A.2 through A.7 of this source (Wilson 1990 [DIRS 100793]) involve the $^{239}Pu + ^{240}Pu$ Series 3 data being qualified for use as a direct input to this report. These data were collected by personnel in association with the YMP and are being qualified in accordance with SCI-PRO-006, Section 6.2.1(K) (bullet 1), and SCI-PRO-001. Method 5 (Technical Assessment) from Attachment 3 of SCI-PRO-001 is used to qualify these data. For Method 5, the "action to be taken" is (b), determination that confidence in data acquisition or developmental results is warranted. A facsimile of the Data Qualification Plan (Attachment 6 of SCI-PRO-001) is presented in Appendix III.

- Wilson, C.N. 1990. *Results from NNWSI Series 3 Spent Fuel Dissolution Tests.* PNL-7170. Richland, Washington: Pacific Northwest Laboratory. ACC: NNA.19900329.0142. [DIRS 100793]

Method 5 (Technical Assessment) from Attachment 3 of SCI-PRO-001 is used to qualify these data. The rationale for using this method for this document is that there is no record of the QA plans under which the data were collected in the original source (i.e., scientific journal or

publication). These evaluations were performed by a subject matter expert independently from the data collection or data reduction process.

Qualification process attributes used in the technical assessment of the data are selected from the list provided in Attachment 4 of SCI-PRO-001 and represent the acceptance criteria used to determine if the data are qualified. Process attributes used specifically for data qualification in this report are:

- *Qualifications of personnel or organizations generating the data are comparable to qualification requirements of personnel generating similar data under an approved program that supports the YMP License Application process or post closure science.*
- *The extent to which the data demonstrate the properties of interest (e.g., physical, chemical, geologic, mechanical).*
- *Extent and quality of corroborating data or confirmatory testing results.*
- *The environmental conditions under which the data were obtained if germane to the quality of data.*

*Justification for qualification of the data***:** The purpose of exercise is to qualify the $^{239}Pu + ^{240}Pu$ Series 3 data in Tables A.2 through A.7 of the study by Wilson (1990 [DIRS 100793]) for use as a direct input to this report.

The $^{239}Pu + ^{240}Pu$ Series 3 data (Wilson 1990 [DIRS 100793], Tables A.2 through A.7) are being qualified in accordance with SCI-PRO-001. The qualification process used for these data involves the method of corroborating data in accordance with SCI-PRO-001. This qualification process is designed to provide the desired level of confidence for the data in its intended use for this report.

The experimental work described by Wilson (1990 [DIRS 100793]) was performed at Pacific Northwest National Laboratory (PNNL). PNNL is, and has been for years, one of the few resources in the U.S. with the ability to perform complex laboratory investigations with spent nuclear fuel. The results of the investigations are generally published as PNNL reports and eventually are published in peer-reviewed literature. The experimental investigations of spent nuclear fuel corrosion were performed under the auspices of the Yucca Mountain Project; the experimental conditions chosen were based on the environmental conditions anticipated in the repository. The experiments represent probably the only laboratory work performed that specifically addresses the formation of plutonium colloids from spent nuclear fuel produced under immersion conditions. The quality of the PNNL investigations and the Project-specific design of the experiments provide confidence that the resulting data are reliable.

The author of the report, Dr. Chuck Wilson, was a senior author or a coauthor on over 40 PNNL reports, task plans, and peer-reviewed publications related to spent nuclear fuel corrosion. Dr. Wilson has a Doctorate from the University of Washington (1974) and a B.S. from the University of Washington (1969) in Ceramic Engineering (Cum Laude). Dr. Wilson has worked on the Basalt Waste Isolation Pilot Program and was principal investigator for spent nuclear fuel

radionuclide release in support of the Yucca Mountain repository in 1984. He has coauthored papers with other well-respected scientists within the Yucca Mountain Program, including Drs. Henry Shaw, Carol Bruton, Walt Gray, Robert Einziger, and Virginia Oversby.

As described in the source document (Wilson 1990 [DIRS 100793], Acknowledgements), the Westinghouse Hanford Company (WHC) and PNNL developed these data for the YMP. The work was conducted under Contract No. W-7405-ENG-48 and the YMP–approved WHC/PNNL quality assurance programs, which met the contractual quality assurance requirements. The laboratory activities were completed under the WHC QA program, from February 1986 to May 1987, and much of the data evaluation and the preparation by Wilson (1990 [DIRS 100793]) were performed under the PNNL QA program. This work was transferred from WHC to PNNL in June 1987 as part of the Hanford site contract consolidation effort. The WHC and PNNL QA programs were reviewed and approved by Lawrence Livermore National Laboratory, which managed the waste package task for YMP and treated WHC and PNNL as suppliers. Technical implementing documents, including test plans, test procedures, and technical drawings were reviewed and approved by Lawrence Livermore National Laboratory and WHC prior to their implementation, and determined to be technically adequate for the collection and analyses of the data. The report by Wilson (1986 [DIRS 171996]) also included an appendix that identified all test instructions, technical procedures, and analytical procedures, including solution and solids analyses, and burnup/radiochemical analyses. The initial evaluation of the overall data quality has determined that the controls and methods used to plan, collect, and analyze the data in question were adequate when compared to generally accepted scientific and engineering practices at the time the data were generated. It should also be noted that the spent nuclear fuel release data reported by Wilson (1990 [DIRS 100793]) has been used in several project products.

Series 1 and 2 tests preceded Series 3 tests and were conducted using the same methodology as in Series 3 testing by WHC personnel, of whom most were involved in all three series tests. The comparison of the Series 1 (Wilson 1985 [DIRS 102147], Tables A.3 through A.9) and Series 2 test results (Wilson 1987 [DIRS 102150], Tables A.2 through A.9) to the Series 3 test results indicates consistency between current and previous testing.

Conclusion: The input data from Wilson (1990 [DIRS 100793]) is qualified for the intended use in this report.

APPENDIX III
DATA QUALIFICATION PLANS

INTENTIONALLY LEFT BLANK

III. DATA QUALIFICATION PLANS

Data Qualification Plan

Complete only applicable items.

QA: QA
Page 1 of 1

Section I. Organizational Information

Qualification Title

Adsorption of Actinides onto Colloids as a Function of Time, Temperature, Ionic Strength, and Colloid Concentration, Waste Form Colloids Report for Yucca Mountain Program (Colloid Data Summary from 1999 to 2000 Research). (2000) Lu, N.; Conca, J.; Parker, G.R.; Leonard, P.A.; Moore, B.; Strietelmeier, B., and Triay, I.R. LA-UR-00-5121. Los Alamos, New Mexico: Los Alamos National Laboratory. ACC: MOL.20031204.0108 [DIRS 166315].

Requesting Organization

PA/NFE

Section II. Process Planning Requirements

1. List of Unqualified Data to be Evaluated

The data contained within this report regard the surface area of iron oxides and colloid concentration, which are directly applicable to the colloid model.

2. Type of Data Qualification Method(s) [Including rationale for selection of method(s) (Attachment 3) and qualification attributes (Attachment 4)]

Method 5, Technical Assessment- The rationale for using this method for this document is that there is no record of the QA plans under which the data were collected in the original source (i.e., scientific journal or publication). These evaluations were performed independently from the data collection or data reduction process and by a subject matter expert. For Method 5, Technical Assessment, the "action to be taken" is (b), determination that confidence in data acquisition or developmental results is warranted

Qualification process attributes used in the technical assessment of the data are selected from the list provided in Attachment 4 of SCI-PRO-001, which represent the acceptance criteria used to determine if the data are qualified. Process attributes used specifically for data qualification in this report are:

- *Qualifications of personnel or organizations generating the data are comparable to qualification requirements of personnel generating similar data under an approved program that supports the YMP License Application process or post closure science.*
- *The extent to which the data demonstrate the properties of interest (e.g., physical, chemical, geologic, mechanical).*

3. Data Qualification Team and Additional Support Staff Required

Qualification Chairperson- Edgar Buck
Data Qualification Team Member- David Sassani and Wendy Mitcheltree

4. Data Evaluation Criteria

SCI-PRO-006, Section 6.2.1(K bullet 1) and SCI-PRO-001. Method 5, Technical Assessment (SCI-PRO-001, Attachment 3) are used to qualify these data for the intended use in this report.

5. Identification of Procedures Used

SCI-PRO-006- *Models*- Section 6.2.1 (K Bullet 1)
SCI-PRO-001- *Qualification of Unqualified Data*

6. Plan coordinated with the following known organizations providing input to or using the results of the data qualification

For use in the document- MDL-EBS-PA-000004 Rev 03

Section III. Approval

GAF 10/12/07

Qualification Chairperson Printed Name	Qualification Chairperson Signature	Date
Edgar Buck ← FOR	David J. Sassani	10/08/2007
Responsible Manager Printed Name	**Responsible Manager Signature**	**Date**
Geoff Freeze	Geoff Freeze	10/8/07

SCI-PRO-001.1-R1

Data Qualification Plan

Complete only applicable items.

QA: QA
Page 1 of 1

Section I. Organizational Information

Qualification Title

Results from NNWSI Series 3 Spent Fuel Dissolution Tests. PNL-7170. Richland, Washington: Pacific Northwest Laboratory. 1990. Wilson, C.N. ACC: NNA.19900329.0142 [DIRS 100793].

Requesting Organization

PA/NFE

Section II. Process Planning Requirements

1. List of Unqualified Data to be Evaluated

The data contained within this report regard the $^{239}Pu + {}^{240}Pu$ Series 3 data in Tables A.2 through A.7 of *Results from NNWSI Series 3 Spent Fuel Dissolution Tests* (Wilson 1990 [DIRS 100793]).

2. Type of Data Qualification Method(s) [Including rationale for selection of method(s) (Attachment 3) and qualification attributes (Attachment 4)]

Method 5, Technical Assessment- The rationale for using this method for this document is that there is no record of the QA plans under which the data were collected in the original source (i.e., scientific journal or publication). These evaluations were performed independently from the data collection or data reduction process and by a subject matter expert. For Method 5, Technical Assessment, the "action to be taken" is (b), determination that confidence in data acquisition or developmental results is warranted

Qualification process attributes used in the technical assessment of the data are selected from the list provided in Attachment 4 of SCI-PRO-001, which represent the acceptance criteria used to determine if the data are qualified. Process attributes used specifically for data qualification in this report are:

- *Qualifications of personnel or organizations generating the data are comparable to qualification requirements of personnel generating similar data under an approved program that supports the YMP License Application process or post closure science,*
- *The extent to which the data demonstrate the properties of interest (e.g., physical, chemical, geologic, mechanical);*

3. Data Qualification Team and Additional Support Staff Required

Qualification Chairperson- Edgar Buck
Data Qualification Team Members- David Sassani and Wendy Mitcheltree

4. Data Evaluation Criteria

SCI-PRO-006, Section 6.2.1(K bullet 1) and SCI-PRO-001. Method 5, Technical Assessment (SCI-PRO-001, Attachment 3) are used to qualify these data for the intended use in this report.

5. Identification of Procedures Used

SCI-PRO-006- *Models*- Section 6.2.1 (K Bullet 1)
SCI-PRO-001- *Qualification of Unqualified Data*

6. Plan coordinated with the following known organizations providing input to or using the results of the data qualification

For use in the document- MDL-EBS-PA-000004 Rev 03

Section III. Approval

Qualification Chairperson Printed Name	Qualification Chairperson Signature	Date
Edgar Buck ← FOR	GAF 10/12/07	10/08/2007
Responsible Manager Printed Name	**Responsible Manager Signature**	**Date**
Geoff Freeze	Geoff Freeze	10/8/07

SCI-PRO-001.1-R1

APPENDIX IV
CRITICAL REVIEW

INTENTIONALLY LEFT BLANK

IV. CRITICAL REVIEW

A critical review by technical specialist James Krumhansl (Sandia National Laboratories) was performed in accordance with Attachment 4 of SCI-PRO-006 as a model validation method per *Technical Work Plan for Waste Form Testing and Modeling* (BSC 2006, [DIRS 177389]). The group manager for the Near-Field Environment (NFE) team (Geoff Freeze) directed the critical review per Section 6.3.2 of SCI-PRO-006, as part of the NFE group manager's determination regarding the adequacy of model validation. The critical reviewer selected by the NFE group manager is independent of the development, checking, and review of the documentation for the models (and submodels) for colloids, including documents providing inputs to the colloids models, and meets the defined criteria for selection within Appendix B of the TWP (BSC 2006, [DIRS 177389]).

Qualifications of the technical specialist Jim Krumhansl include that he has both a B.A. and Ph.D. in geology, and has specialized in aqueous geochemistry as it pertains to the transport and deposition of metals in natural groundwater systems. For the past 30 years, he has also worked at Sandia National Laboratories on a variety of topics related to the treatment and disposal of nuclear wastes. He has extensive experience in the development of backfills, including those that employ various kinds of clay, and has also conducted studies directed at identifying the waste package corrosion products that are actually formed in situ proximate to such backfills. A second pertinent qualification is the body of knowledge he has gained during his extensive research to develop radionuclide "getters," principally finely grained (occasionally colloidal) oxide-hydroxide materials with a select propensity for scavenging radioisotopes that travel in ground water as anions (I, Tc, Se, etc.). A parallel research interest of his is the chemistry of the largely colloidal hydrous iron and silicate precipitates residing in the HLW tank bottoms at Hanford and Savannah River. Over the years, he has conducted both laboratory and modeling studies to understand what factors govern their mechanical, thermal, and chemical stability as well as their ability to sequester radionuclides. The technical specialist has relevant Project experience including training to quality assurance procedures.

The intended use of the colloid models is given the TWP (BSC 2006 [DIRS 177389], Table 2-2) as:

> Describe the abstraction of the colloids process model for the waste form and engineered barrier component calculations to be performed for TSPA-LA.

The overall criterion for the critical reviewer to apply to all evaluations of the various colloid models (and their submodels) is given in the TWP (BSC 2006, [DIRS 177389], Table 2-3) as:

> Assessment of the activities will be qualitative and considered successful if deemed defendable by the independent technical reviewer.

In addition to the above overall criterion, there are seven specific questions to be answered in Appendix B of the TWP (BSC 2006 [DIRS 177389], Section B.2.3). In addition to these, Appendix B also specifies the same four general questions that are listed in Table 2-3 of the TWP (BSC 2006 [DIRS 177389]) for the colloid models. The direction in the TWP is for the

critical reviewer to answer each question and provide the reasoning underlying any "yes/no" answers to them.

A facsimile of the critical reviewer's letter report addressing these questions and the overall criterion for the colloids models (and submodels) is attached below. Note that, in the TWP (BSC 2006 [DIRS 177389]) and the letter report, the critical review is referred to as an independent technical review.

Sandia National Laboratories
Operated for the U.S. Department of Energy by
Sandia Corporation
Albuquerque, New Mexico 87185-0754

Date: June 14, 2007

To: Geoffrey A. Freeze

From: James L. Krumhansl Date 6/14/07

QA/QA

Subject: Independent Technical Review for Model Validation of the *Waste Form, and In-Drift Colloids-Associated Radionuclide Concentrations: Abstraction and Summary*

The purpose of this memo is to document my independent technical review of the *Waste Form, and In-Drift Colloids-Associated Radionuclide Concentrations: Abstraction and Summary* (ANL-EBS-PA-000004 Rev 03A; May 2007; i.e., the "In-Drift Colloids" model) conducted using the criteria provided for the review within Section *.(2.2.1.3, p. 28-30) and Appendix B* of the *Technical Work Plan for Waste Form Testing and Modeling* (TWP-WIS-MD-000018 Revision 01; August, 2006) and following the instructions given in 6.3.2 of procedure SCI-PRO-006 Revision 02 - 51809. As indicated in the Attachment 4 of the AMR, and in the TWP, the goal of this review is to assess whether the model is appropriate for its intended use. In this manner, this independent technical review provides input to the Manager of the work being evaluated so that the Manager may make a determination on the adequacy of model validation. Based on my evaluation of the "In-Drift Colloids" model approach and implementation, I find that the conceptual aspects of the system are well covered, the geochemical system is comprehensively represented, and assumptions are generally justified. The representation of uncertainty is generally appropriate for the intended use of the model and our degree of understanding of the processes involved. Some minor aspects of the model dealing with the interface between the "In-Drift Colloid" model and the volcanic intrusion scenario are rather unique to the YMP program perspective so the relevant supporting documents should be explicitly cited. My overall conclusion, however, is that **the "In-Drift Colloids" model is appropriate for its intended use.**

Purpose/Intended Use of the "In-Drift Colloids" model:

The purpose/intended use of the "In Drift Colloids" model is given in the TWP, Table 2.2 (p. 35).

"Describe the abstraction of the colloids process model for the waste form and engineered barrier component calculations to be performed for TSPA-LA."

Exceptional Service in the National Interest

Further elaboration is provided in Section 1 of the AMR:

"The model describes the types and concentrations of colloids: (1) that could be generated in the waste package from degradation of the waste forms and the corrosion of the waste package materials, (2) produced from the steel components of the repository and their potential role in radionuclide transport, and (3) present in natural waters in the vicinity of Yucca Mountain. In addition, sorption and desorption characteristics and mechanisms of colloids anticipated in the repository are addressed and discussed."

Objectives of the Current Revision:

The current AMR is a revision of an earlier document which is being conducted in response to review comments made regarding its content. The specifics to be addressed in preparing this revision are elaborated on further in the TWP (Sec. 1.2.2; p. 9-10):

"This report (BSC 2005 [DIRS 174290]) will be revised to address IVRT issue EBS-21 and any NRC additional information needed (AIN) items (ENFE 3.05 AIN-1, TSPAI 3.42 AIN, TSPAI 3.30 AIN-1, and ENFE 4.06 AIN-1)……

……This activity also includes work to bolster the technical basis for other parts of the model. Specifically, the work that is needed to bolster the technical basis includes the following:

Reassess radionuclide sorption onto stationary and colloidal corrosion products formed by the internal steel components of the waste package; work conducted under this TWP will be coordinated and integrated with the Near-Field Environment Department's work on radionuclide sorption onto corrosion products.

Model commercial spent nuclear fuel and DOE spent nuclear fuel colloids

Model sorpton of urantum and other low solubility elements onto colloids

Improve defensibility for Kd distributions

Discuss applicability of the competitive sorption models, developed by the Near-Field Environment Department, to the colloids models; this work is to be coordinated and integrated with the work that the Near-Field Environment department is planning to address competitive radionuclide sorption onto corrosion product substrates

Limit sorption based on the sorption site density; this work is to be coordinated and integrated with the work that the Near-Field Environment department is planning to address the effects of the limited sorption site density

Address uncertainty in the 10^{-7} Molar plutonium irreversible glass colloids concentration

Bolster defensibility for low-colloid concentration at high ionic strengths

Assess use of Zarrabi et al. (2003 [DIRS 171238]) data for iron corrosion products colloid concentrations. This assessment will be based on the discussion of corrosion product colloid concentrations in the TSPAI 3.30 letter to be sent to the NRC.

Improve the technical basis for the upper end for iron corrosion products colloids
specific surface area distribution consistent with the surface areas provided for corrosion products in related work to be performed by the Near-Field Environment department."

The critical review is conducted according to the specific questions provided in Appendix B of the TWP. The TWP (Section 2.2.1.3; p. 28-31) also enumerates specific objectives to be achieved by this version of the AMR. These objectives have been abstracted and are included, as appropriate, in italics, with the various specific questions set out in Appendix B of the AMR.

Summary:
"Assessment of the activities will be qualitative and considered successful if deemed defensible by the independent technical reviewer."

The approaches taken to model the difficult, complex, and poorly constrained problems addressed in this AMR were found to provide a representation of nature that is both reasonable and comprehensive. Building this model entailed making a variety of assumptions as well as combining direct experimental observations with theoretical approaches. This activity was successful and conducted in ways which I find to be defensible.

Specific Issues from Appendix B:
1) Have all elements that are likely to have dose-significant colloid-facilitated transport been modeled?

The list of radionuclides considered is supported by ANL-WIS-MD-000006 Rev 02 "Radionuclide Screening", March 2007. Radionuclides selected are also in general agreement with those considered to be important by various independent sources; foreign radioactive waste management programs and overall radionuclide inventories that have been calculated for nuclear fuels at various degrees of burn-up. In making these selections appropriate consideration was given to the degree of radioactive decay which will occur between the time when the waste is emplaced and when exposure becomes a matter of concern, and various competing natural radionuclide transport modes.

2) Have enough types of colloids been modeled to adequately capture the phenomenon of colloid facilitated transport within the waste package and drift?

Yes, all of the principal components in the repository (spent fuel, waste glasses, waste canister materials) are represented in the AMR, and their degradation mechanisms are adequately modeled.. The choice of surrogates, ZrO_2 for mixed metal oxides and meta-autunite for the oxidation product of UO_{2+x} fuel, is appropriate. Among the various possible choices of waste canister corrosion products iron oxide was the appropriate pick because it will be the dominant component in the debris formed as waste packages corrode. Of the materials formed by this corrosion process it is also the component for which there is a substantial body of evidence supporting its ability to scavenging trace constituents from solutions. Choosing as the representative "groundwater colloid" is a correct and pragmatic choice as it is the component in natural (inorganic) colloids with the highest specific surface area and greatest exchange capacity.

3) Is uncertainty in the reversibility of attachment of radionuclide's to each colloid type adequately captured?

The first objective is to reassess reversibility of radionuclide sorption onto stationary and colloidal corrosion products formed by the internal steel components of the waste package.(2.2.1.3, p. 28)

The second objective is to reassess models for formation of radionuclide-bearing colloids from degradation of waste forms: high-level radioactive waste glass, commercial spent nuclear fuel, and DOE spent nuclear fuel. .(2.2.1.3, p. 29)

Yes, the topic is treated in a manner which is appropriate to each individual type of colloid and waste form. Where there is the greatest concern regarding reversibility – with iron oxide corrosion products – the model goes to significant lengths to capture both reversible and irreversible behaviors (Sections 6.3.12.1; 6.3.12.2) as well as considers even more elaborate approaches (Section 6.4). Smectite clays (the surrogate for groundwater colloids) have a layered atomic structure and there is a vast amount of published literature documenting their propensity for these materials to engaging in reversible ion exchange processes. Consequently, as is appropriate, all the radionuclide exchange processes involving this colloid (as a naturally occurring colloid) are assumed by the model to be reversible (even Pu, Th and Am). The layered nature of the meta-autunite (for uranophane) structure, is similar to that of a smectite, which is why it was appropriate to apply reversible exchange models for radionuclide sorption (and desorption) onto to this colloid as well. The treatment of the smectite colloid that develops from degrading waste glass is exceptional in that the retention of Th, Am and Pa is regarded as not being reversible. However, this assessment is supported by direct experimental observation (section 6.3.3). The underlying cause for this distinction is that, rather than being "sorbed" in the classical manner, on these materials the actinides are
Apparently "imbedded" in the colloids as discrete particles (Fig. 6-19).

4) For elements where there is little or no data, are the ranges of Kds provided adequate for the intended purpose?

The third objective is to model sorption of uranium and other low solubility elements onto colloids and to improve defensibility of the associated K_d distributions

Yes, the particular instance referred to here relates primarily to the uranium (VI) colloids, for which there is very little data. However, the actinides (mostly Pu actually), are the constituent of greatest concern (given their relative abundance and higher specific activity) and, fortunately, the Kd values for these radionuclide's can be related directly to experimental observations. For the other radionuclide's it was necessary to make some creative assumptions and extrapolations based on very little data. These estimates, however, were good enough to allow for semi-quantitative assessments of the performance of colloids loaded with these constituents, and they were found to be of trivial importance relative to the overall colloidal transport of radionuclides. Thus, the spotty data available on this topic would not be a factor which adversely impacts the validity or utility of this AMR.

5) For elements where there is data, are the ranges of Kds provided adequate for the intended purpose?

Yes, the origins of these data are uniformly well documented and the experimental conditions cited are appropriate to the range of physical conditions to be expected in the YMP facility. The authors deserve praise for what was apparently a significant effort to perform a comprehensive review of all available data sources. As a consequence, the Kd CDF's which were developed for each radionuclide do indeed span whole range values which are credible for the YMP project. Section 7 is successfully validates these selections by referring to additional independent sources of Kd data compiled by widely respected institutions such as the US EPA and NAGRA.

6) Are the colloid concentration ranges reasonable for transport within the drift both during and after the time frame of waste form and waste package degradation?

Yes colloid ranges are certainly reasonable. Considerable care was taken to evaluate the natural abundance of colloids in groundwater's (6.3.1.1) and much experimental evidence for the other types of (man made) colloids is assembled in the other appropriate sections of Section 6. These data were, in turn, used to develop CDF functions describing the probability that a particular colloid concentration would be encountered. A second aspect of the model development was to derive a tool for assessing whether colloids would (or would not) be stable at a particular pH and ionic strength. This tool was then populated with parameters which would provide a conservative perspective on colloidal stability (see Section 7.1.1 for the best discussion on this topic). Section 6.6 contains a rather detailed account of how the time and spatial scaling factors were evaluated, and the treatment was found to be pragmatic and defensible. Section 6.5.1 describes the logic used to combine the stability limit assessment for each colloid, the CDF describing what particle abundances might be expected in a particular colloid and (not pertinent to this question) how the radionuclide loading on the colloids was determined. Thus, the colloidal transport model reflects both the solution chemistry in question and waste type(s) that are present.

Alternative models for iron oxide were also considered (Section 6.4, Table 6-19) and screened out due to a lack of supporting data, and because the existing model was seen to be conservative with respect to these "improvements". The existing models are also generally conservative because of processes that were explicitly omitted: impact of filtration in the waste package and the trapping of colloids at the vapor-liquid interfaces to name two. Finally, in the case of iron oxide an allowance was made for a small probability that a colloid would exist above the modeled stability limit. This was done to accommodate experimental observations, and was called for in the TWP. Significant effort was expended (Section 7) to validate key parameters for the different colloidal materials using independent data. The arguments were particularly persuasive for the most important colloid: iron oxide corrosion products. Although their use is not explicitly addressed (or required) by the models presented in this version of the AMR, the text also qualifies site density and specific surface area data for the different colloid phases. These would find application if, in the future, the decision was made to use a surface complexation approach to predict the scavenging of trace element from solution. This is also addresses a need that is was explicitly called out in the TWP.

7) Is the dependence of colloid concentration on ionic strength and pH appropriate for TSPA purposes?

The fourth objective is to bolster defensibility for low colloid concentration at high ionic strengths and to partially address KTI 3.42 AIN. This activity will address changes in colloid concentrations when the pH and ionic strength change from regions in which the colloid suspensions are stable to those in which the suspensions are unstable (2.2.1.3, p. 30).

The fifth objective is to assess use of data provided by Zarrabi et al. (2003 [DIRS 171238]) to assess iron corrosion product colloid concentrations.

The sixth objective is to improve the technical basis for upper end for iron corrosion products colloids specific surface area.

Yes, the model employed (DLVO theory) represents a state-of-the-art model. The author(s) correctly point out that only dilute colloidal suspensions are to be expected, if for no other reason than waste and waste package degradation will be very slow - by design. As a consequence using a computational formalism that models the interaction of just two particles is appropriate. The variability in pH and ionic strengths evaluated with this model (or actually the several models developed to treat different types of colloids, see Table 6-1) are reasonable for the environments in question and are consistent with project reports explicitly documenting the ranges for these variables. The DLVO is used for each material in a similar manner so that the relative stability limits for each colloid can be compared with ease. With regard to waste package corrosion products, it is acceptable to establish a non-zero probability that some colloids would exist at concentrations greater than those predicted by the DLVO model (Fig. 6-20B). This approach is valid since the "fudge" made in direct response to experimental observations (and was called for in the TWP). Not evaluating colloid restabilization at very high strength (Section 6.3.10) is justified since such a process could only occur locally and would not operate over any sizable distance outside of the waste package. As specified in the TWP, data by Zarrabi et al. (2003, DIRS 171238) was critically reviewed and included as appropriate in this update of the model database.

General issues to be addressed:

8) Do the models of corrosion product colloid stability and attachment of radionuclides adequately cover the range of possible behavior or bound the behavior of *corrosion product colloids* in facilitating radionuclide transport within the drift?

Yes, the assignment of dual sorption (reversible and irreversible) is a reasonable approach. It is also likely that iron oxide will dominate the sorptive properties of both the colloidal corrosion products and the (much larger) amount of waste package corrosion material that is not mobile. Thus, developing the ability to model radionuclide equilibrium between the two sinks is essential to the overall success of the prediction. The calculated stability limit for iron oxide colloids (Fig. 6-5) agrees well with the trend illustrated in the validation section of the report (Fig. 7.5). The calculated CDF describing particle size distributions is also in reasonable agreement with what was obtained from an independent source (fig. 7-7), except in so far as an exception was made to allow a small percentage of very concentrated Fe-rich colloids (as is described initially in 7.1.4, and called for in the TWP) to exist beyond the stability field provided by the DLVO-based calculation. The option of using either a Kd or kinetic basis for calculating radionuclide loadings onto iron oxide (6.5.1.4 steps 4B or 4C) is a reasonable and pragmatic

choice given the state of the available data and our evolving understanding of the various processes that impact the surface chemistry of iron oxide sorbants. The screening processes that eliminated several alternate models for iron oxide colloids (summarized in Table 6-19) are also acceptable for the same reasons. It also appears that qualitatively the process of using the current model rather than one that was screened out is conservative. Kd CDF parameters (Table 6-15) are within the range which would be expected from the very large amount of literature available regarding sorption onto iron oxides generally. The approaches used to described kinetic factors (if step 4C is used; see Section 6.5.1.4, page 6-79) are also acceptable. Generally, the discussion in Chapter 7 – Model Validation – supports the model developed in Chapter 6 of the AMR for waste package corrosion products. Relative to transport in the drift (as opposed to the source of the colloid in the waste package), the AMR model would re-calculates the status of the colloid once it is exposed to a new fluid in the invert (Section 6.5.2), so the treatment is sufficient for that environment as well. By ignoring possible attractions between the invert-filling material(s) the colloids the model provides a generally conservative picture of transport in the drift.

9) Do the models of waste form colloid stability and attachment of radionuclides adequately cover the range of possible behavior or bound the behavior *of waste form* **colloids (glass, commercial spent nuclear fuel and defense spent nuclear fuel) in facilitating radionuclide transport within the drift?**

Generally yes, though the explanation has three different facets.

1. ZrO_2: Zirconium dioxide is used as a proxy for metal oxide colloids generated from spent fuel – the reasons for the choice are explained clearly (Section 5.5, p. 5-2) and substituting a single surrogate for a unquantifiable heterogeneous mix of materials is a pragmatic choice which allows for at least a semi quantitative evaluation of a problem that formerly could not be addressed. In compiling their model the authors have exhausted the store of available data on ZrO_2 so validation from independent sources could not be achieved in the manner of the iron oxide treatment (#8, above). However, Fig. 7.3 (regarding independent testing of spent fuel) does suggest that the release of Pu and Am containing colloid is very slow so that the model probably samples an appropriately low range of colloidal concentrations at the source (e.g., the surface of the spent fuel undergoing alteration). Treating the uptake of Pu, Am and Th as irreversible probably does reflect a valid assessment of the crystallochemical state of these radionuclides in such materials. Movement of the colloid from the source area within the waste package into the drift should not entail any physical of chemical changes not accounted for in the model.
2. Meta-autunite (for Uranophane): It is noteworthy that: (1) relative to dissolved uranium the transport of uranium as a colloid represents only a small fraction of the total uranium transport, (2) relative to other colloidal components (notably iron oxide), the transport of Pu, Am and other radionuclides on uranium (VI) colloids is calculated to be relatively unimportant and, (3) uranium colloid transport only requires Level 1 validation. Relative to the model; the substitution of the colloidal properties (surface area, zeta potential, etc.) of similar structurally related uranium minerals is acceptable in developing a model for the stability limits of meta-autunite colloids (Fig. 6-14). The required CDF for uranium (VI) colloids as a function of particle sizes is the result of direct measurements (Fig. 6-15) and does not depend on the mineralogic identity of the particles. With regard to requisite Kd distributions, one expects that that the actinides are the constituent of greatest concern (by virtue of their greater abundance and specific activity) and the values use are based on direct experimental results on uranophane (Fig. 6-16). No processes are expected to operate in the drift which are not already accounted for in

the model and which would change the general assessment of unimportance attached to this type of colloid.

3. Smectite Clays: Because similar materials occur naturally in tuffs the mecities derived from glass alteration would be expected to be equally stable in the drift and within the waste package. The stability of such colloids as a function of ionic strength is broadly described in the literature and in the AMR model supported by experimental data (Fig. 6-8), as are the stability limits on smectite suspensions as a function of the combined effects of pH and ionic strength (Fig. 6-9). The association of such particles with irreversible Pu Am and Th was established experimentally (Fig. 6-4), as was the CDF which defines the loading of Pu onto such materials (Fig. 6-10). The process for selecting the range of Pu values to be evaluated from the CDF is clearly documented (Table 6-4 and associated text, p. 6-14) and is defensible. The stability of the mineral substrate and the defined irreversibility of the radionuclide uptake means that when the colloid exits the waste package and enters the drift only concern changes in colloidal stability (in response to new fluid chemistries in the invert) - which is explicitly dealt with by the extended model (Section 6.5.2),.

10) Do the models of ground water colloid stability and attachment of radionuclides adequately cover the range of possible behavior or bound the behavior of *ground water colloids* **(e.g., smectite clays) in facilitating radionuclide transport within the drift?**

Yes, much of what was said for #9-3 is applicable here as well. That these materials are indigenous to the host rock indicates that as long as the invert remains principally crushed tuff (and concrete is absent) these materials will not have stability issues outside the waste package. Kd values were derived from a comprehensive survey of relevant literature (see Section 6.3.12.1) and found to generally be in agreement with other reputable tabulated sources (NAGRA, US EPA, etc. – see Section 7.1.5) In this case all radionuclide uptake is treated as being reversible (even Pu, Th and Am). This is appropriate since the loading process would one of ion-exchange onto a pre-formed mineral substrate rather than co-formation of various phases adjacent to an actively altering waste-glass surface. Since the radionuclide retention processes are treated as being reversible, and the extended model recalculates the state of the colloid once it exits the waste package (steps 5 and 6, sections 6.5.2.1 and 6.5.2.2), the model is adequate for predicting "transport within the drift."

11) Are the models adequate and appropriate for their intended use?

Generally, yes, the models are both adequate and appropriate, as elaborated on in the above discussions.